

Unconventional Homogeneous and Heterogeneous Asymmetric Organocatalysis

Inaugural-Dissertation

zur

Erlangung des Doktorgrades

der Mathematisch-Naturwissenschaftlichen Fakultät

der Universität zu Köln

vorgelegt von

Ji-Woong Lee

aus Seoul (Südkorea)

Köln 2013

Berichtersteller: Prof. Dr. Benjamin List

Prof. Dr. Hans-Günther Schmalz

Prof. Dr. Axel Klein

Tag der mündlichen Prüfung: 26 June 2013

TABLE OF CONTENTS

TABLE OF CONTENTS	I
ABSTRACT.....	IV
LIST OF ABBREVIATIONS	V
ACKNOWLEDGEMENTS.....	IX
1. INTRODUCTION	1
2. BACKGROUND	4
2.1. Catalysis.....	4
2.2. Catalytic Asymmetric Organic Synthesis.....	5
2.3. Asymmetric Synthesis of Enantioenriched Carbonyl Compounds	7
2.4. Ketene Dithioacetals and Thioacetals	11
2.5. BINOL-Based Brønsted Acid Catalysis	13
2.6. Heterogeneous Asymmetric Organocatalysis	14
2.7. Textile materials	18
3. OBJECTIVES OF THIS Ph.D. WORK.....	21
4. RESULTS AND DISCUSSION.....	25
4.1. Preparation of α -Substituted Lactones and Hydrocoumarins and Their Dithioketeneacetals.....	25
4.1.1. Preparation of α -Substituted Lactones.....	25
4.1.2. Preparation of α -Aryl Hydrocoumarins.....	26
4.1.3. Preparation of α -Aryl Hydrocoumarins.....	27
4.1.4. Application of the Claisen Rearrangement for the Preparation of α -Alkyl Hydrocoumarins	28
4.1.5. Preparation of α -Alkyl Hydrocoumarins via NHC Catalysis	32
4.1.6. Preparation of Ketene Dithioacetals.....	33
4.2. Asymmetric Protonation Reactions of Ketene Dithioacetals	34
4.2.1. Asymmetric Protonation of Ketene Dithioacetals Derived from Lactones.....	34
4.2.2. Asymmetric Protonation of Ketene Dithioacetals Derived from α -Alkyl Hydrocoumarins	37
4.2.3. Asymmetric Protonation of Ketene Dithioacetals Derived from α -Aryl Hydrocoumarins	40
4.2.4. Asymmetric Protonation of Ketene Dithioacetals Derived from α -Alkyl Hydrocoumarins with SF ₅ -Substituted BINOL-Phosphoric Acids.....	45
4.2.5. Application of Enantioenriched Dithioacetals.....	47
4.2.6. Reaction Mechanism of Asymmetric Protonation Reaction of Ketene Dithioacetals.....	52
4.3. Heterogeneous Asymmetric Organocatalysis	55
4.3.1. Recycling of a Brønsted Acid Catalyst	55
4.3.2. Immobilization of Cinchona Alkaloids and Its Derivatives – Conventional Approach.....	57
4.3.3. Immobilization of Cinchona Alkaloids and Its Derivatives – Photochemical Approach	60

4.3.4.	Textile Asymmetric Organocatalysis - Design	63
4.3.5.	Preparation of Cinchona Alkaloid Derivatives.....	63
4.3.6.	Preparation of Chiral Textile Organocatalysts	64
4.3.7.	Application of Textile Organocatalysts	67
4.3.8.	Application of Textile Organocatalysts to Continuous Reaction	77
4.3.9.	Preparation of Various Textile Organocatalysts.....	81
4.3.10.	Preparation of DMAP Related Textile Organocatalysts and Their Applications.....	82
4.3.11.	Preparation of Achiral Brønsted Acid Immobilized Textile Catalysts.....	90
4.3.12.	Preparation of Chiral Brønsted Acid Immobilized Textile Catalysts.....	91
4.3.13.	Applications of Chiral Brønsted Acid Immobilized Textile Catalysts.....	99
4.3.14.	Preparation of Chiral Secondary Amine Immobilized Textile Catalysts	100
4.3.15.	Preparation and Application of Further Textile-Immobilized Organocatalysts.....	102
4.3.16.	Investigations on the Immobilization Mechanism	106
5.	SUMMARY.....	114
5.1.	Deracemization of α -Substituted Hydrocoumarins <i>via</i> Asymmetric Protonation of Ketene Dithioacetals	114
5.2.	Textile Organocatalysis.....	118
6.	OUTLOOK.....	124
6.1.	Asymmetric Protonation of Ketene Dithioacetals	124
6.2.	Textile Organocatalysis.....	127
7.	EXPERIMENTAL PART	131
7.1.	General Experimental Conditions	131
7.2.	Synthesis of BINOL-Based Brønsted Acid Catalysts.....	134
7.2.1.	Preparation SF ₅ -Substituted Phosphoric Acid 56n	134
7.2.2.	Preparation 6,6'-Adamantyl Substituted Phosphoric Acid'	136
7.2.3.	Preparation H ₈ -BINOL Derived Phosphoric Acid	137
7.2.4.	Preparation 3,3'-Pentafluorophenyl Substituted BINOL-Phosphoric Acid	139
7.2.5.	Preparation 3,3'-(3,5-(<i>t</i> Bu) ₂ C ₆ H ₃) BINOL-Phosphoric Acid.....	140
7.3.	General Procedure for the Preparation of Dithioketene acetals from Lactones	141
7.4.	General Procedure for the Preparation of Coumarins and Hydrocoumarins and their dithioketene acetals	143
7.4.1.	Preparation of α -Aryl Coumarins and Hydrocoumarins.....	143
7.4.2.	General Procedure for the Preparation of α -Aryl Coumarins and Hydrocoumarins	152
7.4.3.	Typical Procedure for the Preparation of α -Methyl Hydrocoumarin	153
7.4.4.	Typical Procedure for the Preparation of α -Prenyl Hydrocoumarin.....	154
7.4.5.	General Procedure for the Preparation of Hydrocoumarin Ketene Dithioacetals and Their Asymmetric Protonation.....	157
7.4.6.	Typical Procedure for the Preparation of Ketene Dithioacetals from Benzaldehyde	162

TABLE OF CONTENTS

7.4.7.	Typical Procedure for the Preparation of Ketene Dithioacetals from α -Arylaceticacids.....	163
7.4.8.	Preparation of Dithiols.....	164
7.4.9.	General Procedure for Asymmetric Protonation Reactions	167
7.4.10.	Gram-scale Deprotection and Application of Thioacetal-Protected Hydrocoumarin Products – Oxidative Hydrolysis.....	173
7.4.11.	Application of Thioacetal-Protected Hydrocoumarin Products via Reductive Cleavage to the Synthesis of (S)-Equol.....	174
7.5.	X-ray Structure Analysis Parameters.....	175
7.5.1.	X-ray Structure Analysis Parameters for 64g	175
7.5.2.	X-ray Structure Analysis Parameters for <i>rac</i> - 65g	180
7.5.3.	X-ray Structure Analysis Parameters for 65k	184
7.5.4.	X-ray Structure Analysis Parameters for (S)- 30g	188
7.6.	Preparation of Organocatalysts for Immobilization.....	193
7.6.1.	Preparation of DMAP Derivatives.....	193
7.6.2.	Preparation of Cinchona Alkaloid Derivatives.....	195
7.6.3.	Preparation of Phosphate Derivatives for Immobilization on Textiles	198
7.6.4.	Preparation of MacMillan-Type Catalyst.....	201
7.6.5.	Preparation of Proline-Derivative.....	202
7.7.	General Procedure for the Preparation of Organocatalyst-Immobilized Textile Catalysts	203
7.8.	General Procedure for Applications of Textile Catalysts	204
7.8.1.	General Procedure for Acylation of Phenol 96	204
7.8.2.	General Procedure for Catalytic Carbondioxide Fixation Reaction	205
7.8.3.	General Procedure for Hydroetherification of Alkene	205
7.8.4.	General Procedure for Desymmetrization of Anhydrides 76 and Recycling Experiments.....	206
7.8.5.	General Procedure for Desymmetrization of <i>meso</i> -Anhydrides	206
7.8.6.	Recycling Experiments for Desymmerization Reaction of 76a	208
7.8.7.	Synthesis of 4- <i>tert</i> -Butyldiphenylsilyloxy Glutaric Anhydride 76h	216
7.8.8.	Typical Procedure for Desymmetrization of <i>meso</i> -Anhydride 76h using a Continuous Circulatory Reactor.	218
7.8.9.	Typical Procedure for Radical-Mediated Reaction of “Monomeric” Amide and Cinchona Alkaloids.	219
7.8.10.	X-ray Structure Analysis Parameters for CSA-Sulfonamide 203	225
8.	BIBLIOGRAPHY.....	228

ABSTRACT

This work describes developments of i) a catalytic asymmetric protonation reaction of ketene dithioacetals using a chiral Brønsted acid as a catalyst and ii) a heterogeneous catalysis using textiles as solid support materials. First, for an asymmetric protonation reaction of ketene dithioacetals, we have disclosed a facile preparation of various lactones and hydrocoumarins. The formation and application of ketene dithioacetals was well demonstrated and fully characterized. The key enantiodetermining step, an asymmetric protonation reaction, was smoothly catalyzed by BINOL-based Brønsted acids. The desired dithioacetal protected hydrocoumarins were obtained in good yields and high enantioselectivities. The utility of the obtained enantioenriched products were further demonstrated by synthesizing a natural product and conducting a large scale reaction. Secondly, we have successfully demonstrated a facile preparation of textile-immobilized heterogeneous catalysts. As a general method, photochemical reaction conditions can provide diverse solid-supported organocatalysts within one-step from inexpensive starting materials. Further applications and mechanistic studies revealed the high efficiency and application potential of the presented methodology.

Diese Arbeit beschreibt die Entwicklung von i) einer katalytisch asymmetrischen Protonierung von Ketendithioacetalen mit einer chiralen Brønstedsäure als Katalysator und ii) heterogene Katalyse unter Verwendung von Textilien als Trägermaterialien. Im ersten Teil berichteten wir zunächst über eine einfache Darstellung von verschiedensten Lactonen und Hydrocoumarinen. Die Bildung und Verwendung von Ketendithioacetalen wurde gut gezeigt und alle Verbindungen vollständig charakterisiert. Der enantiodiskriminierende Schlüsselschritt wurde glatt durch BINOL-basierte Brønstedsäuren katalysiert. Die gewünschten Dithioacetal-geschützten Hydrocoumarine wurden in guten Ausbeuten und mit hohen Enantioselectivitäten erhalten. Die Nützlichkeit der erhaltenen enantiomerenangereicherten Produkte wurde darüber hinaus durch die Synthese eines Naturstoffes und die Durchführung einer Reaktion im großen Maßstab demonstriert. Im zweiten Teil konnten wir erfolgreich die einfache Darstellung von auf Textilien immobilisierten heterogenen Katalysatoren zeigen. Als allgemeine Methode können fotochemische Reaktionsbedingungen verschiedenste geträgerte Organokatalysatoren in einem Schritt und aus günstigen Startverbindungen liefern. Darüber hinaus stellten Anwendungen und mechanistische Untersuchungen die hohe Effizienz und das Anwendungspotenzial der vorgestellten Methodik heraus.

LIST OF ABBREVIATIONS

Ac	acetyl
AcO	acetate
Adm	adamantyl
Alk	alkyl
Aliph	aliphatic
app.	apparent
Ar	aryl, aromatic
aq.	Aqueous
ax	axial
calcd	calculated
BINAP	2,2'-bis(diphenylphosphino)-1,1'-binaphthyl
BINOL	1,1'-bi-2-naphthol
Bn	benzyl
Boc	<i>tert</i> -butyloxycarbonyl
BSA	Bis(trimethylsilyl)acetamide
Bu	butyl
Calcd	calculated
cat.	catalyst/catalytic
CND	Cinchonidine
CN	Cinchonine
conv.	Conversion
CSA	camphorsulfonic acid
Cy	cyclohexyl
d	doublet
d	day(s)
DFT	density functional theory
DIAD	diisopropyl azadicarboxylate
DKR	dynamic kinetic resolution
DME	dimethyl ether
DMF	dimethylformamide
DMSO	dimethylsulfoxide
DOSY	diffusion ordered spectroscopy
DPP	diphenylphosphoric acid
DPPA	diphenylphosphoryl azide
DYKAT	dynamic kinetic asymmetric transformation
dr	diastereomeric ratio

LIST OF ABBREVIATIONS

E	electrophile
EI	electron impact
ee	enantiomeric excess
EM	exact mass
<i>ent</i>	enantiomer(ic)
eq	equatorial
equiv	equivalent(s)
er	enantiomeric ratio
Et	ethyl
ESI	electrospray ionization
<i>g, gr</i>	gram(s)
GC (GC-MS)	gas chromatography (gas chromatography coupled with mass detection)
h	hour(s)
HMDS	hexamethyldisilazane
HOMO	highest occupied molecular orbital
HPLC	high performance liquid chromatography
HQN	Hydroquinine
HRMS	high resolution mass spectrometry
HPLC	high performance liquid chromatography
KMDS	potassium hexamethyldisilazane (potassium bis(trimethylsilyl amide))
KR	kinetic resolution
LC-MS	liquid chromatography coupled with mass spectrometer
LDA	lithium diisopropylamide
Lit.	literature
LUMO	lowest unoccupied molecular orbital
<i>m</i>	<i>meta</i>
m	multiplet
M	molar (concentration)
M	metal
<i>m</i> CPBA	<i>meta</i> -chloroperbenzoic acid
Me	methyl
Mesityl	mesityl (2,4,6-trimethylphenyl)
MM	molecular mechanics
MS	mass spectrometry, molecular sieves
Ms	methylsulfonyl
MTBE	methyl <i>tert</i> -butyl ether
MW	molecular weight
<i>m/z</i>	atomic mass units per charge
<i>n</i>	normal

N	normal (concentration)
n.a.	not available
NaHMDS	sodium hexamethyldisilazane (sodium bis(trimethylsilyl amide))
NBS	<i>N</i> -bromosuccinimide
NCS	<i>N</i> -chlorosuccinimide
n.d.	not determined
NHC	<i>N</i> -heterocyclic carbene
NMR	nuclear magnetic resonance spectroscopy
N.R.	no reaction
Nu-H/Nu	nucleophile
<i>o</i>	<i>ortho</i>
P	product
<i>p</i>	<i>para</i>
PA	Polyamide
PCC	pyridinium chloro chromate
Pd	palladium
PEG	polyethyleneglycol
PET	polyethyleneterephthalate
PETA	pentaerhthritol triacrylate
Ph	phenyl
Phth	Phthalic
Pr	propyl
<i>p</i> TSA	<i>para</i> -toluenesulfonic acid
Py	pyridine
QD	Quinidine
QN	Quinine
quint	quintet
QN	quinine
<i>rac.</i>	racemic
r.t.	room temperature (rt)
sc	super critical
sept	septet
sext	sextet
SM	starting material
<i>t</i>	<i>tert, tertiary</i>
t	triplet
TAC	triallyl cyanurate
TEAA	triethyl ammonium acetate
TEOS	tetraethyl orthosilicate

LIST OF ABBREVIATIONS

Tf	trifluoromethylsulfonyl
TFA	trifluoroacetic acid
THF	tetrahydrofuran
TLC	thin layer chromatography
TMEDA	tetramethylethylenediamine
TMS	trimethylsilyl
TPP	Triphenylpyrylium tetrafluoroborate
Ts	<i>para</i> -toluenesulfonyl
wt	weight

ACKNOWLEDGEMENTS

I would like to extend my sincerest thanks to Prof. Dr. Benjamin List for the opportunity to work in his wonderful research group and to experience the most exciting and cutting-edge chemistry. I am indebted to him for the exceptional trust and unlimited freedom given to me for the academic support. His wonderful and generous personality, which I can not even try to describe with my English skills, have inspired my every second of my life in Mülheim that I will not forget forever.

I would also like to thank assistant professors Dr. Nuno Maulide and Dr. Martin Klußman who have volunteered their time and knowledge by leading various Ph.D. seminars, total synthesis exercises, POC seminars and MOS competitions. All these activities were highly beneficial to construct my chemical knowledge and communication skills, which were not guaranteed without their effort.

I am grateful to Prof. Dr. Hans-Günther Schmalz for accepting to review this thesis, and to Prof. Dr. Axel Klein and Dr. Martin Klußman for serving on my defence committee. I also thank Teresa Oliveira, Manuel Mahlau, Viviana Valerio, Qinggang Wang, Mattia Monaco, Sébastien Prévost and Monika Lindner for kindly proofreading this work and for their valuable suggestions.

I would like to thank Adrienne Hermes and Alexandra Kaltdsis for their advice and support in various forms, and all of the technician staff for providing me with valuable catalysts and their routine assistance in the lab, especially Marianne Hannappel, Simone Marcus, Hendrik van Thienen, Pascal Wallkamp and Arno Döring. I thank our GC department, as well as the HPLC and mass departments for their generous support. I am indebted to my labmates from the List, Klußman and Maulide groups for sharing chemicals, catalysts, ideas and insight especially Nathalie Dupré and Alberto Martinez. For all the valuable discussions, I'd like to thank especially Ilija Čorić, Olga Lifchits, Mattia Monaco, Joyram Guin, and Sébastien Prévost whose creativity and chemical intuition have been a source of my Ph.D. study in Mülheim.

Additionally, I would like to thank Dr. Thomas Mayer-Gall and Dr. Klaus Opwis from Deutsches Textilforschungszentrum Nord-West e.V. in Krefeld for their initialization and collaboration of the project with endless creativity and endeavour.

Finally, I would like to thank the people for their non-optional endurance and support: my parents and friends in Korea, scientific family from Suwon including Prof. Song and his wife and my "Portuguese family" in Lisbon, Villa-Nova and Teresa Oliveira.

1. INTRODUCTION

Catalysis has contributed greatly to chemical industry by lowering the activation energy of certain chemical processes and facilitating the reaction sequence to afford desired products with higher selectivity under more benign and milder reaction conditions (Figure 1-1). Arguably, the biggest breakthrough of chemical processes on Earth has been the synthesis of amino acids billions of years ago. According to the hypothesis from the Miller–Urey’s experiments in mid-20th century, a primordial soup could be transformed into several amino acids in the presence of an energy source (electrical sparks) or “catalyst”.^{1,2} It seems reasonable that in the primitive environment, various inorganic materials could act as catalysts for this astonishing “reaction” ultimately leading to the formation of Life. Since the blossoming of Life, most chemical reactions in nature are promoted by catalysts or enzymes which, in turn, were also produced by (enzymatic) catalysis. By investigating enzymes’ operations, organic chemists have been able to mimic their performance to convert raw materials into more valuable chemical substances even more selectively and efficiently.

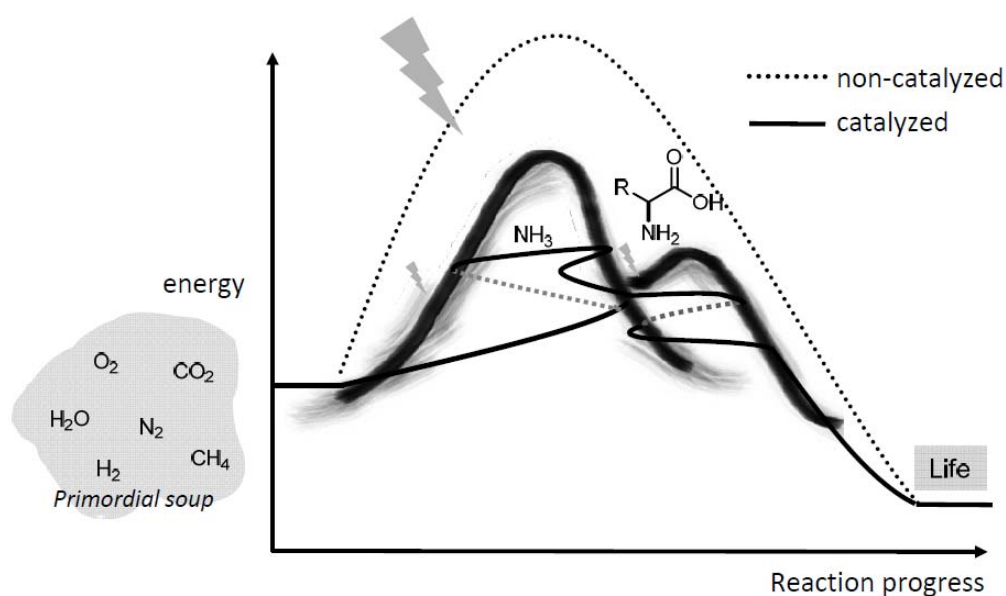
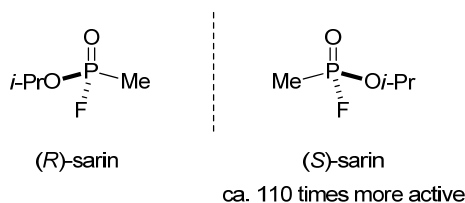


Figure 1-1. Reaction coordinates for non-catalyzed and catalyzed reaction of “Origin of Life”.

On the other hand, surprisingly, nature had already chosen (or been forced to choose) only one enantiomer from the energetically identical racemate to construct Life. This “accidental” event provided us an important message about selectivity. Although the origin of this selectivity remains unclear,^{3,4} it is believed that a small imbalance of a racemic amino acid or sugar could be amplified to the enantiomerically pure level via a chemical⁵ and/or physical⁶ process. The importance of the specific properties of chiral molecules is expressed in the existence of all biological matters as single enantiomers of amino acids, sugars, lipids and nucleotides. Therefore, all biologically active compounds such as drugs and agrochemicals can show different bioactivity depending on the chirality of the molecules. The different biological activity of two enantiomers was tragically

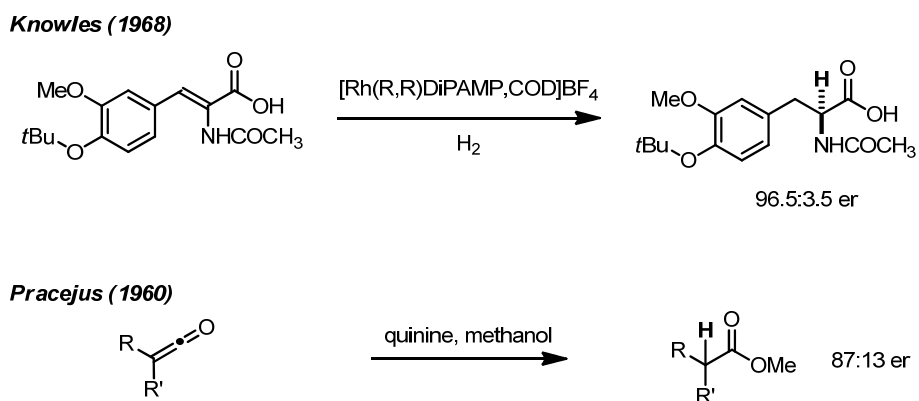
1. INTRODUCTION

demonstrated by the Thalidomide effect.⁷ Although the enantiomers can be racemized in vivo, its use as a racemate by pregnant women resulted in a number of birth defects in the late 1950s. The other example of chirality on phosphorous atom is shown in Scheme 1-1. Sarin is a nerve agent, which is volatile, odorless and colorless liquid. It is known that (*S*)-form of sarin and its derivatives (*G-series*) are more active due to their greater binding to acetylcholinesterase than (*R*)-form.⁸



Scheme 1-1. Two enantiomers of sarin, a nerve agent.

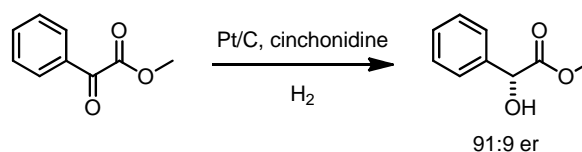
Therefore, it has become even more important to access enantiomerically pure biologically active compounds by using simple methodologies. Although chiral auxiliaries and resolutions have been employed as major tools for the preparation of chiral molecules, asymmetric catalysis seems to be an appealing alternative from an economic and environmental point of view. For example, the synthesis of L-DOPA was dramatically improved by replacing triphenylphosphine from Wilkinson's catalyst with a chiral phosphine ligand for catalytic asymmetric hydrogenation.^{9,10,11} Prior to this work, Bredig and Fiske had already reported asymmetric cyanohydrin synthesis using cinchona alkaloids, albeit in low enantiopurity.¹² About fifty years later, Pracejus had reported asymmetric catalysis using a cinchona alkaloid as catalyst to achieve useful enantioselectivity of α -phenyl methylpropionate (87:13 er) *via* an asymmetric protonation reaction.¹³ The use of an organic molecule as a sole chiral source as well as a catalyst was surprisingly neglected for centuries.



Scheme 1-2. Early examples for catalytic asymmetric catalysis: transition metal and organocatalysis.

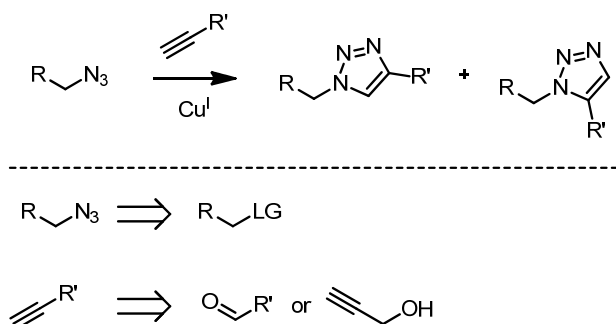
Another striking example was reported by Orito in 1979 by employing a cinchona alkaloid and a heterogeneous platinum catalyst for the reduction of α -keto esters (91:9 er, Scheme 1-3).¹⁴ This pioneering work demonstrated the possibility of asymmetric heterogeneous catalysis by decorating a bulk transition metal surface with cinchonidine (**CND**). Modification of the heterogeneous material could lead to a recyclable enantioselective catalyst although the interaction between the organic molecule and the solid surface is not

permanent. Nonetheless, the obtained high enantioselectivity inspired various efforts to develop more efficient heterogeneous chiral catalysts which derived from homogeneous catalysts.¹⁵

Orito (1979)

Scheme 1-3. Asymmetric hydrogenation using a CND-modified Pt catalyst.

Although heterogeneous catalysis has been investigated in an effort to increase the practicability of chiral homogeneous catalysts *via* immobilization, it has often been limited to inorganic materials and styrene-based polymers,¹⁶ such as Merrifield's resin.¹⁷ There is no doubt that polymeric resins have provided tremendous advantages in solid-state synthesis, especially in polypeptide synthesis. Although their applications in solid-state synthesis and catalyst immobilizations have been investigated for decades, their industrial uses are generally limited to ion-exchange resins.¹⁸ Heterogenization could also be achieved *via* non-covalent immobilization of chiral catalysts in aqueous media or ionic liquids for easy separation. However, this process requires highly polarized catalysts or "fluorous-tags".¹⁹ Generally, procedures for the immobilization of homogeneous catalysts or reagents require sophisticated modifications of both catalyst and solid support. Recent developments of "click chemistry" have been providing a general tool to connect two complex components under neutral reaction conditions for example, azide-alkyne cycloaddition (Scheme 1-4).²⁰

"Click chemistry"

Scheme 1-4. Cycloaddition of azides and alkynes, Huisgen cycloaddition.

This reaction shows perfect atom economy and a broad substrate scope as well as high chemical yields of the desired conjugated products.²¹ Also, the high selectivity of the reaction enables its application in various fields of science, including functionalization of polymeric materials. Nevertheless, this functionalization requires pre-modification of the polymers with alkyne or azide functional groups.²² Therefore, a direct preparation of chiral catalyst-functionalized polymeric heterogeneous material is still advantageous. In the following chapters, we will discuss a research program regarding the efficient preparation of optically pure compounds from simple starting materials and the use of simple heterogeneous catalysts which can be employed in various organic transformations with high practicability and robustness.

2. BACKGROUND

2.1. Catalysis

Perhaps the most common and familiar catalysts in modern human society are catalytic converters which convert harmful gases (NO_x, SO_x and hydrocarbons) to “greener” chemicals such as water, CO₂ and N₂ (Figure 2-1). A mixture of metal oxides (SiO_x, AlO_x and TiO_x) with various heterogeneous transition metals (Pt, Pd and Rh) provides highly efficient catalytic reactions to convert undesired “products” to desired products with high selectivity and robustness. This combination of different catalysts provides efficient oxidation and reduction reactions in a single chamber by taking advantage of the high surface area for interconversion of gaseous substrates on the solid phase (Figure 2-1).

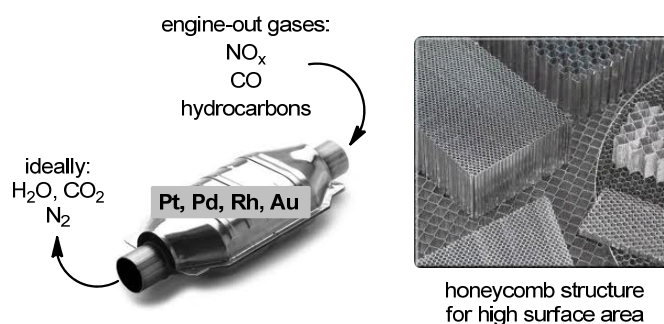
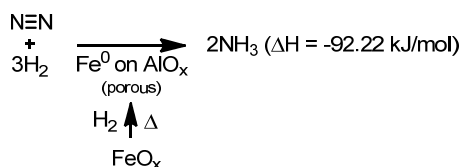


Figure 2-1. Catalytic converter for automobiles.

Another great breakthrough for a chemical process by using heterogeneous catalysts was made by Fritz Haber, who implemented the reaction for conversion of nitrogen gas to ammonia, which is important for fertilizers and explosive materials (Scheme 2-1).²³ It is speculated that half of the proteins in the human bodies is originated from the Haber-Bosch process. The highly active metallic iron catalyst is generated from magnetite by exposing it to reducing conditions by removing oxygen. The catalyst retains its heterogeneous property with high porosity which leads to higher catalytic activity due to the accessible surface area. The mechanism of the reaction was extensively investigated by Gerhard Ertl, awarded with the Nobel Prize for chemistry in 2007.²⁴



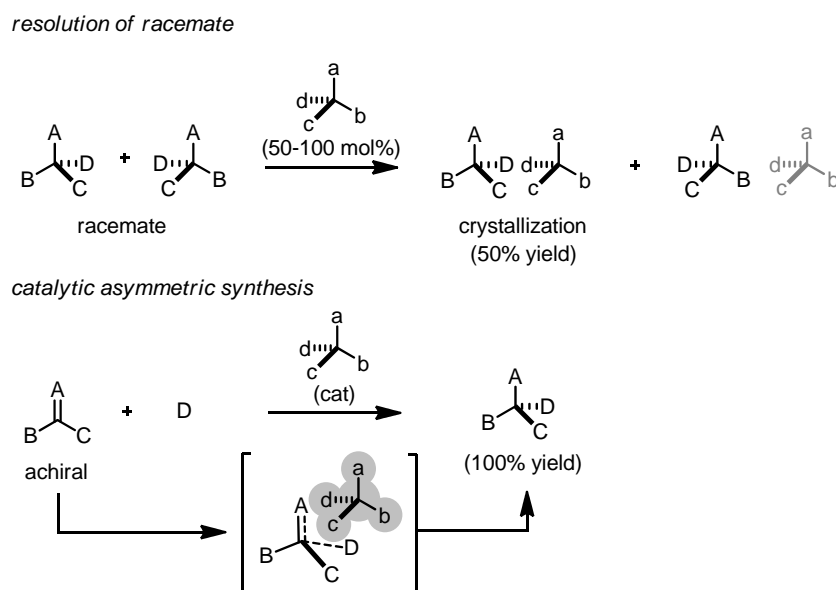
Scheme 2-1. Haber-Bosch process.

As shown in the two previous examples (Figure 2-1 and Scheme 2-1), the catalytic transformation of molecules is of great importance due to its direct impact on human life, society and environment. Recent developments in chemical industry, particularly pharmaceutical, agrochemical and material industry, have challenged organic

chemists to provide fine chemicals under practical reaction conditions. Since the natural world largely consists of single enantiomers, the importance of asymmetric organic synthesis can not be overlooked due to the differences in pharmacokinetics and pharmacodynamics of chiral drugs and agrochemicals.²⁵

2.2. Catalytic Asymmetric Organic Synthesis

Carbon atoms with sp^3 hybridization can connect up to four different atoms, thereby generating a chiral center. The pioneering resolution of tartaric acid by Pasteur^{26,27} led chemists to investigate other types of chiralities such as axial, helical and planar chirality in the field of organic synthesis. Due to practicality, a crystallization-induced resolution of racemic compounds using naturally-occurring chiral molecules has been predominant in asymmetric synthesis. However, in this case, the maximum yield of the desired enantiomer is limited up to 50% (Scheme 2-2). Recent developments of catalytic asymmetric synthesis using a chiral catalyst and an achiral substrate have proved to be efficient in constructing chiral molecules with precise control of the stereogenic units.

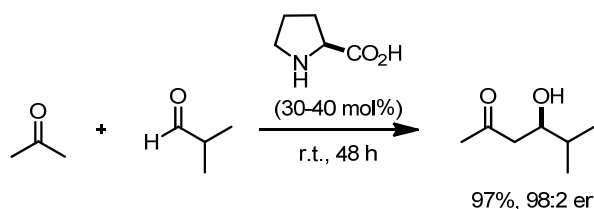


Scheme 2-2. Conventional methods for resolution of a racemate and catalytic asymmetric synthesis.

As introduced in Chapter 1, transition metal catalysts have dominated the field of asymmetric catalysis for more than three decades. This is due to their high activity and selectivity for various asymmetric transformations, such as oxidation, reduction and addition reactions to “activated” electrophiles. Extremely high selectivities can also be achieved for diverse reactions using Nature’s great tools, enzymes. The substrate scope is generally narrower than in transition metal catalysis due to the high specificity of the catalytically active centers of enzymes. However, the recent development of engineered-enzymes which can co-operate with additional organic modifiers or even transition metal catalysts, shows potential for further applications of enzymatic asymmetric catalysis.^{28,29}

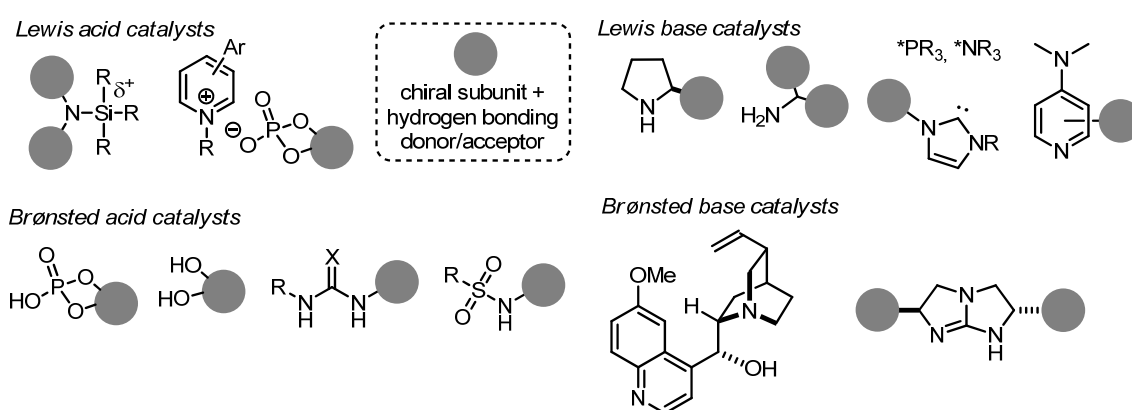
2. BACKGROUND

In the beginning of the 21st century, a great breakthrough was made by List and others in the field of catalytic asymmetric synthesis. A small organic molecule was identified as an efficient catalyst for various transformations which were not amenable with conventional transition metal catalysis.³⁰ Due to its operationally simple reaction conditions and its environmentally friendly nature, proline catalysis has been recognized as a representative example of organocatalysis (Scheme 2-3). Although the catalyst had already been utilized in the synthesis of Hajos-Parrish lactone,³¹ the potential applicability of the reaction was completely neglected by the chemical society.



Scheme 2-3. Proline-catalyzed direct aldol reaction.

After this pioneering work, as shown in Scheme 2-4, various organocatalysts have been developed with unique and unprecedented activity and enantioselectivity for numerous asymmetric transformations started with amino catalysis.³² From small organic molecules such as amino acids and cinchona alkaloids to highly engineered Brønsted acid catalysts, the high potential of organocatalysts should not be underestimated. The key of successful organocatalysis might be the “bifunctionality” of the catalysts. Since organocatalysts lack the highly reactive *d*-orbitals typical of transition metal catalysts, “bifunctionality” of organocatalysts might be crucial for their successful performance. Highly polarized reaction intermediates or transition states could be stabilized by bifunctional organocatalysts *via* cooperational effects, which facilitate reactions and also induce high stereoselectivities.



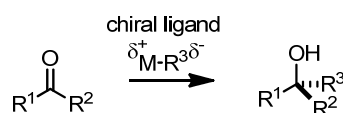
Scheme 2-4. General scheme for rationalization of different classes of organocatalysts.

However, due to the fact that organocatalysis often requires high catalyst loading, strenuous research enabled the development of diverse organocatalysts with remarkable catalytic activity.³³ Additionally, in contrast to transition metal catalysis using chiral ligands, organocatalysts can be recovered during a workup process by taking advantage of the basic nature of nitrogen-based catalysts.³⁴ Moreover, various investigations were

focused on the immobilization of organocatalysts to improve recyclability. Polymer-supported organocatalysts are particularly interesting in contrast to immobilization of ligand-transition metal systems. The robust nature of organocatalysts would indeed avoid the "leaching-out" of the catalytically active species. For the above mentioned reasons, organocatalysis is now one of the most important tools in asymmetric catalysis together with transition-metal catalysts and bio-catalysts. An increasing number of applications of organocatalysts in natural product synthesis and fine chemical production will stimulate more research aimed at the development of more active and selective organocatalysts.

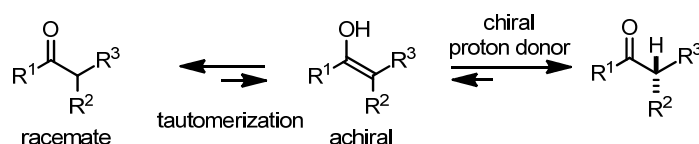
2.3. Asymmetric Synthesis of Enantioenriched Carbonyl Compounds³⁵

Among the numerous asymmetric transformations, a well-established strategy to generate a stereogenic center on a carbon atom is the addition of nucleophiles into carbonyls to produce secondary or tertiary alcohols (Scheme 2-5).^{36,37} The electrophilicity of carbonyl substrates could be enhanced by addition of electron deficient metal reagents together with chiral ligands to create a chiral environment for the addition reaction.



Scheme 2-5. Catalytic asymmetric 1,2-addition of nucleophiles onto carbonyls.

Besides the electrophilic 1,2-addition reaction, carbonyl compounds can also be used in asymmetric protonation reactions to generate enantioenriched compounds. The inherent equilibrium of carbonyl compounds containing adjacent α -protons could lead to keto-enol tautomerization and subsequent asymmetric protonation in the presence of a chiral proton donor (Scheme 2-6). However, due to the acidity of the α -proton of both the substrate and the product, possible racemization of the product must be prevented by controlling the reaction conditions. The reaction can proceed *via* kinetic resolution of the starting materials depending on the activity of the chiral proton donor or additional bases, or dynamic kinetic resolution since the intermediate enol species is achiral. This reaction could provide a general method to access carbonyl compounds bearing a stereogenic tertiary center in α -position.

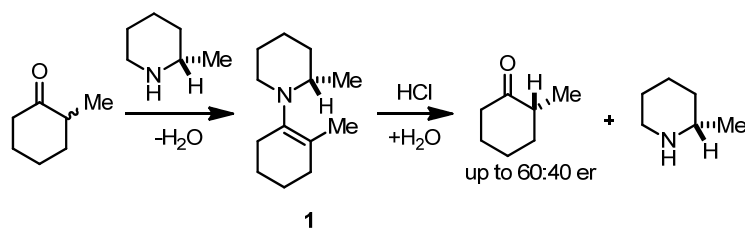


Scheme 2-6. Asymmetric protonation using chiral proton donors.

In 1975, Yoshikawa and coworkers reported a pioneering enamine asymmetric protonation reaction. The chiral enamine intermediate **1**, prepared through an azeotropic procedure could undergo hydrolysis to afford

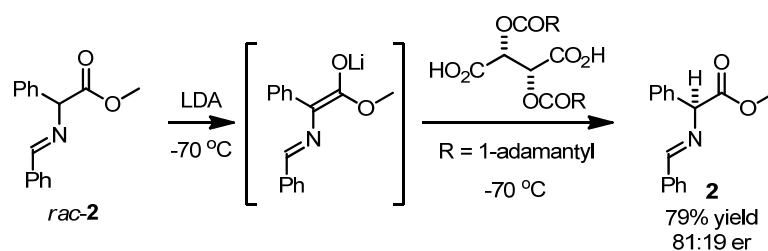
2. BACKGROUND

optically active ketones albeit with low enantioselectivity (60:40 er, Scheme 2-6).³⁸ Various attempts using chiral acids and different chiral amines showed no further improvement in terms of enantioselectivity.



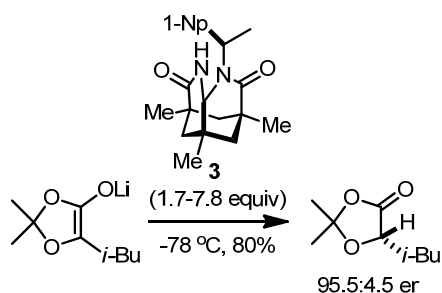
Scheme 2-7. Asymmetric protonation of a chiral enamine.

Another pioneering work for asymmetric protonation was reported in 1978 by Duhamel by using modified tartrate as proton donor. After formation of the lithium enolate of racemic Schiff base **2** using LDA, protonation with sterically biased chiral acid at low temperature ($-70\text{ }^{\circ}\text{C}$) provided α -amino acid derivative **2** with good enantioselectivity (81:19 er, Scheme 2-8).³⁹ Further investigation revealed that the enantiomeric ratio could be improved to 85:15 er by using a chiral base for the deprotonation. This result implies the interaction of the chiral amine with acid or lithium cation during the protonation reaction.⁴⁰



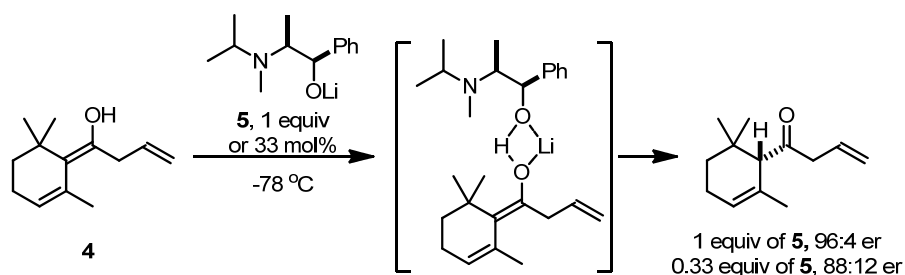
Scheme 2-8. Asymmetric protonation of a lithium enolate using chiral acids.

In 1990, Rebek made a breakthrough in asymmetric protonation reactions by using a novel chiral proton donor **3** derived from Kemp's tricarboxylic acid (Scheme 2-9).⁴¹ The α -hydroxyester derivative was obtained exclusively with high enantioselectivity (95.5:4.5 er). The authors suggested that the proton is buried in the chiral pocket, which could induce the high enantioselectivity of the process. The bifunctional nature of the amide group could also be a key factor by organizing the reactants in a chiral environment.



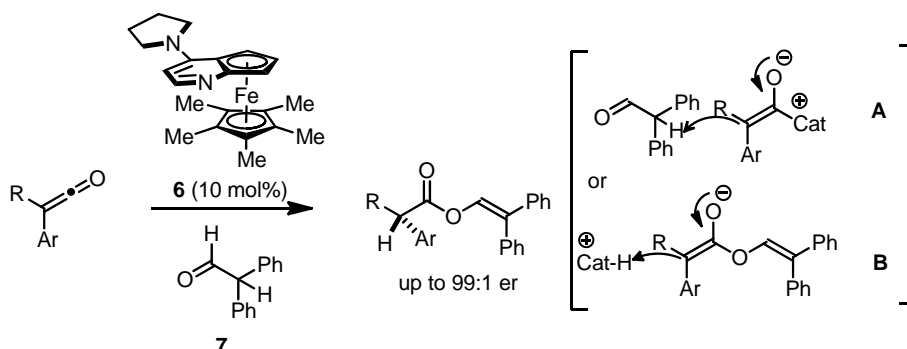
Scheme 2-9. Asymmetric protonation of cyclic enolate using Kemp's acid derivative.

The typical asymmetric protonation reaction requires deprotonation as a separate step. However, in 2007 Fehr reported an elegant method using an enol as a substrate (Scheme 2-10).⁴² Although the reaction is limited to the stable enol **4**, the asymmetric tautomerization reaction was realized by using a chiral base to afford the desired ketone in 96:4 er. The authors also observed a strong non-linear effect of the asymmetric process, which suggests that aggregated lithium species are involved in the enantiodetermining step. Moreover, the use of catalytic amount of lithium alkoxide **5** (33 mol%) leads to the product with lower selectivity (88:13 er). However, a chiral tertiary amine-promoted asymmetric protonation can not be excluded. Nonetheless, to the best of our knowledge, this is the only example of direct protonation of an enol/enolate using a chiral catalyst.



Scheme 2-10. Asymmetric protonation of enol substrate using chiral lithium alkoxide.

For a catalytic asymmetric protonation to be possible, the substrate should be able to undergo the protonation reaction under mild conditions, which would prevent racemization of the final product. For example, ketenes could suffer from a nucleophilic attack by catalyst **6** and then undergo protonation by the aldehyde **7** to afford the aldehyde derived enolate, which eventually replaces the chiral catalyst (Scheme 2-11-A).⁴³ Alternatively, due to the basicity of the catalyst and the presence of the acidic α -proton in aldehyde **7**, the reaction can proceed *via* a Brønsted acid mechanism. A proton transfer from the aldehyde to the catalyst could generate a chiral Brønsted acid catalyst which would then protonate the enolate species. Nevertheless, the employment of a nucleophilic catalyst (10 mol%) was successful in terms of enantioselectivity of the obtained α -disubstituted esters (up to 99:1 er).

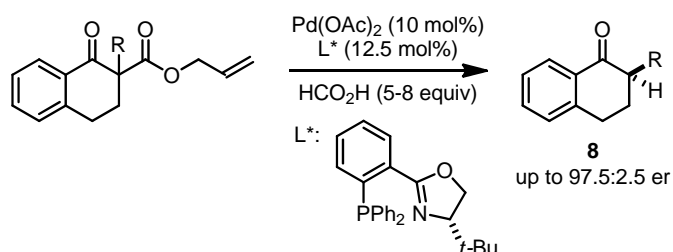


Scheme 2-11. Catalytic asymmetric protonation of ketene.

Transition-metal catalysis has also been applied in asymmetric protonation reactions by using allylestere as substrates.⁴⁴ In the presence of a palladium catalyst, the substrate could be converted to chiral α -tetralones

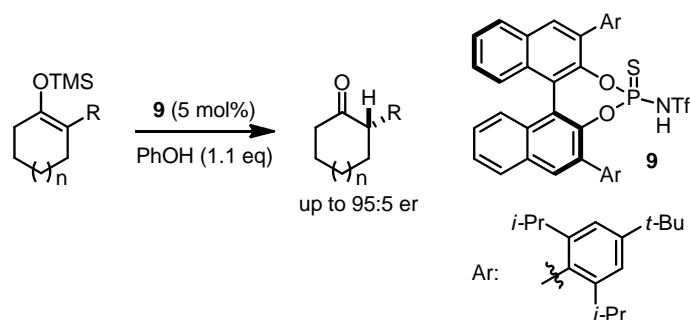
2. BACKGROUND

(Scheme 2-12). The reaction is believed to proceed *via* π -allyl formation/decarboxylation and protonation reaction from the racemic starting materials. This enantioconvergent process could be modified in the absence of formic acid to afford allylated products with a quarternary stereogenic center (Tsuji reaction⁴⁵ and Carroll rearrangement⁴⁶). The use of a large excess of formic acid leads to the protonated products **8** in high enantioselectivity (up to 97.5:2.5 er).



Scheme 2-12. Palladium catalyzed decarboxylative asymmetric protonation.

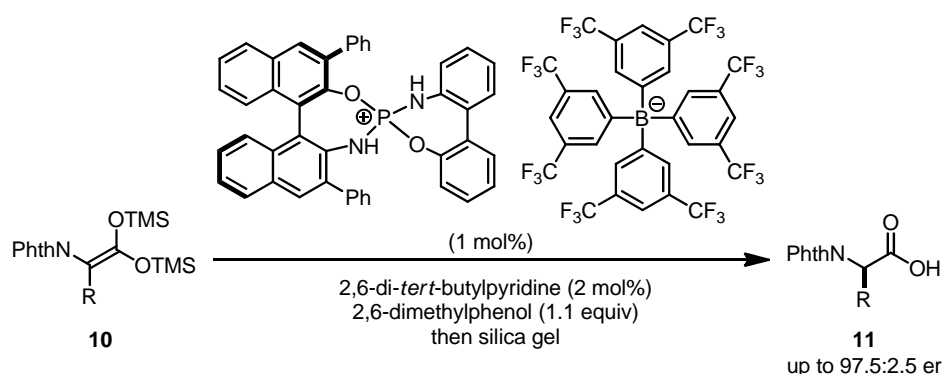
Since the pioneering work by Yoshikawa, Duhamel and Rebek regarding asymmetric protonation reactions using a stoichiometric chiral proton source, it was a formidable challenge to employ a chiral Brønsted acid catalyst with a stoichiometric achiral proton source for the asymmetric protonation of enolates. Although the reaction mechanism is simple to understand, a facile protonation of the enolate from an achiral proton source should be efficiently prevented. After several decades, a catalytic asymmetric protonation reaction using a chiral Brønsted acid was realized by Yamamoto's group.⁴⁷ Using sterically hindered, strong Brønsted acid catalyst **9**, high enantioselectivities were obtained in the presence of phenol as a stoichiometric proton donor, which was eventually converted to the silyl-protected alcohol (Scheme 2-13). The exact reaction mechanism is not yet clear; however, the authors suggested the formation of an oxonium ion from the protonated phenol, in the presence of the chiral counter anion. Also, they speculated that subsequent desilylation of the substrate by phenol could facilitate the whole reaction sequence.



Scheme 2-13. Asymmetric protonation of a silyl enolether using a Brønsted acid catalyst.

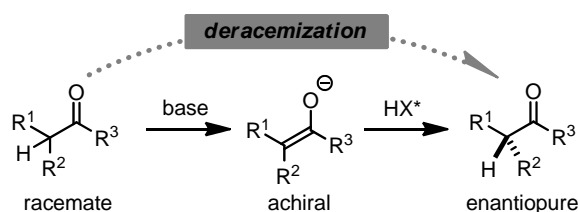
Further advances in Brønsted acid-catalyzed asymmetric protonation reactions were realized by Ooi in the synthesis of α -amino acid derivatives **11** using an organocatalyst (Scheme 2-14).⁴⁸ The new catalytic motif, *P*-spiro diaminodioxaphosphonium barfate, showed remarkable enantioselectivity for the asymmetric protonation of ketene disilylacetals **10** in the presence of a sterically bulky achiral base and a proton source.

The utility of the methodology was demonstrated by the preparation of Boc-protected amino acids without erosion of the obtained enantioselectivities.



Scheme 2-14. Asymmetric protonation of ketene disilylacetals.

As shown so far, asymmetric protonation reactions could easily provide α -stereogenic centers of carbonyl compounds using a chiral proton source (catalytic or stoichiometric). Also, as Duhamel suggested,⁴⁹ the process could be seen as a stepwise deracemization, since the starting material is racemic and the reaction proceeds through an achiral reaction intermediate.⁵⁰

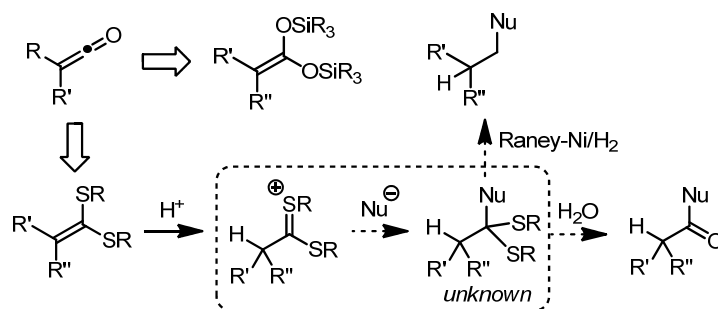


Scheme 2-15. Deracemization of carbonyl compounds *via* asymmetric protonation.

2.4. Ketene Dithioacetals and Thioacetals

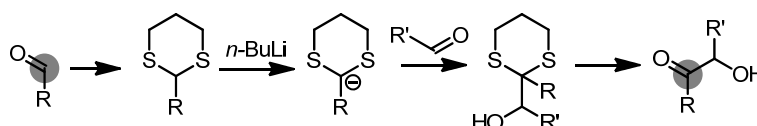
As mentioned in the previous chapter (Scheme 2-11), ketene could undergo asymmetric protonation easily in the presence of a chiral base as a catalyst although the reaction mechanism is not clear.⁴³ Since this substrate can be quite reactive due to its high electrophilicity, the ketene disilylacetal has been utilized as shown in Scheme 2-14. The sulfur version of ketene disilylacetals (ketene dithioacetals) has been utilized as an equivalent of ketene for organic synthesis as a protecting group. Additionally, ketene dithioacetals easily undergo protonation reactions in the presence of Brønsted acids (Scheme 2-16).⁵¹ Moreover, the dithioacetal products could be potentially useful for further derivatization by hydrolysis or reductive cleavage using Raney-Nickel.⁵² However, an intermolecular reaction with the cationic intermediate and nucleophile to afford chiral dithioacetals has never been reported, although the desired product could be transformed into various synthetically useful intermediates *via* a simple deprotection step.

2. BACKGROUND



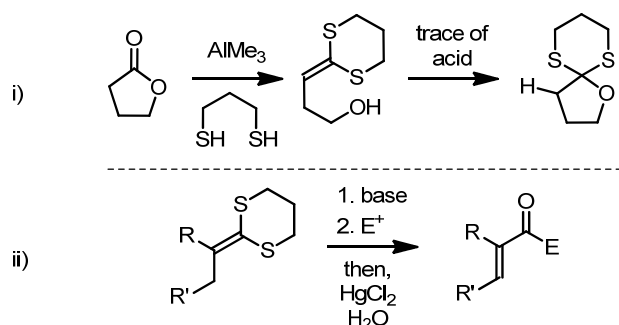
Scheme 2-16. Ketene dithioacetals as chemical equivalent of ketenes.

Due to the facile deprotection of dithioacetals, carbonyl compounds such as aldehydes can be protected to prevent undesired nucleophilic attacks or to generate carbanions which show an *umpolung* reactivity (Scheme 2-17).⁵³ In the latter case, after completion of the reaction, dithioacetals can simply be deprotected *via* oxidative hydrolysis to afford β -hydroxy carbonyl compounds. This reaction sequence has been applied to various natural product syntheses.⁵⁴



Scheme 2-17. Umpolung reactivity of thioacetals.

Another application of dithioacetals was reported in 1973 by E. J. Corey.⁵⁵ The formation of ketene dithioacetal starting from lactone **A** was achieved using AlMe₃ and 1,3-dithiol (Scheme 2-18 (i)). Surprisingly, the obtained ketene dithioacetal spontaneously undergoes cyclization in the presence of trace amounts of Brønsted acid. Further development of this reaction was realized with acyclic substrates for the reaction with electrophiles in the presence of a base (Scheme 2-18, (ii)).⁵⁶

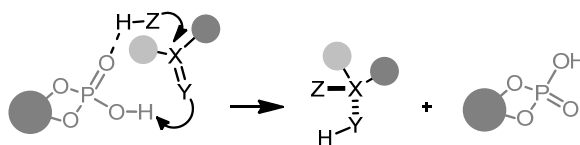


Scheme 2-18. i) Spontaneous cyclization of a ketene dithioacetal in the presence of trace amounts of acid, ii) Application of ketene dithioacetal's *umpolung* reactivity.

The observed facile cyclization of the ketene dithioacetal in the presence of an acid catalyst could be useful. Since numerous new chiral Brønsted acids have been developed in the last decades for various purposes, the reactivity of ketene dithioacetals with novel chiral Brønsted acids would in principle be able to afford various enantioenriched products.

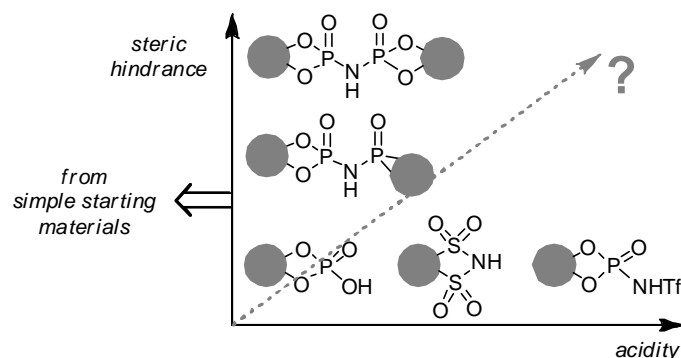
2.5. BINOL-Based Brønsted Acid Catalysis

The development of new chiral Brønsted acids could be beneficial to solve various synthetic problems in asymmetric catalysis, considering the possible interaction of these bifunctional catalysts with most organic functional groups, similar to Lewis acid catalysts.⁵⁷ Although a chiral thiourea catalyst was reported in 1998 by Jacobsen,⁵⁸ further development of metal-free hydrogen bonding-mediated asymmetric catalysis was overlooked for the next decades. In 2003, Rawal reported a TADDOL catalyst⁵⁹ for hetero Diels-Alder reactions to afford heterocyclic compounds with excellent enantioselectivity. These results suggested that fine tuning of hydrogen bonding donor ability could be beneficial to induce an unprecedented reaction profile with high stereoselectivity. In 2004, for example, a BINOL-derived phosphoric acid for imine activation was reported by Akiyama⁶⁰ and Terada⁶¹ independently. After these pioneering examples in asymmetric organocatalysis, research efforts were focused on the preparation of various BINOL-based phosphoric acids and their derivatives, and their application in asymmetric catalysis.⁶² Due to the bifunctionality of the phosphate functional group, it is believed that the phosphoric acid can activate carbonyl, imine and olefin substrates *via* interaction with hydrogen-bonding donors and acceptors simultaneously in a chiral pocket (Scheme 2-19).



Scheme 2-19. Working hypothesis of the phosphoric acid catalysis.

Although BINOL-based phosphoric acids had already showed high activity and enantioselectivity, various research groups developed further derivatives of BINOL-phosphate to overcome limitations, expand the substrate scope and access more challenging reactions. More acidic chiral Brønsted acid catalysts were developed by List³³ and Yamamoto⁶³ containing a disulfonimide and triflimide functionality, respectively, which might be beneficial as a stable chiral counter anion. Moreover, to induce high enantioselectivity, the List group introduced *N*-phosphinylphosphoramidate⁶⁴ and imidodiphosphoric acid⁶⁵ which show extremely high stereoselectivity for unbiased small substrates in asymmetric transformations. Particularly, in the case of imidodiphosphoric acid, the authors suggested that the C_2 -symmetry of the catalyst is crucial to minimize the possible number of catalyst isomers for the selective stabilization of the transition state or reaction intermediate. Various research programs in our laboratory are aimed at meeting these two basic requirements - steric hindrance for enantioselectivity and stronger acidity for the unprecedented activity of BINOL-based Brønsted acid catalysts (Scheme 2-20). Recently, the List group reported SPINOL as a surrogate for the BINOL-backbone, which showed higher enantioselectivity for the kinetic resolution of homoaldols although the synthesis of the catalyst requires several transformations from commercially available starting materials.⁶⁶ Although further progress on the development of new chiral Brønsted acids can not be limited only to the BINOL-backbone, the privileged axially chiral BINOL backbone is still attractive since it is very accessible in enantiopure form, and easy to derivatize for further applications.

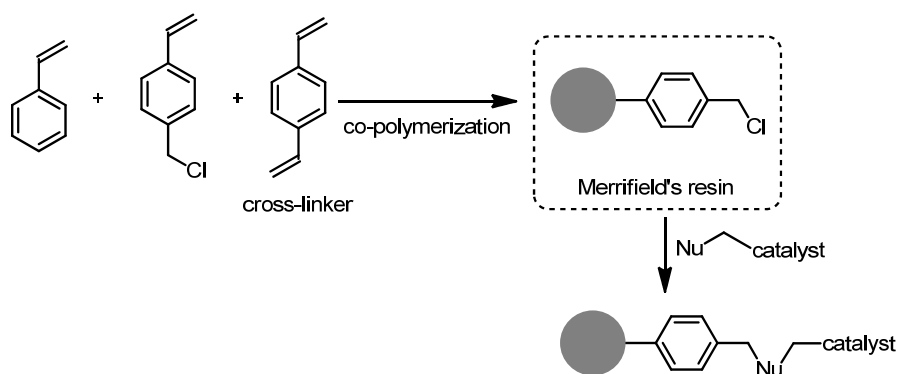


Scheme 2-20. Representative developments of chiral Brønsted acid catalysts with a BINOL-backbone.

2.6. Heterogeneous Asymmetric Organocatalysis

The considerable development of organocatalysis has inspired a variety of fields of chemical sciences during the last decades, not only as a surrogate of metal and biocatalysis but also as a general tool for the asymmetric synthesis of complex molecules. Increasing attention to environmentally friendly and green chemistry also caused exponential growth of the field of organocatalysis, which shows metal-free reaction conditions. Due to their nature as small organic molecules, organocatalysts are generally easier to handle compared to transition metal catalysts. On the other hand, separation of the final (organic) product from the "organic" catalyst becomes more arduous. Various transition-metal catalysts have been used in heterogeneous form to increase the economical and practical utility; practical heterogeneous organocatalysts however have yet to be developed. Moreover, recent developments of pharmaceutical, agrochemical and fine-chemical industry highlight the importance of complex organic molecules as active ingredients. To construct organic molecules selectively and efficiently, it is highly required to promote an organic transformation within an efficient (chiral) catalytic system.

To increase the utility of organocatalysts, it would be desirable to prepare recyclable catalysts. For a bulk chemical process, easy purification and recovery of catalyst are of great concern due mainly to economic and related environmental aspects. The simplest way to connect organic molecules to solid materials is perhaps by using reactive functionalized polymeric materials, such as Merrifield's resin (Scheme 2-21).¹⁷



Scheme 2-21. General approach for polymer-supported organocatalysts.

This pioneering simple functional-polymer synthesis revolutionized various fields of science, particularly solid-state synthesis of polypeptides. Also, Merrifield's resin has been applied in the synthesis of immobilized chiral ligands for asymmetric transition metal catalysis.⁶⁷ Applications of resin-bound reagents and scavengers in the preparation of chemical libraries were documented by Steven Ley.⁶⁸ Using the same strategy, the reaction of modified organocatalysts with a proper nucleophile and Merrifield's resin can easily afford immobilized organocatalysts. However, the formation of Nu-C bonds is usually not quantitative. The unreacted polymer backbone could influence the reaction outcome, especially in asymmetric catalysis, by disturbing the chiral environment or by generating the racemic product through a background reaction (Figure 2-2).^{69,70}

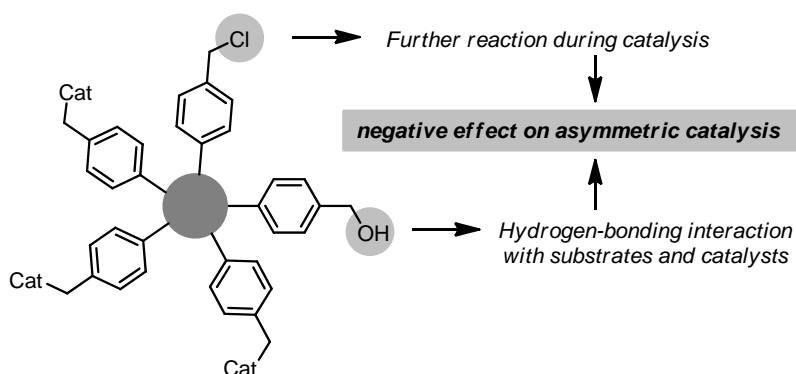


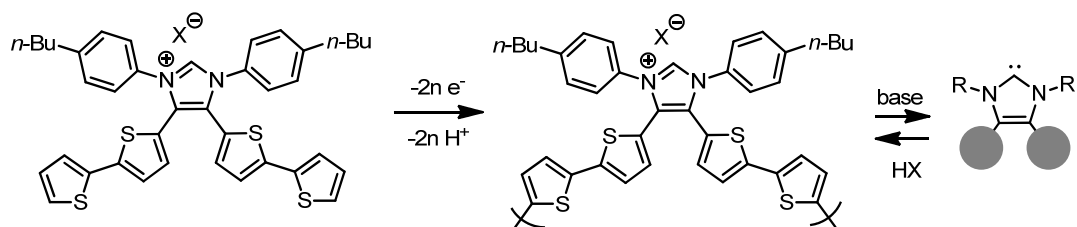
Figure 2-2. Graphical representation of unreacted polymer material's surface.

To overcome this intrinsic problem of the resin-based method, various methodologies have been developed. Since the first report on the synthesis of a dendritic molecule,⁷¹ dendrimers drew significant attention due to their unique molecular structure and modular synthesis. Various catalysts, ligands and reagents were developed using this methodology to provide highly functionalized dendrimers.⁷² However, their synthesis often requires multi-step sequences and the catalytic site can be disturbed due to the proximal interactions of catalysts and backbone structure.

In the same context, the so-called "bottom-up" strategy has been developed by using "polymerizable" catalysts. For example, thiophene could be utilized as a "polymerizable" unit *via* a self-oxidative coupling reaction to afford a polythiophene structure thereby providing a heterogeneous property which has been frequently applied in material chemistry for the preparation of conducting polymers.⁷³ This strategy was amenable for the

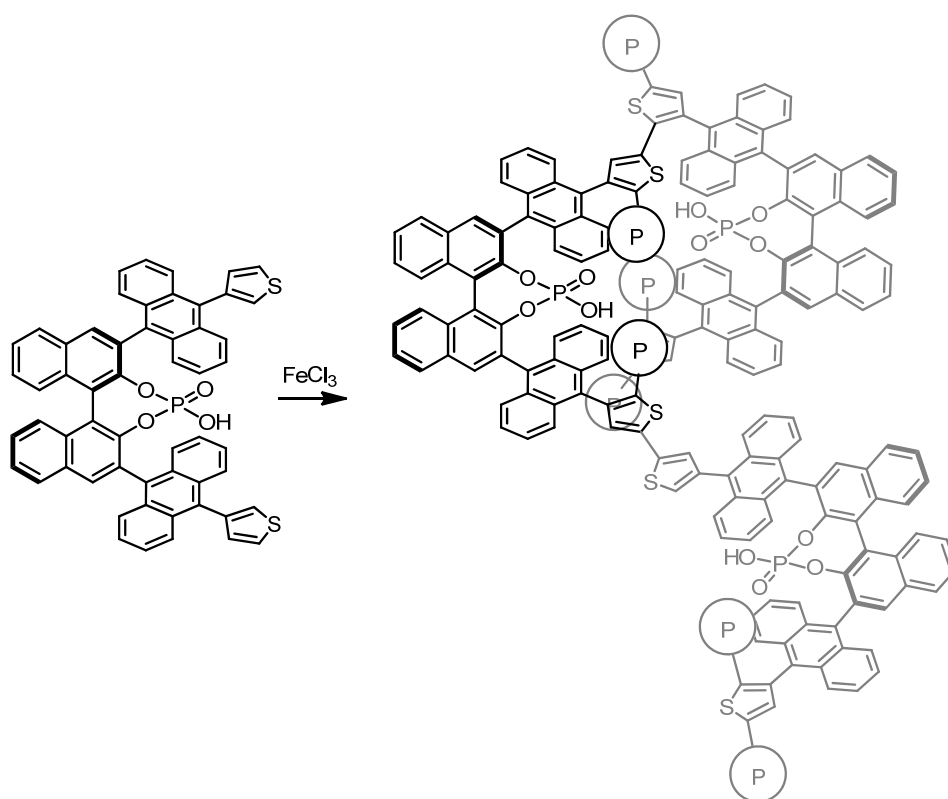
2. BACKGROUND

polymerization of metal-carbene complexes and imidazolium salts (Scheme 2-22).⁷⁴ The obtained imidazolium salt was applied to the benzoin condensation and recycled by treating with HCl to regenerate the imidazolium salt, which could be used for three iterative cycles.



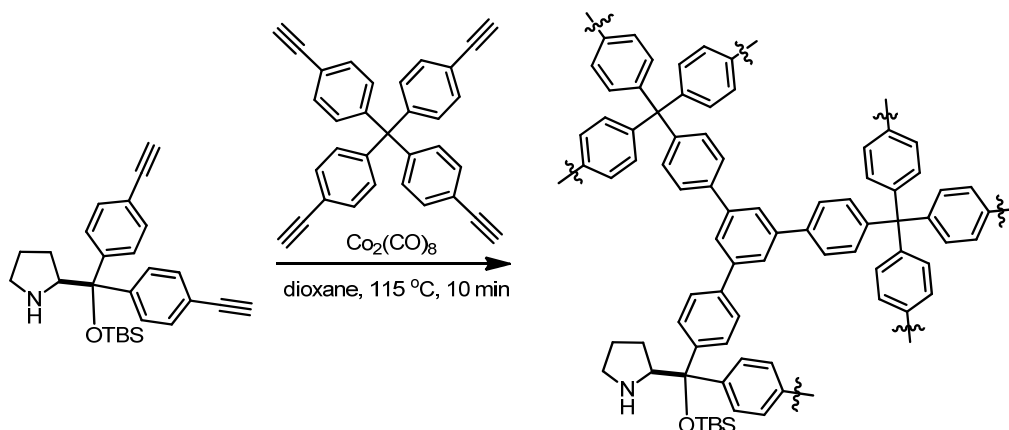
Scheme 2-22. Electrochemical polymerization of a thiophene functionalized imidazolium salt.

This methodology was also utilized to prepare a chiral Brønsted acid catalyst with 3,3'-thiophene and 9-thiophene-anthracene substituted BINOL-phosphate catalysts (Scheme 2-23).⁷⁵ However, the alteration of the catalytically active site might result in inferior activity and enantioselectivity. Also, the stability of the phosphoric acid under oxidative reaction conditions is not clear. Nonetheless, the application of thiophene polymerization in the preparation of chiral heterogeneous catalysts is quite straightforward. If one can control the conformation or polymerization degree in the catalytically active center, high enantioselectivities for asymmetric transformations could be expected.⁷⁶



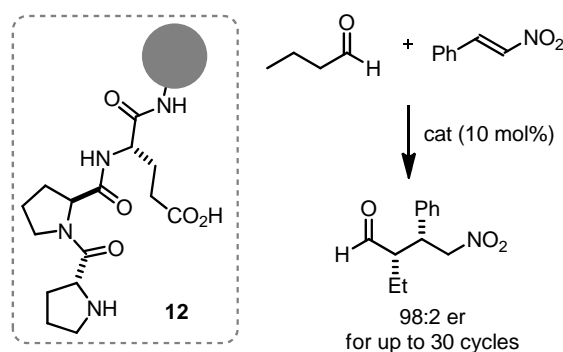
Scheme 2-23. Oxidative coupling of a thiophene-functionalized BINOL-phosphoric acid.

Another example of the “bottom-up” strategy was reported by Wang *et al.* by employing the Jorgensen-Hayashi catalyst (Scheme 2-24).⁷⁷ The authors employed the well-established methodology for the synthesis of porous materials.⁷⁸ The process could construct an intrinsically porous material with the embedded desired functionality inside. Remarkably, the preparation of the heterogeneous catalyst was extremely facile and complete within 10 minutes. Nevertheless, the obtained catalyst showed low recyclability (up to three consecutive runs).



Scheme 2-24. Preparation of heterogeneous Jorgensen-Hayashi catalyst in a porous material.

Perhaps the most stable polymeric organocatalyst is the poly-peptide based catalyst developed by Wennemers.⁷⁹ The optimum catalytic activity was obtained by using Tenta-Gel as a solid support, which bears a PEG (polyethyleneglycol) spacer. The catalytic activity and enantioselectivity of catalyst **12** remained high for 30 cycles by using 10 mol% of catalyst **12**.



Scheme 2-25. Tenta-gel supported polypeptide catalyst for Michael addition reaction.

As summarized in this chapter, there is no general method to prepare a heterogeneous organocatalyst from simple starting materials without resorting to sophisticated modification steps. The use of a pre-modified styrene-based resin could provide a facile immobilization of organic molecules. However, this methodology usually provides low catalyst loading and only modest activity and enantioselectivity compared to the corresponding homogeneous catalysts, due to the alteration of the microenvironment. Ionic liquids and fluorosolvents could be used for immobilization of highly polarized or fluorine-tagged catalysts, respectively.

2. BACKGROUND

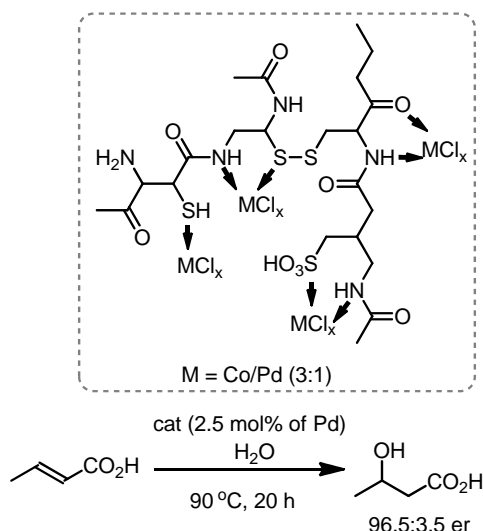
However, these methodologies show no economic advantage up to date due to the high cost of ionic liquids and fluorine-tagged molecules. Polyethyleneglycols are often used as bio-available and biodegradable polymer supports, since they are soluble in organic solvents resulting in high concentration of active catalyst. The recovery of the catalyst could be achieved by adding a non-polar solvent to extract the catalyst.⁸⁰ However, their highly polar backbone with polyether linkage could influence catalysis which requires non-polar environment.

In conclusion, it would be highly desirable to provide heterogeneous catalysts *via* “click-chemistry”, without generating any by-product, in one-step from highly accessible, inexpensive and abundant starting materials. Ideally, heterogeneous catalysts should retain their catalytically active centers as in homogeneous catalysis to give the same reaction outcome.

2.7. Textile materials

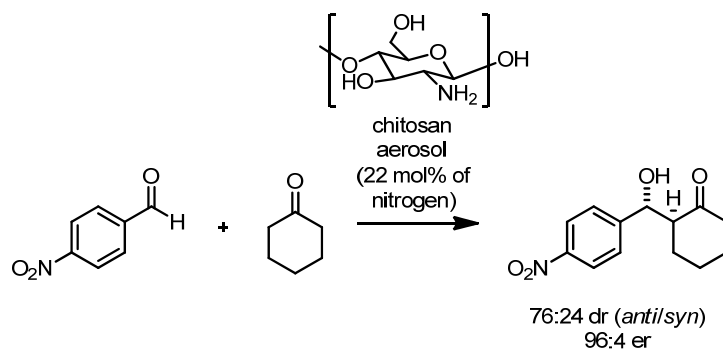
Textile materials have been utilized by human beings since pre-historical times. They can easily be obtained from plants, insects and animals and modified to protect human skin. Since the industrial revolution period, development of synthetic textiles made a great breakthrough by providing inexpensive and durable materials *via* simple condensation/polymerization of diacids and diamines.⁸¹ Although textile materials are abundant in human society, the application of textile materials in the scientific area is quite rare. To the best of our knowledge, most applications of textile materials are limited to the field of material chemistry, as a solid support of nanomaterials.⁸² The immobilization of nanomaterials was conducted *via* physical absorption of nanomaterials, such as carbon nanotubes and graphene, onto textile materials to increase the flexibility of electronic devices.

Only one example of asymmetric catalysis using textile materials has been reported, using wool as a chiral ligand for a transition metal catalyst.⁸³ Excellent enantioselectivity and recyclability (up to 6 cycles) were achieved under the optimized reaction conditions. Although the result shows tremendous potential applicability to various reactions, no further investigation was conducted using the same concept of asymmetric catalysis.



Scheme 2-26. Wool-Pd/Co catalyzed asymmetric hydration of unsaturated carboxylic acids.

The absence of applications of textile materials in organic synthesis might be due to the lack of reactivity of these materials, in contrast to Merrifield's resin. Cotton could be used for the immobilization of catalysts and reagents since it possesses numerous hydroxyl groups in the chiral environment, which might be possible to apply in asymmetric catalysis. However, its abundant hydroxyl groups could prevent a selective immobilization of catalysts and reagents. For example, chitosan was reported as a primary amine catalyst for the aldol reaction.^{84, 85} To increase the availability of the chitosan catalyst, the authors prepared an aerosol-chitosan catalyst, which shows good activity and enantioselectivity for the aldol reaction.



Scheme 2-27. Chitosan catalyzed aldol reaction.

Other types of available biopolymers, such as gelatine and casein (Figure 2-3) were evaluated as chiral ligands for transition metal catalyzed reactions.⁸⁶ However, due to the complexity of the binding mode of chiral ligands to metals, it would be hard to understand the exact mode of reaction and to develop more general methods for desired transformations. Nonetheless, the application of biopolymers shows great potential not only in transition metal catalysis, but also in asymmetric organocatalysis in the near future.

2. BACKGROUND

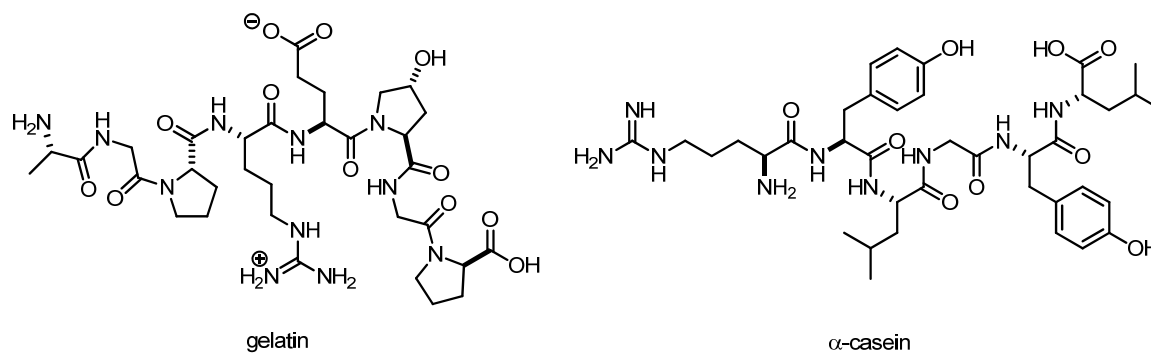
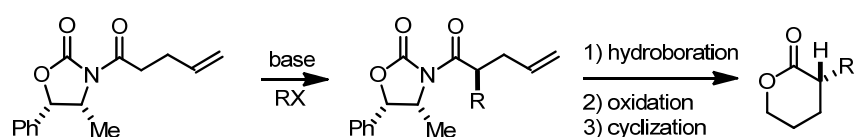


Figure 2-3. Representative structures of gelatin and α -casein.

Surprisingly, there is no precedent of using synthetic textile materials as solid support for organic molecules. Several attempts were made by the Schollmeyer group and others *via* grafting synthetic textiles with organic molecules under UV irradiation.⁸⁷ This methodology was extended to the immobilization of proteins as a biocatalyst.⁸⁸ Although the catalytic activity and recyclability of the immobilized bio-catalyst was not extensively investigated, this reaction could perhaps provide a direct immobilization methodology of organic molecules on solid supports.

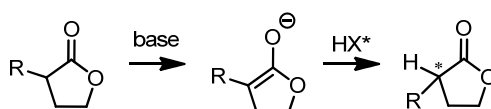
3. OBJECTIVES OF THIS Ph.D. WORK

Although catalytic asymmetric syntheses have shown great applicability to the synthesis of enantioenriched molecules, no reaction has been developed to access chiral lactones with α -stereogenic centers using organocatalysts. The state-of-the-art synthesis of chiral lactones relies on the use of Evans' auxiliary *via* stereoselective alkylation and subsequent hydroboration, oxidation and cyclization (Scheme 3-1).⁸⁹ Although this methodology provides enantiopure lactones with a reliable substrate scope, catalytic synthesis of chiral lactones would be more beneficial from an atom economical point of view.⁹⁰



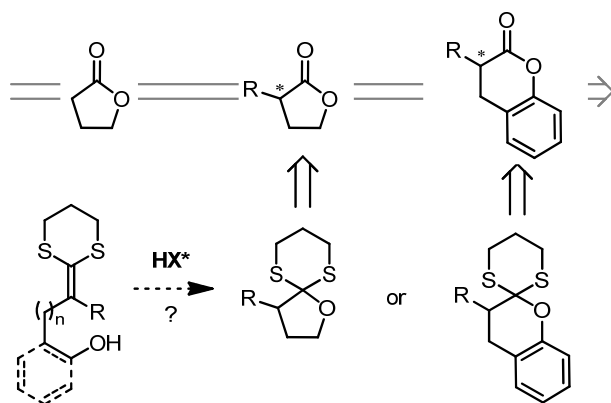
Scheme 3-1. State-of-the-art synthesis of enantioenriched lactones.

The first objective of this Ph.D. work focused on the asymmetric protonation of lactone enolates (Scheme 3-2). Due to the low stability of lactone enolates, it would be desirable to find an alternative reaction pathway to establish α -stereogenic centers. Moreover, the requirement of a stoichiometric amount of a proton source could be synthetically not feasible due to the severe background protonation reaction which results in racemic product.



Scheme 3-2. Asymmetric protonation of enolate anions with chiral Brønsted acid.

As mentioned in Chapter 2.4, ketene dithioacetal was susceptible to undergo spontaneous cyclization under acidic conditions (Scheme 2-18). We therefore became interested in exploring the possibility to obtain chiral dithioacetal-protected lactones in the presence of chiral Brønsted acid catalysts *via* asymmetric protonation of ketene dithioacetals (Scheme 3-3).



Scheme 3-3. Asymmetric protonation of ketene dithioacetals to afford chiral lactones and hydrocoumarins.

Moreover, α -aryl hydrocoumarin⁹¹ and chroman derivatives (isoflavonoids)⁹² are naturally abundant biologically active molecules as shown in Figure 3-1. Despite their tremendously attractive biological properties, asymmetric synthesis of this class of molecules is quite rare. Namely, an enantioselective preparation of α -aryl hydrocoumarins is completely unknown.

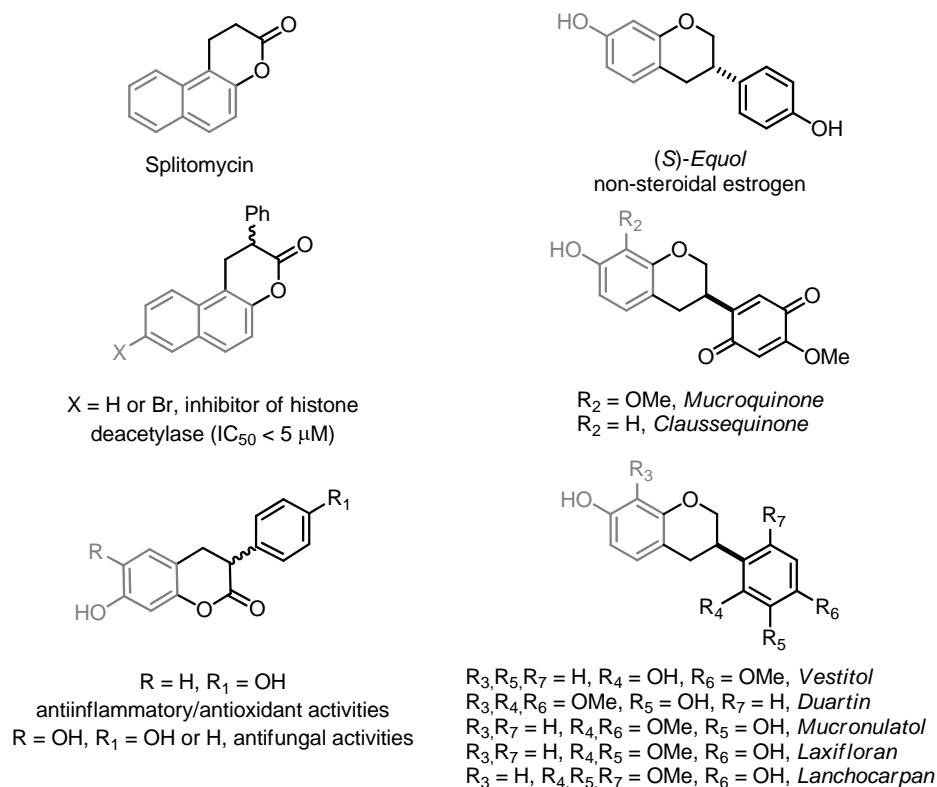
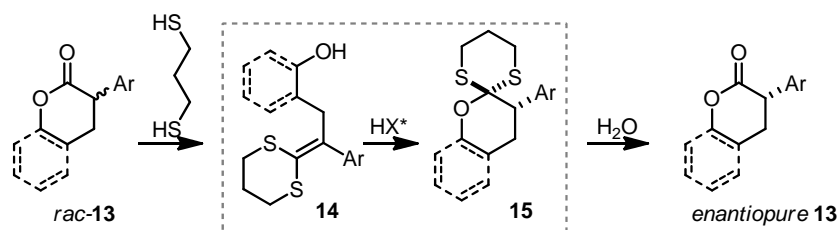


Figure 3-1. Selected examples of chiral α -aryl hydrocoumarins and chromans.

Therefore, we decided to investigate the deracemization process starting from α -substituted cyclic esters **13**, such as lactones and hydrocoumarin *via* a catalytic asymmetric protonation reaction to afford the cyclized products **15**. To accomplish this goal, the development of new chiral Brønsted acid catalysts would be necessary. Moreover, the modification of the obtained enantioenriched dithioacetal products would require

further investigation to retain the enantiopurity. This novel methodology to access enantiopure lactones and hydrocoumarins **13** could then, in principle, be extended to the asymmetric total synthesis of natural products.



Scheme 3-4. Deracemization of cyclic esters *via* catalytic asymmetric protonative cyclization.

Another objective of this Ph.D. work focused on heterogeneous catalysis. Observing the lack of a general method for the preparation of heterogeneous chiral organocatalysts, we became interested in using new materials, particularly textiles as solid supports. By collaboration with *Dr. Thomas Mayer-Gall* and *Dr. Klaus Opwis* from the Textile Institute in Krefeld, we wanted to investigate the potential of textile materials as a new platform for heterogeneous catalysis (Figure 3-2).

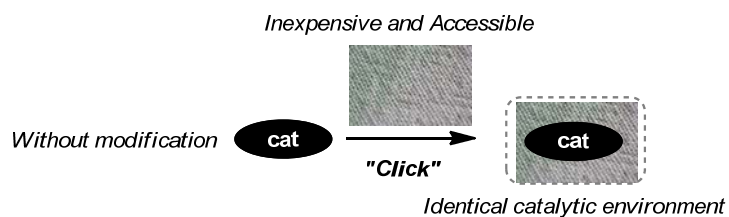


Figure 3-2. A facile immobilization of organocatalysts on solid supports.

When establishing a new approach to access heterogeneous systems from robust materials, textiles show numerous obstacles. First of all, due to their low reactivity, they require a strong activation energy to modify the surface with organic molecules, such as UV-light. The need for photochemical reaction conditions could have a detrimental effect on organic molecules. Secondly, for efficient asymmetric catalysis to take place, the active site of the catalyst should be in an identical environment as it would be in the corresponding homogeneous catalysts. To achieve this goal, studies of the immobilization mechanism would be highly desirable, although light-induced free-radical generation reaction conditions could give a complex reaction outcome. Third, to provide a general methodology for the preparation of heterogeneous catalysts, various organocatalysts should be possible to immobilize independently of their functionality. This can prove challenging since a number of organic functional groups are light-sensitive and can undergo photochemically-induced decomposition pathways (Figure 3-3). It might be helpful to employ a crosslinker to prevent an irradiation-induced damage on organic molecules and to increase the catalyst loading by forming cross-linked polymers.⁹³ The goal of this Ph.D. work was to contribute in the research field of heterogeneous catalysis by providing a general tool for the immobilization of organocatalysts to afford “*textile organocatalysts*” under photochemical reaction conditions.

3. OBJECTIVES OF THIS Ph.D. WORK

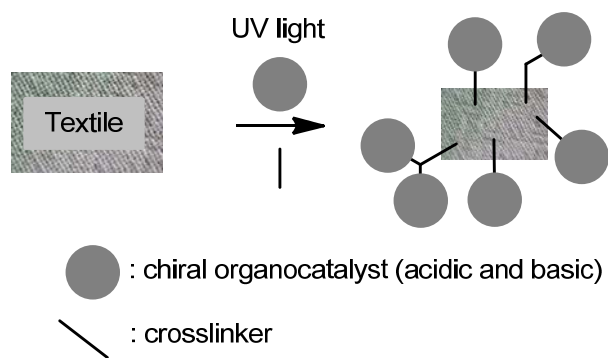
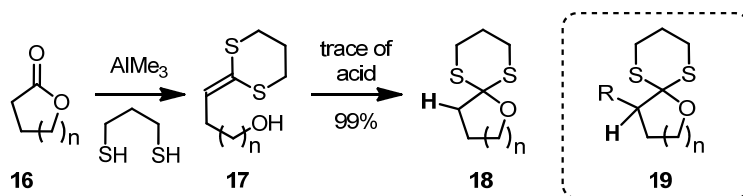


Figure 3-3. The ideal immobilization of organocatalysts on textile materials.

4. RESULTS AND DISCUSSION

4.1. Preparation of α -Substituted Lactones and Hydrocoumarins and Their Dithioketeneacetals

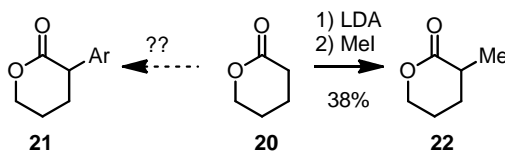
During our investigation on chiral anion-directed radical cation catalyzed reactions, it was discovered that ketene dithioacetal **17** could be transformed into cyclic compound **18** during silica column chromatography. The cyclization is indeed catalyzed by a Brønsted acid catalyst to afford the desired product in quantitative yield. As mentioned in Chapter 2.4, this transformation had already been reported by Corey *et al.* in 1973 for the protection of esters and carboxylic acids from undesired nucleophilic attacks (Scheme 4-1).^{55,56} We presumed that if one can prepare dithioketene acetals from α -substituted lactones, we could obtain enantioenriched orthodithioesters **19** by using chiral Brønsted acid catalysts. Therefore, we commenced our study by preparing various α -substituted lactones and related hydrocoumarin substrates.



Scheme 4-1. The cyclization of ketene dithioacetal by Corey *et al.*

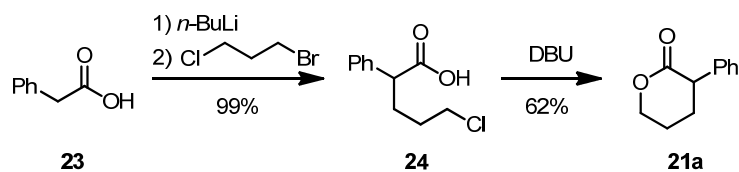
4.1.1. Preparation of α -Substituted Lactones

In the literature, there is no general procedure documented for the preparation of α -aryl lactones with high yields. Methylation of δ -valerolactone (**20**) was conducted by using freshly prepared LDA and methyl iodide albeit in low yield (Scheme 4-2). However, in general, it is quite challenging to access to α -aryl δ -valerolactone (**21**) using conventional strategies starting from unsubstituted δ -valerolactone.



Scheme 4-2. Preparation of α -substituted δ -valerolactones.

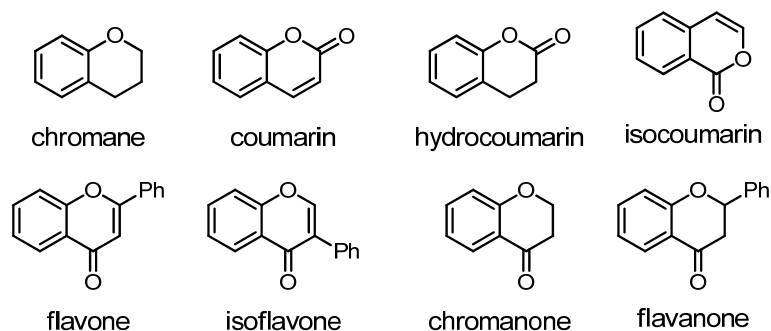
In the case of the five-membered ring system, it has been reported that α -bromo γ -butyrolactone can undergo a Ni-catalyzed arylation reaction using arylboronic acids.⁹⁴ However, the desired product was obtained with only low yield (12 % yield). Therefore, a different strategy was employed starting from phenylacetic acid. After alkylation with dihalide and subsequent cyclization, α -phenyl δ -valerolactone **21a** could be obtained in moderate yield (Scheme 4-3).⁹⁵



Scheme 4-3. Preparation of α -phenyl δ -valerolactone (21a).

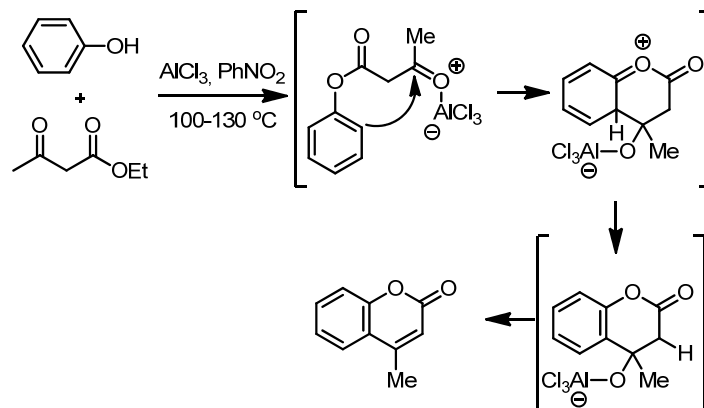
4.1.2. Preparation of α -Aryl Hydrocoumarins

Coumarins are common naturally occurring products as a second metabolite from plants. For example, coumarin is responsible for the scent of new-mown hay and has been utilized in the perfume industry as an ingredient. Flavones, isoflavonoids and neoflavonoids which are based on the benzopyran core, often exist in enantiomerically pure form in nature (Scheme 4-4). Moreover, due to their vast biological activity in interacting with various receptors, these classes of molecules have been attractive targets for the organic synthesis community.⁹⁶



Scheme 4-4. General structures of naturally occurring benzopyrone derivatives.

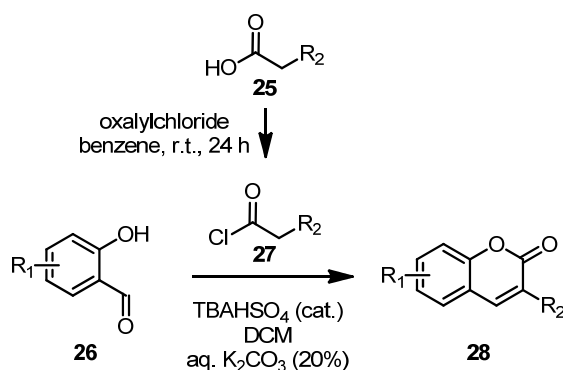
The Pechmann condensation can provide 4-substituted coumarins from phenol and β -carbonylestere in the presence of a Lewis acid at high temperature (Scheme 4-5).⁹⁷ However, the reaction conditions require long reaction time and high temperature, which can limit the utility of the methodology. Also, the Friedel-Crafts reaction step is limited to relatively electron-rich aromatic groups.



Scheme 4-5. The Pechmann condensation.

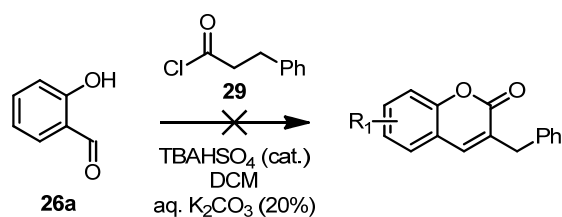
4.1.3. Preparation of α -Aryl Hydrocoumarins

Further efforts to access various α -substituted coumarins were initiated by substrate preparation starting from α -aryl coumarins. The synthesis is reported by using biphasic reaction conditions and a phase-transfer catalyst (PTC).⁹⁸ Gratifyingly, the reaction conditions using catalytic amounts of PTC provided a general methodology to α -aryl coumarins **28**. The desired coumarins **28** were obtained by precipitation in protic solvents (methanol or ethanol, Scheme 4-6).



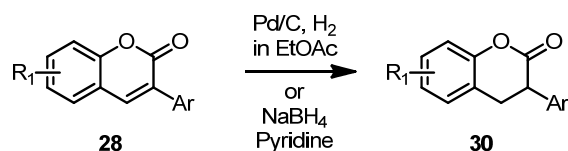
Scheme 4-6. A general procedure to access α -aryl coumarins **28**.

Unfortunately, the reaction is not operative with aliphatic acyl chloride **29** (Scheme 4-7) which could be ascribed to the lower acidity of the α -proton of the carbonyl, crucial for the aldol condensation reaction.



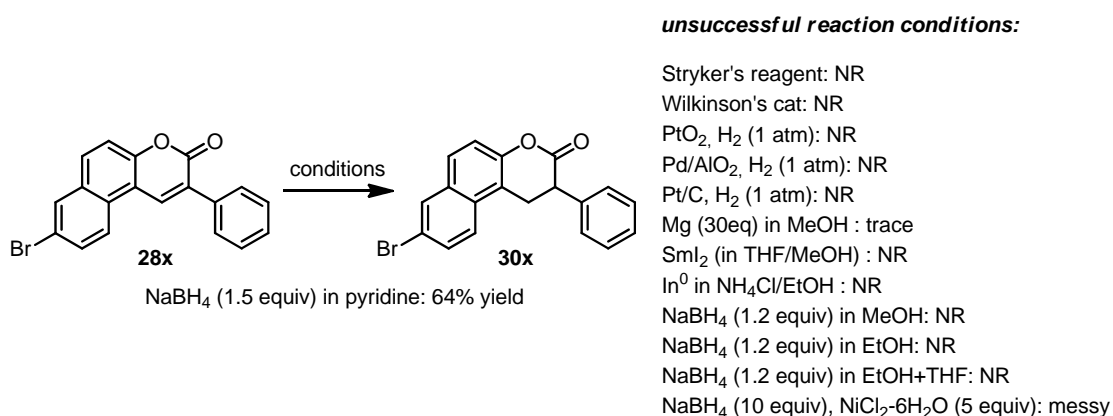
Scheme 4-7. The condensation reaction with hydrocinnamylchloride (**29**).

The reduction of coumarins **28** was conducted using Pd/C under hydrogen atmosphere. Sterically bulky substrates were reduced using high hydrogen pressure (up to 30 bar, Scheme 4-8). Halogen-substituted coumarins were problematic for the palladium-catalyzed hydrogenation. Therefore, the halogenated substrate was subjected to NaBH₄ reduction conditions in pyridine as solvent. Pyridine is known to activate NaBH₄ to increase the reactivity of the hydrides.⁹⁹ On the other hand, when the reaction was conducted in methanol, low conversion or a complex reaction mixture was obtained.



Scheme 4-8. Reduction of α -aryl coumarins to α -aryl hydrocoumarins.

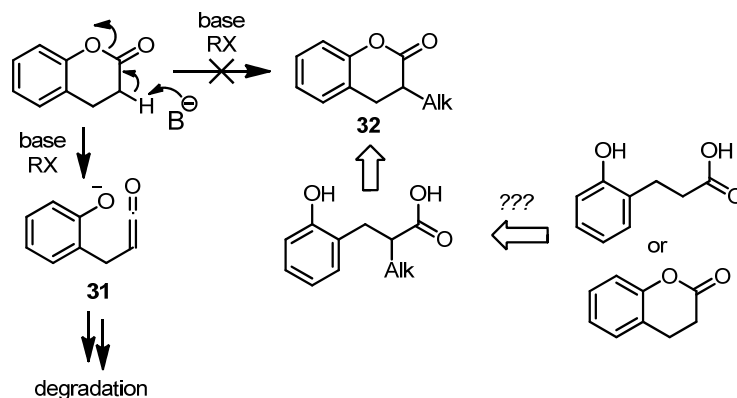
For example, coumarin **28x** did not undergo reduction using molecular hydrogen and a transition metal catalyst due to the sterical bulkyness and reactivity of the bromide (Scheme 4-9). Various reaction conditions using magnesium(0), samarium(II) or indium(0) afforded complete recovery of the starting material or complex reaction mixtures. Fortunately, the reduction of the substrate was accomplished by using NaBH_4 in pyridine to afford the desired product **30x** with synthetically useful yields.



Scheme 4-9. Different reaction conditions for the reduction of coumarin **28x**.

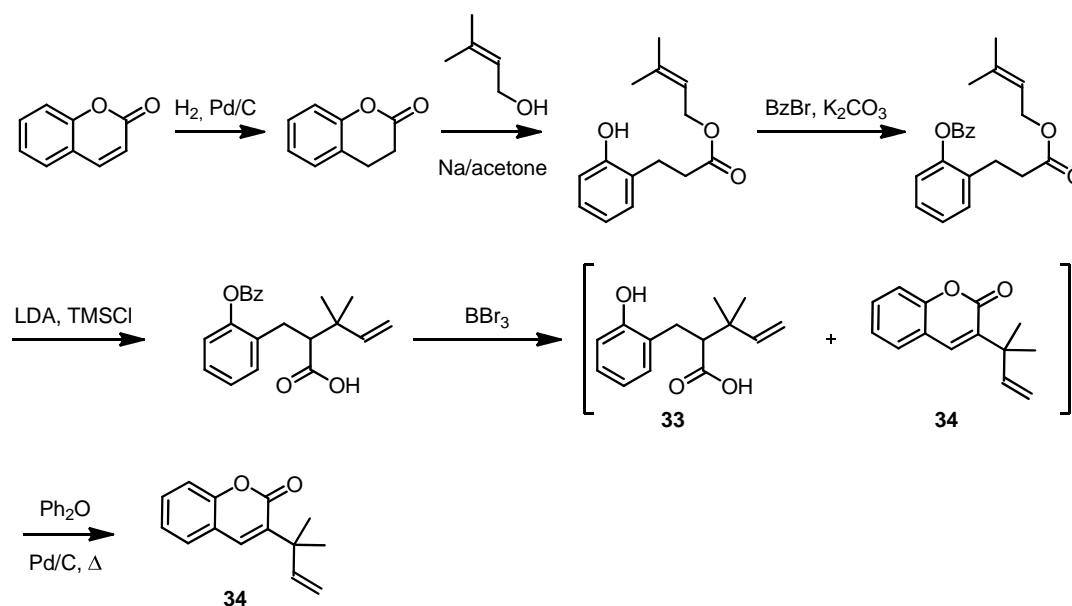
4.1.4. Application of the Claisen Rearrangement for the Preparation of α -Alkyl Hydrocoumarins

To prepare a variety of hydrocoumarin substrates, we became interested in performing the α -alkylation of hydrocoumarins as a general solution for the preparation of α -alkylated hydrocoumarins **32**. Unfortunately, several attempts to alkylate hydrocoumarins were not successful. This fact could be ascribed to the formation of the ketene **31** via E_2 elimination of the phenol group under basic reaction conditions (Scheme 4-10). Moreover, through α -alkylation it is virtually impossible to install a bulky substituent due to the low reactivity of the sterically bulky alkylating reagents.



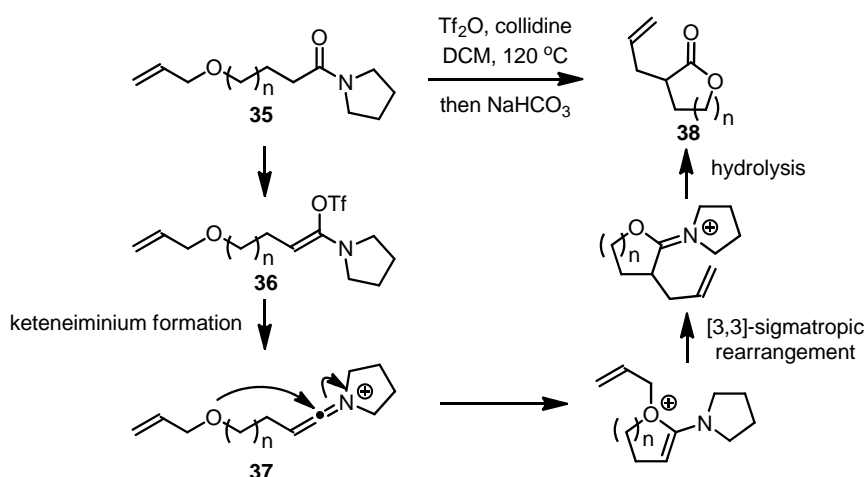
Scheme 4-10. Unsuccessful general approach to the α -alkyl hydrocoumarins.

A synthesis of coumarin derivatives *via* Ireland-Claisen rearrangement has been reported. However, it requires the tedious protection-deprotection of a functional group (phenol) and additional modification steps to afford the α -alkylated hydrocoumarin **34** from a mixture of ring-opened acid **33** and the coumarin derivative (Scheme 4-11).¹⁰⁰



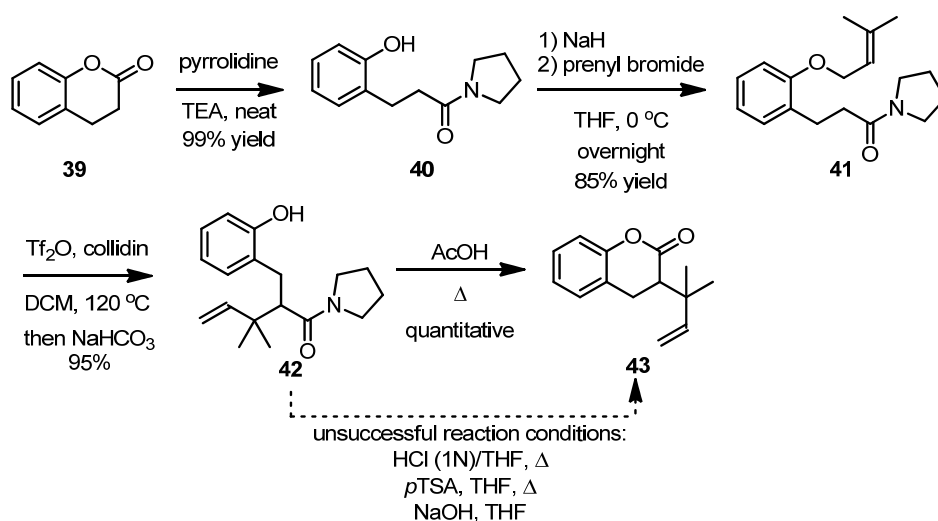
Scheme 4-11. Application of Ireland-Claisen rearrangement in α -isoprenyl hydrocoumarin synthesis.

Recently, the Maulide group reported a novel transformation of ether-tethered amides **35** into a variety of α -substituted lactones *via* [3,3] sigmatropic rearrangement (Scheme 4-12).^{101,102} This methodology operates by forming a keteniminium ion intermediate **37**, which is highly electrophilic in nature. The keteniminium intermediate¹⁰³ is then attacked by the oxygen of the allyl ether functional group. Subsequent rearrangement and hydrolysis generates lactone **38**. Due to the advantages of this methodology, namely i) simple reaction conditions, ii) high accessibility of the starting materials and iii) relatively high yield and a broad substrate scope, the employment of this protocol for the preparation of α -alkyl, particularly α -prenyl, hydrocoumarin derivatives was pursued.



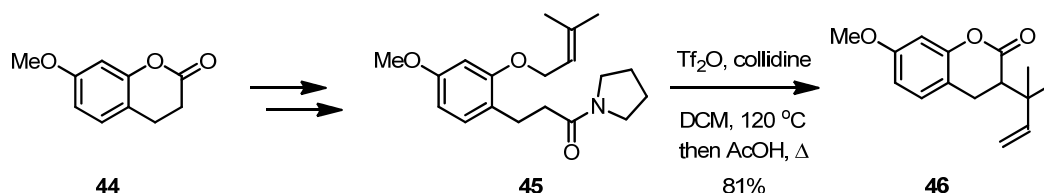
Scheme 4-12. [3,3] Sigmatropic rearrangement of amide to afford α -allyl lactone **38**.

Initially, as already discussed, the starting materials were easily accessible from unsubstituted hydrocoumarin **39**. By treating hydrocoumarin **39** with pyrrolidine as a solvent at room temperature, the desired product **40** was obtained by precipitation from the solution (Scheme 4-13). Alkylation of phenol **40** with prenyl bromide afforded the arylether **41** in good yield. Under the standard rearrangement reaction conditions as described in the literature (microwave irradiation, 120 °C in DCM, 0.2 M, 7 min), the starting material **41** was completely consumed. However, the desired product **43** was not formed and ^1H NMR analysis of the crude reaction mixture along with further screening of work-up conditions revealed that the obtained compound was the ring-opened amide **42** as a mixture with collidine. Numerous attempts to convert the phenol product **42** to the hydrocoumarin derivative **43** failed due to the high leaving group ability of phenol. Fortunately, in acetic acid as a solvent under reflux temperature, the pyrrolidine amide could be hydrolyzed to afford hydrocoumarin **43** with excellent yield. The obtained hydrocoumarin derivative **43** has been synthesized as an unsaturated form (coumarin, **34**) *via* the Ireland-Claisen reaction in 5 steps.



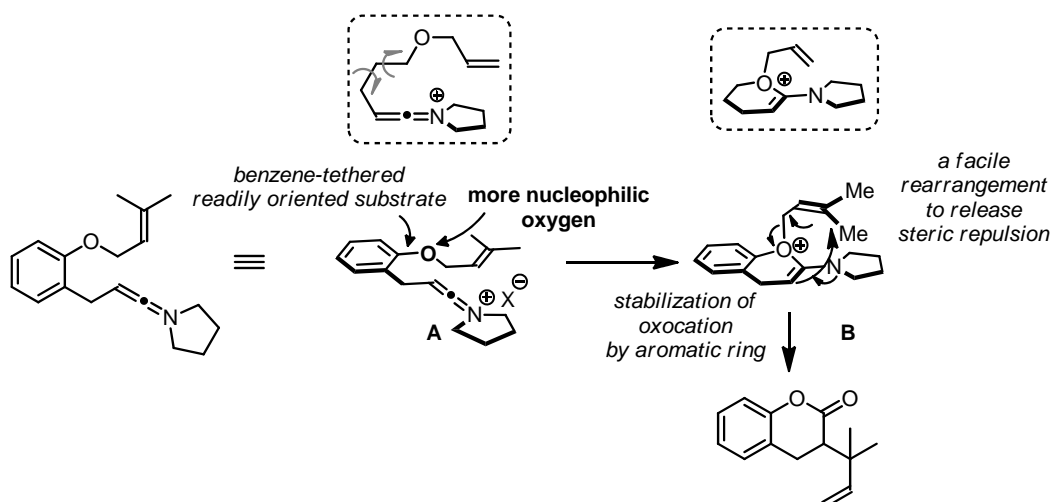
Scheme 4-13. Preparation of the starting material and application to the [3,3]-sigmatropic rearrangement.

A parallel investigation on the application of the [3,3]-sigmatropic rearrangement reaction was pursued (Scheme 4-14). Substrate **44** was used, since it possesses an electron-rich aromatic ring, which could prevent the facile hydrolysis of the iminium intermediate to phenol. Nevertheless, the reaction outcome was identical to the previous reaction (Scheme 4-13). Pleasingly, the desired product **46** was obtained by treating the intermediate with acetic acid at reflux temperature with good isolated yields. The obtained hydrocoumarin **46** was then subjected to the ketenedithioacetal formation reaction (See next chapter).



Scheme 4-14. Application to the [3,3] sigmatropic rearrangement for the substrate **44**.

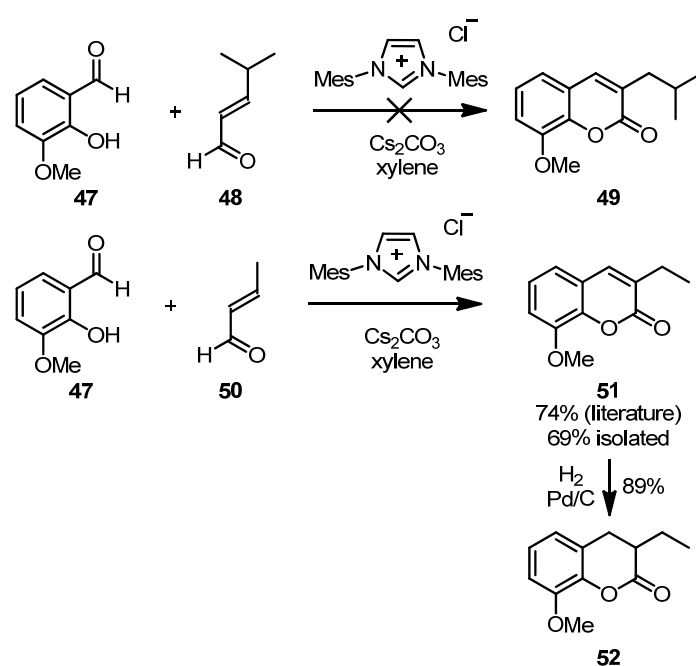
Surprisingly, the obtained yields of the rearrangement reaction are higher than the reported substrates derived from lactones.¹⁰³ Moreover, the [3,3]-sigmatropic rearrangement reaction could be conducted at room temperature, without microwave heating. It is noteworthy that the keteniminium intermediate could be generated and undergo [3,3]-sigmatropic rearrangement reaction smoothly without harsh reaction conditions. These results can be explained by the aromatic backbone, which places the nucleophilic oxygen in closer proximity to keteniminium ion, facilitating the attack (**A**, compare with the structure in the box). Moreover, this substrate further stabilized the oxonium ion by electron-rich aromatic substrates (**B**, compare with the structure in the box). It would be interesting to install a gem-dimethyl substituent on the benzylic position to see the Thorpe-Ingold effect in this reaction (Scheme 4-15).¹⁰⁴



Scheme 4-15. Rationale of the higher reactivity of the benzene-tethered substrate compared to the aliphatic substrate **35**.

4.1.5. Preparation of α -Alkyl Hydrocoumarins via NHC Catalysis

After the successful application of a Claisen-like rearrangement for the preparation of α -isoprenyl hydrocoumarins, we became interested in relatively small substituents, such as *n*-alkyl substituted hydrocoumarins. NHC-catalysis could be used to access this class of molecules as reported by Bräse *et al.* (illustrated in Scheme 4-16).¹⁰⁵ Although sterically hindered aldehyde **48** gave no conversion under the reaction conditions, α -ethyl coumarin **51** could be prepared with good chemical yield. Then coumarin **51** was reduced to afford the corresponding hydrocoumarin **52** with good isolated yield.

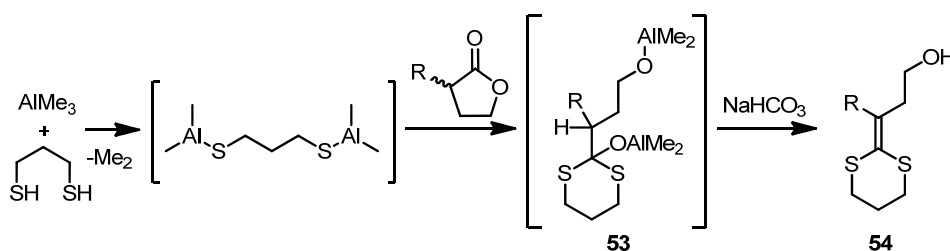


Scheme 4-16. NHC-catalyzed α -alkyl coumarin formation reaction and preparation of hydrocoumarin **52**.

Having various hydrocoumarins in our hands, we moved to preparation of the corresponding ketene dithioacetals, which are potentially highly reactive and useful for catalytic asymmetric transformations.

4.1.6. Preparation of Ketene Dithioacetals

The preparation of ketene dithioacetals using AlMe_3 and dithiol as reagents was reported by Moeller *et al.*¹⁰⁶ All the lactones and hydrocoumarin substrates were smoothly converted to the desired products. It is noteworthy that, after the addition of the lactone substrate the O- AlMe_2 complex **53** was formed, which has to be hydrolyzed under basic conditions to give ketene dithioacetal (Scheme 4-17). In general high yields of the ketene dithioacetal **54** were obtained. In the case of electron rich hydrocoumarins, higher reaction temperature was often required to obtain the desired product.



Scheme 4-17. Reaction mechanism of the ketenedithioacetal formation.

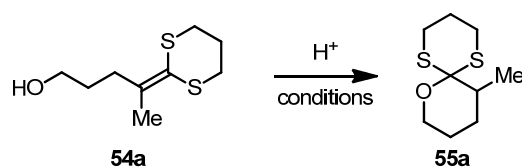
As mentioned previously, the obtained ketene dithioacetals are easily cyclized in the presence of acid catalysts. For example, during column chromatography, ketene dithioacetal **54a** started to undergo cyclization with a conversion above 60% (by ^1H NMR analysis). Also, in dichloromethane or chloroform, ketene dithioacetals usually cyclize spontaneously without any additional acid catalysts due to the trace amount of HCl existent in the solvents. The contamination with this cyclized product, which exists as a racemate, can be problematic for the asymmetric catalysis. The optimal approach to the ketene dithioacetal synthesis is circumventing silica chromatography. To avoid purification, it is crucial to verify the complete conversion of the lactone substrate. After treatment with aq. solution of NaHCO_3 in distilled diethylether, the reaction mixture can usually be purified with a short column with ethylacetate, diethylether, MTBE and hexane as eluents.

4.2. Asymmetric Protonation Reactions of Ketene Dithioacetals

4.2.1. Asymmetric Protonation of Ketene Dithioacetals Derived from Lactones

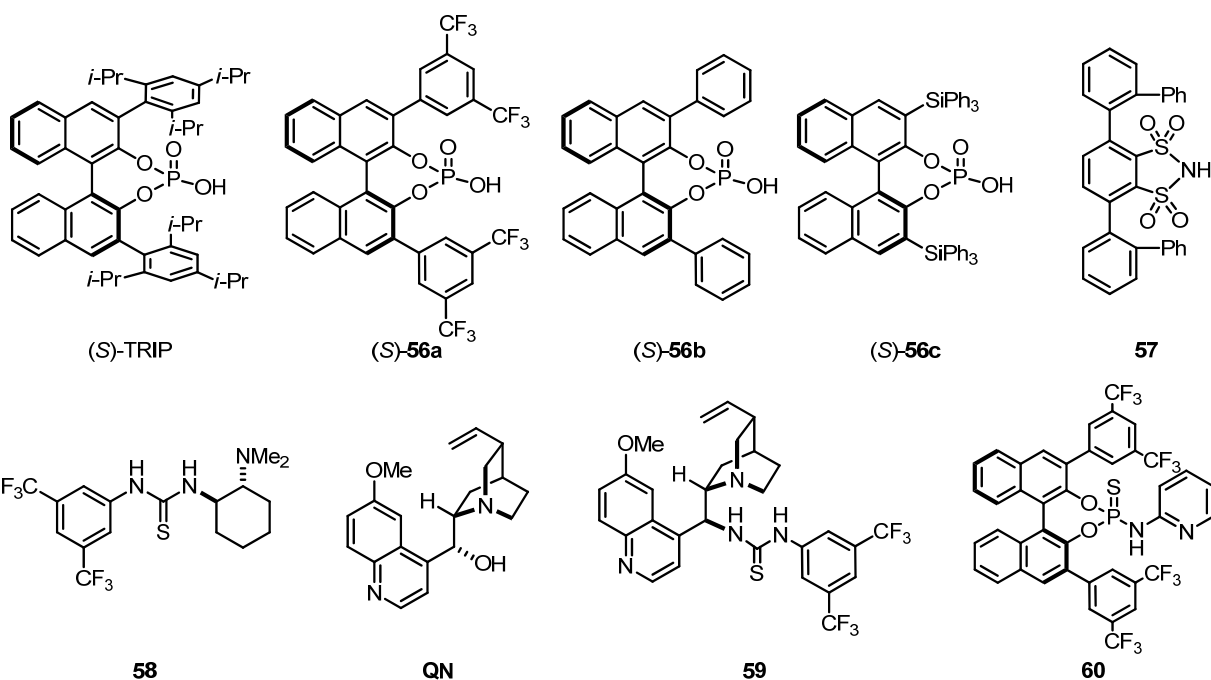
Due to the high reactivity of ketene dithioacetals, any kind of Brønsted acid could catalyze the cyclization reaction under mild reaction conditions, even during silica gel column chromatography. The racemic product was obtained by using diphenylphosphate (DPP) as a catalyst (entry 1 in Table 4-1). Although the cyclization occurred under very mild reaction conditions, initial screening of the reaction conditions proved to be quite disappointing.

Table 4-1. Optimization of the reaction conditions for the asymmetric protonation of substrate **54a**.



Entry	Catalyst (mol%)	Solvent	Conc.	Temp	Time (h)	Yield (%)	er	MS 4Å
1	DPP	DCM	0.1 M	r.t.	1 h	99	50:50	X
2	(<i>S</i>)-TRIP	DCM	0.1 M	r.t.	16 h	99	56:44	X
3	(<i>R</i>)-TRIP	DCM	0.088 M	r.t.	16 h	99	41.5:58.5	X
4	(<i>S</i>)-TRIP	DCM	0.09 M	r.t.	21 h	99	60:40	50 mg
5	(<i>S</i>)-TRIP	benzene	0.09 M	r.t.	21 h	99	59.5:40.5	X
6	(<i>S</i>)-TRIP	DCM	0.04 M	r.t.	20 h	99	58.5:41.5	X
7	(<i>S</i>)-TRIP	CHCl ₃	0.04 M	r.t.	20 h	99	50:50	X
8	(<i>S</i>)-TRIP	pentane	0.04 M	r.t.	5 d	99	46:54	X
9	(<i>S</i>)-TRIP	cHex	0.04 M	r.t.	5 d	<80%	45.5:54.5	X
10	(<i>S</i>)-TRIP	THF	0.04 M	r.t.	44 h	99	50:50	X
11	(<i>S</i>)-TRIP	Et ₂ O	0.04 M	r.t.	-	-	-	X
12	(<i>S</i>)-TRIP	toluene	0.04 M	r.t.	5 d	95	58:42	X
13	(<i>S</i>)-TRIP	benzene	0.04 M	r.t.	5 d	99	61.5:38.5	X
14	(<i>S</i>)-TRIP	MeNO ₂	0.04 M	r.t.	20 h	99	48:52	X
15	(<i>S</i>)-TRIP	EtOH	0.04 M	r.t.	-	-	-	X
16	(<i>S</i>)-TRIP	acetone	0.04 M	r.t.	-	-	-	X
17	(<i>S</i>)-TRIP	DMF	0.04 M	r.t.	5 d	NR	-	X
18	(<i>S</i>)-TRIP	ACN	0.04 M	r.t.	24 h	99	-	X
19	(<i>S</i>)-TRIP	benzene	0.04 M	r.t.	64 h	95	62:38	50mg

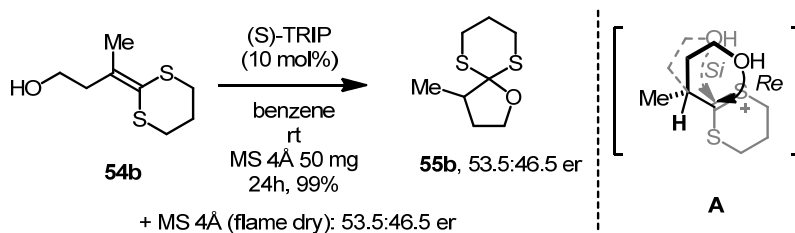
20	(<i>S</i>)-TRIP	benzene	0.08 M	r.t.	64 h	96	60:40	X
21	(<i>S</i>)-TRIP	benzene	0.02 M	r.t.	64 h	64	60.5:39.5	X
22	56a	benzene	0.04 M	r.t.	18 h	95	51:49	X
23	56b	benzene	0.04 M	r.t.	18 h	95	51:49	X
24	56c	benzene	0.04 M	r.t.	43 h	34	49:51	X
25	57	DCM	0.08 M	r.t.-40 °C	3 d	NR	-	X
26	58	DCM	0.08 M	r.t.-40 °C	3 d	NR	-	X
27	QN	DCM	0.08 M	r.t.-40 °C	3 d	NR	-	X
28	59	DCM	0.08 M	r.t.-40 °C	3 d	NR	-	X
29	60	benzene	0.04 M	r.t.	3 d	NR	-	X



As summarized in Table 4-1, the reaction was conducted in a non-polar solvent such as DCM or benzene, to provide a more compact transition state with stronger catalyst-substrate interactions. The reaction was completed in one day, and very low enantioselectivity was obtained with (*S*)-TRIP (entry 2, 56:44 er). The opposite enantiomer was obtained using (*R*)-TRIP as catalyst with a similar level of enantioselectivity (entry 3, 58.5:41.5 er). After solvent screening (entries 5-18), benzene (entry 5) was found to be the optimal solvent and addition of molecular sieves (4Å) proved beneficial in terms of enantioselectivity (entries 4 and 19). Further screening of catalyst included BINOL-based phosphoric acids (**56**, entries 23-24) and bifunctional organocatalysts (**58**, **59** and **QN**, entries 26-29), which showed no improvement in terms of activity and enantioselectivity. The low enantioselectivity obtained could be ascribed to the facile cyclization of the substrate without accessing chiral cavity of the catalyst.

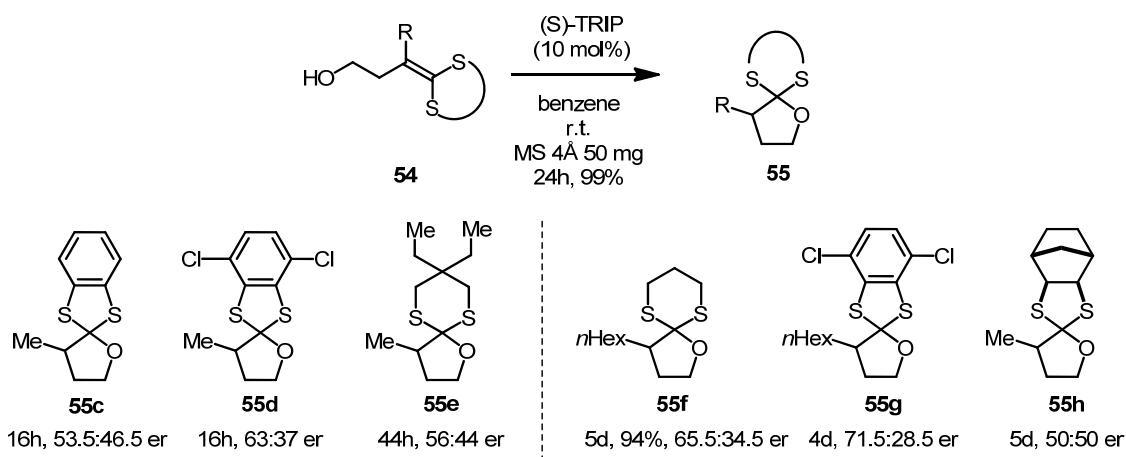
Therefore a substrate with a shorter aliphatic chain such as ketene dithioacetal **54b** was tested for the same reaction. However, the obtained enantioselectivity was inferior (53.5:46.5 er) than with substrate **54a**. This result may imply that the aliphatic backbone is quite challenging to control facial selectivity of the attacking alcohol by phosphoric acid catalyst (**A** in Scheme 4-18).

4. RESULTS AND DISCUSSION



Scheme 4-18. Asymmetric protonation of substrate **54b** derived from γ -butyrolactone.

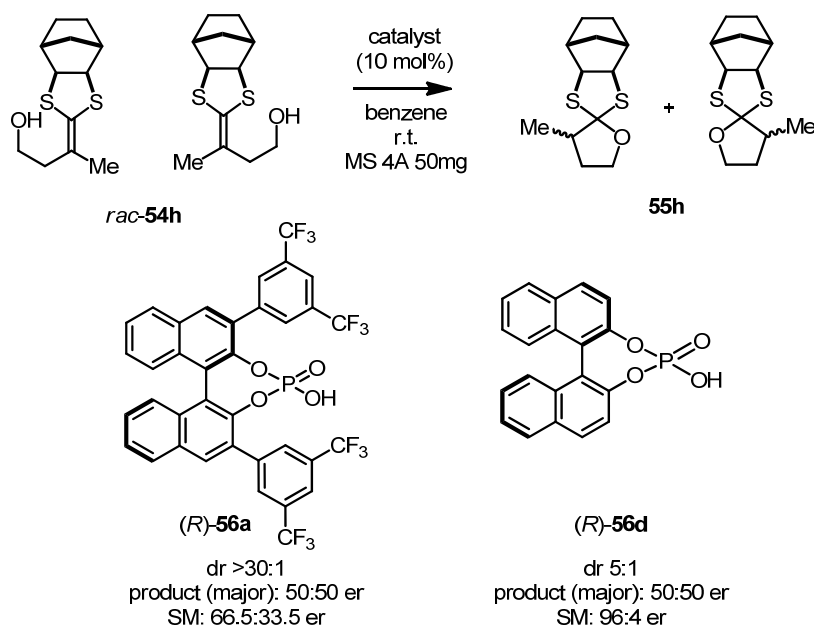
Since substrates **54a** and **54b** are sterically and electronically not feasible to be manipulated except on the dithiol moiety, we decided to modify the dithiol backbone. As described in Scheme 4-19, commercially available 1,2-dithiobenzene (**55c**) and 3,6-dichloro-1,2-dithiobenzene (**55d**) were used for ketene dithioacetal formation reactions and subjected to the asymmetric protonation reaction conditions. In the case of the dithiobenzene (**55c**), it was assumed that the presence of an aromatic group would allow the substrate to interact with the catalyst *via* π - π interaction. Nevertheless, a similar enantioselectivity was observed compared to substrates **54a** and **54b**. Diethylsubstituted 1,3-propane dithiol was prepared using S_8 and dihalide to increase the steric hindrance of the dithiol unit. However, the effect was not remarkable (**55e**, 56:44 er). Fortunately, dichlorobenzene substitution (**55d**) led to a significant increase of enantioselectivity to 63:37 er from 53.5:46:5 er. In the case of α -hexyl substituted lactone derived ketene dithioacetals, generally higher enantioselectivities were obtained compared to α -methyl substituted substrates. Up to 71.5:28.5 er was obtained using 3,6-dichloro-1,2-dithiobenzene (**55g**) as backbone for the ketene dithioacetal. To increase steric hindrance dramatically, we employed a norbornene-derived dithiol as backbone for the ketene dithioacetal, however, only racemic product was obtained (**55h**).



Scheme 4-19. Screening of the dithiol moiety.

Interestingly, although product **55h** was obtained as a racemate, due to the chirality of the starting materials, the kinetic resolution of the ketene dithioacetal occurred with reasonable enantioselectivity. A simple BINOL-phosphate **56d** was identified as a highly enantioselective catalyst for the resolution of ketene dithioacetal **54h** despite the fact that the obtained product was racemic (Scheme 4-20). This reaction profile suggested that the

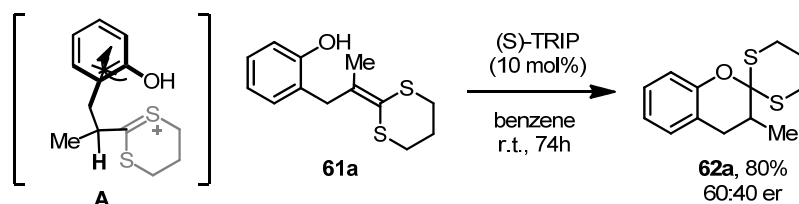
protonation occurred without stereoselectivity to afford the racemic product although one of the racemic starting materials reacts with the catalyst preferentially.



Scheme 4-20. Kinetic resolution of the ketene dithioacetal **54h** with different catalysts.

4.2.2. Asymmetric Protonation of Ketene Dithioacetals Derived from α -Alkyl Hydrocoumarins

We also investigated another substrate class, which generates benzene-fused cyclic compounds, hydrocoumarins. We anticipated that the benzene-fused backbone might reduce entropy to allocate all functional groups for the cyclization reaction (Scheme 4-21, **A**). Although the desired product **62a** was obtained with good yield, the obtained enantioselectivity (60:40 er) was disappointing (Scheme 4-21).



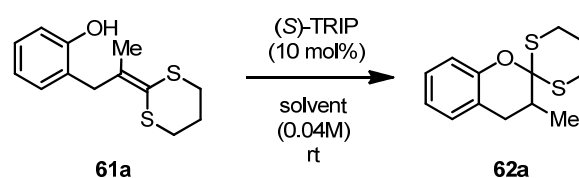
Scheme 4-21. Asymmetric protonation of ketene dithioacetal derived from hydrocoumarin.

Gratifyingly, after a brief screening of the reaction conditions we obtained an encouraging enantioselectivity of 70:30 er in *n*-hexane as a solvent (entry 3 in Table 4-2). High enantioselectivity was obtained in non-polar solvents (entries 3, 9 and 10). In protic and polar solvents, either low conversion or low enantioselectivity was obtained (entries 6-8). Remarkably, the reaction does not require strictly anhydrous reaction conditions (entries 4 and 5), although the protonation step is the enantiodetermining step. Variations on the

4. RESULTS AND DISCUSSION

concentration and reaction temperature did not improve the reaction outcome in terms of reactivity and enantioselectivity (entries 18-20).

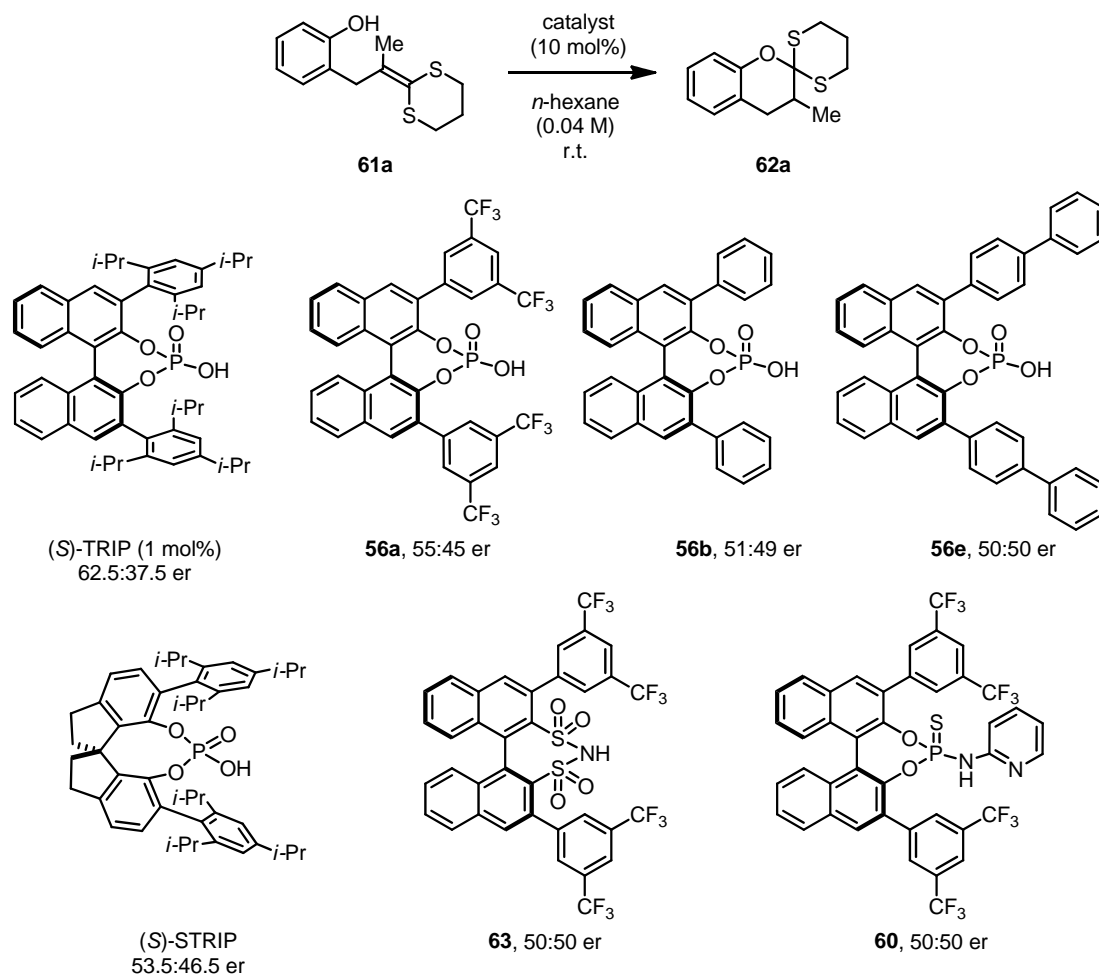
Table 4-2. Solvent screening of asymmetric protonation of ketene dithioacetal **61a**.*



Entry	Solvent	Time	Conversion	er	Remark
1	<i>p</i> -xylene	6d	<50%	66.5:33.5	-
2	DCM	48h	99%	56:44	-
3	<i>n</i> -hexane	67h	99%	70:30	-
4	<i>n</i> -hexane	3d	93%	50:50	under Ar
5	<i>n</i> -hexane	3d	93%	50:50	<i>n</i> -hexane (HPLC grade)
6	THF	3d	93%	50:50	-
7	diethylether	3d	93%	50:50	-
8	acetone	3d	93%	50:50	-
9	<i>n</i> -pentane	24h	-	66:34	trace of product
10	<i>c</i> -hexane	24h	-	65.5:34.5	trace of product
11	methylcyclohexane	24h	-	65:35	trace of product
12	toluene	24h	-	59:41	trace of product
13	<i>o</i> -xylene	24h	-	60:40	trace of product
14	<i>m</i> -xylene	24h	-	56.5:43.5	trace of product
15	chlorobenzene	24h	-	57:43	trace of product
16	1,2-DCE	24h	-	50:50	trace of product
17	1,2-dichlorobenzene	24h	-	55:45	trace of product
18	<i>n</i> -hexane	24h	99%	65:35	0.02 M
19	<i>n</i> -hexane	24h	trace	68:32	0.013 M
20	<i>n</i> -hexane	24h	trace	52.5:47.5	-10 °C (0.04 M)

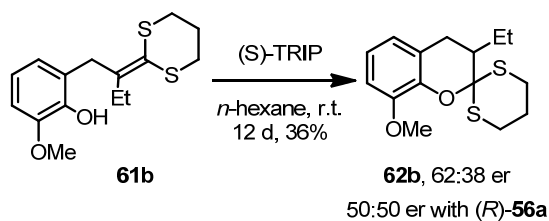
*The reaction was conducted with 0.2 mmol of ketene dithioacetal **61a**.

We next tested various Brønsted acid catalysts as shown in Scheme 4-22. An electron withdrawing substituent or an electron donating substituent on 3,3'-positions of BINOL-based phosphoric acid showed no effect on the enantioselectivity of the reaction (**56a**). The newly developed STRIP catalyst,⁶⁶ which possesses a tighter “bite angle”, was tested but provided inferior enantioselectivity (53.5:46.5 er). Chiral disulfonimide catalyst **63**,³³ which has a remarkable activity by forming a silicon Lewis acid catalyst, was tested for the reaction as a pure Brønsted acid catalyst but gave only racemic product under the reaction conditions. Bifunctional catalyst **60** also gave only racemic product **62a**.



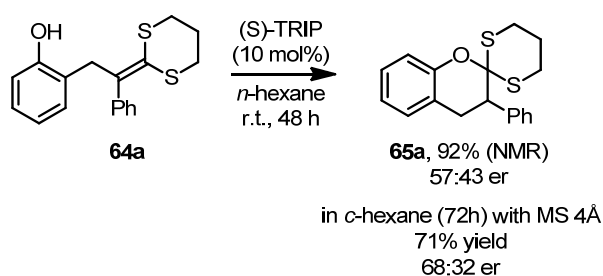
Scheme 4-22. Screening of Brønsted acid catalysts.

The ketene dithioacetal derived from α -ethylhydrocoumarin was also tested under the best reaction conditions, so far. However, only low enantioselectivity was obtained (62:38 er) after 12 days perhaps due to the low reactivity of the substrate with the bulky phosphate (Scheme 4-23).

Scheme 4-23. Asymmetric protonation of α -ethylhydrocoumarin-derived ketene dithioacetal **61b**.

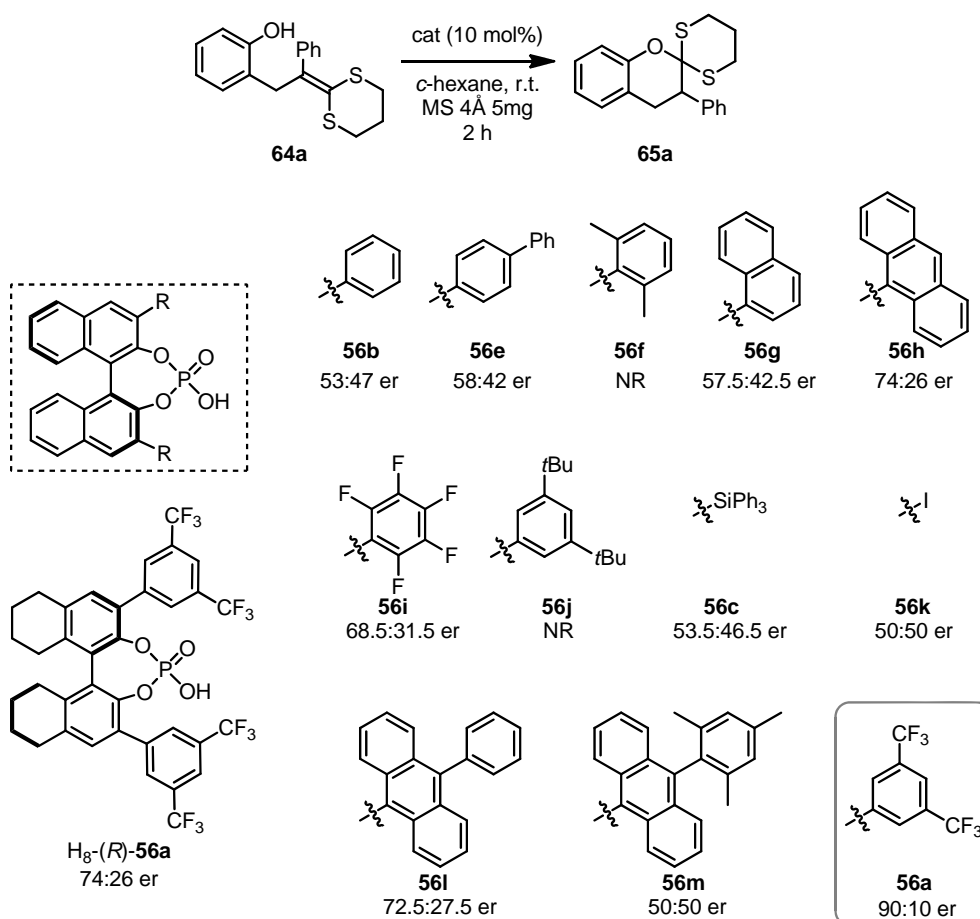
4.2.3. Asymmetric Protonation of Ketene Dithioacetals Derived from α -Aryl Hydrocoumarins

Due to the disappointing results obtained with α -alkyl substrates **61**, we next turned our attention to ketene dithioacetals of α -aryl hydrocoumarins **64**. These substrates are of particular interest since the obtained enantiopure compounds can be useful intermediates to access chiral α -aryl hydrocoumarins and chromanes. Under identical reaction conditions, product **65a** was obtained with low enantioselectivity (57:43 er). However, after solvent and concentration optimization, as well as the study of the effect of additives (different sizes of molecular sieves and water), the enantioselectivity could be increased to 68:32 er (Scheme 4-24).



Scheme 4-24. Optimization of the reaction conditions for the asymmetric protonation of ketene dithioacetal derived from α -phenylhydrocoumarin **30**.

Encouraged by this result, we tested various BINOL-based phosphoric acid catalysts as shown in Scheme 4-25. Remarkably, 9-anthracenyl (**56h**) and 10-phenyl-9-anthracenyl (**56l**) substituents on 3,3-positions of BINOL phosphate induced high enantioselectivity. Surprisingly, bis-trifluoromethyl substituted phenyl (**56a**) was the optimal substituent in terms of activity and enantioselectivity (full conversion after 2 hours in 90:10 er). The H₈-BINOL backbone was also tested for this catalyst, but showed inferior results (H₈-**56a**, 74:26 er). Owing to the electron withdrawing substituents, the reaction could be completed in shorter reaction time with higher enantioselectivity.



Scheme 4-25. Catalyst screening for the asymmetric protonation of ketene dithioacetal **64a**.

To verify the stability of the obtained product, the enantioselectivity was measured over time as shown in Figure 4-1. The observed enantiomeric ratio of dithioacetal **65a** increased with time (10 minutes, 74% conversion, 86:14 er vs 60 minutes, 90% conversion, 90:10 er) was observed. This result implies that the product **65a** does not racemize under the reaction conditions. Instead, the starting material **64a** may be converted to the product through a racemic pathway, which can occur during analysis. It had already been observed that the starting material could cyclize on silica or in dichloromethane, since they contain traces of acid. After this finding, enantiomeric ratios were determined exclusively after full conversion of the ketene dithioacetal to obtain precise values.

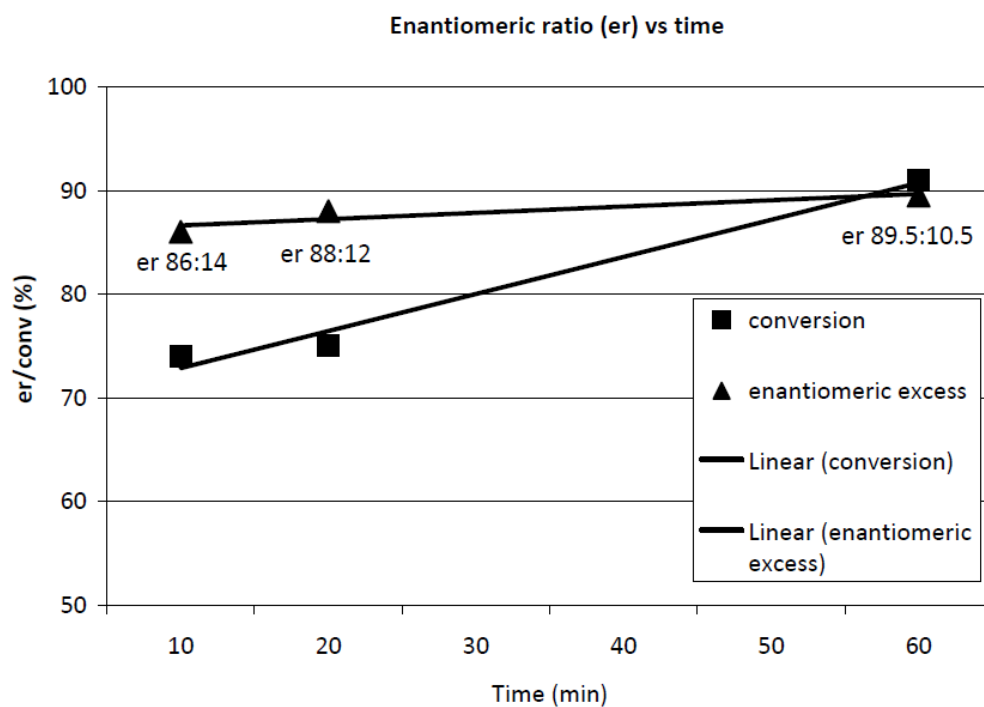
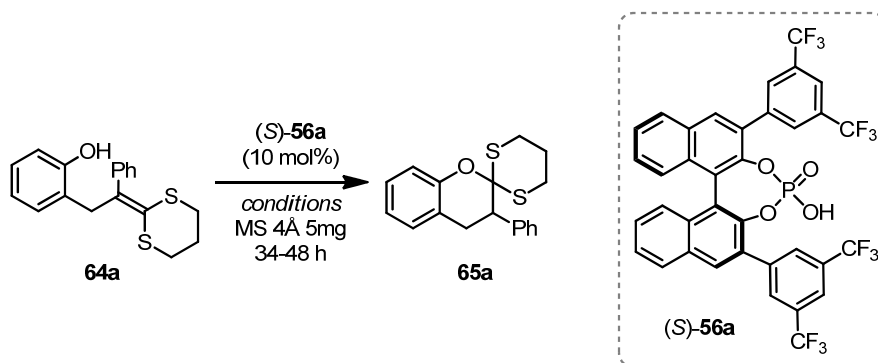


Figure 4-1. Enantioselectivity of the asymmetric protonation of substrate **64a** reaction over time.

Further optimization of the reaction conditions was conducted by varying the reaction concentration, solvent and temperature (Table 4-3). Various non-polar solvents were evaluated for the reaction and cyclohexane and methylcyclohexane were the solvents of choice (entries 5 and 9). Furthermore, decreasing concentration of the reaction led to increased enantioselectivity (entries 10-13). Under highly diluted reaction conditions (0.002 M), the highest enantioselectivity (95:5 er) was obtained, although slightly prolonged reaction time was required (entry 12). Fortunately, under these reaction conditions, the reaction could be conducted with only 0.5 mol% of catalyst loading (entry 13).

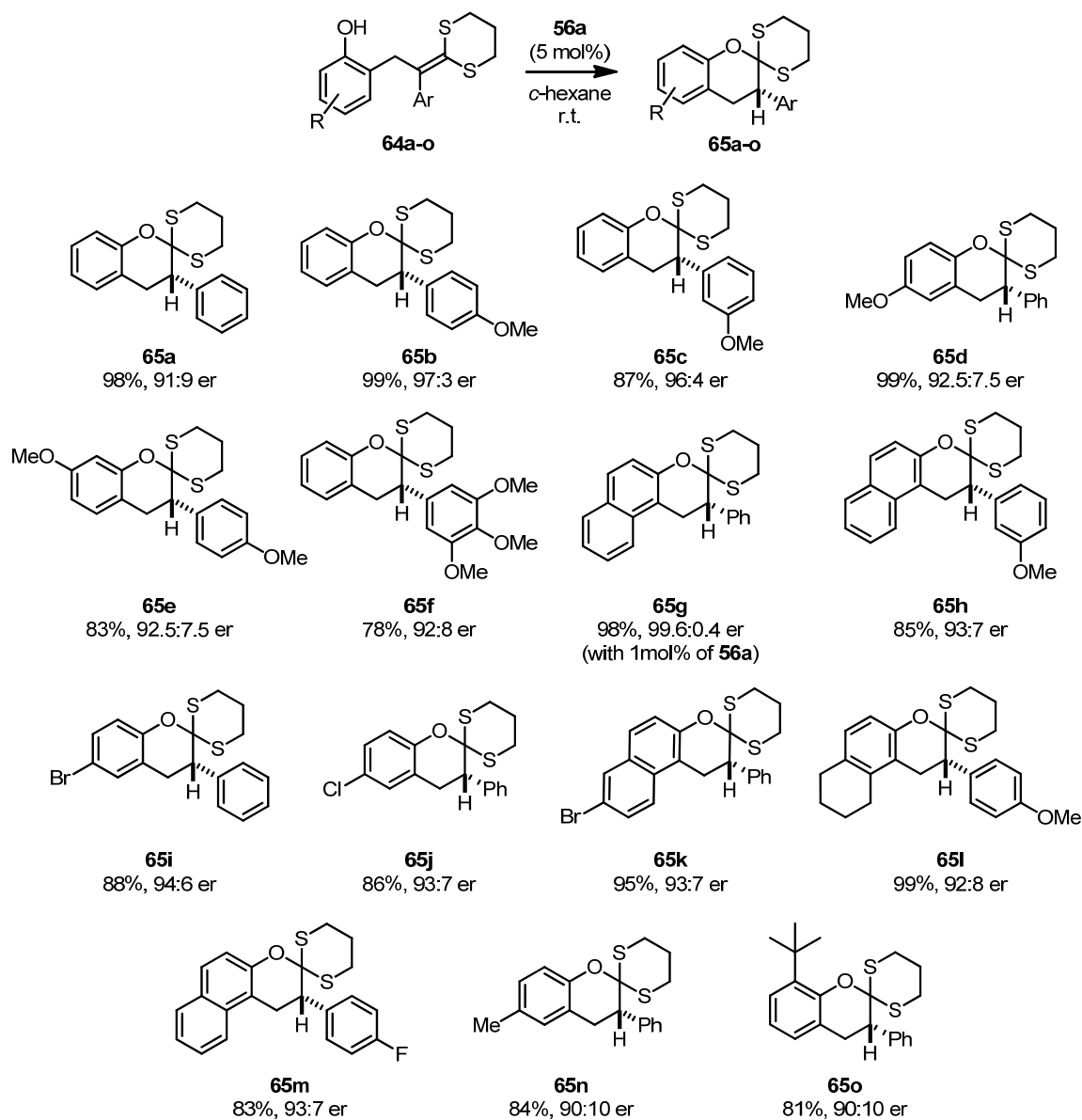
Table 4-3. Solvent and concentration screening for the asymmetric protonation of ketene dithioacetal **64a**.

Entry	Solvent	Concentration	er	remarks
1	<i>n</i> -hexane	0.08 M	87:13	-
2	<i>n</i> -heptane	0.08 M	84.5:15.5	-
3	benzene	0.08 M	84.5:15.5	-
4	toluene	0.08 M	84.5:15.5	-
5	methylcyclohexane	0.08 M	90:10	-
6	<i>i</i> -octane	0.08 M	88.5:11.5	-
7	aliphatine	0.08 M	84.5:15.5	-
8	<i>n</i> -pentane	0.08 M	86:14	-
9	<i>c</i> -hexane	0.08 M	87:13	-
10	<i>c</i> -hexane	0.03 M	90:10	-
11	<i>c</i> -hexane	0.008 M	91.5:8.5	-
12	<i>c</i> -hexane	0.002 M	95:5	reaction time: 60 h
13	<i>c</i> -hexane	0.002 M	94:6	0.5 mol% of catalyst loading

After obtaining the optimized reaction conditions, the substrate screening was conducted by employing various α -aryl hydrocoumarin-derived ketene dithioacetals **64**. As summarized in Scheme 4-26, substrates with electron-donating or withdrawing substituents, which were all tolerated under the reaction conditions, affording the desired product with excellent yield and good enantioselectivity. In general, electron withdrawing substituents indeed facilitate the reaction rate for the cyclization but a satisfactory enantioselectivity was observed (**64i** and **64j**). It is noteworthy that product **64e**, which is a precursor for the synthesis of (*S*)-equol, was obtained with good yield and enantioselectivity (83%, 92.5:7.5 er). Additionally, poly-oxygenated products such as **64f** could be obtained in an enantiomerically enriched form (92:8 er). This class of substrate could be used for the synthesis of various natural product-like molecules. It is noteworthy that dithioacetal **64g** was obtained in excellent enantioselectivity (99.5:0.5 er) with only 1 mol% of catalyst loading, which highlighted this methodology. Product **64g** could be transformed into the corresponding hydrocoumarin, which is α -phenyl substituted Splitomicin, inhibitor of Sir2p in its enantioenriched form. However the deprotection of dithioacetal

4. RESULTS AND DISCUSSION

could be problematic due to the acidic α -proton, which could result in racemization of the product. To improve the synthetic utility of our methodology, we decided to investigate more enantioselective Brønsted acid catalysts for the asymmetric protonation reaction of ketene dithioacetals.



Scheme 4-26. Substrate scope of the asymmetric protonation reaction of substrates **64** catalyzed by catalyst **56a**.

4.2.4. Asymmetric Protonation of Ketene Dithioacetals Derived from α -Alkyl Hydrocoumarins with SF₅-Substituted BINOL-Phosphoric Acids

Since the bistrifluoromethylphenyl-substituted BINOL phosphate **56a** is the most active and enantioselective catalyst for the reaction, we became interested in the sulphur analogue of the trifluoromethyl group, the SF₅ functionality, which is a surrogate for trifluoromethyl group in medicinal chemistry. Due to its five fluorine atoms, it can generate larger steric hindrance in the catalyst pocket, while acting as a stronger electron-withdrawing group than trifluoromethyl group (Figure 4-2).¹⁰⁷ Moreover, it is reported that a SF₅ group could enhance lipophilicity of a molecule significantly (lipophilicity parameters in benzene (π); H = 0, CH₃ = 0.56, CF₃ = 0.88, SF₅ = 1.23).¹⁰⁸ As expected, the catalyst containing SF₅ group (**56n**) provided higher enantioselectivity (95:5 er) under the same reaction conditions compared to the corresponding CF₃ catalyst (91:9 er). Although the catalytic activity is lower compared to the catalyst **56a** this result showed an advantage of sterically demanding and electronically withdrawing substituent SF₅.

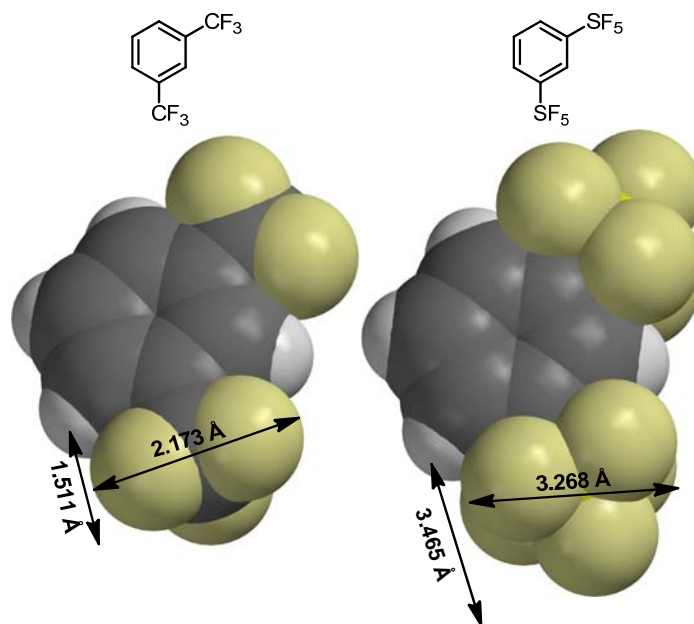
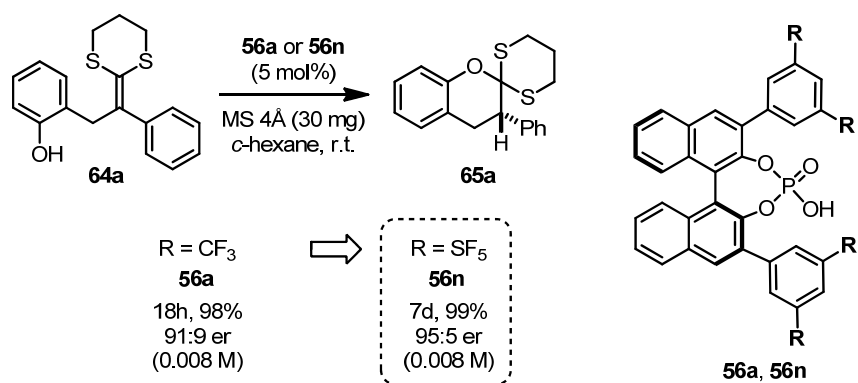


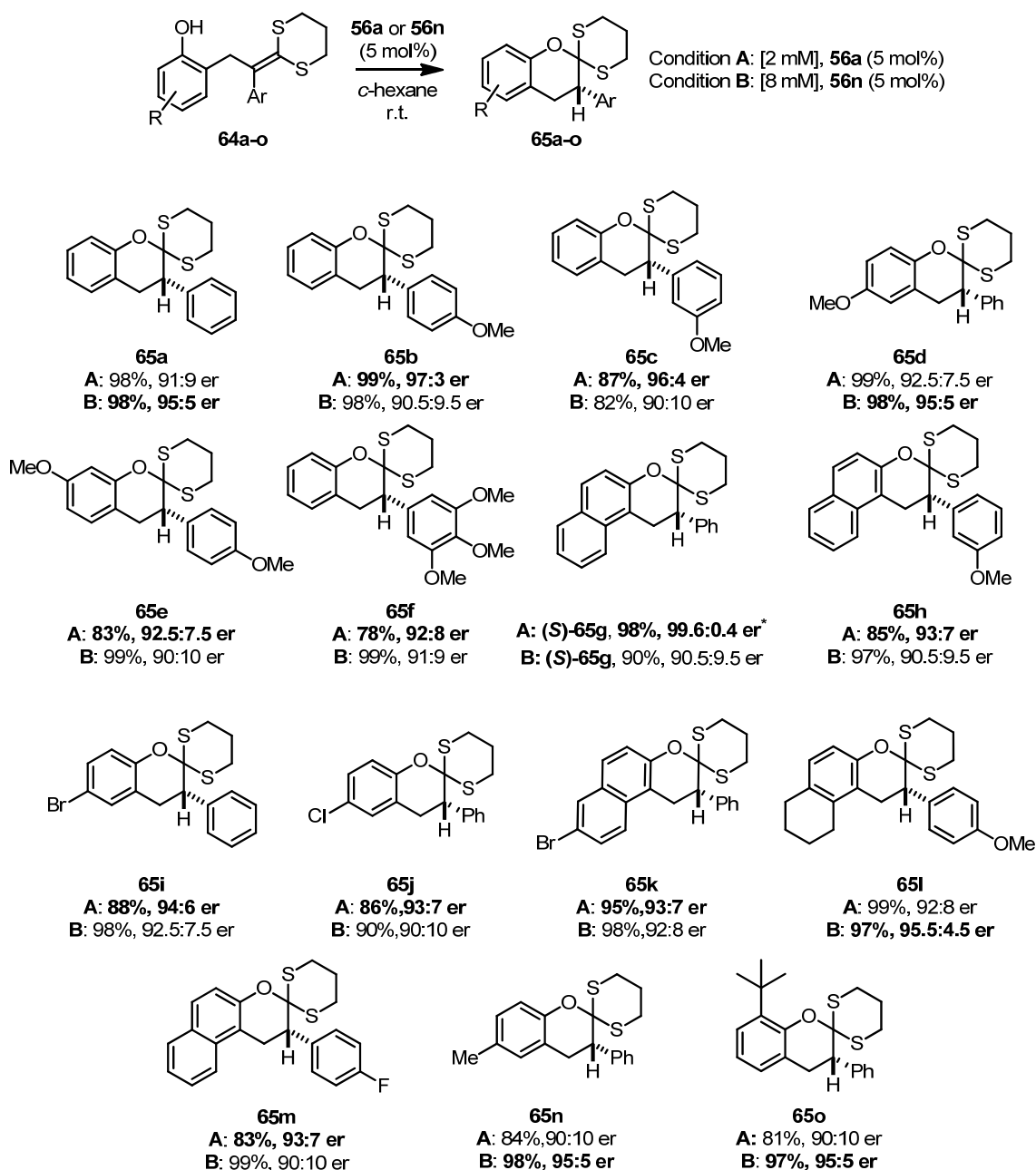
Figure 4-2. Comparison of the sphere models of C₆H₄(CF₃)₂ and C₆H₄(SF₅)₂.

4. RESULTS AND DISCUSSION



Scheme 4-27. Asymmetric protonation of substrate **64a**; Reaction with bis-3,5-CF₃ and -SF₅ phenyl substituted BINOL phosphate **56a** and **56n**.

With the new Brønsted acid catalyst **56n** in hands, the substrate scope was once again evaluated. As summarized in Scheme 4-28, the reaction conditions were optimized for each catalyst separately. The obtained enantioselectivity was generally higher than 95:5 er under slightly diluted reaction conditions for catalyst **56a** and more concentrated reaction conditions for catalyst **56n**. Due to the structural similarity of the catalyst **56a** and **56n**, in general the obtained enantioselectivity did not vary greatly when catalyst **56a** and **56n** were employed. After obtaining satisfactory results in terms of enantioselectivity of the obtained dithioacetals, the deprotection strategy was investigated. As mentioned before, the dithioacetal protecting group can be cleaved by employing reductive reaction conditions or hydrolysis by employing acidic/oxidative reaction conditions. The major concern of this state was to prevent possible racemization of the α -position.



Scheme 4-28. Substrate scope of the asymmetric protonation with catalysts **56a** and **56n**.

*The reactions was carried out with 1 mol% of catalyst 25 mM concentration.

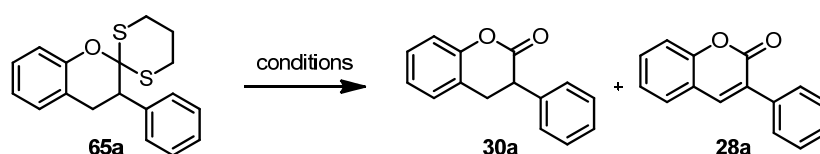
4.2.5. Application of Enantioenriched Dithioacetals

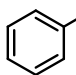
We started our investigation with the oxidative hydrolysis of dithioacetals. We presumed that a Brønsted acid could catalyze the hydrolysis of the dithioorthoester. However, under acidic conditions (in the presence of 50 mol% of DPP), only trace amounts of the desired hydrolyzed product **30a** was obtained after 2 weeks at room temperature. To facilitate the reaction process, an iodine reagent was employed, which can activate sulphur for the hydrolysis step. However, as summarized in Table 4-4, the reaction conditions should be milder to preserve the stereogenic center and generate the desired product **30a** selectively. When PIFA (Iodosobenzene

4. RESULTS AND DISCUSSION

bis(trifluoroacetate)), a well known periodine reagent was employed, only unseparable mixture was obtained under the reaction conditions (entry 1). Highly active periodic acid could convert the dithioacetal to hydrocoumarin but overoxidized-coumarin product **28a** was obtained as a major product (entry 2). Unfortunately, IBX (2-iodoxybenzoic acid) showed no reactivity for this transformation. Gratifyingly, employing the reaction conditions developed by the Nicolaou group,¹⁰⁹ molecular iodine under basic conditions, a facile oxidative hydrolysis was achieved in 2 minutes at room temperature to afford the clean hydrocoumarin product without any overoxidation. Further optimization of the reaction conditions to prevent racemization was conducted by changing the solvent and reaction time (entries 4-8).

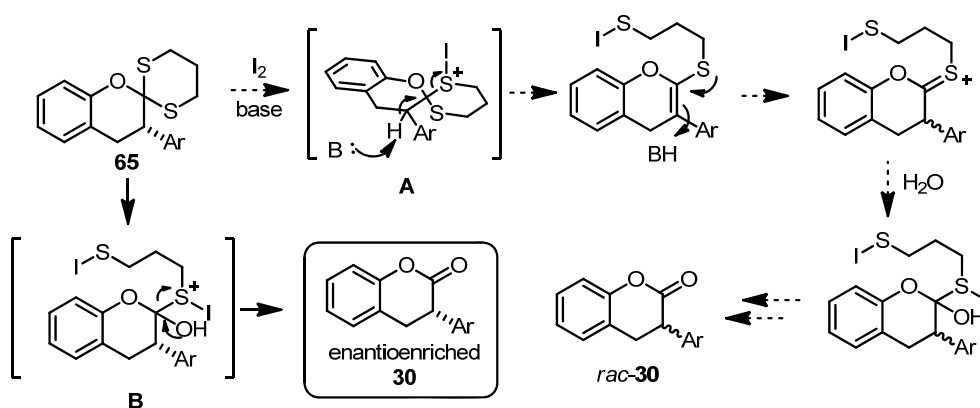
Table 4-4. Optimization of the oxidative hydrolysis of **65a**



Entry	er of 65a	Oxidant	Solvent	Time	comment
1	50:50	 (PIFA, 2 equiv)	THF	10 min	trace product
2	50:50	H ₅ IO ₆ (2 equiv)	THF	15 h	full conversion + 28a (56%)
3	50:50	IBX (1equiv)	THF	1h	no reaction
4	50:50	I ₂ (3.4 equiv) NaHCO ₃ (6.4 equiv)	acetone/H ₂ O	2min	30a (99%) ^a
5	91:9	I ₂ (2 equiv) NaHCO ₃ (4 equiv)	acetone/H ₂ O	10min	30a (26%) ^b 89.5:10.5 er
6	91:9	I ₂ (3.4 equiv) NaHCO ₃ (6.4 equiv)	acetone/H ₂ O	2min	30a (99%) ^a 89.5:10.5 er
7	92.5:7.5	I ₂ (3.4 equiv) /NaHCO ₃ (6.4 equiv)	THF	2min	30a (99%) ^a 92:8 er
8	92.5:7.5	I ₂ (3.4 equiv) /NaHCO ₃ (6.4 equiv)	THF/H ₂ O (5:1)	2min	30a (99%) ^a 91:9 er

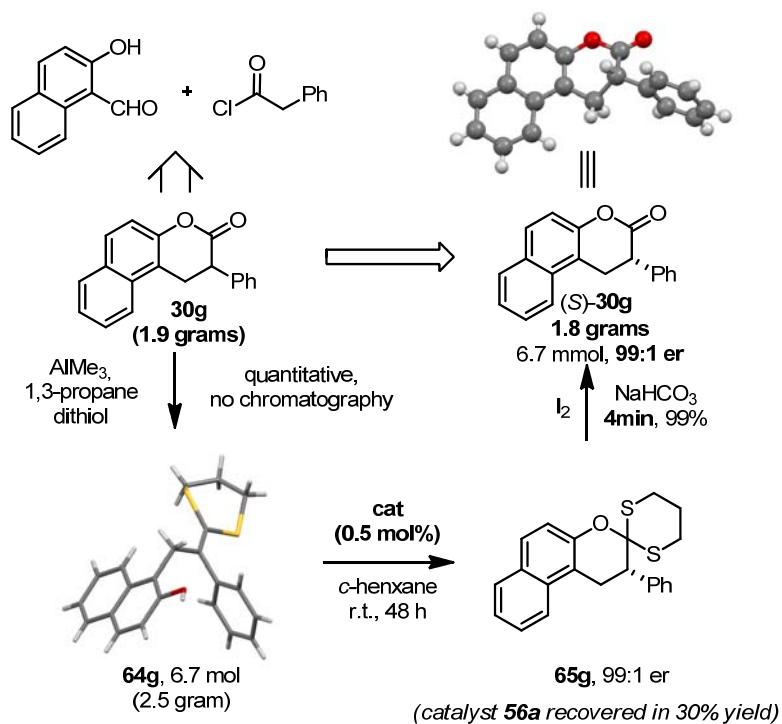
^a Isolated yield, ^b Conversion by ¹H NMR and HPLC analysis.

Finally, with a mixed solvent system (THF/H₂O), the deprotection reaction could be completed within a few minutes without a significant racemization (from 92.5:75 er to 91:9 er). Although the reaction mechanism implies that it is impossible to avoid racemization (intermediate **A** in Scheme 4-29). The maintained enantiomeric ratio from the dithioacetal to hydrocoumarin could be ascribed to the facile hydrolysis rather than deprotonation of the α -proton (intermediate **B** in Scheme 4-29). Also, the α -aryl substituent could sterically inhibit the access of base for the deprotonation and subsequent racemization.



Scheme 4-29. Reaction mechanism for the deprotection of dithioacetals **65** to hydrocoumarins **30**.

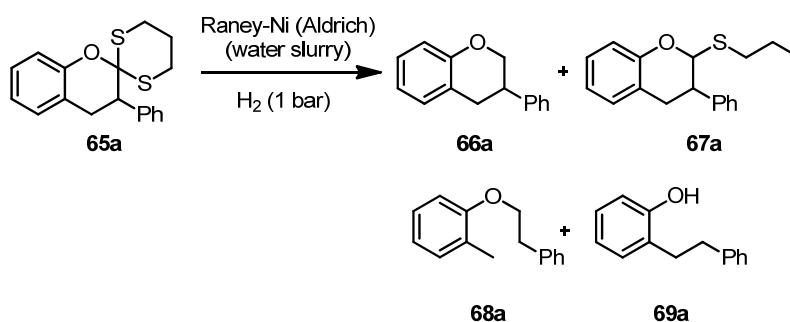
After obtaining the reaction conditions for the deprotection of a dithioacetal to a hydrocoumarin without racemization, a scale-up experiment was performed. Hydrocoumarin **65g** could be obtained from acid chloride and 2-hydroxy-1-naphthaldehyde without any sophisticated purification steps. Under anhydrous reaction conditions, hydrocoumarin **30g** was converted to the corresponding ketene dithioacetal and was precipitated in ice-cold ether solution. After filtration of the ketene dithioacetal, the substrate was dissolved in cyclohexane and treated with catalyst **56a** (Scheme 4-30). Pleasingly, high enantioselectivity (99:1 er) was obtained with only 0.5 mol% of catalyst **56a**. Without isolation of the dithioacetal product, the subsequent oxidative hydrolysis afforded enantiomerically pure (99:1 er) hydrocoumarin with quantitative yield after precipitation in methanol. This deracemization of a hydrocoumarin through asymmetric protonation was accomplished without any silica chromatography in gram scale under mild reaction conditions for each transformation.



Scheme 4-30. Deracemization of hydrocoumarin **30g** via asymmetric protonation reaction.

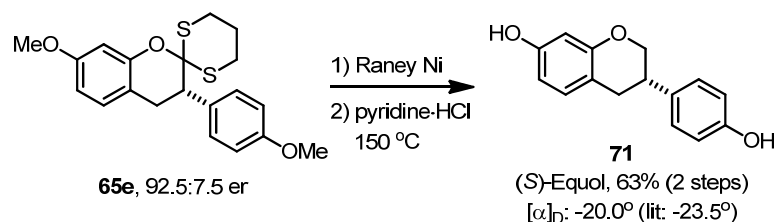
4. RESULTS AND DISCUSSION

Further investigation on the deprotection of dithioacetal **65** was focused on the reductive cleavage to afford chromane derivatives. Dithioacetals protecting groups, are well-known to be easily cleaved under hydrogen atmosphere in the presence of catalytic amounts of Raney-nickel. As shown in Table 4-5, a facile deprotection of dithioacetal was achieved in THF as solvent. In different solvent systems, the conversion was usually lower and the reaction mixture contained a reaction intermediate which could be converted to the desired product after prolonged reaction time. In THF as a solvent after 18 h, the reaction mixture contained various by-products which can be derived from the desired product after further reduction (entry 3). By decreasing reaction time to 15 min, all the starting material was consumed to afford the desired product exclusively (entry 4). Fortunately, the desired product was obtained without significant racemization. Due to the high utility of this methodology, we attempted to employ it in the synthesis of a biologically active molecule.

Table 4-5. Optimization of reductive cleavage of dithioacetal.

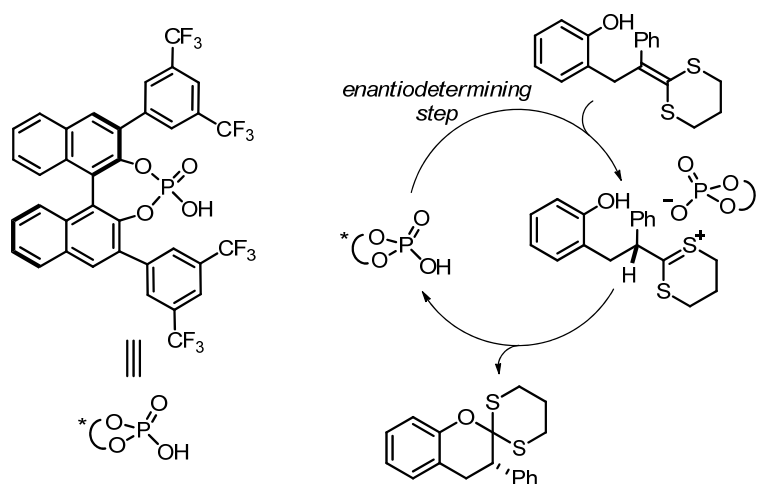
Entry	er of 3a	Solvent	Time	Comment
1	50:50	EtOH/EtOAc (1:2)	18 h	full conversion, complex mixture
2	50:50	THF/EtOAc (1:1)	18 h	full conversion, 66a : 67a = 1:1
3	50:50	THF	18 h	66a + 67a + 68a + 69a
4	91:9	THF	15 min	full conversion, 66a = 87.5:12.5 er

The application of the reductive cleavage of dithioacetal to afford chromane was further demonstrated by using substrate **65e**. As shown in Scheme 4-31, dithioacetal **65e** was smoothly converted to corresponding chromane derivative **70**. Subsequent demethylation with pyridine-HCl under dehydration conditions (using MgSO₄ reflux filter at 150 °C) afforded non-steroidal estrogen (*S*)-equol (**71**) in enantioenriched form. The obtained optical rotation value was smaller than the reported value,¹¹⁰ which can be due to the racemization occurring during the deprotection step as previously observed for substrate **65a** (Table 4-5). However, this natural product synthesis highlights that this methodology could provide easy access to this class of molecules within 4 steps from hydrocoumarins. In contrast, the conventional asymmetric synthesis of (*S*)-equol requires the employment of a chiral auxiliary and transition metal catalysts to afford the desired product in 7-8 synthetic steps.¹¹⁰

**Scheme 4-31.** Reductive cleavage of dithioacetal using Raney-Ni toward asymmetric synthesis of (*S*)-Equol.

4.2.6. Reaction Mechanism of Asymmetric Protonation Reaction of Ketene Dithioacetals

A plausible reaction mechanism is depicted in Scheme 4-32. It is reported that a ketene dithioacetal undergoes immediate protonation in the presence of a Brønsted acid.⁵¹ Therefore, we assumed that the ketene dithioacetal will be protonated immediately by chiral phosphoric acid. This step is the enantiodetermining step of the whole reaction sequence, unless the protonation step is reversible. Electron withdrawing groups on 3,3'-position of the catalyst is critical in terms of enantioselectivity of the process while sterically bulky substituted phosphoric acids showed much inferior results. Therefore, we believe that the enantiodetermining step is affected by the pK_a of the catalyst. Higher enantioselectivity of catalysis can be expected from a tighter ion pairing in the transition state. The cyclization step could be catalyzed by regenerated phosphoric acid or take place spontaneously without catalyst.



Scheme 4-32. Plausible reaction mechanism of the asymmetric protonation of ketene dithioacetal

With the aim of studying the reaction mechanism, preliminary MM (molecular mechanics)-DFT (density functional theory) calculations were conducted using Spartan[®]. A conformation search was conducted using MM and the corresponding most stable conformer was used as a starting geometry for an optimization at the B3LYP/6-31G* level of theory. As shown in Figure 4-3, we presumed that the enantiodetermining step of the reaction must be the protonation step. After protonation, the ionic substrate-catalyst complex could resemble the nearest transition state energetically according to the Hammond's postulate. Each enantiomeric cationic intermediate was complexed with (*R*)-configured BINOL-based catalyst. These two diastereomeric structures then gave two different energy values, which were translated to the proportional distribution of the enantiomer by using Boltzmann's distribution equation. The obtained energy difference between the two diastereomeric complexes is 1.62 kcal/mol, which corresponds to an enantiomeric ratio of 94:6. The experimental enantioselectivity under optimized reaction condition for this typical substrate was 95:5 er, which matches the computational result well.

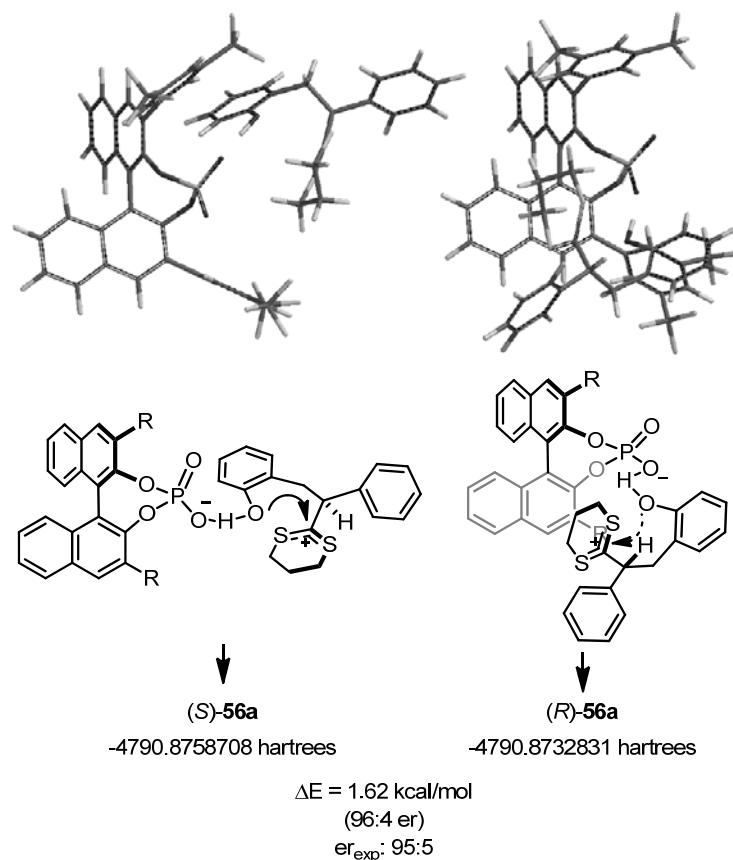
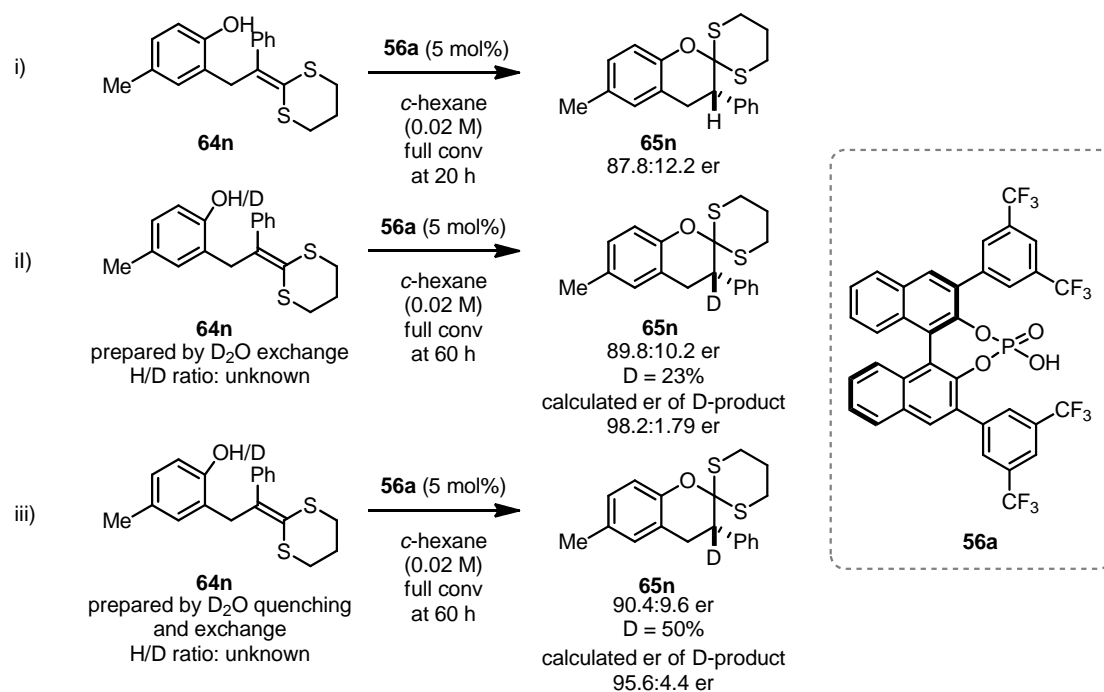


Figure 4-3. MM-DFT calculation of the reaction intermediate-catalyst complex.

Further investigation on the reaction mechanism was conducted by checking the isotope effect in the asymmetric catalysis (Scheme 4-33). However, due to the fast exchange of the phenolic proton in any medium, the H/D ratio was not determined. First, the deuterated substrate **64n** was prepared by exchanging the phenolic proton to deuterium by stirring a solution of substrate in diethylether and D_2O overnight ((ii) in Scheme 4-33). The obtained substrate was treated with neither dehydrating reagent (i.e. Na_2SO_4 or $MgSO_4$) nor silica to prevent further proton exchange. After cyclization under identical reaction condition as protonated substrate **64n**, the obtained product was analyzed by 1H NMR to show 23% deuterium incorporation in the product. Surprisingly, under identical reaction conditions, the deuterated substrate gave a higher enantioselectivity (ca. 90:10 er, eq 2 in Scheme 4-33) than the protonated substrate (ca. 88:12 er, (i) in Scheme 4-33). To gain access to higher deuterium incorporated substrate and product, substrate **64n** was prepared by quenching with $D_2O/NaHCO_3$ to afford the deuterium exchanged ketene dithioacetal (iii). To ensure deuterium incorporation, the substrate was repeatedly submitted to the D_2O /diethylether exchange conditions. Then the asymmetric protonation reaction was conducted under the same reaction conditions to give the cyclized product. As expected, the reaction rate was very slow (60 h, full conversion) compared to the rate of the proton substrate (12 h, full conversion). After complete consumption of the starting material, the H/D ratio was determined by 1H NMR and showed 50% of deuterium incorporation. Although high deuterium incorporation

4. RESULTS AND DISCUSSION

ratio was observed, the obtained enantiomeric ratio (ca. 90:10 er, eq 3 in Scheme 4-33) was similar to that obtained from of product **65n**. We assumed that the reaction with higher D/H ratio substrate is relatively slower than the lower D/H ratio substrate and a racemic background process is more predominant.



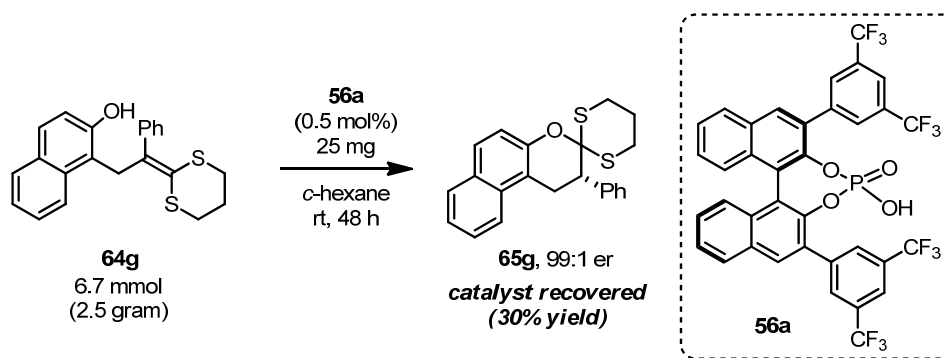
Scheme 4-33. Effects of the deuteration of the phenolic proton for the asymmetric protonation of ketene dithioacetal **64n**.

These results could perhaps be explained by the effect of deuterium in the transition state. Due to the higher atom weight of deuterium compared to a proton, the transition state could be more compact (shorter bond length) than the proton analogue.^{111, 112} Further discussion regarding this subject will be disclosed in the outlook section.

4.3. Heterogeneous Asymmetric Organocatalysis

4.3.1. Recycling of a Brønsted Acid Catalyst

Asymmetric organocatalysis has been providing a general and practical approach to numerous enantiomerically pure complex organic molecules, however its application in industry is often hampered by economic factors. As shown in shown Scheme 4-34, although catalytic amounts (0.5 mol%) of the organic catalyst are used for the catalysis, the recovery of the organocatalyst is not particularly feasible. By column chromatography, only 30% of pure catalyst **56a** could be obtained together with a mixture of unknown compounds.

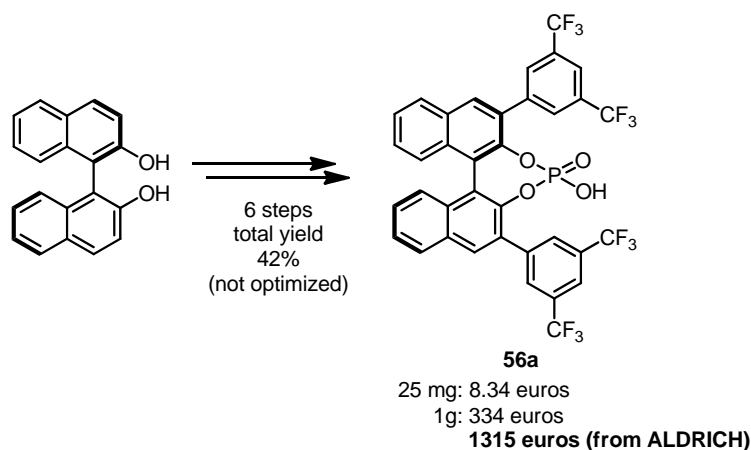


Scheme 4-34. Large scale asymmetric transformation and recovery of the chiral organocatalyst **56a**.

Nonetheless the synthesis of catalyst **56a** is straightforward from inexpensive starting material. As can be seen in Table 4-6, the synthesis requires 6 steps of transformations, which include protection and deprotection sequences. Moreover, the total price of the commercial reagents required for the synthesis cannot be overlooked. The prices of the chemical reagents and solvents necessary for its synthesis are summarized in Table 4-6, excluding any additional costs generated during the work-up and purification steps as well as additional costs (infrastructures, water, electricity and labor). This aspect is clearly related to the environmental effects of chemical industry, since the chemical industry highly demands green processes to decrease the negative effects on nature.

4. RESULTS AND DISCUSSION

Table 4-6. The cost for the synthesis of catalyst **56a**.



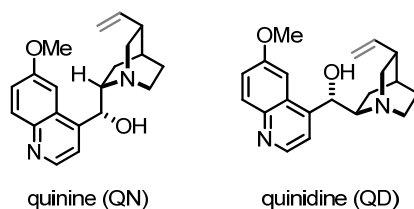
	Aldrich price			Equiv	mmol	MW	mg required	€
	amount	€	€/g					
(R)-BINOL	10	137.5	13.75			286		0.0303
MeI	1000	401	0.401	3.9	0.30	141	42.34	0.016979
K ₂ CO ₃	2500	99.7	0.03988	8	0.62	138.2	85.13	0.003395
acetone	1000	37.5	0.0375	-	-	-	-	1.5
nBuLi 2.5M	1000	102.6	0.1026	3	0.23	-	-	0.1026
TMEDA	1000	386	0.386	2.2	0.17	116	19.26	0.007433
diethylether	1000	58.5	0.0585	-	-	-	-	1.17
bromine	250	490	1.96	13	0.98	159	155.98	0.305713
DCM	1000	93	0.093	-	-	-	-	1.86
BBr ₃	100	307.5	3.075	7	0.38	250.52	93.95	0.288909
Pd(PPh ₃) ₄	5	120	24	0.1	0.0054	1156	6.19	0.148643
POCl ₃	100	479.5	4.795	3	0.16	153	24.59	0.117917
pyridine	1000	174.5	0.1745	-	-	-	-	0.8725
boronic acid	5	86.6	17.32	8	0.43	258	110.58	1.915282
							For 25 mg of catalyst 56a	8.34 €

Immobilization of homogeneous catalysts could be an ideal solution in this context. However, methods to generate economically and environmentally benign heterogeneous catalysts from homogeneous catalysts by employing solid materials are scarce. Most of the catalysts developed so far suffered from low recyclability and inferior selectivity compared to their homogeneous analogues. To provide a general solution for this problem, we decided to develop a very simple immobilization methodology and apply the immobilized catalyst to conventional catalysis and asymmetric catalysis.

4.3.2. Immobilization of Cinchona Alkaloids and Its Derivatives – Conventional Approach

This work has been accomplished in collaboration with Dr. Thomas Mayer-Gall from Deutsches Textilforschungszentrum Nord-West e.V. in Krefeld who conducted all photochemical immobilization reactions.

We commenced our study on the development of a facile preparation of heterogeneous catalysts with Cinchona alkaloids (Scheme 4-33). Due to their multifunctionality, cinchona alkaloids have been utilized as versatile chiral organocatalysts and chiral ligands for numerous organic transformations.¹¹³ Moreover, Cinchona alkaloids possess the olefin functional group inherently, which can be converted to a “polymerizable” reaction center. However, it has been known that the olefin group can hardly participate in polymerization reactions except thiol-ene type reactions under free-radical generation reaction conditions.¹¹⁴ Although significant progress on the development of heterogeneous Cinchona alkaloids derivatives has been reported, these studies are often limited to surface decorators and chiral ligands for transition metal catalysis.^{115,116}



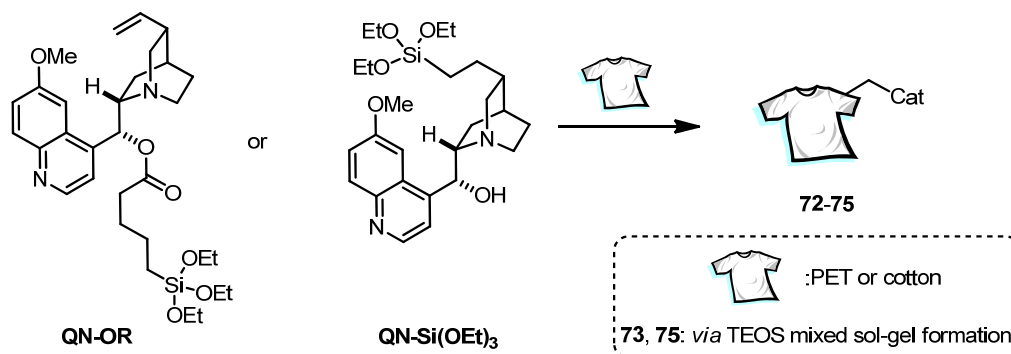
Scheme 4-35. Structures of the pseudoenantiomeric Cinchona alkaloids quinine and quinidine

Cinchona alkaloids, such as quinine (**QN**) and its pseudoenantiomer quinidine (**QD**), possess various functional groups such as quinoline, quinuclidine, a secondary alcohol and a vinyl group. Transformations of any of the functional groups of cinchona alkaloids into “polymerizable” functional groups have been extensively investigated. However, there is no general method for the immobilization of this class of compounds without any modification of the parent compounds.

To provide a general methodology for the immobilization of organic molecules, the polymeric material should be i) inexpensive, ii) highly accessible, iii) easy to handle and iv) durable in the catalysis. To meet these requirements, we found that textile material could be a good candidate. By modifying the surface of the textile materials, we presumed that a facile immobilization of organocatalysts could be realized.

As depicted in Scheme 4-36, cotton as a solid material was used for the immobilization of Cinchona alkaloid derivatives. The immobilization reactions were performed by changing alkoxy groups of orthosilicates (TEOS, tetraethyl orthosilicate) with hydroxyl groups on the surface of cotton. In the case of PET (Polyethylene Terephthalate), sol-gel formation of the catalyst could be expected on the surface. This methodology has been developed and applied to prepare similar heterogeneous catalysts using silica gel as a solid support.¹¹⁷

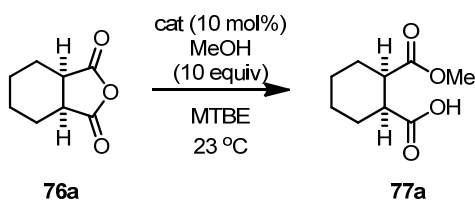
4. RESULTS AND DISCUSSION



Scheme 4-36. Immobilization of quinine derivatives on cotton.

The immobilized catalysts were tested for the desymmetrization of *meso*-anhydride **76a**. As summarized in Table 4-7, the non-immobilized parent cinchona alkaloid, quinine, afforded the desired product with quantitative yield and low enantioselectivity (entry 1, 60:40 er). The blank reactions with cotton (entry 2) and PET (entry 7) without any modification gave significant conversion due to the background reaction. In general, cotton-immobilized catalysts gave only racemic products (entries 3-6). Fortunately, catalyst **PET-72** generated the product with an enantioselectivity comparable to the homogeneous reaction conditions (entry 1 and entry 8, 62:38 er). Therefore we decided to investigate the reaction conditions using this catalyst. The catalysts prepared *via* mixed sol-gel method showed only inferior results (entries 9-11). Moreover, we observed significant leaching-out of the catalyst during the reaction by analyzing the crude reaction mixture (entries 5, 10 and 11).

Table 4-7. Evaluation of textile-organocatalysts **PET/Cotton-72-75**.

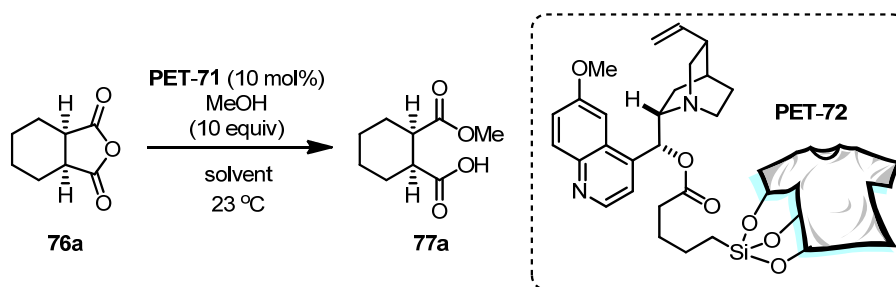


Entry	catalyst	time (h)	conversion (%)	er
1	quinine	18h	100%	60:40
2	blank cotton	18h	70%	50:50
3	cotton-72	18h	100%	60.5:39.5
4	cotton-73	18h	100%	60:40
5 ^a	cotton-74	18h	50%	54:46
6	cotton-75	18h	40%	50:50
7	blank PET	18h	80%	50:50
8	PET-72	18h	100%	62:38
9	PET-73	18h	100%	59.5:40.5
10 ^a	PET-74	18h	40%	50:50
11 ^a	PET-75	18h	40%	50:50

*The reaction was conducted with 1 mmol of anhydride in MTBE (5 mL). The reaction mixture was sonicated for 2 min. The catalyst absorbs almost all of the liquid reaction mixture. ^aThe catalyst leached out during the reaction.

The reaction conditions for the desymmetrization of *meso*-anhydride **76a** with catalyst **PET-71** were optimized by changing the reaction concentration and solvent (Table 4-8). Higher enantioselectivity (69:31 er) was observed under diluted reaction conditions (entry 2). Use of different solvents, however, did not improve the enantioselectivity further (entries 3-12). Moreover, the catalyst was not feasible of being recycled (entry 13). After the first run of the asymmetric reaction, catalyst **PET-71** completely lost its activity and enantioselectivity (54:46 er from 65:35 er). These results could be explained by severe leaching out of the catalyst into the solution. Upon analyzing the reaction mixtures (entries 1-12) by ¹H NMR, we could observe aromatic signals (6%) together with the desired product. This observation could be interpreted as the decomposition or leaching-out of the Cinchona alkaloid catalyst. Due to the weak chemical stability of the silicate under hydrolysis conditions, the immobilized catalysts showed impractical recyclability. This result prompted us to develop a more chemically robust immobilization methodology.

Table 4-8. Optimization of the reaction conditions for catalyst **PET-71** and the recycling experiment.



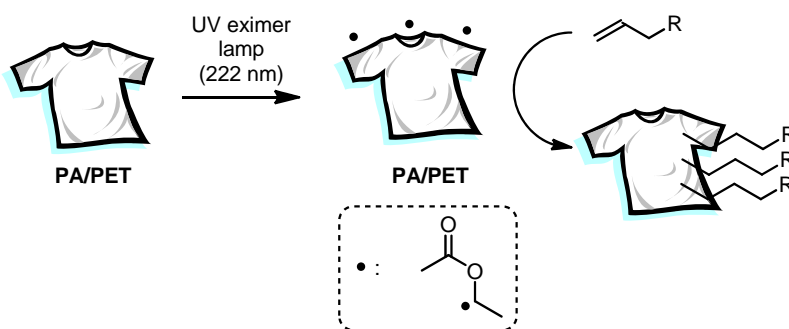
Entry	Solvent	Concentration (M)	time (h)	conversion (%)	er
1	MTBE	0.04 M	24h	100%	65:35
2	MTBE	0.02 M	4 days	99%	69:31
3	THF	0.04 M	42h	99%	62.5:37.5
4	DCM	0.04 M	42h	99%	47.5:52.5
5	toluene	0.04 M	17h	99%	53:47
6	ether	0.04 M	24h	99%	61.5:38.5
7	1,4-dioxane	0.04 M	3 days	99%	64:36
8	ACN	0.04 M	4 days	99%	54.5:45.5
9	benzene	0.04 M	24h	99%	51:49
10	acetone	0.04 M	4 days	99%	58:42
11	hexane	0.04 M	24h	99%	50:50
12	EtOAc	0.04 M	3 days	99%	59:41
13^b	MTBE	0.04 M	4 days	99%	54:46

4. RESULTS AND DISCUSSION

^a Under the same reaction condition, quinine (homogeneous) gave 62:38 er after 24h. ^b The catalyst was reused from entry 1.

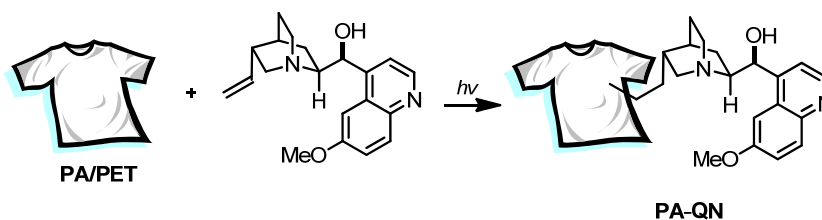
4.3.3. Immobilization of Cinchona Alkaloids and Its Derivatives – Photochemical Approach

It has been reported that textile materials, for example PET, can undergo radical-initiated surface modification under photochemical reaction conditions in the presence of olefin.^{118,119} High energy ultraviolet light can generate radical species on the surface, which can be stabilized by the solid environment.¹²⁰ The subsequent reaction with electron-rich olefin eventually afforded organic molecule immobilized textile material (Scheme 4-37). We decided to use this methodology since it has striking advantages over a conventional immobilization process. First, radical-initiated reaction conditions do not require pre-modification of the solid material or the organic molecules. Second, the carbon-carbon bond formation reaction could lead to permanent immobilization of the organic molecule on the surface. Third, the process is operationally simple and environmentally friendly since it generates no by-products during the immobilization process, in contrast to the conventional immobilization methodologies.



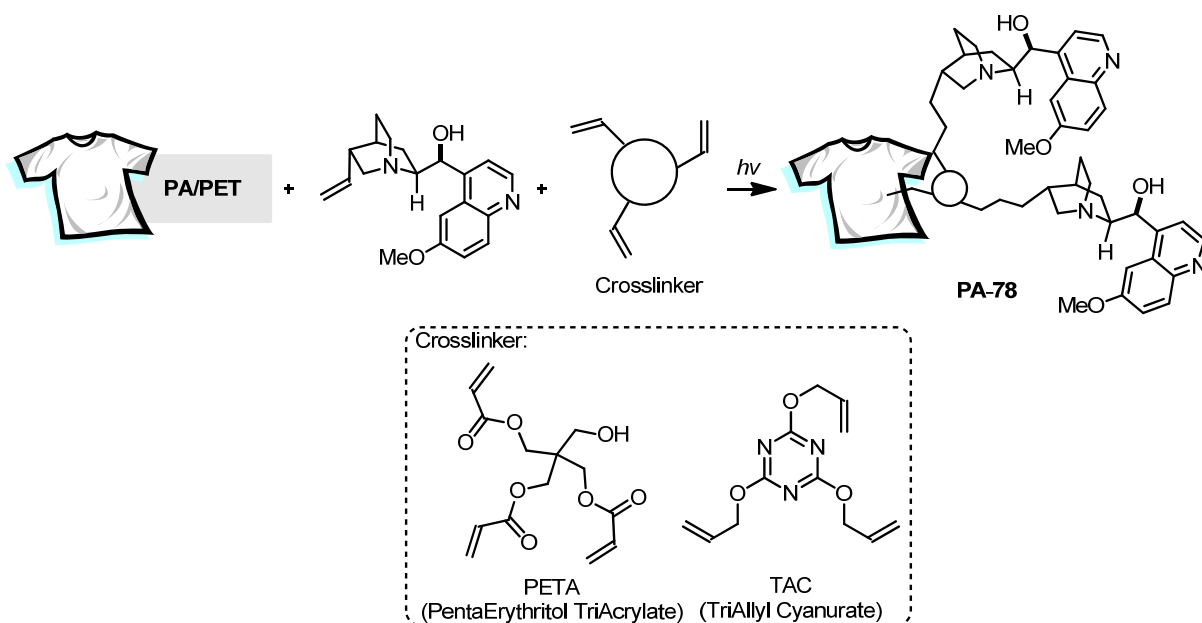
Scheme 4-37. Surface modification of PET under photochemical reaction conditions.

The immobilization reaction was performed as depicted in Scheme 4-38, using the cinchona alkaloid, quinine, PET and Nylon as a polymeric support under UV irradiation conditions. Pleasingly, the reaction indeed afforded the quinine-immobilized textile catalyst. At this stage, the catalyst loading was not determined due to the fact that elemental analysis on nitrogen and carbon provided unreliable results.



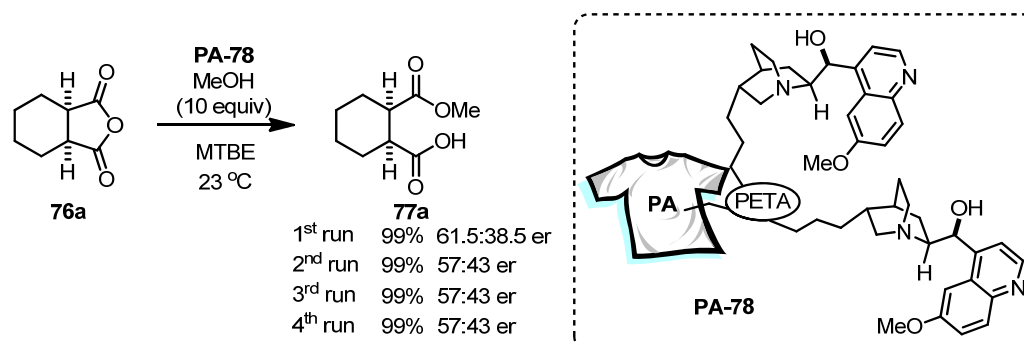
Scheme 4-38. Immobilization of QN on PA/PET under photochemical reaction conditions.

We presumed that the employment of a crosslinker could improve the immobilization efficiency and also could be beneficial for catalytic activity and perhaps for enantioselectivity. It could be helpful to position the chiral catalyst away from the surface, in order to increase the flexibility of the catalyst and prevent any negative effects *via* surface-substrate interactions. As shown in Scheme 4-39, we employed a crosslinker such as PETA (pentaerythritol triacrylate) or TAC (triallyl cyanurate) to improve catalyst loading.



Scheme 4-39. Immobilization of quinine in the presence of crosslinkers, such as PETA and TAC.

As predicted, the catalyst was smoothly immobilized on the surface, as confirmed by testing the catalyst for the catalytic asymmetric transformation (Scheme 4-40). The textile-based catalyst gave the same sense of enantioselectivity for the reaction, which implies that the chemical structure of the organocatalyst was maintained on the surface. Although the obtained enantioselectivity was low, similarly to the corresponding homogeneous reaction conditions (60:40 er), the textile catalyst could be recycled and showed no significant erosion of activity and enantioselectivity. Moreover, until four cycles, the catalyst maintained its activity and enantioselectivity although the second run gave inferior enantioselectivity (57:43 er) than the first experiment (61.5:38.5 er). By analysis of the crude reaction mixture by ^1H NMR, no leaching-out of the chiral catalyst was observed. We presume that the loss of enantioselectivity after the second run can be ascribed to the reorganization of the catalyst on the surface. Nevertheless the recyclability of the catalyst showed the strong potential of this methodology.



Scheme 4-40. Desymmetrization of *meso*-anhydride using **PA-78** and recycling experiments.

As mentioned before, the morphology of the textile material indeed enables a handy and operationally simple process for the recycling procedure (Figure 4-4). The catalyst is extremely easy to handle and can be used without any special concerns contrary to the conventional resin catalysts. If one uses resin-based catalysts or reagents, the major reason for loss of catalytic activity comes from recycling procedures since the filtration and washing process are tedious and error-prone. This disadvantage can be overcome by using chemically benign “tea-bag” equipment, which can contain the resin based catalyst inside. However this procedure is not feasible for large scale applications. Our catalyst indeed showed superior practicability to any other conventional solid support catalysts in terms of morphology, such as powder, granule and (rectangular) resins.



Figure 4-4. Reaction set-up using the textile-based catalyst shown as the white material contained in the vial.

4.3.4. Textile Asymmetric Organocatalysis - Design

Having established the photochemical immobilization reaction conditions, subsequent investigation was focused on immobilization of various organocatalyst. Owing to the simplicity of our methodology, we intended to prepare numerous catalytic systems on textile materials. This process would be ideal if the reaction does not require any pre-modification of polymeric materials or of the organic molecules and the process could be done within not more than one step. Moreover, the active site of the polymeric catalyst should be identical to the corresponding homogenous catalyst to provide the same chiral environment in the case of the chiral organocatalyst.

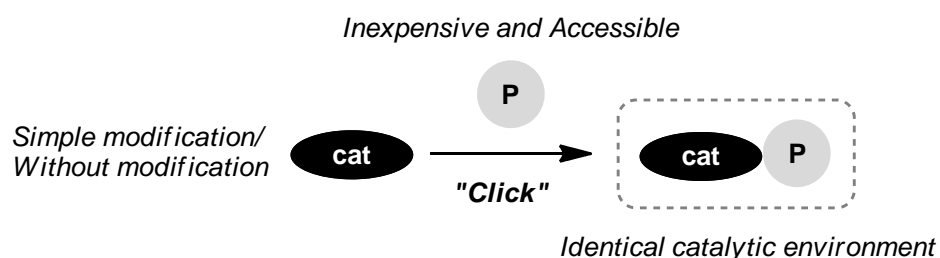


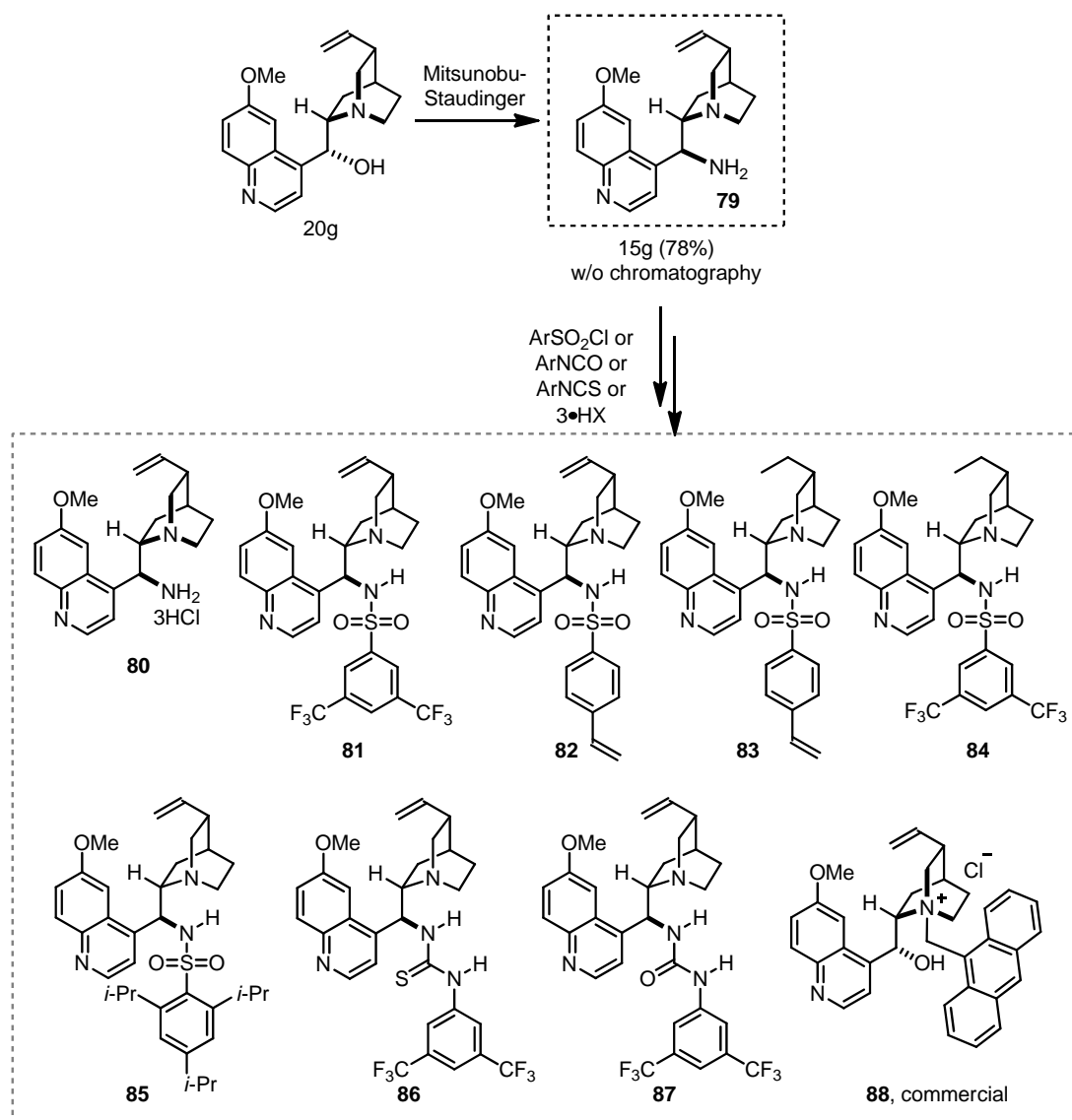
Figure 4-5. Schematic representation of the ideal immobilization procedure for organic molecules on solid materials.

4.3.5. Preparation of Cinchona Alkaloid Derivatives

We commenced our investigation with a chiral organocatalyst derived from cinchona alkaloids. The preparation of 9-*epi*-amino cinchona alkaloid compounds¹²¹ is well known, using the Mitsunobu-Staudinger sequence, even in large scale preparations. We conducted the reaction on a 15 gram scale to afford the desired amine compound **79** with 78% yield, which was stored as a 3•HCl salt to prevent any degradation or decomposition (Scheme 4-41). The product **79** was obtained without silica chromatography. After formation of 3•HCl salt **80**, the product was precipitated in methanol and isolated as an analytically pure form characterized by NMR and HRMS. Moreover, 3•HCl salt **80** can be used as a primary amine catalyst for various asymmetric transformations as it is or after exchanging the anion.¹²² Apart from that, we focused on the synthesis of various bifunctional organocatalysts using the primary amine salt and aryl sulfonyl chloride and aryl iso(thio)cyanates to afford the corresponding sulfonamide catalysts (**81-85**) and (thio)urea catalysts (**86** and **87**)¹²³ (Scheme 4-41). Particularly, sulfonamide-based organocatalysts drew our attention because of their high acidity¹²⁴ and unique single hydrogen-bonding donor ability.¹²⁵ Thiourea and urea catalysts are versatile and highly selective organocatalysts owing to their bifurcated hydrogen bonding since various hydrogen bonding donor catalysts would be desirable. In this context, squaramide-based catalysts,¹²⁶ phosphinamide catalyst¹²⁷ and dimeric organocatalysts¹²⁸ were developed and applied to asymmetric catalysis.

4. RESULTS AND DISCUSSION

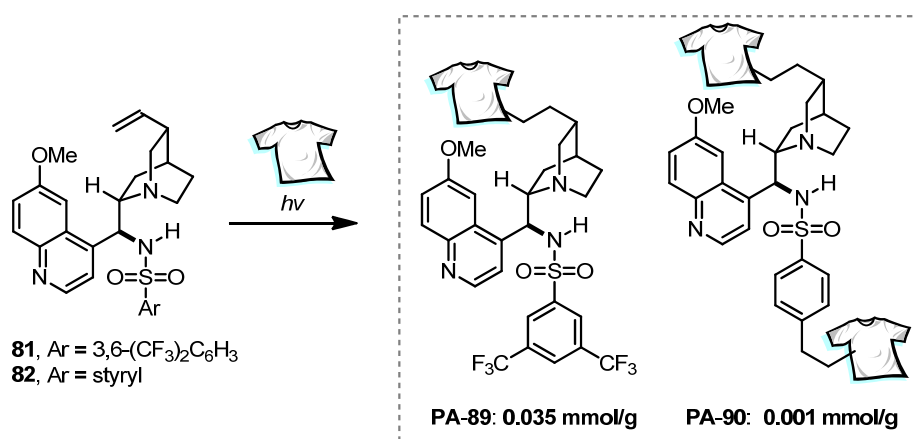
Fortunately, the quinine-derived sulfonamide-based catalyst showed an inherent advantage from an analytical perspective. Due to its sulfur atom and fluorine atoms, it is easier to determine the catalyst loading on the solid materials by elemental analysis. The synthesis is straightforward to afford the desired product after short column chromatography with usually quantitative yields in multi-gram scale.



Scheme 4-41. Synthesis of cinchona alkaloid derived organocatalysts

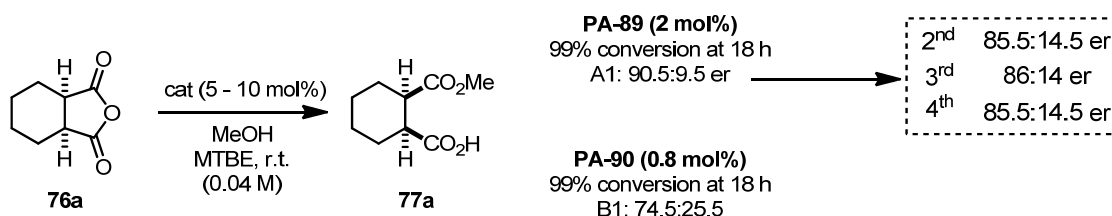
4.3.6. Preparation of Chiral Textile Organocatalysts

Textile catalysts derived from chiral bifunctional organocatalysts **PA-89** and **PA-90** were simply prepared by using polyamide (PA) as a solid support *via* irradiation with a ultraviolet excimer lamp (220 nm). As depicted in Scheme 4-42, the catalyst loading was determined by elemental analysis of sulfur. The styrene-substituted sulfonamide catalyst was also tested at this stage to confirm the effect of the styrene group on the immobilization process. Although the catalyst loading on the textile was very low compared to **PA-89** (0.001 mmol/g), the catalytic activity and enantioselectivity of catalyst **PA-90** were also tested for comparison.



Scheme 4-42. Immobilization of sulfonamide catalysts on polyamide (PA).

Pleasingly, catalyst **PA-89** showed good activity (99% conversion at 18 h) and enantioselectivity (90.5:9.5 er) with only 2 mol% of catalyst loading. Due to the low catalyst loading on the polymer of catalyst **PA-90**, only 0.8 mol% of catalyst was employed for the asymmetric reaction and therefore it gave inferior results (74.5:25.5 er). This enantioselectivity could perhaps be improved by using a higher catalyst loading. However, from a practical point of view, we concluded that catalyst **PA-89** is more efficient since the immobilization gave a higher catalyst loading than **PA-90**. The recyclability of catalyst **PA-89** was also tested using the same catalyst for the next runs. As observed before, although the catalyst lost some enantioselectivity (86:14 er from 90.5:9.5 er) after the first run, the enantioselectivity was retained within the next four cycles.



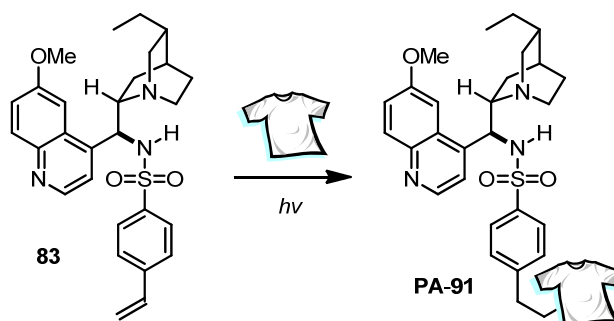
Scheme 4-43. Evaluation of catalytic activity, enantioselectivity and recyclability of **PA-89** and **PA-90**.

Further optimization of the catalyst loading was conducted by varying the irradiation time and the concentration of monomeric catalyst for the immobilization reaction. For this purpose, catalyst **83** was prepared by using the corresponding sulfonyl chloride from *p*-stryrenylsulfonate sodium salt with thionylchloride. The hydroquinine derivative was prepared *via* reduction of 9-*epi*-aminoquinine with Pd/C and H₂. As summarized in Table 4-9, a higher concentration of monomer during the immobilization provided textile catalyst **PA-91** with higher catalyst loading. Double irradiation of the textile was optimal to increase the catalyst loading on both sides of the textile (after the first irradiation, the other side of the textile was irradiated under the same conditions). Increasing the irradiation time to 20 minutes (twice 10 minutes) generated the textile catalyst with higher catalyst loading (entry 7). Up to 0.0704 mmol/g of catalyst loading was achieved by using PETA as crosslinker (entry 4). However, in the case of **83**, a severe film formation occurred and the catalyst lost its activity and enantioselectivity dramatically after the first asymmetric transformation. Therefore the styrene

4. RESULTS AND DISCUSSION

group as a polymerization center was avoided since it may be too reactive under the employed photochemical reaction conditions.

Table 4-9. Optimization of catalyst loading using catalyst **83**.



Entry	mmol of 83 /g of textile	Irradiation time	Catalyst loading (mmol/g)
1	0.05	2 x 5 min	0.0118
2	0.1	2 x 5 min	0.0124
3	0.2	2 x 5 min	0.0204
4*	0.3	2 x 5 min	0.0704
5	0.3	2 x 5 min	0.0276
6	0.4	2 x 5 min	0.0319
7	0.3	2 x 10 min	0.0525

*PETA was used as cross linker (0.17 mmol/g of textile)

After establishing that repeated irradiation was the key to improve the catalyst loading while keeping its enantioselectivity, the effect of the irradiation time on the catalyst loading was investigated in more detail with various cinchona alkaloid-derived catalysts **81**, **82** and **83** (Figure 4-6). Although the styrene-modified catalyst **82** has been confirmed to be sensitive under photochemical and free-radical reaction conditions, the three different catalysts were screened to see the effect of the functional groups under different photochemical reaction conditions. By changing the irradiation time, all three catalysts showed the highest catalyst loading at 20 minutes of irradiation time. This result could indicate that long irradiation time was required for the high catalyst loading on the textile. However, extended irradiation with UV-light is not beneficial, probably due to decomposition of the catalyst. Therefore, optimization of the irradiation conditions for each catalyst might be necessary. Higher catalyst loading was achieved in the case of catalyst **83**. Relatively lower catalyst loading was observed with **81** and **82** catalysts. Particularly, catalyst **82** showed an extremely low catalyst loading, which could be ascribed to the random polymerization with two different “polymerizable” centers, resulting in film formation *via* non-covalent bonding immobilization on the surface. It is noteworthy that all the catalysts were washed with various organic solvents after the immobilization reaction (methanol, dichloromethane and acetone) to remove non-bound polymeric materials before analysis and application to asymmetric catalysis.

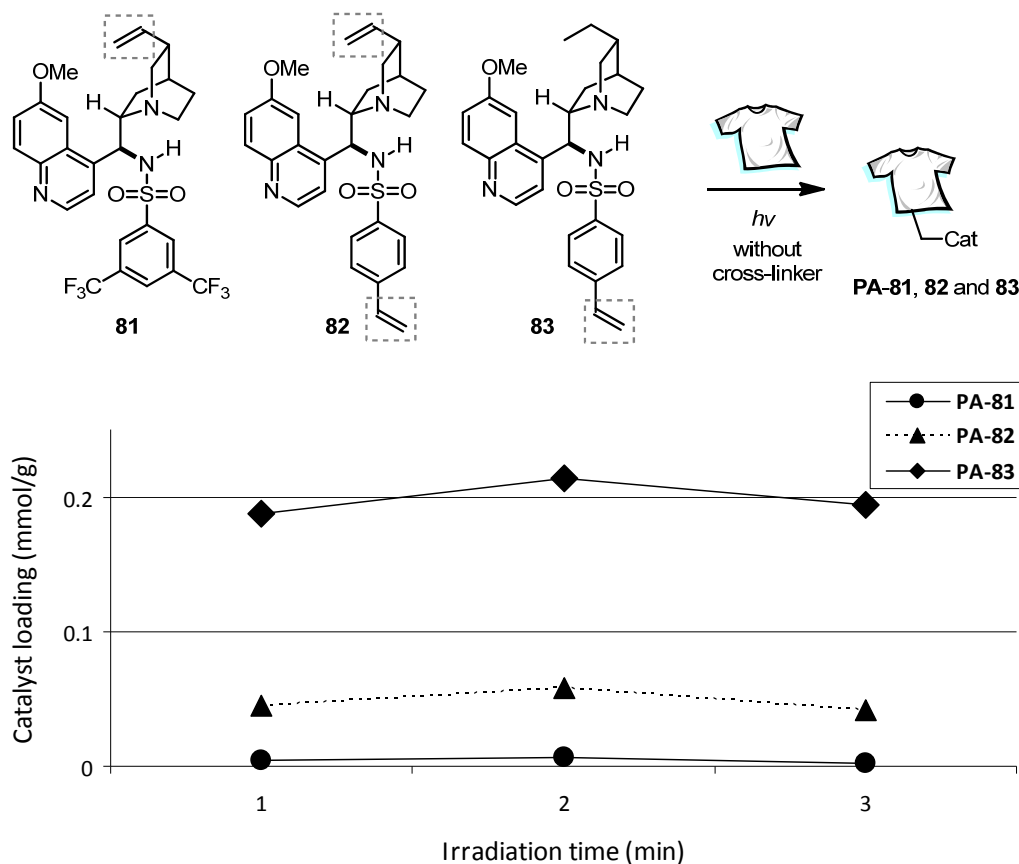


Figure 4-6. Relationship between irradiation time and catalyst loading. (See entries 2-4 in Table 4-10 for details)

4.3.7. Application of Textile Organocatalysts

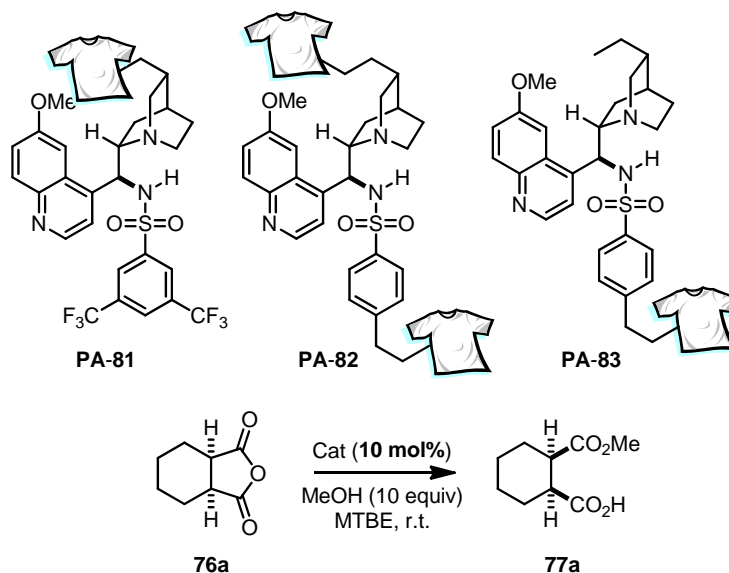
The catalytic activity and enantioselectivity of the prepared catalysts is summarized in Table 4-10. With catalyst **PA-81**, as depicted in Figure 4-6, the highest catalyst loading on the textile was achieved by irradiating for 20 minutes. The enantioselectivity of the textile catalyst **PA-81** was higher than the other catalysts with different irradiation time (entry 3, 69:31 er). Even after longer irradiation time (30 min) with higher monomer concentration (0.25 mmol/g of textile) for the immobilization reaction, the catalyst loading was lower than the result with shorter irradiation time (compare entries 3 and 5). However, the catalyst showed better enantioselectivity (entry 5, 77:23 er). In the presence of crosslinker PETA for the immobilization, the catalyst loading on the textile was not improved (0.146 mmol/g) and the enantioselectivity decreased considerably (47:53 er, entry 6).

In the case of catalyst **PA-83**, generally lower catalyst loading on textile material was observed (0.03-0.042 mmol/g, **PA-81**: 0.070-0.214 mmol/g, entries 13-16). However, the catalyst derived from short irradiation time (10 min) showed surprisingly a high enantioselectivity (86.5:13.5 er, entry 13). No significant improvement was observed by increasing the concentration of monomer **83** and irradiation time for the immobilization reaction (entries 14-16). Moreover, the immobilization with longer irradiation time in the presence of PETA cross-linker afforded a large film formation, resulting in no catalyst loading on the textile (entries 12 and 18). Unfortunately, catalyst **PA-82** showed unacceptable catalyst loading without cross-linker (entries 7-12) and showed no

4. RESULTS AND DISCUSSION

significant activity in the desymmetrization of *meso*-anhydride **76a**. The immobilization reaction with crosslinker showed no improvement in terms of catalyst loading and catalytic activity (entry 14).

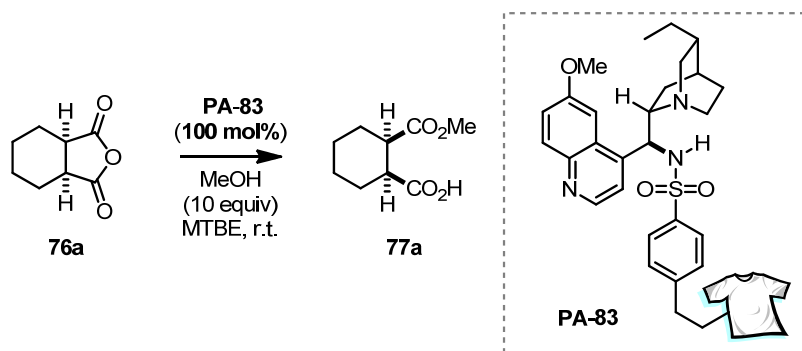
Table 4-10. Relationship between monomers structure and enantioselectivity.



Time (min)	Conc. (mmol/g)	Entry	PA-81		PA-82			PA-83		
			Cat loading (mmol/g)	er	Entry	Cat loading (mmol/g)	er	Entry	Cat loading (mmol/g)	er
10	0.05	1	0.002	-	7	0.030	86.5:13.5	13	0.166	56.5:43.5
10	0.1	2	0.004	-	8	0.045	80:20	14	0.188	62.5:37.5
20	0.1	3	0.007	-	9	0.058	73.5:26.5	15	0.214	69:31
30	0.1	4	0.002	-	19	0.042	76.5:23.5	16	0.194	66:34
30	0.25	5	0.014	-	11	n.d.	-	17	0.070	77:23
30	0.1	6*	0.001	-	12*	n.d.	-	18*	0.146	47:53

*Catalyst was prepared in the presence of PETA (0.03 mmol/g of textile)

Although the obtained enantioselectivities were not satisfactory, the catalysts were used for the recycling experiments to investigate their stability. As summarized in Table 4-11, catalyst **PA-83** was tested for a second cycle with 100 mol% of catalyst loading to confirm its maximum enantioselectivity and higher enantioselectivities were observed in all cases. However, the enantioselectivities were still lower than in the homogeneous reaction conditions with less than 5 mol% of catalyst loading (with catalyst **81** 97:3 er was observed). Surprisingly, the catalyst prepared with cross linker (PETA) showed the opposite sense of enantioinduction (40:60 er) compared to the other catalysts and homogeneous systems (entry 6). This result implies that the catalyst is immobilized in a different mechanism to generate a completely different chiral environment. Therefore, we kept in mind that the cross-linker could affect the conformation of the catalyst on the surface by offering a different polymerization pathway.

Table 4-11. Recycling experiment of catalyst **PA-83**.

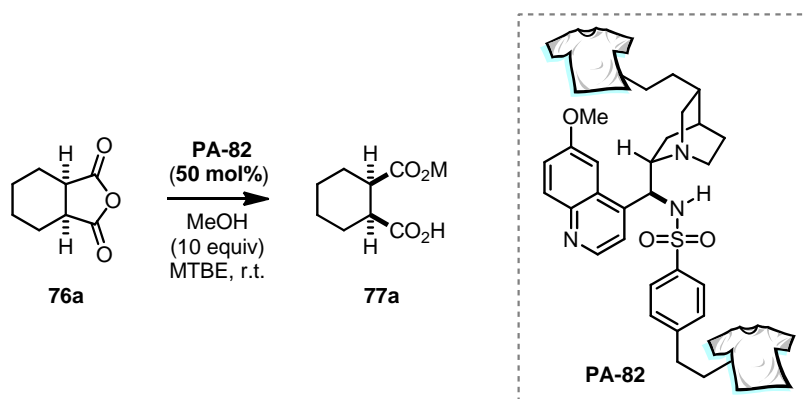
entry	Time (min)	Conc. (mmol/g)	Cat loading (mmol/g)	er 1 st cycle	er 2 nd cycle ^a
1	10	0,05	0,166	56.5:43.5	73.5:26.5
2	10	0,1	0,188	62.5:37.5	77.5:22.5
3	20	0,1	0,214	69:31	84:16
4	30	0,1	0,194	66:34	86:14
5	30	0,25	0,070	77:23	86:14
6*	30	0,1	0,146	47:53	40:60

*The catalyst was prepared in the presence of PETA (0.03 mmol/g of textile). ^a100 mol% of catalyst was used.

The next recycling experiment was performed with catalyst **PA-82**. As shown in Table 4-12, the desymmetrization reaction was conducted by using 50 mol% of textile catalyst. Although the catalyst loading was increased to 50 mol% from 10 mol%, the enantioselectivities of catalyst **PA-82** showed no significant improvement. The catalysts prepared with shorter irradiation time and higher monomer concentration (**82**) showed superior performance in terms of enantioselectivity (entries 2 and 3). Until the third recycling experiment, the catalysts showed no erosion of activity and enantioselectivity. These results prompted us to develop more enantioselective textile catalysts which generate an identical chiral environment without forming a film on the surface. Until now, the major problem of the immobilization method was film formation due to non-selective polymerization. This reaction was most significant when the cross-linker was employed. Although catalyst **PA-82** in Table 4-10 did not provide any appreciable amount of catalyst loading on the surface, we decided to utilize the irradiation conditions from Table 4-9 (double irradiation) for the catalyst **81** since the reaction conditions greatly improve catalyst loading. Since catalyst **81** is the most active and enantioselective as a homogenous catalyst, we focused on the optimization of the preparation of the textile catalyst with **81** with reasonable catalyst loading.

4. RESULTS AND DISCUSSION

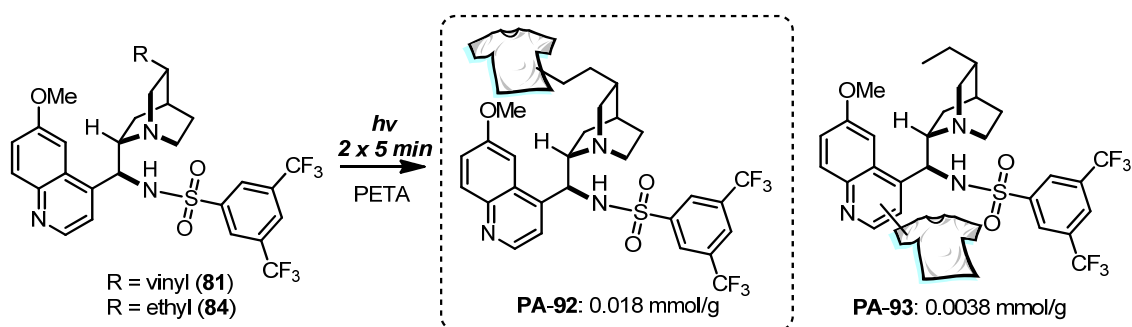
Table 4-12. Recycling experiment of catalyst **PA-82**.



Entry	Time (min)	Conc. (mmol/g)	Cat loading (mmol/g)	PA-82		
				er 1 st cycle	er 2 nd cycle ^a	er 3 rd cycle ^a
1	10	0,05	0,030	86.5:13.5	89:11	
2	10	0,1	0,045	80:20	92:8	92.5:7.5
3	20	0,1	0,058	73.5:26.5	92.5:7.5	94:6
4	30	0,1	0,042	76.5:23.5	90:10	-
5	30	0,25	n.d.	-	-	-
6*	30	0,1	n.d.	-	-	-

*Catalyst was prepared in the presence of PETA (0.03 mmol/g of textile). ^a50 mol% of catalyst was used.

To fulfill this purpose, textile immobilized bifunctional catalysts **PA-92** and **PA-93** were prepared using double irradiation conditions in the presence of crosslinker PETA. Notably, catalyst **81** showed a reasonable catalyst loading, which was confirmed by elemental analysis and XPS measurements in the presence of cross-linker PETA. Interestingly, catalyst **84** could also be immobilized under identical photochemical reaction conditions albeit with lower catalyst loading (0.0038 mmol/g, **PA-93**). We presumed that this “background” immobilization, without olefin functional group, could be attributed to random polymerization with the electron-rich quinoline ring, although concrete mechanistic supports have yet to be found. Nonetheless, literature procedures using free-radical reaction conditions support that the reaction occurs mainly in the olefin functional group.¹²⁹



Scheme 4-44. Immobilization of sulfonamide-based catalyst **81** and **84**.

The presence of sulfur and fluorine atoms was clearly confirmed by XPS measurements. As shown in Figure 4-8, blank polyamide material showed no considerable amount of fluorine and sulfur in contrast to catalyst PA-92 in Figure 4-7.

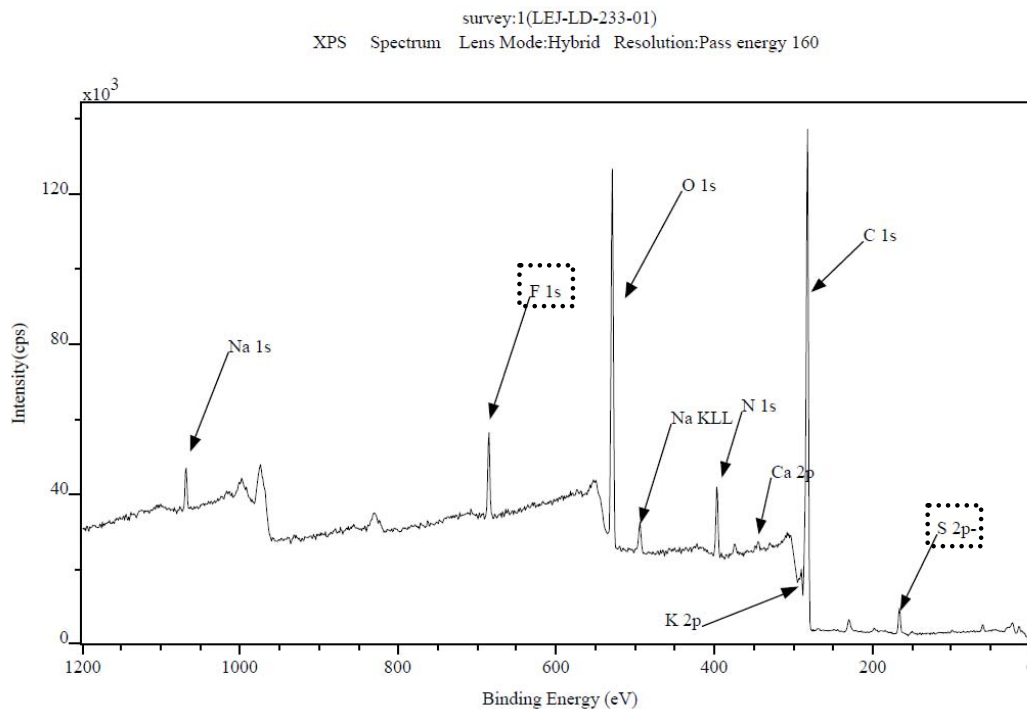


Figure 4-7. XPS spectrum of catalyst PA-92.

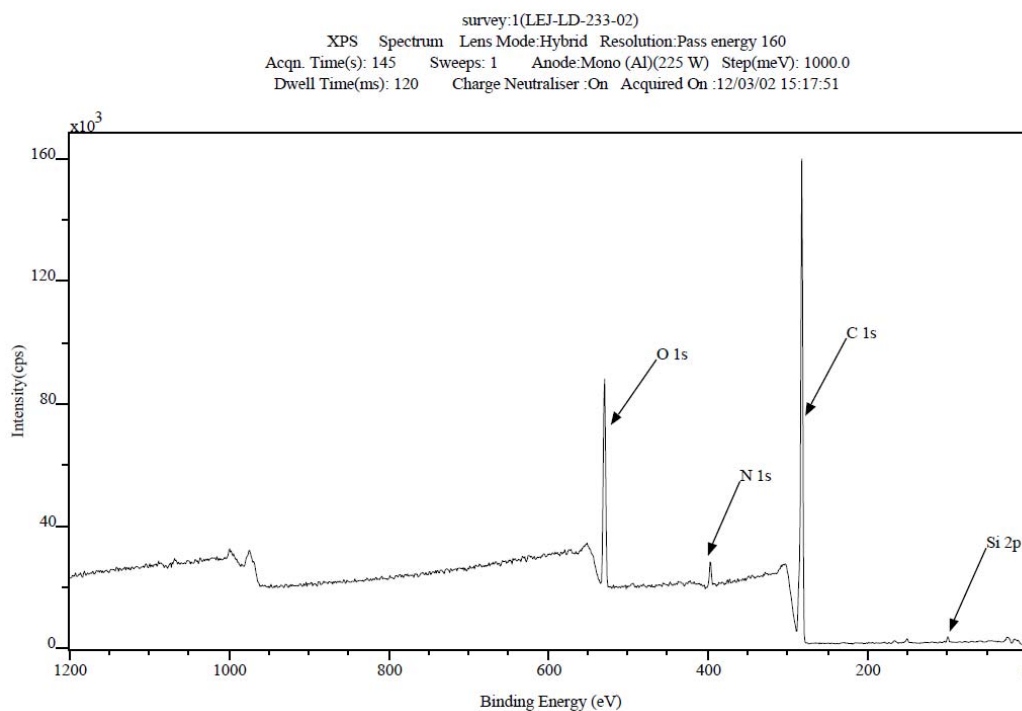


Figure 4-8. XPS spectrum of blank polyamide.

4. RESULTS AND DISCUSSION

Further SEM (scanning electron microscopy) revealed that the catalyst showed no significant defects on the surface and no non-selective film formation (Figure 4-9). At this stage, the catalyst could not be characterized by SEM with higher resolution due to the roughness of the catalyst's surface. Further studies using spin coating of textile catalyst on silicon wafer for high resolution AFM and SEM analysis will be conducted in the future (by Dr. Thomas Mayer-Gall).

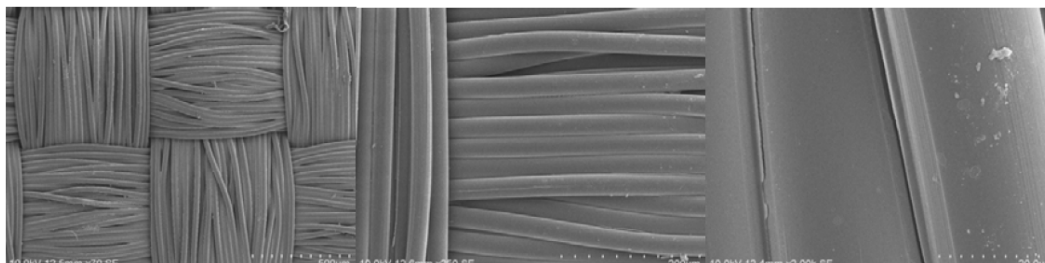
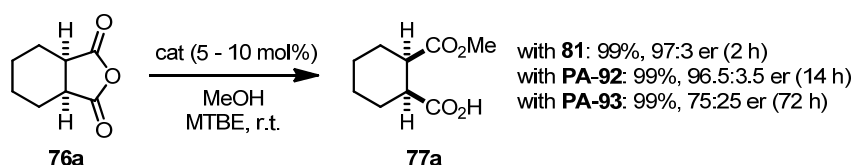


Figure 4-9. Low resolution SEM images of catalyst PA-92.

The catalytic activity was tested in the desymmetrization reaction of *meso*-anhydride **76a**. As summarized in Scheme 4-45, catalyst PA-92 showed comparable enantioselectivity to the corresponding homogeneous catalyst **81** (**81**: 97:3 er, PA-92: 96.5:3.5 er). This encouraging result could be explained by the modular immobilization of the monomeric catalyst **81** in the presence of cross-linker PETA. Moreover, the shorter irradiation time during the immobilization reaction could prevent possible decomposition and/or partial modification of the catalyst. Although the recovered monomeric catalyst showed no significant change by ¹H NMR analysis, longer irradiation clearly provided a negative effect on the catalyst loading and its activity and enantioselectivity (Figure 4-6).

Textile catalyst PA-92 prepared from monomer **84** which lacks the olefin moiety showed inferior results in terms of enantioselectivity (75:25 er, Scheme 4-45). Therefore we concluded that the catalyst with the olefin moiety induces highly selective immobilization. In the absence of the olefin group, the immobilization can occur randomly and generate a non-selective chiral environment, resulting in lower enantioselectivity.



Scheme 4-45. Desymmetrization of *meso*-anhydride **76a** using textile catalysts PA-92 and PA-93.

These findings led us toward understanding of the immobilization mechanism. In the case of the catalyst with styrene as a “polymerizable” center, the given high radical stability of benzylic radical leads to the self-polymerization without anchoring the catalyst to the textile surface individually. This polymerization indeed generates film formation on the surface. Therefore, the catalytically active site could be oriented in a somehow crowded environment due to random polymerization although a large amount of chiral catalyst could be immobilized on the surface (Figure 4-10). The result in Table 4-11 (entry 6) with the opposite sense of enantioselectivity underscores the alteration of the chiral environment through non-selective polymerization.

In some cases, the polymerization could be beneficial due to the cooperative effect of two catalysts in the transition state.¹³⁰ In our case, the bifunctional catalyst could be deactivated through acid-base interaction. Therefore, proximal interaction of each chiral catalyst should be prevented to increase catalytic activity and enantioselectivity. Moreover highly branched polymeric catalysts could be problematic in terms of recyclability because if a chemical bond between the solid support and organic polymer is cleaved, larger amounts of the chiral catalyst will be leached out.

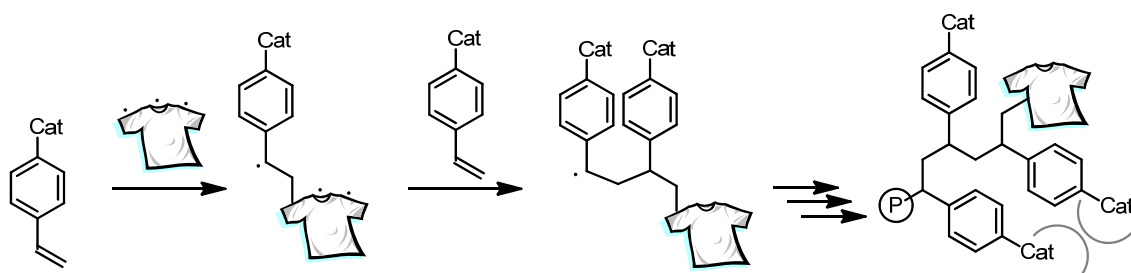


Figure 4-10. Immobilization reaction with styrenyl substituent under photochemical reaction conditions.

Figure 4-11 shows a textile catalyst, which suffers from significant film formation. The polymeric catalyst on the surface could be mechanically unstable under reaction conditions. This property of the textile catalyst could result in low recyclability.

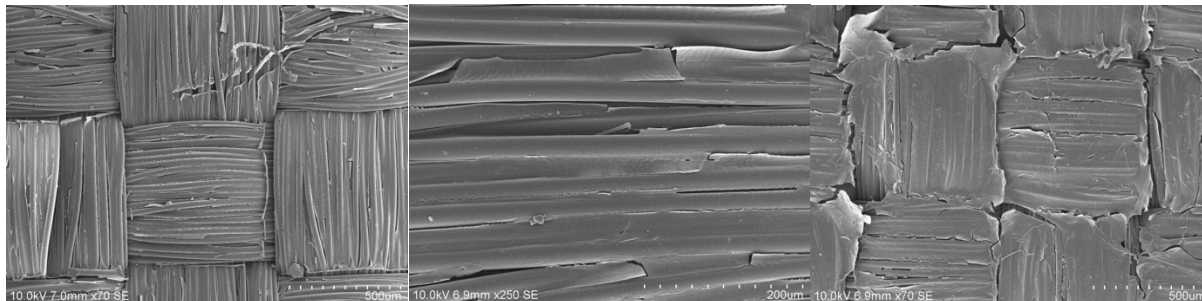


Figure 4-11. SEM images of textile surface with severe film formation.

In this context, the immobilization reaction with catalyst **81** showed advantages over the styrene functional group (Figure 4-12A). First, the relatively low reactivity of the olefin could significantly decrease free-radical polymerization of the catalyst itself. Therefore, each catalyst monomer can anchor to the solid surface *via* covalent bonding, which will eventually increase the stability of the textile catalyst dramatically. Moreover, each catalyst can retain its chiral environment individually. By employing a cross-linker properly, the space between the catalyst and solid support could be controlled (Figure 4-12B). All these advantages can explain the obtained high enantioselectivity of catalyst **PA-92** under heterogeneous reaction conditions. Therefore we decided to further investigate the stability of the textile catalyst by repeating asymmetric catalysis with the same catalyst.

4. RESULTS AND DISCUSSION

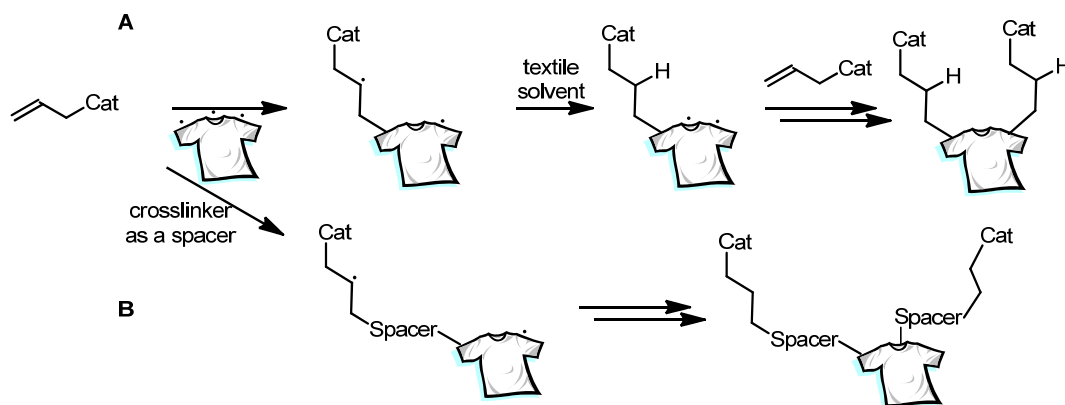


Figure 4-12. Immobilization reaction with olefin substituent under photochemical reaction conditions (A) without cross-linker, (B) with cross-linker as spacer.

With the highly enantioselective textile catalyst **PA-92**, subsequent recycling experiments were conducted. As shown in Figure 4-13, the catalyst presents indefinite stability under the reaction conditions. More than 250 cycles of asymmetric catalysis were achieved by using a single textile catalyst sheet. The detailed reaction conditions can be found in Chapter 7.8.6. The catalyst loading was varied by changing the amount of the substrate since we used the same catalyst in the glass vial for all the recycling experiments. The highest enantioselectivity (98:2 er) was obtained by using 30 mol% of catalyst loading (cycle 3) and the lowest enantioselectivity was observed (81:19 er) when 1 mol% of catalyst was used (cycle 8). During the recycling experiments, reaction conditions were optimized by varying the concentration of substrate and the equivalents of methanol. In all cases, quantitative yields of the desired hemiester were observed by checking ^1H NMR spectrum of the crude reaction mixture after decanting and evaporating the solvent. After each cycle, the catalyst was washed with MTBE (10 mL x 3) and then simply dried over airflow. Further recycling experiments were conducted by using 10 - 50 mol% of catalyst loading but showed no significant difference in terms of activity and enantioselectivity. To show the fate of catalyst **PA-92** we selected the reaction conditions which give a higher er than 95:5 with a minimum amount of catalyst. With 6 -7 mol% of catalyst loading, a higher er than 95:5 was achieved by using 6 equivalents of methanol as the nucleophile. The amount of the solvent (MTBE) was fixed to 14 mL. The catalytic activity and enantioselectivity diminished very slowly under these reaction conditions. After 150 cycles, an enantiomeric ratio of 94:6 er was frequently observed. Furthermore, after 230 cycles, the average enantiomeric ratio for 10 cycles was 93.5:6.5 er. This slight decrease in enantioselectivity could simply be compensated by using 10 mol% of catalyst loading (95:5 er, 231st cycle). It should be noted here that this degree of recyclability with such a robust catalyst maintaining excellent levels of selectivity has never been observed in heterogeneous organocatalysis. During more than 200 recycling experiments, none of the reactions failed. This result underlined our methodology as a powerful and extremely convenient tool for the immobilization of catalysts. Further applications of our methodology to the preparation of solid supported reagents would be desirable.

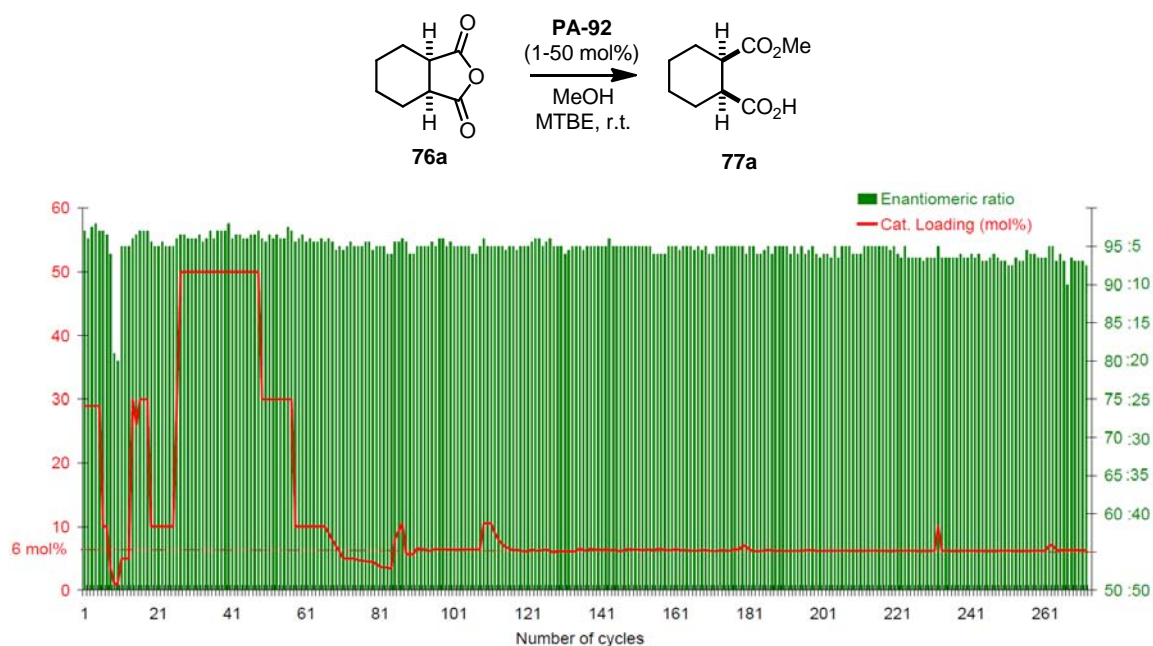


Figure 4-13. Recycling experiments of catalyst **PA-92** for the desymmetrization reaction of *meso*-anhydride **76a**.

As already shown in Figure 4-9 and Figure 4-11, the film formation on the surface of textile catalyst **PA-92** was remarkably lower, as confirmed by low resolution SEM spectroscopy (LRSEM, low resolution SEM, compare the images from Figure 4-11). Moreover, mechanic stability of the catalyst was confirmed by checking LRSEM, which shows no significant alteration of the structure on the surface after several recycling experiments. This observation supports our hypothesis that the degree of film formation could be inversely proportional to the recyclability of the textile catalyst. Having uniform polymerization on the surface could indeed lead to a robust textile catalyst, which can be used for indefinite cycles for asymmetric catalysis.

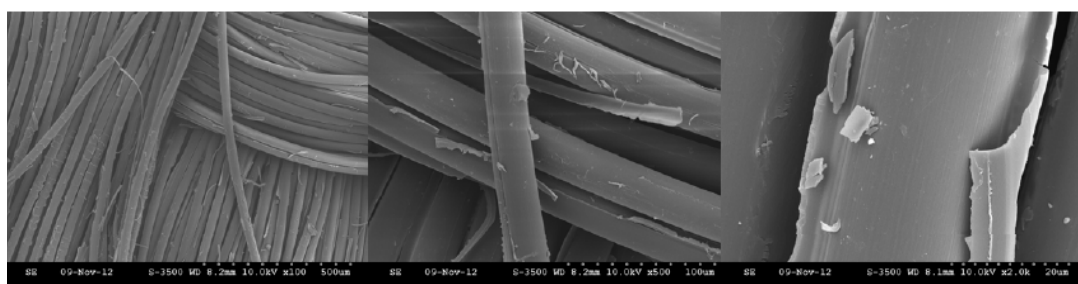
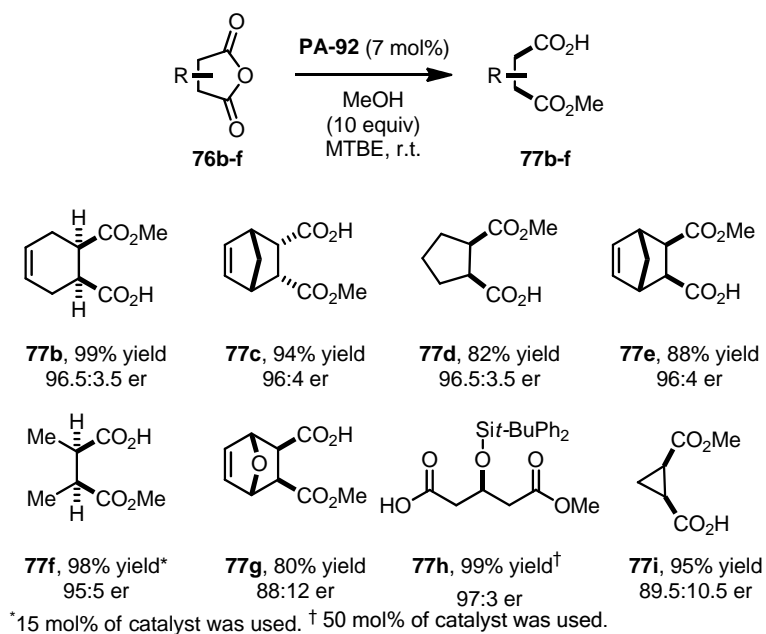


Figure 4-14. Low resolution SEM images of **PA-92** catalyst after several recycling experiments.

After obtaining successful results with catalyst **PA-92**, we decided to explore the substrate scope of the heterogeneous catalyst. A total of eight sheets of **PA-92** were prepared and analyzed by elemental analysis to determine the catalyst loading and showed similar values in all cases (See analysis data in Chapter 7.6). For the substrate scope, we used 7 mol% of catalyst loading and 10 equivalents of methanol in MTBE. As expected, high enantioselectivity (up to 96.5:3.5 er) was obtained for various cyclic anhydrides (Scheme 4-46). Bi- and tricyclic anhydrides (**76b-e**) required longer reaction time due to the steric effect, particularly for the oxygen-

4. RESULTS AND DISCUSSION

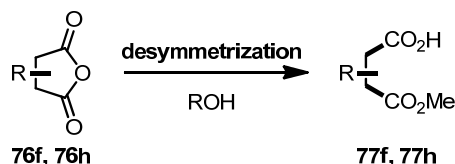
containing substrate (**77g**, 88:12 er, 72 h). Monocyclic *meso*-anhydrides were also tested, however, they gave lower enantiomeric ratios (**77f**, **77h** and **77i**). By increasing the catalyst loading, higher enantioselectivities were observed in the case of dimethyl succinic anhydride (**76f**) and glutaric anhydride derivatives (**76h**).



Scheme 4-46. Substrate scope for the desymmetrization of *meso*-anhydrides using catalyst **PA-92**.

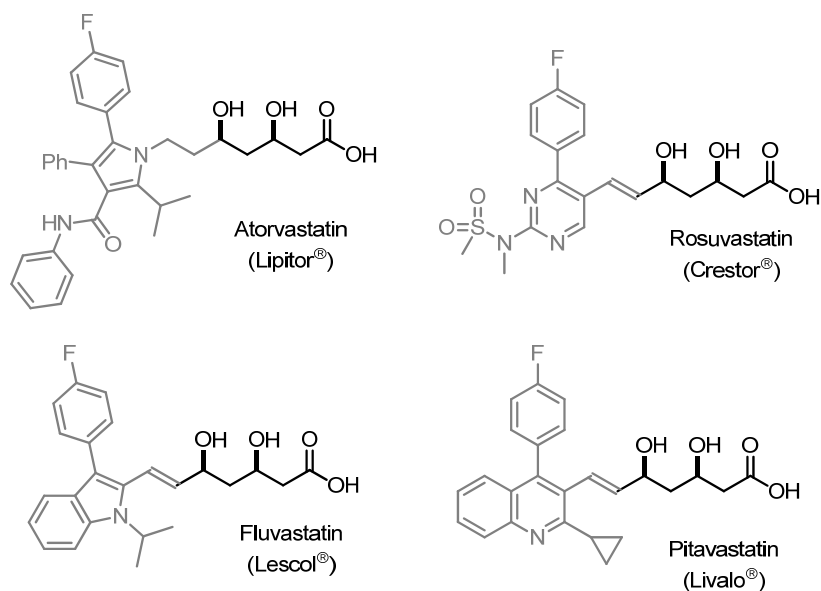
4.3.8. Application of Textile Organocatalysts to Continuous Reaction

We were particularly interested in the optimization of reaction conditions for monocyclic anhydrides. Succinic and glutaric *meso*-anhydrides can be converted to enantiomerically pure dicarbonyl compounds through desymmetrization with nucleophiles (Scheme 4-47).



Scheme 4-47. Desymmetrization of monocyclic *meso*-anhydrides.

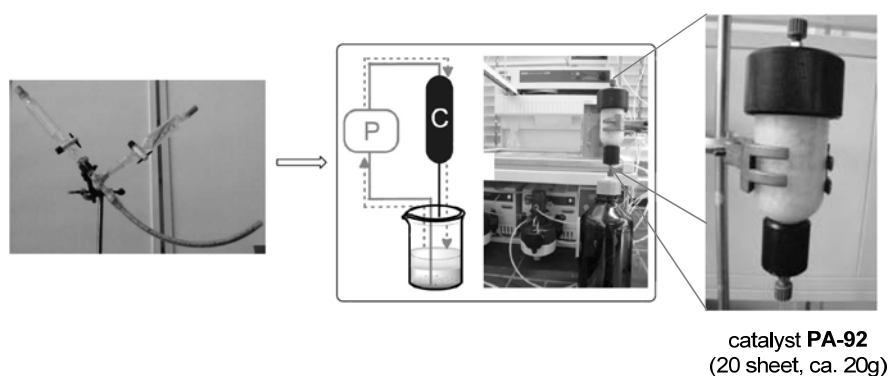
Moreover, the conversion of 4-hydroxy glutaric anhydride **76h** to the corresponding hemiemester **77h** is a highly important transformation since the obtained product can be used for the synthesis of statin derivatives, clinical drugs for lowering cholesterol levels (Scheme 4-48). Statins, for example Atorvastatin (Lipitor®) generated more than 10 billion dollars revenue each year after 2011. All the statin derivatives contain a β,δ -hydroxy carboxylic acid moiety which is derived from 4-hydroxy glutaric anhydride as a precursor in nature. We believed that our methodology could provide a practical approach to this class of molecules.



Scheme 4-48. Structures of statin derivatives, blockbuster drugs.

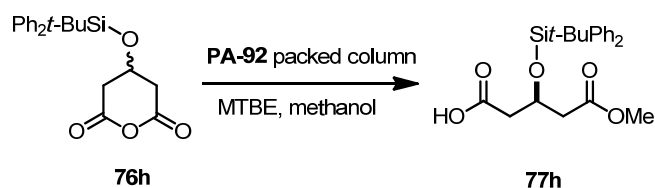
4. RESULTS AND DISCUSSION

As shown in Scheme 4-49, the textile catalyst **PA-92** was applied to the continuous reactor system. Due to the flexibility and stability of the textile catalyst, we could prepare a “catalytic PET tube” by putting the textile catalyst in the PET tube and using it as a column for continuous reaction. To control the flow rate more precisely, we adopted a MPLC (medium performance liquid chromatography) equipment to install the textile catalyst. The textile catalyst (20 sheets, ca. 20 grams) was packed into the empty BÜCHI cartridge. The reaction mixture was circulated by a pump and supplied back to the reaction mixture batch. This reaction set-up is believed to be more efficient than conventional reactions with glass flask and stirring.



Scheme 4-49. Continuous fixed-bed reactor containing a column packed with catalyst **PA-92**.

To confirm this hypothesis, we conducted various experiments with the fixed-batch reactor with the **PA-92** packed column in the MPLC system and the batch reaction system. The reaction was conducted using 1-2 gram of substrate **76h** in MTBE as a solvent. The amount of methanol was increased to 30 equivalents to improve the reaction rate due to the relatively low reactivity of the silylated glutaric anhydride **76h**. As shown in entry 1, Table 4-13, with a batch system and magnetic stirring only low conversion was observed after 66 h (25% conversion) in low enantioselectivity (85.5:14.5 er). Having a MPLC fixed-batch continuous reactor system, the flow rate for the desymmetrization reaction was screened. By increasing the flow rate from 3 to 7.5 mL/min, the conversion and enantioselectivity of the process is higher (entries 2-4, up to 93.5:6.5 er). Increasing the concentration afforded the product in lower enantioselectivity (93:7 er) with a similar reaction rate (entry 5). Further increase of the flow rate provided a lower reaction conversion and enantioselectivity (61% conversion, 89:11 er, entry 6), perhaps due to the less efficient mass transfer. With an optimal flow rate (7.5 mL/min) excellent enantioselectivity was obtained, by decreasing the amount of the substrate from 2 gram to 0.87 gram (entry 10). As shown in Scheme 4-50, the continuous reactor was iteratively used after washing the column with additional MTBE. More than 10 cycles were conducted under optimized reaction conditions to give enantioenriched hemiester **77h** in quantitative yield (99% yield and up to 97:3 er, Figure 4-15).

Table 4-13. Optimization of the reaction conditions for the fixed-bed reactor.

Entry	Flow rate (mL/min)	Substrate amount (76h) (g)	Time	Conversion (%)	er
	0				
1 ¹	(batch system with stirring)	2 g	66h	25%	85.5:14.5
2	3	2 g	66h	39%	87.5:12.5
3 ²	5	2 g	68 h	50%	90.5:9.5
4	7.5	2 g	60h	73%	93.5:6.5
5 ³	7.5	2 g	50h	67%	93:7
6	12.5	2 g	64h	61%	89:11
7 ²	25	1 g	22 h	90%	96:4
8 ³	25	1 g	48 h	99%	96:4
9 ²	12.5	1 g	21h	98%	96:4
10 ²	7.5	870 mg	22h	95%	97.5:2.5

*Reaction conditions: substrate and MeOH (30 equiv) in MTBE (200 mL) were circulated through a catalyst **PA-92** packed column (20 sheets) at room temperature. Conversions were detected by analyzing ¹H NMR spectra. ¹The reaction was carried out in an 500 mL Erlenmeyer flask with a magnetic stirring bar. Otherwise, all the reaction parameters were identical. ²The reaction was carried out with 100 mL MTBE. ³The reaction was carried out under diluted conditions (MTBE 150 mL).

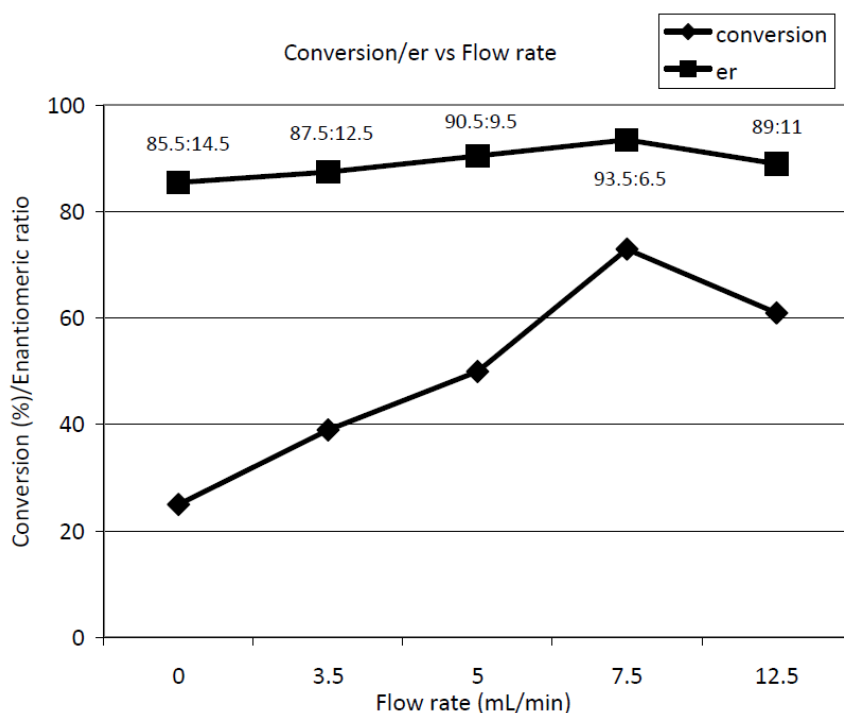
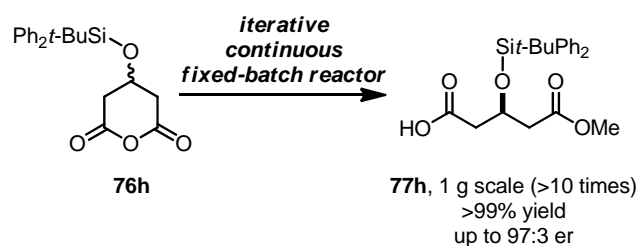


Figure 4-15. Graphical representation of Table 4-13.



Scheme 4-50. Iterative continuous fixed-bed reaction for the desymmetrization of anhydride **76h**.

The reaction conditions of the MPLC-fixed bed reactor are remarkable, since the catalyst shows high robustness and high pressure could be applied in the system. There is no leaching-out of catalyst to the organic solution. The desired product was simply purified by evaporating the remaining solvent and methanol without further purification. This methodology clearly shows practical advantages over the conventional polymeric catalyst. No special concern was required for the preparation of the catalyst and further application in asymmetric catalysis. Therefore we became interested in other organocatalysts which could be potentially useful after immobilization.

4.3.9. Preparation of Various Textile Organocatalysts

Based on the previous results, we decided to demonstrate the generality of our immobilization methodology by preparing various textile catalysts. As shown in Figure 4-15, although we have already achieved excellent results with a bifunctional organocatalyst, sulfonamide catalyst **81-85**, there are numerous different classes of organocatalysts. Therefore, we focused on the preparation of various textile organocatalysts which can potentially be applied in organic synthesis.

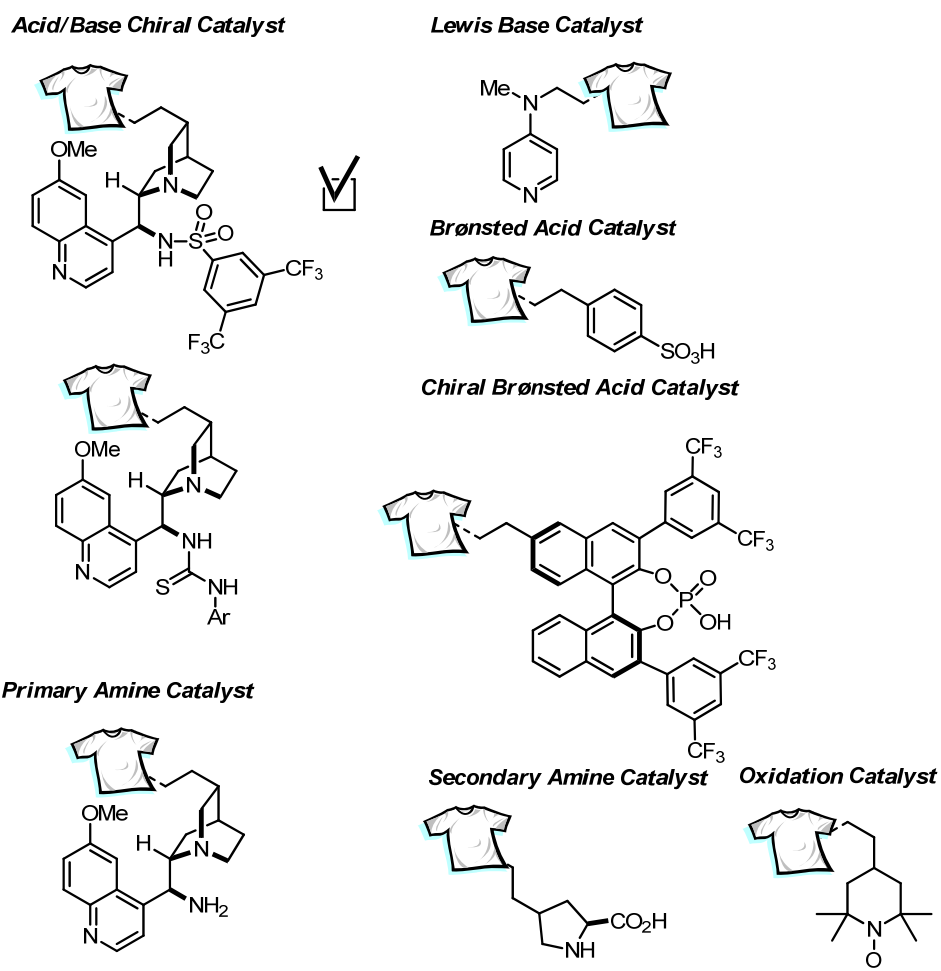
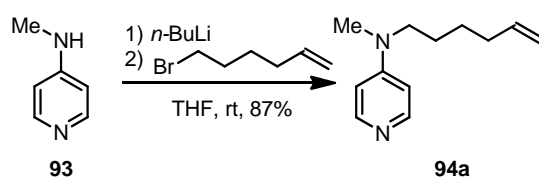


Figure 4-16. A schematic plan for the preparation of various textile organocatalysts.

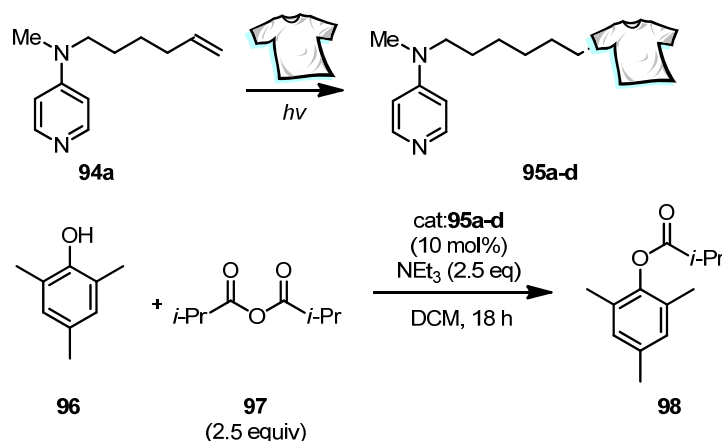
4.3.10. Preparation of DMAP Related Textile Organocatalysts and Their Applications

Due to the wide use of DMAP derivatives in organic synthesis as Lewis basic acyl transfer catalysts,¹³¹ we decided to investigate DMAP derivatives as candidates for the immobilization on textile materials. Although DMAP possesses a highly electron rich, photo-labile pyridine moiety, we commenced our investigation with an olefin functionalized DMAP derivative (**94**) to induce a specific immobilization of the olefin functionality. The substrate **94a** was easily prepared by treating 4-methylaminopyridine (**93**) with *n*-BuLi followed by alkylhalide. The desired product **94a** was obtained with good yield after silica chromatography (Scheme 4-51).



Scheme 4-51. Preparation of DMAP derivative **94a**.

The optimization of the immobilization reaction conditions was conducted, as summarized in Table 4-14. Since we had already optimized various parameters for the immobilization with bifunctional catalyst **94a**, we briefly checked the irradiation time and number of repetitions as well as the effect of cross-linker PETA with polyamide as a solid support. Gratifyingly, catalyst **PA-95** was obtained with a similar catalyst loading to **PA-92** (0.01136 mmol/g), after the repeated irradiation sequences in the presence of PETA (entry 2). In this case longer irradiation time provided only a slightly diminished catalyst loading. With the catalyst in our hands (**95a-d**), we investigated the catalytic activity in the acyl transfer reaction with sterically bulky phenol **96** and acyl donor **97** using catalysts **95a-d**. As expected, catalyst **PA-95b** showed superior activity for the acylation reaction compared to the other catalysts (entry 2). Higher “catalyst loading” could directly imply higher catalytic activity, although the same amount of the catalyst was used for the catalytic transformation (10 mol%). We presumed that the presence of the cross-linker during the immobilization could improve the flexibility of the catalyst by positioning the catalyst away from the solid support, which could provide higher efficiency of the mass-transfer of substances during the catalysis.

Table 4-14. Optimization of immobilization reaction conditions for **94a**.

Entry	94a (mmol/sheet)	Irradiation time (repeat N° x min)	PETA (mmol/sheet)	PETA: 94a	Catalyst loading (mmol/g)	Acylation conversion to 98 (%)
1	0.3	2 x 5	0	-	0,00744 (95a)	21
2	0.3	2 x 5	0.17	1 : 1.75	0,01136 (95b)	60
3	0.3	2 x 10	0	-	0,00731 (95c)	18
4	0.3	2 x 10	0.17	1 : 1.75	0,01126 (95d)	30

*ICP/OES for sulfur containing materials: After soxhlet extraction, a textile was subjected to a microwave digestion with HNO_3 (69 % ROTIPURAN® Supra) and sulphur contents was measured by ICP/OES and calibrated with Merck single element standard.

The recyclability of catalyst **PA-95b** was further investigated. As illustrated in Figure 4-17, the catalytic activity was retained for more than 10 cycles. The conversion was detected by GC/MS and confirmed by isolating the acylated product (cycles 1 and 2: 99% conversion, 95% isolated yield). It should be noted here that after the 3rd cycle, the catalytic activity diminished slightly (from 99% to 84% conversion). Loss of activity could be compensated by washing the catalyst with triethylamine after completion of the reaction (5-8th cycles: up to 99% conversion) due to the remaining acid, which can deactivate the catalyst.

4. RESULTS AND DISCUSSION

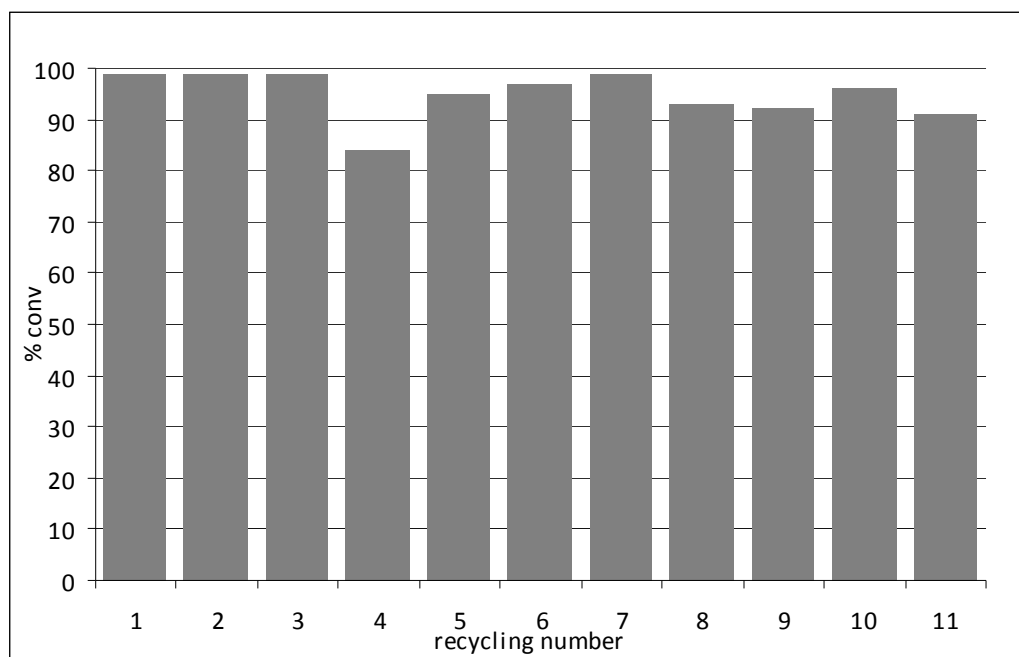
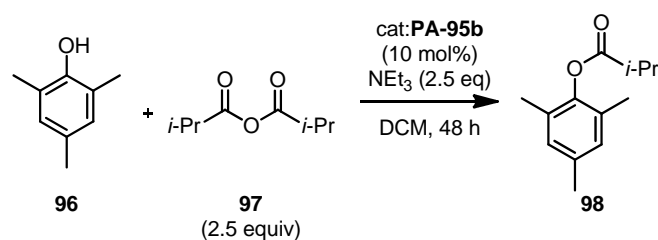
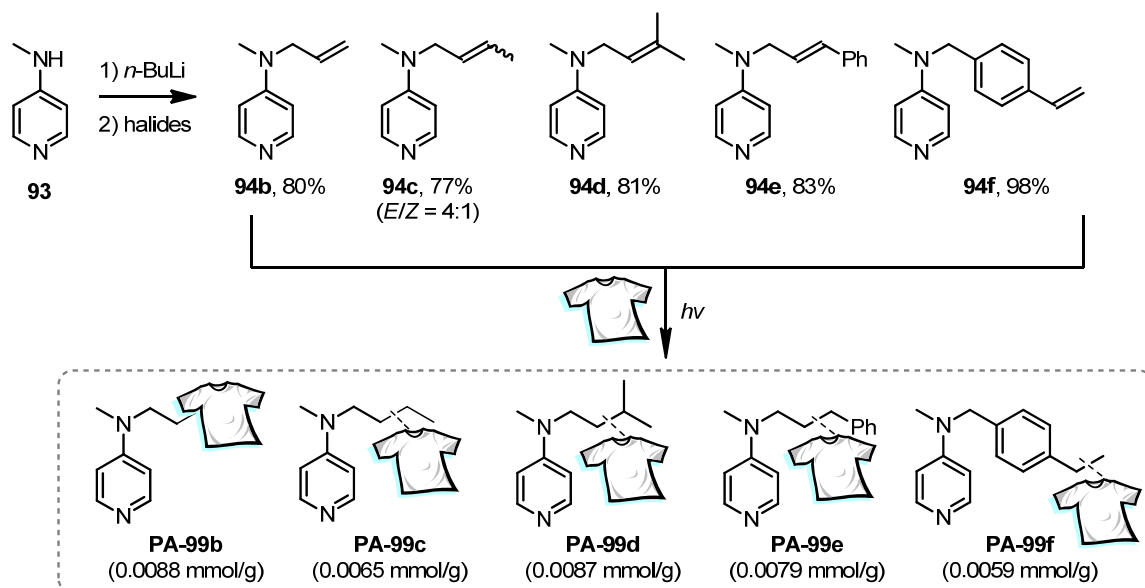


Figure 4-17. Recycling experiments of catalyst **PA-95b** for the acylation reaction of phenol **96**.

Since the DMAP derivatives are easily accessible, we decided to investigate the relationship between structure and activity of the catalysts. As summarized in Scheme 4-52, various DMAP derivatives were prepared according to the same synthetic procedure used for DMAP derivative **94a**. In general, the desired products were obtained with high yield under the reaction conditions after chromatographic purification. In the case of 2-butene-substituted DMAP derivative **94c**, an *E/Z* mixture (4:1) was isolated and used for a further immobilization step. After preparation of various DMAP derivatives, the corresponding immobilized textile catalysts were prepared according to the procedure from entry 2 in Table 4-14, which proved to be the best. All the textile catalysts **PA-99** were successfully prepared under identical photochemical reaction conditions.

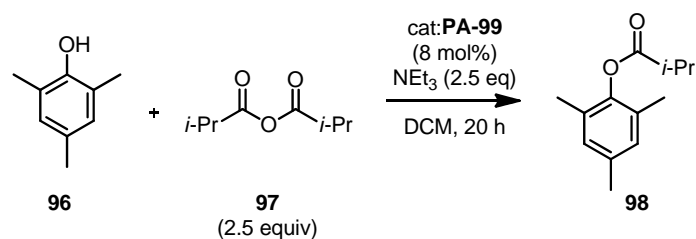


Scheme 4-52. Preparation of various DMAP derivatives **94b-f** and their immobilization.

As summarized in Table 4-15, the activity of these new catalysts was tested under identical reaction conditions (8 mol% of catalyst loading for 20 h). The conversion of the starting material, phenol, was recorded by checking GC/MS. In this case, higher catalyst loading does not guarantee higher catalytic activity. Although **PA-99b** (42% conversion, entry 1) showed the highest catalyst loading on the textile, its catalytic activity was inferior compared to **PA-99d** (64% conversion, entry 4). In Figure 4-18, a direct comparison of the relative catalyst activity is presented. A longer side chain and higher substitution on the olefin are beneficial in terms of catalytic activity as observed in the case of **PA-99b-d** (entries 1, 2, 3 and 4). This effect is quite general in heterogeneous catalysis due to a more efficient mass transfer and higher flexibility of the catalytically active site.¹³² Olefins with higher substitution can in principle provide a more stable radical intermediate, which facilitates selective immobilization without any side reaction. However, the styrene moiety gave inferior catalytic activity although the catalyst immobilization was quite efficient (**PA-99e**, entry 5). Surprisingly, parent DMAP could be immobilized even without any olefin functionality and showed comparable catalytic activity for the acylation reaction (entry 7). The immobilization reaction of DMAP itself, as well as its catalytic activity, was surprising when considering the absence of an olefin functionality. We assumed that under photochemical reaction conditions DMAP can undergo one electron oxidation and subsequent hydrogen abstraction to generate a radical species which could be immobilized on the textile. If the reaction is not productive, this species should undergo iminium formation to afford the demethylated compound. We will discuss this in the following chapter with detailed mechanistic studies on the immobilization process in Chapter 5.

4. RESULTS AND DISCUSSION

Table 4-15. Catalytic activity of various DMAP-derivatives **94** immobilized textile catalysts (**PA-95b** and **PA-99b-f**).



Entry	Monomers	Average conversion (%) ¹
1	<p style="text-align: center;">95a-d</p>	42
2	<p style="text-align: center;">PA-99b</p>	29
3	<p style="text-align: center;">PA-99c</p>	35
4	<p style="text-align: center;">PA-99d</p>	64
5	<p style="text-align: center;">PA-99e</p>	24
6	<p style="text-align: center;">PA-99f</p>	26
7	<p style="text-align: center;">PA-DMAP (0.0064 mmol/g)</p>	54

*Unless otherwise indicated, the irradiation reaction was performed by following the general procedure. Monomer **1** (0.3 mmol/sheet) was used in the presence of PETA (0.17 mmol/sheet) for 5 minutes (2 times).

¹Conversions were detected by GC/MS and ¹H NMR for phenol **96** to acylated product **98**.

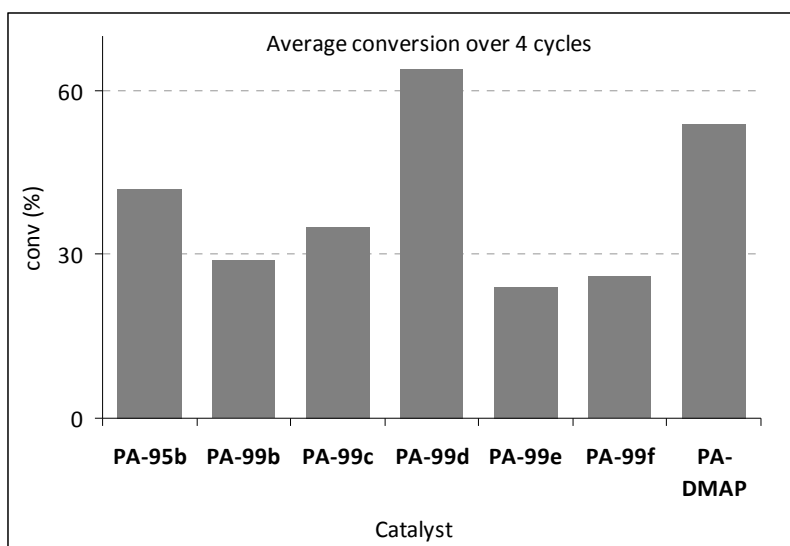
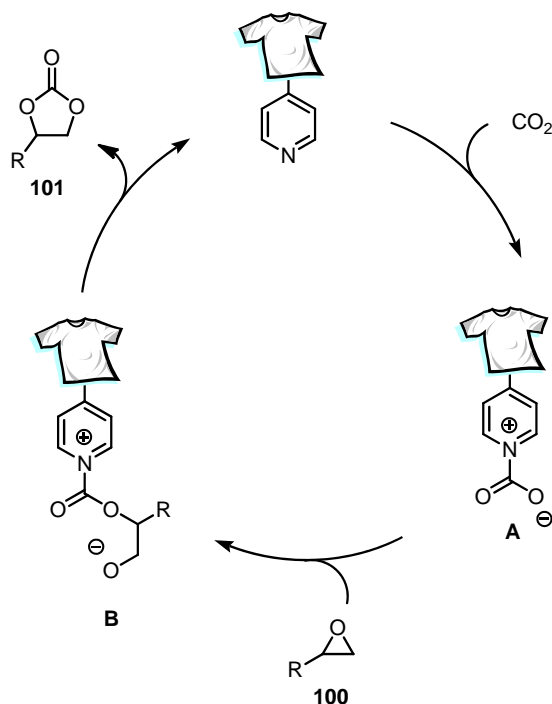


Figure 4-18. Catalytic activity of textile-immobilized DMAP derivatives **PA-95b** and **PA-99b-f**.

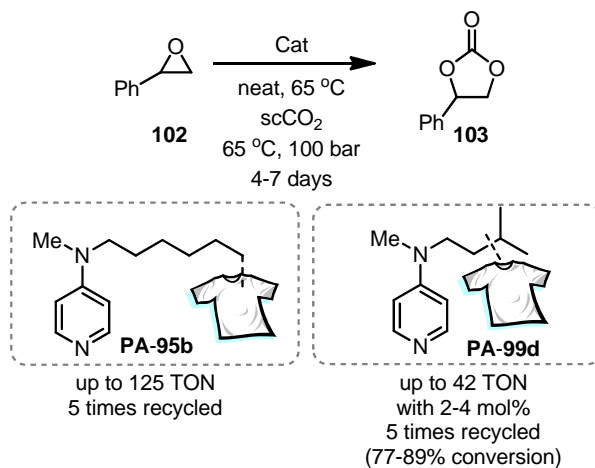
(Graphical presentation of Table 4-15)

After establishing the immobilization process with Lewis basic DMAP-derived catalysts **94**, we turned our attention to another application of DMAP catalysts. It is well known that, due to the nucleophilic nitrogen DMAP is often applied to cyclic carbonates formation reaction (Scheme 4-53). The reaction requires an epoxide **100** to react with DMAP-CO₂ adduct **A**. The subsequent ring-closing reaction can afford cyclic carbonate **101** and liberate the catalyst for the next turnover. This reaction has been investigated with various organocatalysts (DMAP, NHC and other organic bases) and transition metal complexes. Thus, we decided to apply the DMAP-derived textile catalysts for the cyclic carbonate formation reaction.



Scheme 4-53. Proposed reaction mechanism for the Lewis base-catalyzed cyclic carbonate formation reaction using a DMAP-derived textile catalyst.

After brief optimization of the reaction conditions with the two best catalysts **PA-95b** and **PA-99d**, reasonable results could be obtained for the catalytic cyclic carbonate formation reaction using epoxide and CO₂. The reaction was conducted in supercritical CO₂ at high temperature. The catalysts could be recycled without any erosion of activity and used for up to 5 cycles (Scheme 4-54). Analysis of the reaction mixture and isolation of the cyclic carbonate revealed that there is no significant polymerization reaction of the epoxide (up to 89% conversion and 85% isolated yield). **PA-DMAP-1** showed reasonable TON (up to 125). However, we could not observe high conversion (more than 80% conversion) using catalyst **PA-95b**. Although the reason for this observation is not yet entirely clear, the catalyst could be replaced by **PA-99d**, which showed the highest activity in the acylation reaction (entry 4 Table 4-15). High conversion was observed by employing 2-4 mol% of catalyst **PA-99d** to afford a clean cyclic carbonate with good conversion. Although the reactions require prolonged reaction time in general (4-7 days), this result highlights the unprecedented stability of our catalysts under harsh reaction conditions (at high temperature and pressure). Although it is still unclear how the reaction intermediate is formed and converted to the desired product, we presume that the hydrogen-bonding donor ability of the surface could contribute to stabilize the reaction intermediate. As illustrated in Figure 4-19, the pyridinium carbonate zwitterionic species could react with epoxide to afford the reaction intermediate. Then, depending on the chain length of the catalyst, the mode of stabilization of the intermediate could be different. It would be interesting to study the effect of chain length/structure of the side chain on the catalytic activity. This plausible interaction between the surface of the textile catalysts and the reaction intermediate could be applied to other catalytic systems to improve activity and even selectivity of a process.



Scheme 4-54. Cyclic carbonate formation reaction under the optimized reaction conditions using catalysts **PA-95b** and **PA-99d**.

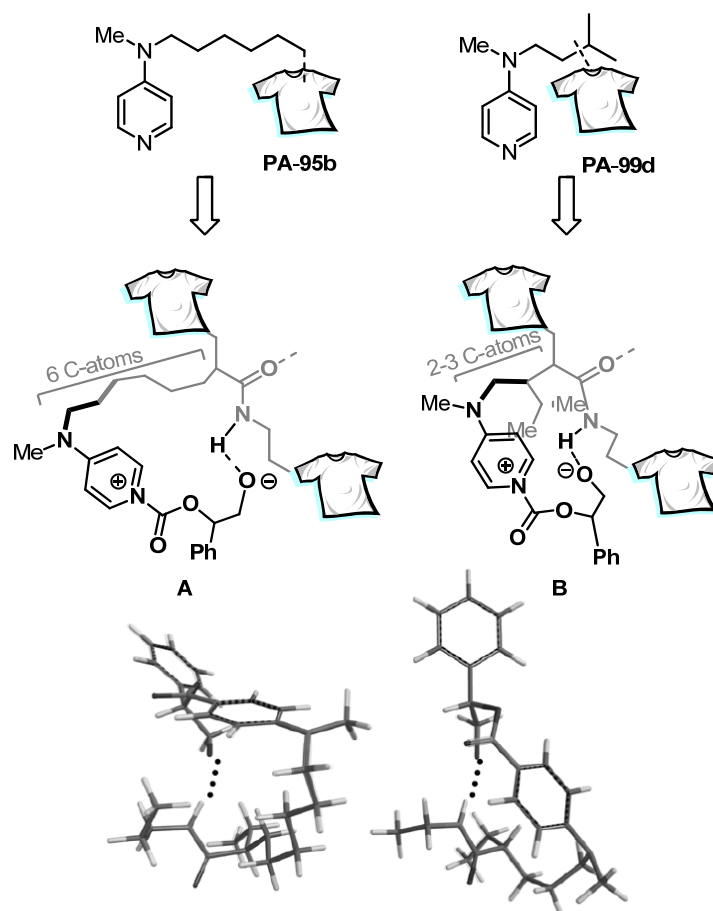
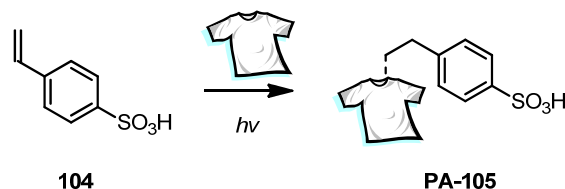


Figure 4-19. Plausible reaction intermediate in the cyclic carbonate formation reaction with catalysts **PA-95b** and **PA-99d** and their MM-DFT (B3LYP/6-31G*) optimized structure.

4.3.11. Preparation of Achiral Brønsted Acid Immobilized Textile Catalysts

After establishing the immobilization reaction conditions for Lewis basic DMAP-derived catalysts **94**, we became interested in immobilized Brønsted acid textile catalysts. Due to their broad utility in organic synthesis in the lab and industry, it is highly desirable to provide stable and practical heterogeneous Brønsted acid catalysts. We commenced our study on textile Brønsted acid catalysts with an achiral acid, *p*-styrosulfonic acid. As summarized in Table 4-16, a facile immobilization of the commercially available Brønsted acid **104** on the textile was achieved easily. The catalyst loading was confirmed by elemental analysis of the sulfur. In the case of the Brønsted acid catalyst, the catalyst loading was not affected by irradiation time but the presence of the cross-linker greatly improved the loading (entries 1 and 2). Longer irradiation gave no improvement (entry 3) even in the presence of PETA during the immobilization reaction.

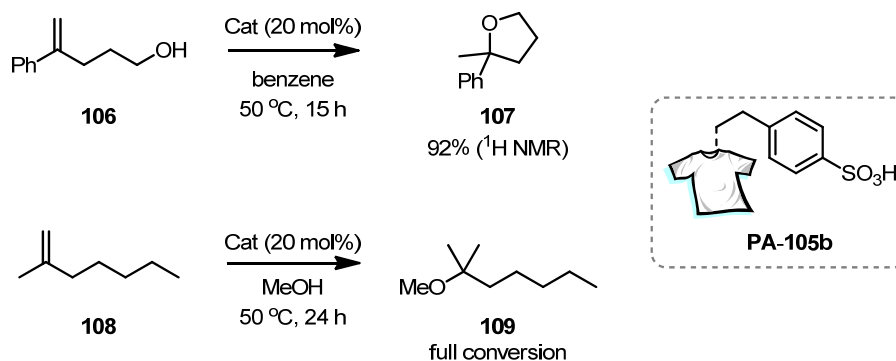
Table 4-16. Preparation of *p*-styrosulfonic acid immobilized textile catalysts



Entry	mmol/g of sheet	time [min]	Loadings [mmol/g]
1	0.3	2 x 5	0.0081 (PA-105a)
2*	0.3	2 x 5	0.022 (PA-105b)
3	0.3	2 x 10	0.028 (PA-105c)
4*	0.3	2 x 10	0.024 (PA-105d)

*Cross-linker PETA was used (0.17 mmol/g of sheet).

The catalytic activity was briefly tested by applying catalyst **PA-105b** to Brønsted acid-catalyzed reactions. As shown in Scheme 4-55, hydroetherification reactions were conducted using catalyst **PA-105b**. A catalytic amount of textile catalyst **PA-105b** could promote the intramolecular cyclization reaction of alkene **106** (donated by Dr. Sebastien Prévost) to afford tetrahydrofuran derivative **107** with good yield. Further investigation on the intermolecular hydroetherification of non-activated alkenes was conducted using 2-methyl-heptene (**108**) as an isobutene surrogate in methanol as solvent. Full conversion of the starting material was detected, however, selectivity to the desired product could not be determined due to the difficulty with the separation. Nonetheless, this result highlights the facile immobilization strategy, which can provide access to highly acidic heterogeneous catalysts, which are easy to handle and applicable in various organic transformations.

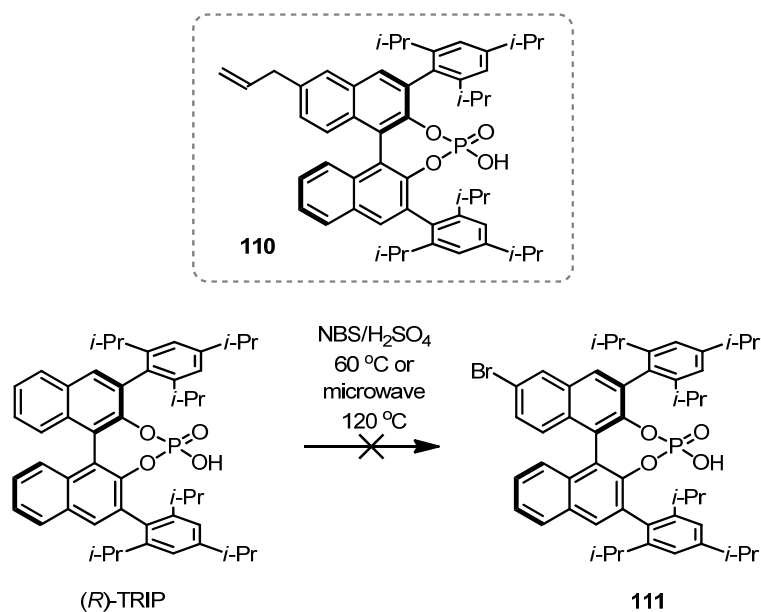


Scheme 4-55. Catalytic hydroetherification of alkenes **106** and **108** using Brønsted acid immobilized textile **PA-105b**.

4.3.12. Preparation of Chiral Brønsted Acid Immobilized Textile Catalysts

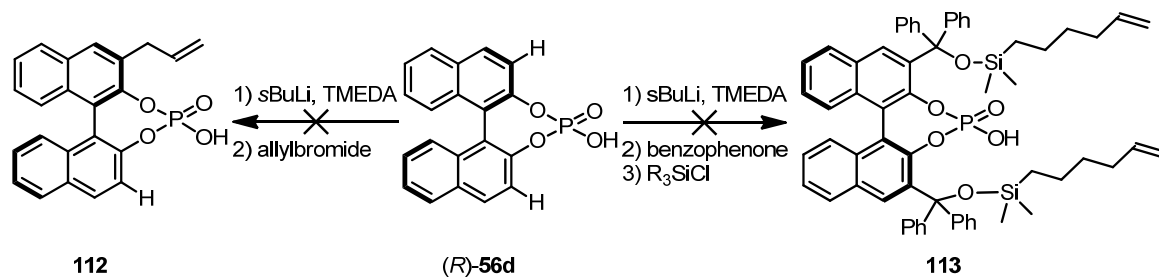
Due to an ongoing project in our group to prepare more selective and active Brønsted acid catalysts, we became interested in the preparation of immobilized chiral Brønsted acid catalysts. As briefly discussed in chapter 4.3.1, it is of great interest to recover and recycle chiral Brønsted acid catalysts due to their high cost and tedious preparation steps. A recent report on heterogeneous Brønsted acid catalysts showed only moderate activity and enantioselectivity due to the alteration of the chiral environment.⁷⁵ Surprisingly, although the progress on asymmetric catalysis with chiral Brønsted acid catalysts is remarkable, heterogeneous asymmetric catalysis with Brønsted acid catalysts is quite rare. Here, we describe our preliminary results on the endeavour to develop an efficient chiral Brønsted acid immobilized textile catalyst.

We commenced our investigation by preparing an olefin-tethered TRIP catalyst. TRIP is one of the most efficient phosphoric acids-based catalysts in terms of enantioselectivity due to its bulky substituent at the 3,3'-positions of the BINOL backbone. To access compound 6-allyl-TRIP **110**, we tested a direct bromination reaction of TRIP catalyst (Scheme 4-55). However, only starting material (*S*)-TRIP was recovered under the harsh reaction conditions. Therefore, we decided to install bromine before the formation of phosphoric acid. It is noteworthy that, our target molecule was mono-allyl compound **110** since the 6,6'-diallyl-TRIP compound was expected to generate non-selective polymerization.

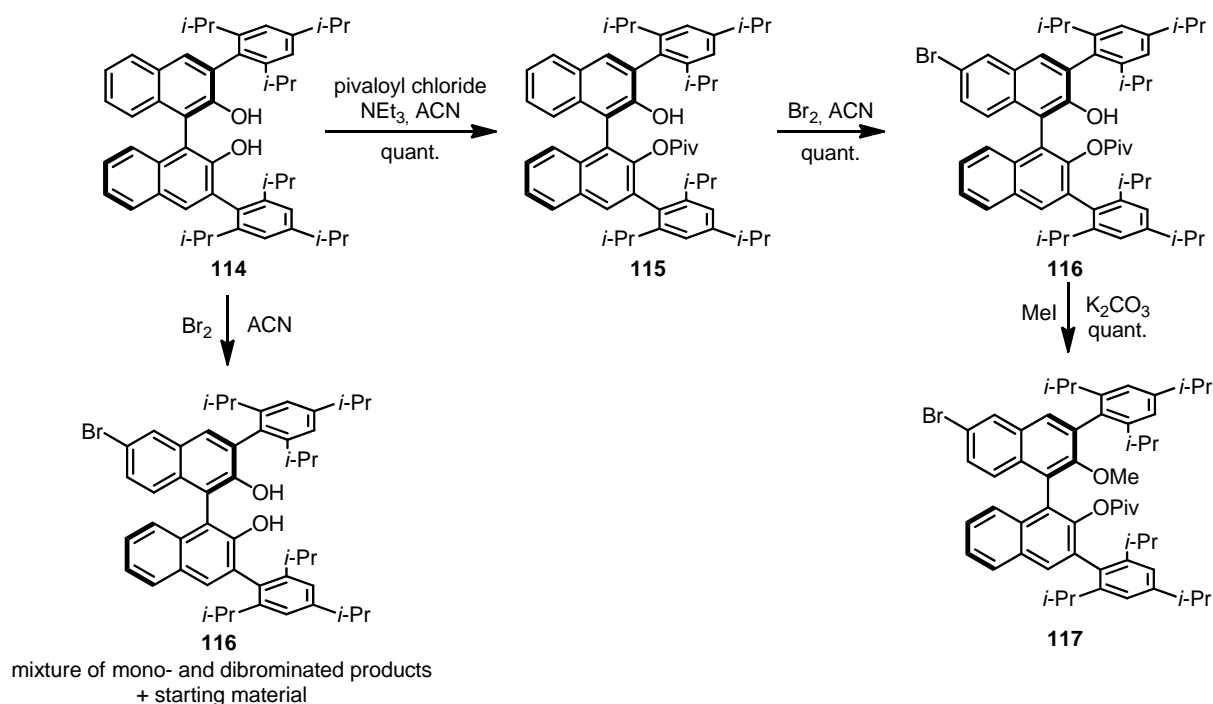


Scheme 4-56. Direct bromination of TRIP catalyst.

Meanwhile, we also tried to functionalize the 3,3'-positions by using the phosphate functionality of BINOL phosphate (*R*)-**56d** as a directing group. Nonetheless, no significant amount of desired products **112** or **113** was detected by treating BINOL-phosphate with *s*BuLi (2 equiv.) and subsequent addition of electrophiles (Scheme 4-57).

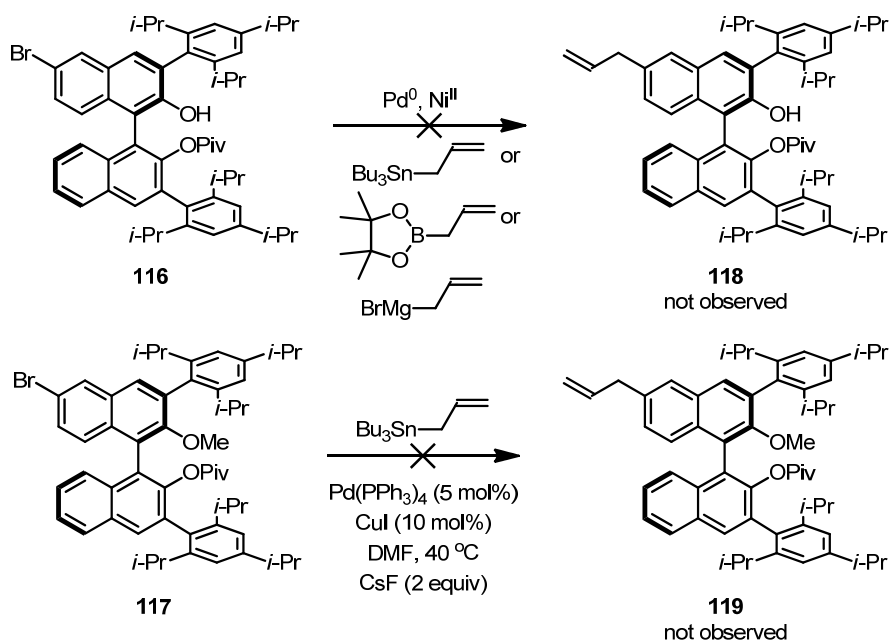
Scheme 4-57. Direct functionalization of phosphate **56d**.

A more “conventional” synthesis of an olefin-functionalized TRIP catalyst was commenced with TRIP-diol **114** (donated by Hendrik van Thienen and Marianne Hannappel, AK List). The protection of one phenol with pivaloyl chloride to afford mono phenol **115** was necessary for the selective bromination,¹³³ since the bromination reaction with TRIP-diol **114** was completely non-selective and afforded an inseparable complex mixture (Scheme 4-58). The desired mono-brominated compound **116** was isolated with excellent yield after silica chromatography and was then converted to methyl-protected compound **117** to prevent any negative effect during the cross-coupling reactions.



Scheme 4-58. Protection and selective bromination of TRIP-diol.

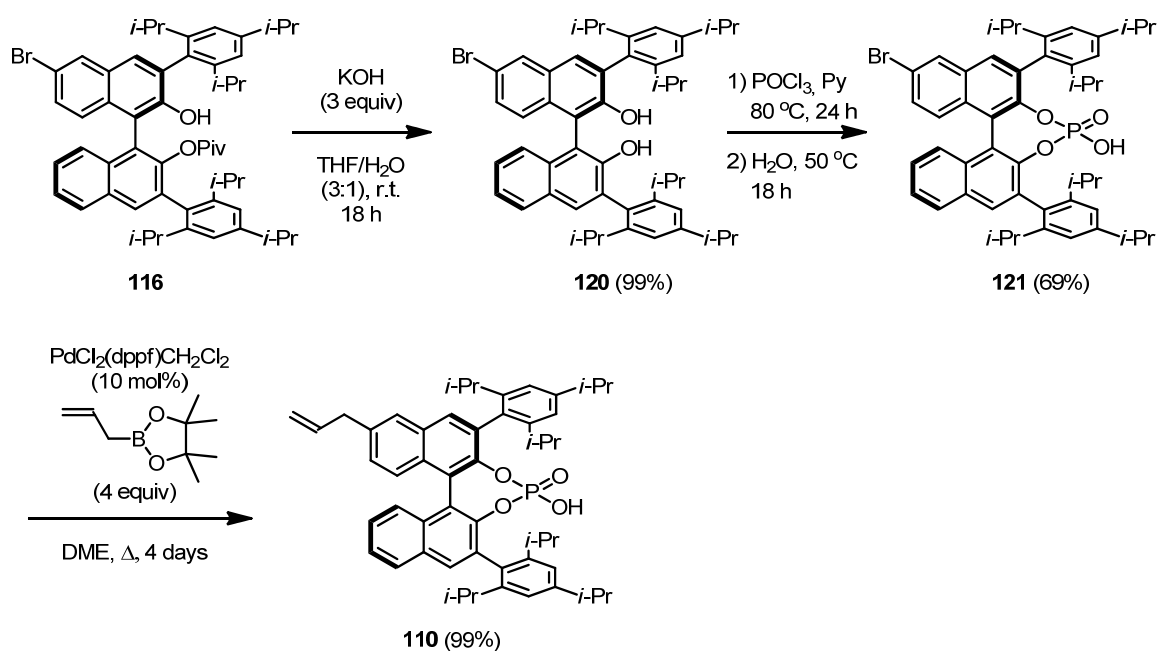
Under the palladium catalyzed Stille, Kumada and Suzuki coupling reaction conditions, the desired product **118** was never observed, using different palladium sources and bases (Scheme 4-59). In the case of the Kumada coupling reaction conditions, a small amount of deprotected diol was observed by crude ¹H NMR. To overcome this problem, methoxy-protected substrate **117** was prepared as shown in Scheme 4-58 and submitted to the Stille coupling reaction conditions. Unfortunately, also in this case no desired product **119** was observed (Scheme 4-59).



Scheme 4-59. Attempted cross-coupling reactions of the arylbromide and allyl donors.

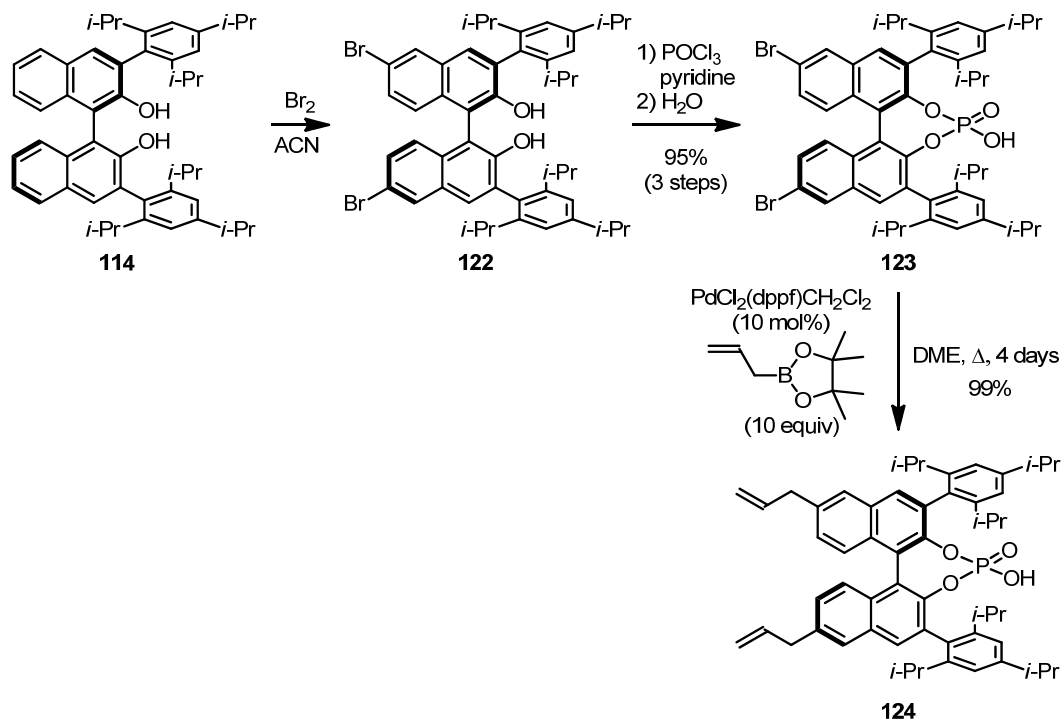
4. RESULTS AND DISCUSSION

After obtaining disappointing results for the preparation of allyl-tethered TRIP catalyst **110**, we decided to install the allyl group in a late stage. For this purpose, we prepared the phosphoric acid with the bromide on the 6 position of the BINOL backbone (**121**) with good overall yield (Scheme 4-60). Gratifyingly, desired product **110** was isolated with quantitative yield under Suzuki coupling reaction conditions. Surprisingly, the phosphate group stays intact during the cross-coupling reaction.¹³⁴ We could conclude that the BINOL phosphate is at least “innocent” under basic conditions,¹³⁵ and more practical for the Suzuki reaction than the phenol or protected phenol (OMe or OCOR) substrates. After establishing the reaction conditions for the allylation reaction for BINOL-derived phosphate substrate, we next focused on the preparation of different types of phosphates for further immobilization reactions.



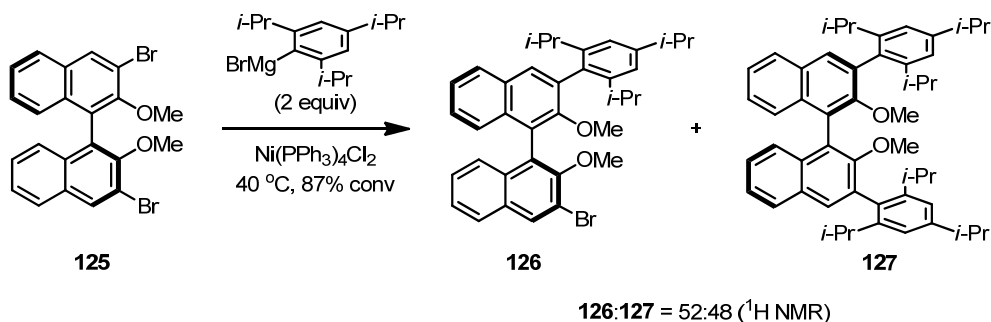
Scheme 4-60. Preparation of 6-allyl-BINOL-TRIP catalyst **110**.

As illustrated in Scheme 4-61, 6,6'-dibromo TRIP diol phosphate **123** was easily prepared from diol **114** in good isolated yield. Obtained phosphate **123** was then subjected to the Suzuki coupling reaction conditions to afford desired product **124** in excellent yield.



Scheme 4-61. Preparation of 6,6'-allyl TRIP phosphate **124**.

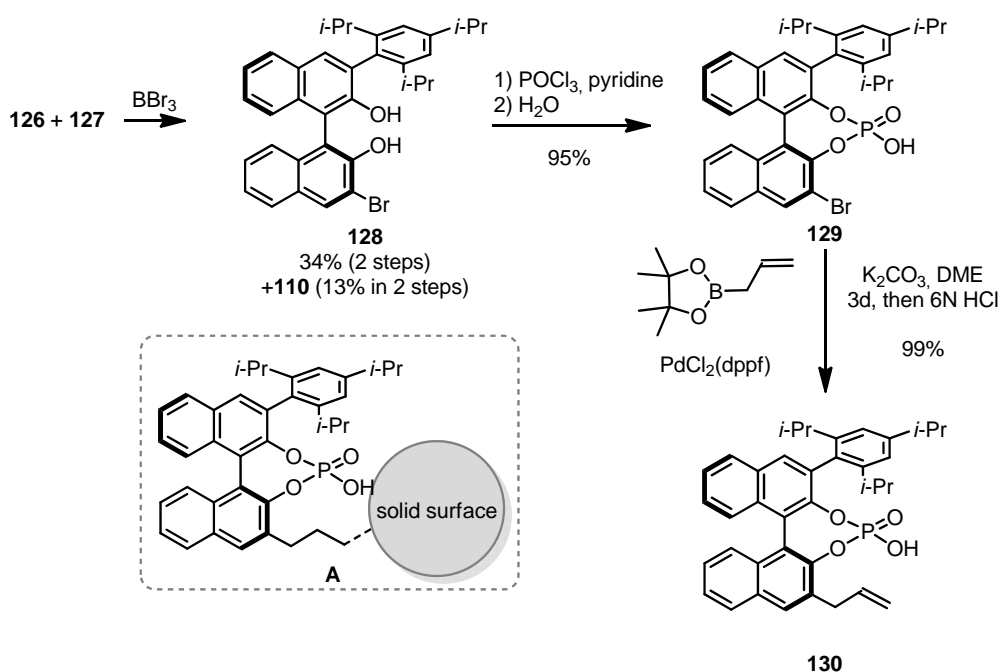
We have observed that, during the Kumada coupling reaction to prepare TRIP-diol **114**, the main byproduct was mono-TRIP coupled product **126**. We optimized the reaction conditions to provide mono-TRIP substituted BINOL bromide **126** to install allyl group on the 3'-position later on. As shown in Scheme 4-62, the desired product was obtained as the major product (52:48 ratio of **126:127**) in synthetically useful yield. The separation of the obtained mixture was not feasible at this stage, due to the high hydrophobicity of the molecules. Therefore, we conducted the deprotection of the mixture under the standard reaction conditions to afford a mixture of two diols, which were easily separated by silica chromatography (Scheme 4-63).



Scheme 4-62. Preparation of mono-TRIP substituted BINOL bromide **126**.

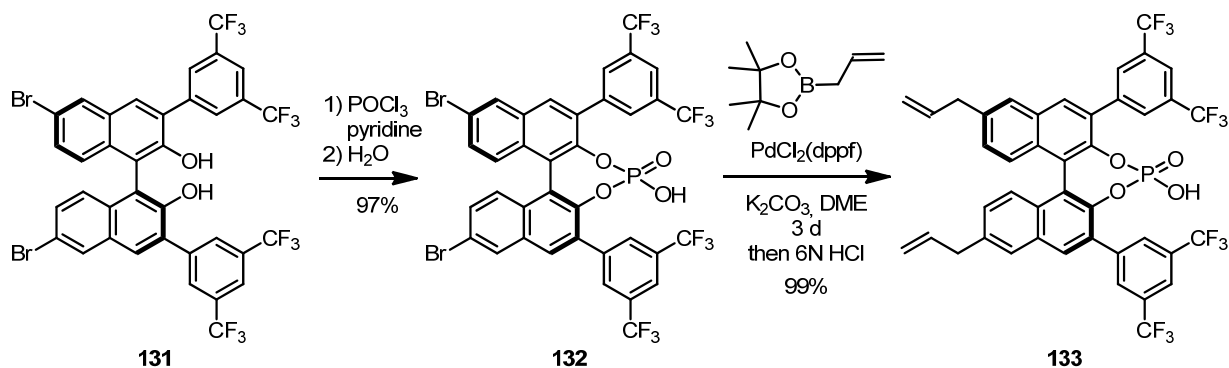
4. RESULTS AND DISCUSSION

Afterwards, the separated diol **128** was smoothly converted to corresponding phosphate **129** and allylated product **130** (Scheme 4-63). This particular phosphate drew our attention due to its possible advantage after the immobilization reaction. High enantioselectivities could be expected, since the bulk solid surface is just next to the catalytically active site (Scheme 4-63A). Although this phenomenon could lead to a diminished catalytic efficiency compared to the homogeneous catalysis, a possible positive confinement effect of the heterogeneous environment prompted us to further investigation.



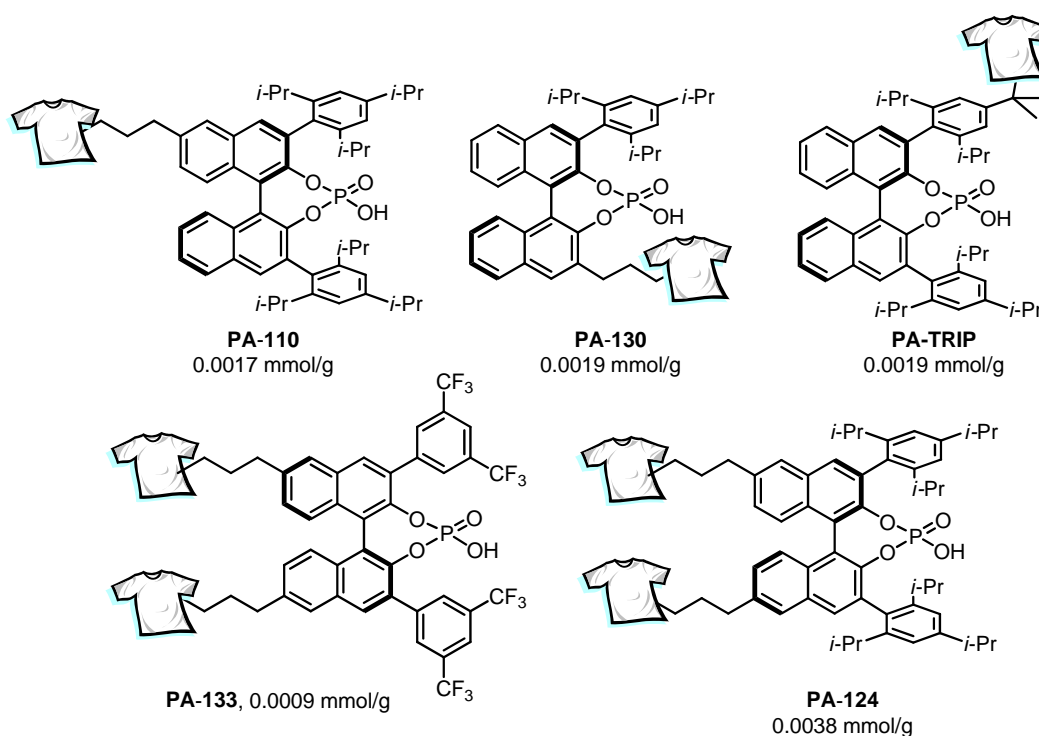
Scheme 4-63. Preparation of 3-TRIP-3'-allyl phosphate **130**.

To investigate the asymmetric protonation reaction (previously discussed in Chapter 4.2) under heterogeneous reaction conditions, we also prepared the 3,3'-bis(CF_3)₂Ph-substituted phosphoric acid with 6,6'-allyl substitution. As shown in Scheme 4-64, the desired product **133** was obtained without any difficulty starting from the diol in high yield (*diol 131* was donated by Dr. Nathalie Dupré).



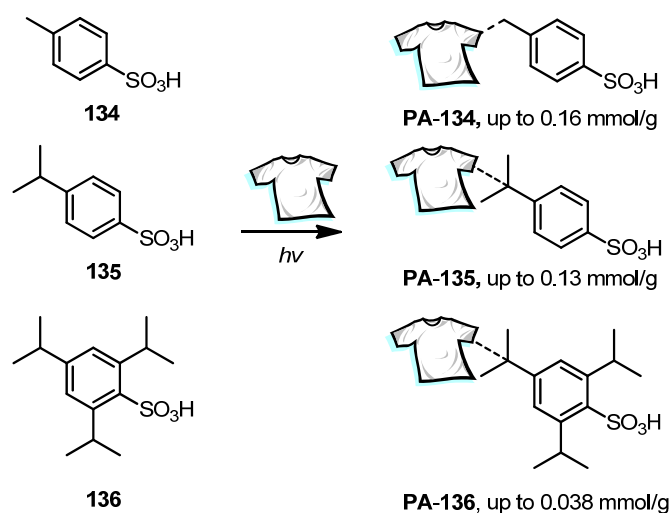
Scheme 4-64. Preparation of 3,3'-bis(CF_3)₂Ph substituted phosphoric acid **133**.

After preparation of various phosphoric acid derivatives with olefin substituents, we subjected the monomers to the immobilization reaction conditions (Scheme 4-65). As expected, the catalysts were easily immobilized and the catalyst loadings were confirmed by elemental analysis on phosphorous atom. However, generally low catalyst loadings were observed (up to 0.0038 mmol/g). This value is about 10% of the average catalyst loading obtained with the other functionalities tested (Brønsted bases and sulfonates). Surprisingly, the simple TRIP catalyst without any other functionality could also be immobilized on the textile to afford catalyst **PA-TRIP**. This reaction gave a catalyst loading similar to the mono-allyl TRIP-immobilized textiles **PA-110** and **PA-130**. We presumed that the reaction might occur at the isopropyl functional group, *via* hydrogen abstraction. This result was particularly surprising, since it implies that all the prepared TRIP-derivatives could be randomly polymerized on the isopropyl group.



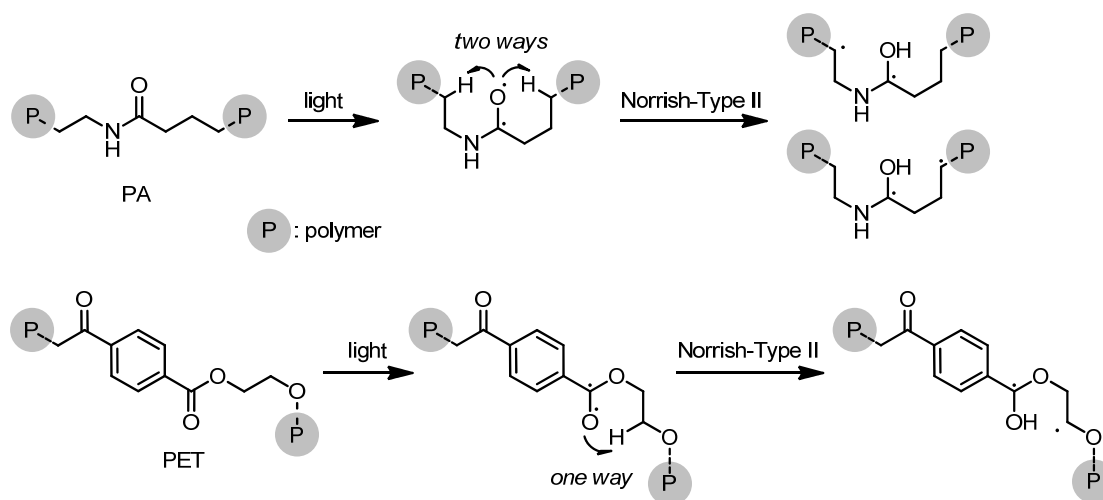
Scheme 4-65. Immobilized phosphates on polyamide.

The immobilization process on the textile through the isopropyl group was further proved by irradiating various sulfonic acid derivatives (**134-136**) under identical photochemical reaction conditions (Scheme 4-66). The immobilization reactions were conducted with and without crosslinker. In general, the catalyst loading of the sulfonic acids was higher in the absence of the crosslinker PETA. Moreover, higher catalyst loading was observed with polyamide than with PET as solid support, as expected since it was assumed that the nitrogen atom on the surface could stabilize radical species.



Scheme 4-66. Immobilization of *p*-toluene and *p*-cumene sulfonic acids and their derivatives on polyamide.

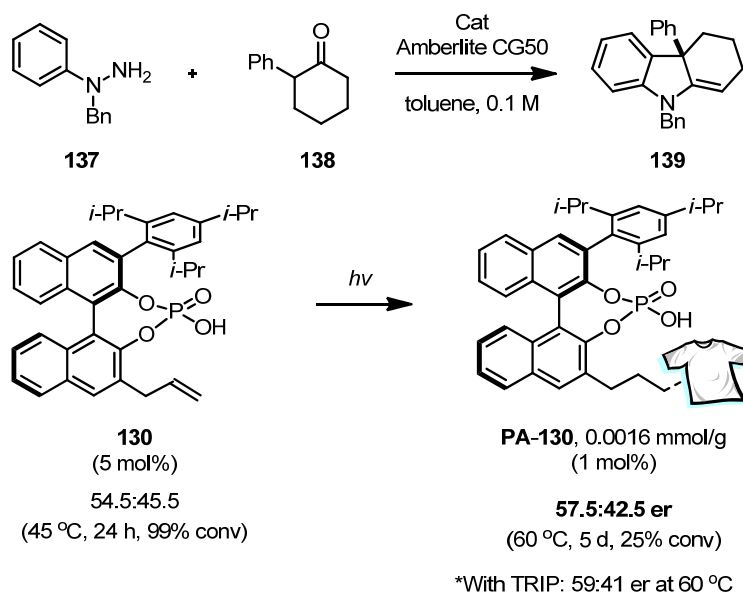
Additionally, PET intrinsically has less chance for facile 1,5 hydride-shifts, like Norrish type II reaction to take place (Scheme 4-67). For this reason, PA could be more susceptible than PET to induce a higher concentration of surface radicals under photochemical reaction conditions, which can then be captured by the organic substrate. Although the immobilization mechanism and the structure of the C-C bond connection are still unclear, this methodology could provide a facile immobilization of a variety of organocatalysts without any pre-functionalization. Further mechanistic studies on the immobilization process are highly desirable (*vide infra* for mechanistic studies on the immobilization of olefins and DMAP derivatives). Nonetheless, it is strongly believed that our methodology could be used for any organic substances as catalysts or reagents, except in the case of bearing a functional group, which is sensitive to the photochemical reaction conditions.



Scheme 4-67. Norrish-Type II reaction of PA and PET.

4.3.13. Applications of Chiral Brønsted Acid Immobilized Textile Catalysts

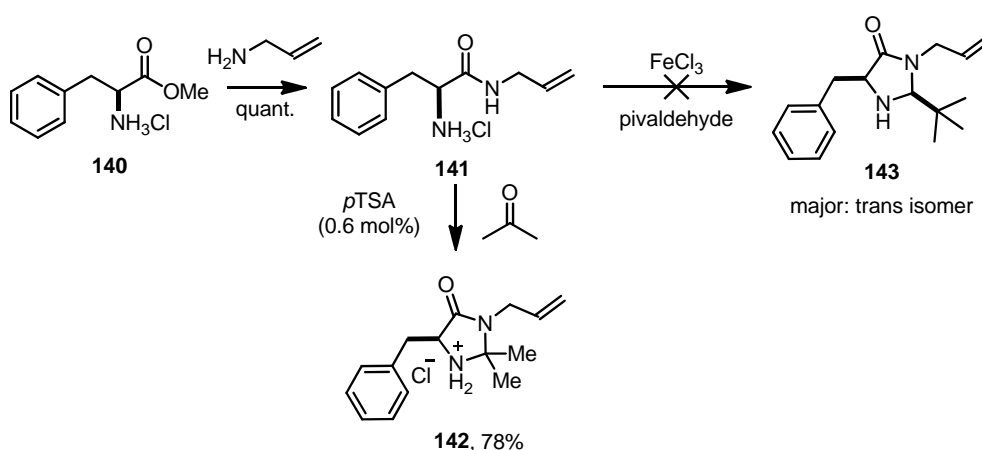
After the preparation of chiral Brønsted acid immobilized textile catalysts, we attempted to apply the obtained catalysts in asymmetric catalysis. However, all the textile catalysts derived from chiral Brønsted acids showed only moderate activity and low enantioselectivity for various asymmetric transformations. This observation could be ascribed to the low catalyst loading or decomposition of the catalytically active site, the phosphate. Phosphate groups are known to be used as photo-labile protecting groups for peptide synthesis.¹³⁶ Nevertheless, textile catalyst **PA-130** was employed for the catalytic asymmetric Fischer indolization reaction.¹³⁷ Monomer **130** was also tested for the reaction separately, to confirm the effect of the immobilization reaction. Under the homogeneous reaction conditions, product **139** was obtained in good conversion with low enantioselectivity (54.5:45.5 er). Unfortunately, heterogeneous catalyst **PA-130** was not as active (25% conversion with 1 mol% of catalyst loading). However, a slight increase of enantioselectivity was observed (57.5:42.5 er) compared to the homogeneous catalyst **130**, which could perhaps be due to the confinement effect induced by the heterogenous catalyst, as already suggested in Scheme 4-63.



Scheme 4-68. Application of Brønsted acid immobilized textile catalyst **PA-130** in the asymmetric Fischer indolization reaction (performed by Dr. Alberto Martinez)

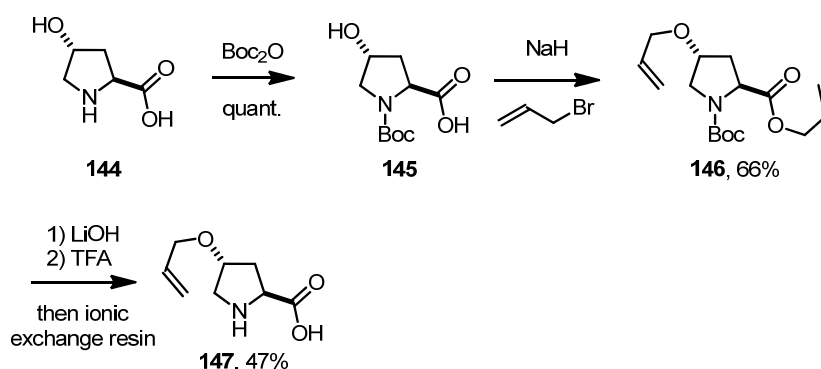
4.3.14. Preparation of Chiral Secondary Amine Immobilized Textile Catalysts

Since the year 2000, secondary amine catalysts for carbonyl functionalization have emerged as one of the most privileged organocatalysts, since they can provide extremely high stereoselectivity for various asymmetric catalysis processes. Among them, proline and MacMillan's catalyst demonstrate the power of covalent bonding catalysis, which utilizes enamine and iminium intermediates as chiral and reactive species. Due to the basicity of secondary amine catalysts, their recovery can be achieved by a simple acid/base workup procedure or simple precipitation and filtration.¹³⁸ Nonetheless, it would be desirable to provide a general method for the immobilization of secondary amine catalysts. As shown in Scheme 4-69, MacMillan's catalyst derivative **142** was prepared using a modified reported procedure.¹³⁹ Unfortunately, the catalyst with a *tert*-butyl substituent **143** could not be prepared, due to the low selectivity towards the *cis*-product under the reaction conditions (Scheme 4-69).

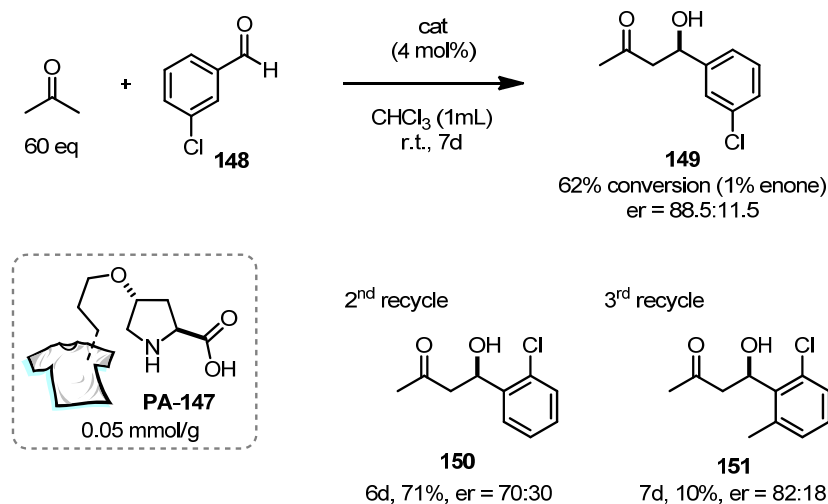


Scheme 4-69. Preparation of N-allyl MacMillan's catalyst.

On the other hand, a proline derived olefin-tethered catalyst was prepared starting from 4-hydroxy proline (**144**), according to the reported procedure (Scheme 4-70).¹⁴⁰ The isolation of final product **147** was achieved using acidic ion exchange resin.

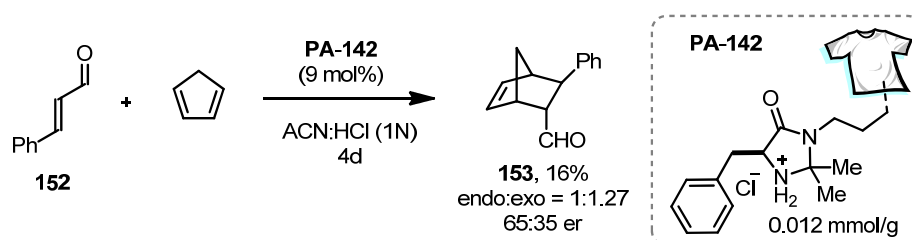
Scheme 4-70. Preparation of 4-allyloxy-L-proline (**147**).

After the preparation of monomers **142** and **147**, the immobilization of the secondary amine catalysts was conducted using polyamide as a solid support under the optimized reaction conditions. Unfortunately proline derivative **147** was not suitable for the immobilization process, and we could only obtain low catalyst loading on polyamide (up to 0.05 $\mu\text{mol/g}$). Nonetheless, the catalytic activity was evaluated by performing an aldol reaction of acetone with electron deficient aldehydes. The textile catalyst was recovered and reused for further cycles and showed reasonable activity and enantioselectivity (up to 88.5:11.5 er).



Scheme 4-71. Evaluation of Proline-immobilized textile catalyst **PA-147**.

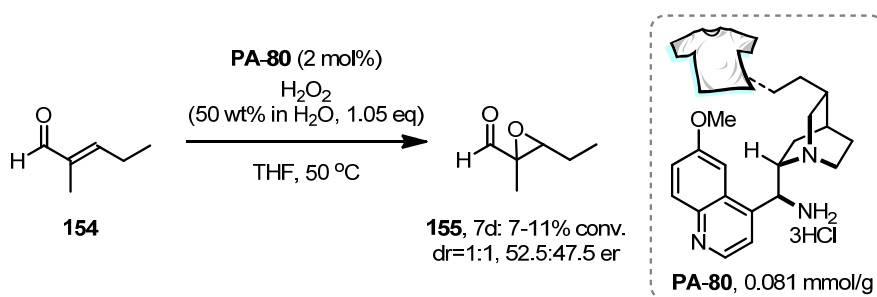
The evaluation of the MacMillan-type catalyst immobilized textile **PA-142** was conducted by employing the catalyst for the Diels-Alder reaction of cyclopentadiene and enal **152** (Scheme 4-72). However, only low yield (up to 16%) and enantioselectivity of product **153** (up to 65:35 er) was observed after 4 days. The low activity and enantioselectivity of secondary-amine immobilized textile catalysts **PA-142** and **PA-147** could be ascribed to the low catalyst loading on the surface. In contrast to the tertiary amine catalysts, the secondary amine catalysts were not able to be immobilized efficiently. This result is perhaps due to the low mass transfer rate of the substrates, since the reaction requires covalent bonding intermediates. Also, various parasitic intermediates of the reaction could be a reason for the inefficient catalysis.



Scheme 4-72. Evaluation of MacMillan-type catalyst immobilized textile **PA-142**.

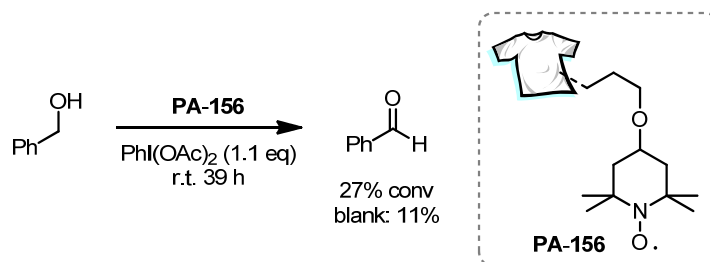
4.3.15. Preparation and Application of Further Textile-Immobilized Organocatalysts

Besides secondary amine catalysts, primary amine catalysts were also considered as an effective candidate for amino catalysis, due to the less congested amine center, which facilitates formation of enamine and iminium intermediates.¹⁴¹ As shown in Scheme 4-73, quinine-derived primary amine salt **80** was immobilized on textile with a reasonable catalyst loading (0.081 mmol/g). The catalytic activity of textile catalyst **PA-80** was tested for the epoxidation of α -branched enal **154** using H_2O_2 as a nucleophilic oxidant. However, only low conversion was detected with neglectable enantioselectivity (up to 11% conversion, up to 52.5:47.5 er). This reaction outcome could be explained by the formation of the *N*-oxide of the catalyst under the reaction conditions.^{142,143} The irreversible catalyst modification could be faster than the transformation of the substrate. Since the formation of the reaction intermediate with the solid supported catalyst and substrate is critical for the catalytic turnover, the observed low activity of the heterogeneous catalyst could be expected.



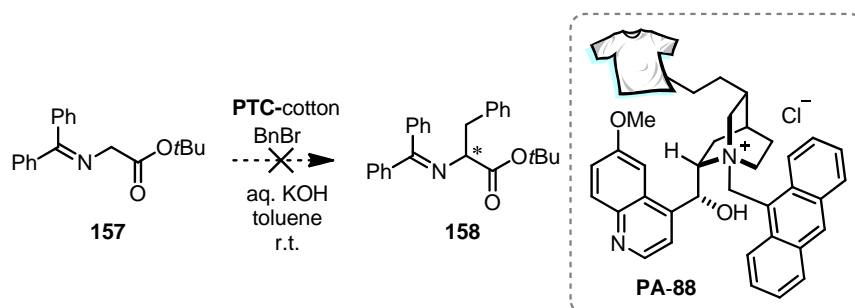
Scheme 4-73. Evaluation of primary-amine immobilized textile catalyst **PA-80**.

We could not obtain positive results of aminocatalysts after immobilization due to the possible reaction of the amine under photochemical reaction conditions *i.e.* oxidation and formation of *N*-oxide. Therefore we wondered about the possibility of *N*-oxide radical catalysts, which are usually used for the catalytic oxidation reaction of alcohols. As shown in Scheme 4-74, TEMPO could be immobilized and used for primary alcohol oxidation. However, textile catalyst **PA-156** was found to be less efficient than background reaction (with only $\text{PhI}(\text{OAc})_2$) due to the heterogeneous environment. Since TEMPO possesses a radical functionality, the photochemical reaction conditions can affect the radical stability during the immobilization, leading to inferior results in the catalytic transformation.¹⁴⁴



Scheme 4-74. Textile catalyst **PA-156** catalyzed oxidation of a primary alcohol.

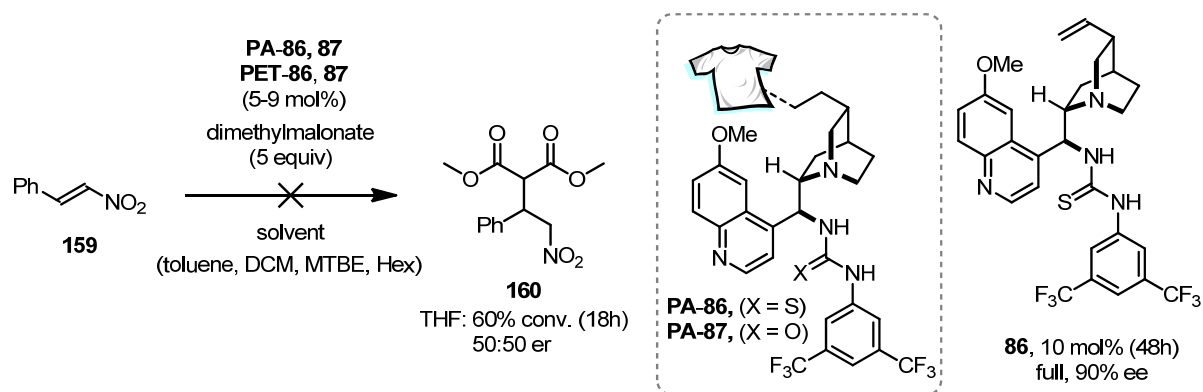
We were also interested in phase-transfer catalysts because of their vast application potential in the asymmetric α -functionalization of carbonyl compounds.¹⁴⁵ The commercially available catalyst **88** was immobilized according to our optimized photochemical reaction conditions. Unfortunately, the catalytic system gave no conversion for the alkylation reaction with textile catalyst **PA-88** (Scheme 4-75). Due to the multiphasic reaction conditions of heterogeneous phase-transfer catalysis, the catalyst should be well-designed for catalytic activity and selectivity. Since the interaction between the aqueous phase and the organic phase through PTC is critical, we immobilized the PTC catalyst on cotton, which possesses abundant free hydroxyl groups. We presumed that the surface of cotton can act as a surrogate for the aqueous phase, enhancing proximity of the catalytic species to encounter the inorganic substrate (KOH) in the organic solvent. We conducted the reaction without water to confirm this hypothesis, but unfortunately, only low conversion was observed.



Scheme 4-75. Application of PTC-immobilized textile catalyst **PA-88**.

Among the various bifunctional organocatalysts, a (thio)urea catalyst is one of the most versatile organocatalysts since they contain a bifurcated hydrogen bonding donor. In contrast to other hydrogen bonding donor functionalities (alcohols, amides and acids), (thio)ureas can stabilize (or coordinate) two lone pairs or negative charges delocalized on two atoms, for example, carbonyl and nitro compounds. The catalytic activity and enantioselectivity of their chiral variants were well demonstrated since the last decade.¹⁴⁶ However, the preparation of polymer-supported (thio)urea catalysts and their applications are quite rare. We decided to immobilize quinine-based (thio)urea catalysts **86** and **87** on PA and PET. A reasonable catalyst loading was achieved for both PA and PET using the standard immobilization conditions. However, the catalytic activity was much lower than the corresponding homogeneous catalysts (48h, full conversion, 95:5 er, Scheme 4-76). In THF, reasonable catalytic activity was obtained, but unfortunately led to racemic product **160** (60%, 50:50 er). These results imply that the photochemical immobilization conditions could affect the (thio)urea functionality resulting in poor catalytic activity and enantioselectivity. It is known that thioureas can be decomposed under free-radical polymerization at high temperature (110 °C).^{147,148}

4. RESULTS AND DISCUSSION



Scheme 4-76. Application of (thio)urea catalyst immobilized textiles **PA-86** and **PA-87**.

Due to the higher activity of catalyst **PA-86** in polar solvents (i.e. THF), although the obtained enantioselectivity is negligible, we presumed that the (thio)urea catalyst can interact with the surface *via* hydrogen bonding. As illustrated in Figure 4-20, by MM optimization of the immobilized catalyst fragment, the sulfonamide catalyst **PA-92** showed no interaction between the amide and any functionality of the catalyst. However, the thiourea catalyst **PA-86** shows strong hydrogen bonding interaction between the proton of the amide. This interaction could completely change the conformation of the catalyst resulting in inferior catalytic activity and/or low enantioselectivity. Although two CF_3 groups can induce high acidity of the ortho proton of the aryl group to interact with the oxygen (or sulfur) of the (thio)urea, the proximal interaction between the solid support and the catalyst could be more predominant. Further optimization of the immobilization process of (thio)urea catalysts could be achieved by using different cross-linkers to prevent the surface-catalyst interactions.

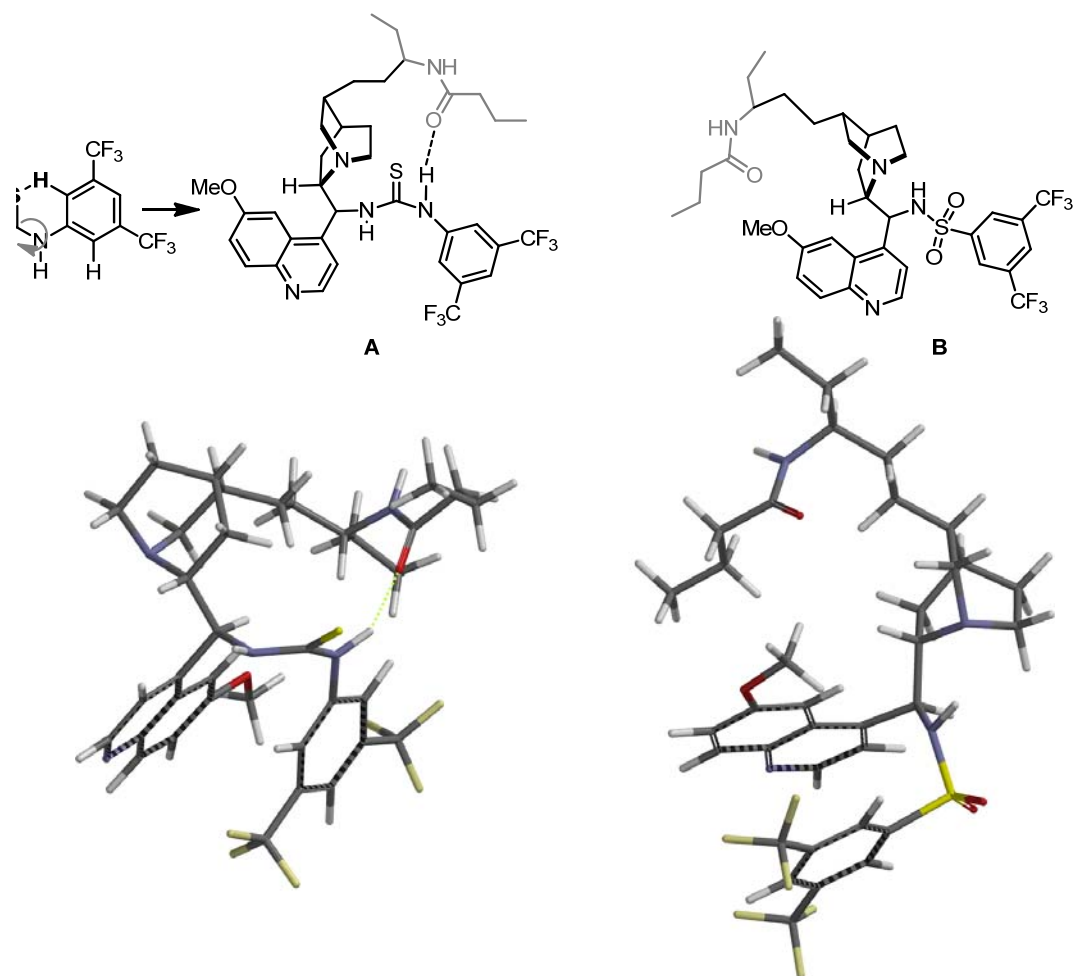
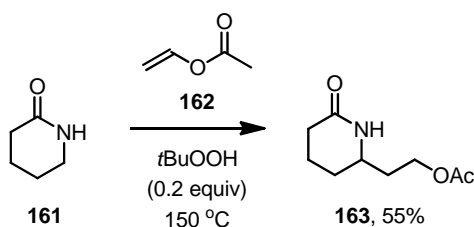


Figure 4-20. MM-optimized structures A and B.

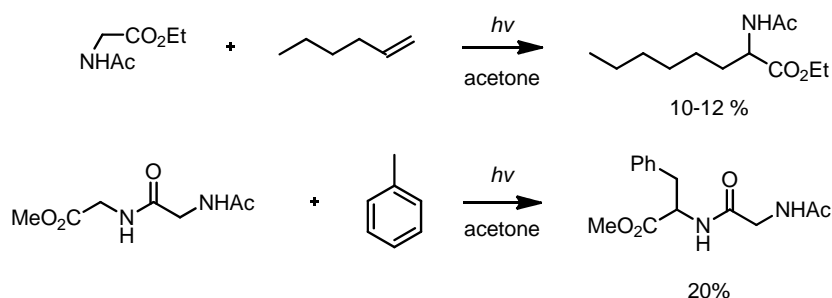
4.3.16. Investigations on the Immobilization Mechanism

After having established a highly efficient immobilization method for various organocatalysts, we were interested in elucidating the immobilization mechanism. It has been reported from BASF and Nikishin *et al.* that a cyclic amide, for example δ -lactam (**161**) can undergo functionalization under free-radical generation conditions to give a linear compound (Scheme 4-77).^{149, 150} This reaction is believed to proceed *via* radical generation on the lactam ring, which can be stabilized by the α -heteroatom (nitrogen), and subsequent quenching with an olefin **162** to give the product. Although the obtained yield is moderate, this functionalization is quite remarkable.



Scheme 4-77. Functionalization of δ -lactam (**161**) under free-radical generation conditions.

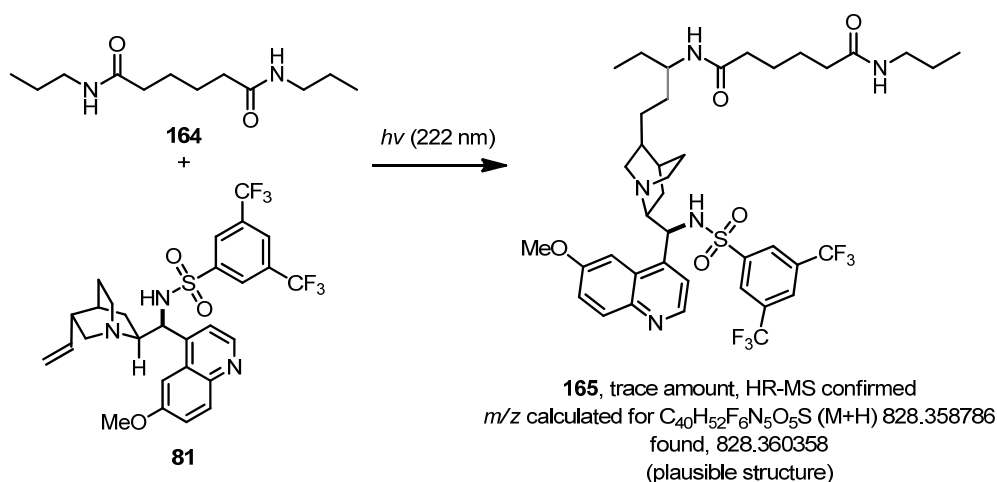
Moreover, amino acid derivatives can participate in alkylation reactions in the presence of olefins and toluene under photochemical reaction conditions (Scheme 4-78).^{151, 152} Therefore, we decided to investigate the immobilization reaction mechanism by treating organocatalysts with a monomeric amide under either photochemical reaction conditions or free-radical generation reaction conditions.



Scheme 4-78. Alkylation of amino acid derivatives under photochemical reaction conditions.

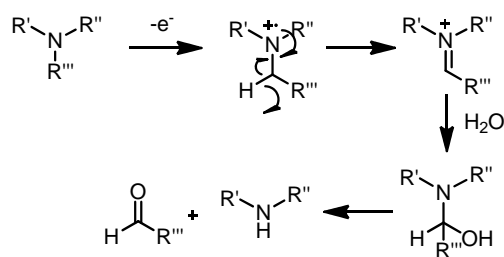
As shown in Scheme 4-79, catalyst **81** was irradiated in the presence of polyamide derivative **164**. The crude reaction mixture showed no significant conversion of the starting material, even after longer irradiation time (10-60 min). Fortunately, we could obtain trace amounts of the desired product (less than 0.1% yield), which was analyzed by high resolution mass, confirming the molecular weight of the coupled product ($M+H$: 828.360358, **165**). We currently have no structural information regarding this reaction, although we could assume that the olefin reacts with the radical species generated on the amide to give the most stable radical species. Alternatively, the reaction could occur through the generation of the allylic radical on the

organocatalyst, then the recombination of two radical species could generate the proposed structure as shown in Scheme 4-79.



Scheme 4-79. Photochemical reaction of “monomeric” amide **164** and sulfonamide **81**.

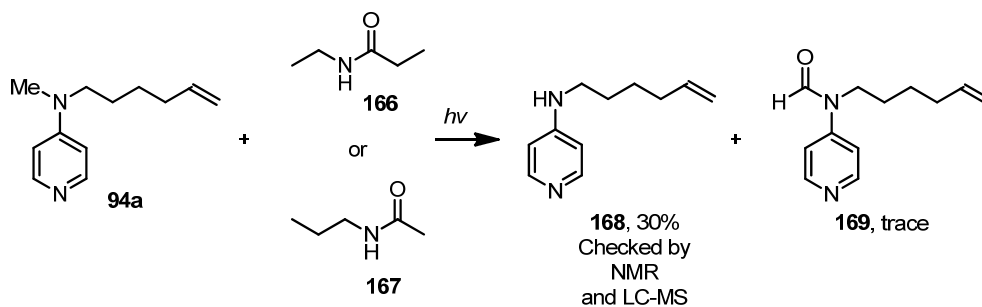
Encouraged by this result, we turned our attention to DMAP derivatives. As shown in Chapter 4.3.10, parent DMAP could also undergo the photochemical immobilization reaction. This unprecedented result prompted us to investigate the mechanism. In the case of electron-rich amines, after one-electron oxidation a tertiary amine radical cation can be converted into the iminium species due to the higher acidity of the α -proton (Scheme 4-80).¹⁵³ Then this reactive species could undergo various reaction pathways. In the presence of moisture, this intermediate can be hydrolyzed to afford the demethylated compound.



Scheme 4-80. Plausible reaction mechanism for the cleavage of tertiary amines.

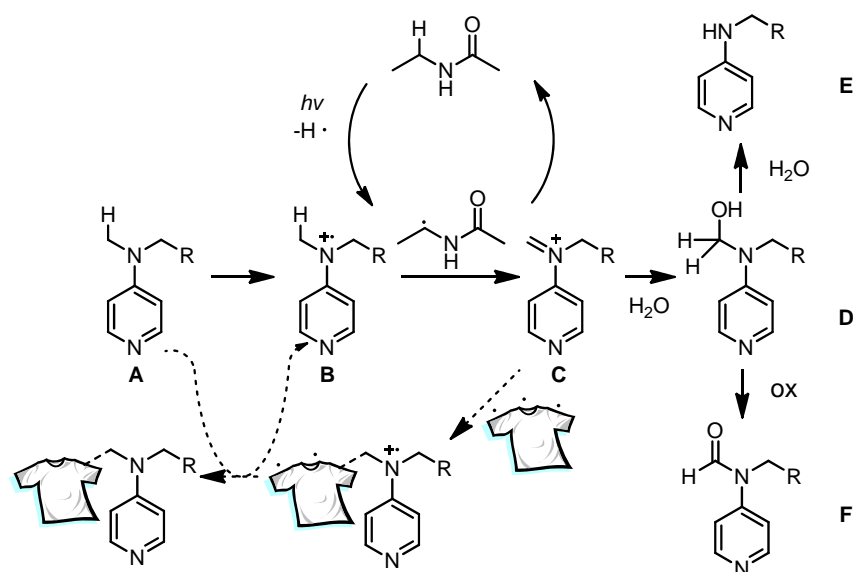
As shown in Scheme 4-81, DMAP derivative **94a** was subjected to identical photochemical reaction conditions as in the immobilization reactions in the presence of amide **166** or **167**. By analyzing the crude mixture with NMR spectroscopy, we could observe demethylated compound **168** as the major product although the conversion is quite low (<30% conversion). The other by-product, formamide **169**, was observed, which can be explained by the mechanism shown in Scheme 4-80.

4. RESULTS AND DISCUSSION



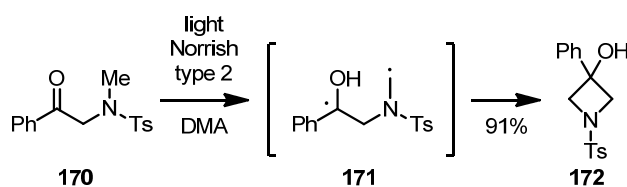
Scheme 4-81. Photochemical reaction of DMAP-derivative **94a** and amides **166** and **167**.

A plausible reaction mechanism for the photochemical reaction of DMAP derivative **94a** is depicted in Scheme 4-82. Under the photochemical reaction conditions, the substrate could be oxidized to afford radical cation **B**. Then the radical on the amide could abstract the hydrogen of radical cation **B** to give iminium ion **C**, which can then be attacked by water to give hemiaminal **D**. Further hydrolysis could afford secondary amine **E**. Further oxidation under photochemical reaction conditions could afford formamide **F**. The reaction mechanism involving the textile for the immobilization reaction is depicted with dashed arrows. *In-situ* formed iminium intermediate could react with a radical on the textile surface¹⁵⁴ to give the immobilized catalyst in a radical cationic form, which can be then reduced by another equivalent of the substrate in a propagation mechanism. This hypothesis could explain the immobilization of DMAP on the textile without any olefin functional group, as described in Chapter 4.3.10. It is noteworthy that, in the presence of olefin functional group, the immobilization with the olefin will be predominant. Additionally, the chain length and olefin substitution have a remarkable effect on catalyst loading and catalytic activity (Figure 4-18). This result once again indicated that the olefin functionality is the reaction center for the immobilization. However, the immobilization mechanism involving the formation of iminium intermediate **C** and subsequent radical addition from the surface cannot be ruled out.

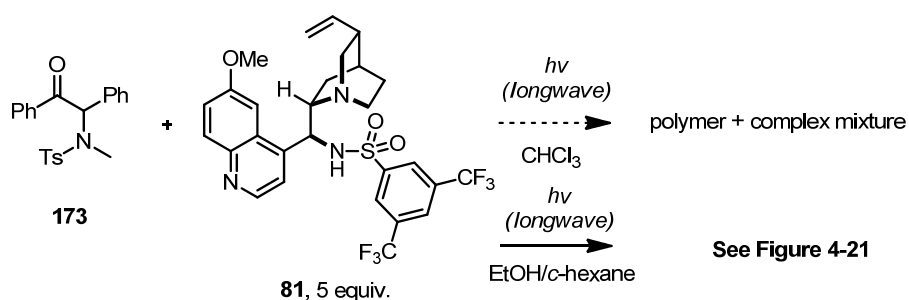


Scheme 4-82. Plausible reaction mechanism for DMAP derivatives under photochemical reaction conditions.

Further investigation on the immobilization reaction mechanism was conducted using substrate **170** and **173**, which undergoes typical Norrish type II reaction (Scheme 4-83).¹⁵⁵ Although excess of sulfonamide **81** was used to minimize the intramolecular cyclization for the irradiation reaction in the presence of substrate **173** (longwave, >300nm in chloroform), a complicated mixture was obtained (Scheme 4-84). Fortunately, the reaction mixture in ethanol/c-hexane as a mixed solvent system gave a new species after irradiation (Figure 4-21). Although the assignment of the obtained compound was not straightforward, we could observe the disappearance of the olefin signal of sulfonamide **81**. Additionally, we could obtain the mass of the compound, which corresponds to the coupled product **175** (Scheme 4-85). Substrate **173** usually undergoes a Norrish type-2 reaction leading to intramolecular cyclization. However, in the presence of sulfonamide **81** (5 equiv.), the two radical species could be generated *via* Norrish type-1 reaction pathway, which can then be trapped by the olefin (**81**) to afford the coupled product **175**.



Scheme 4-83. Reported photocyclization of ketone **170**.



Scheme 4-84. Photochemical reaction of substrate **173** and **81**.

4. RESULTS AND DISCUSSION

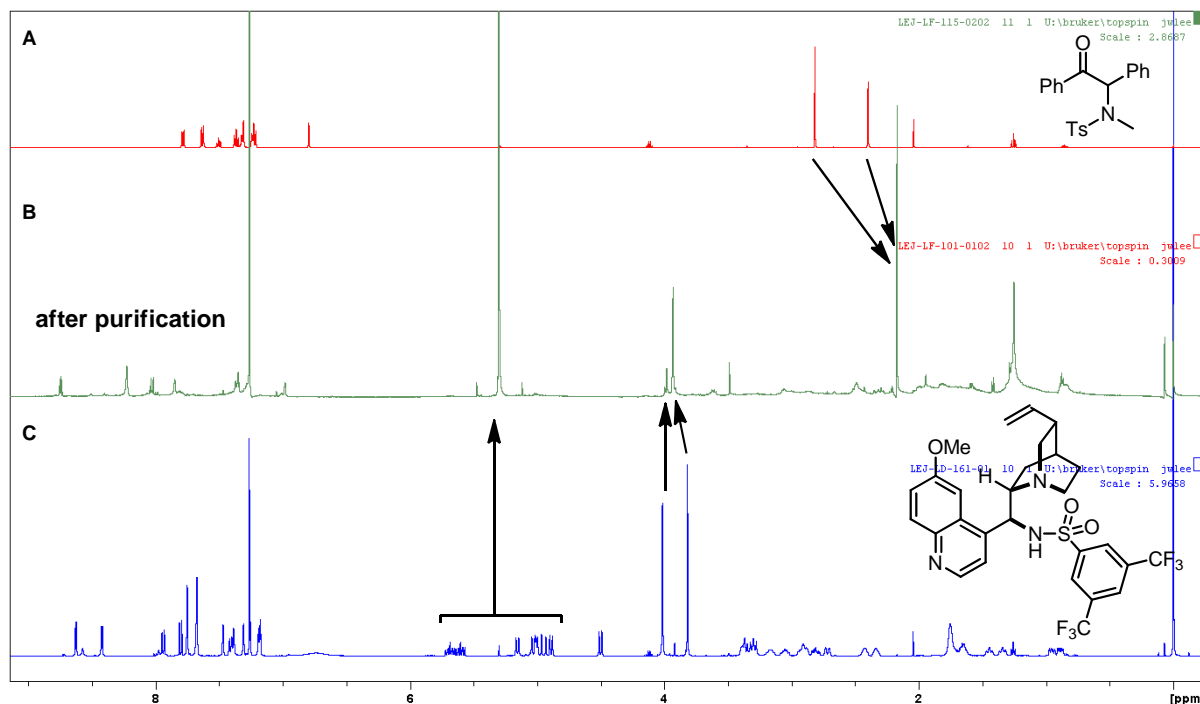
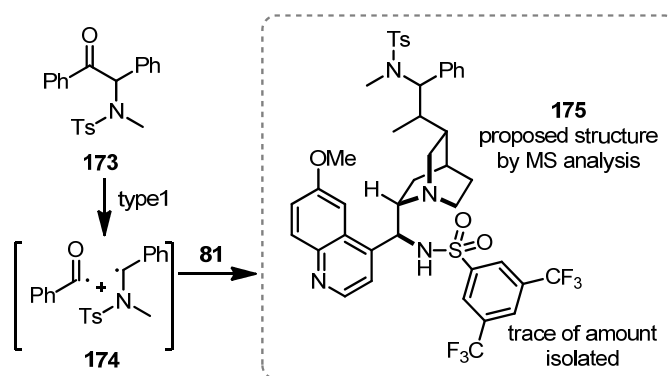


Figure 4-21. ^1H NMR spectra for Scheme 4-84, **A:** substrate **173**, **B:** reaction mixture after purification, **C:** **81**.

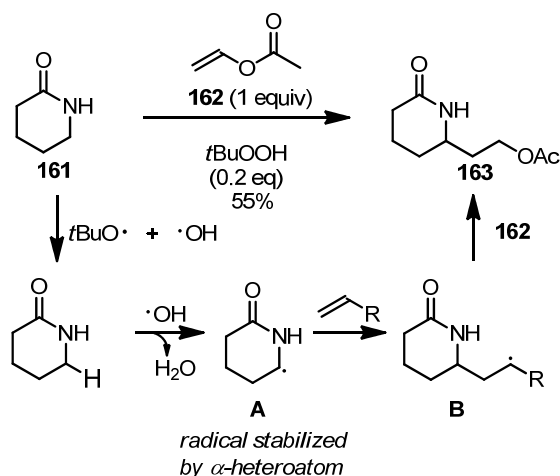


Scheme 4-85. Proposed structure **175** from MS analysis.

Since we could only obtain coupled-product **175** in trace amounts (< 1% yield), the reaction mechanism of immobilization is still unclear. Nonetheless, all these reactions were conducted under homogeneous reaction conditions, in contrast to the immobilization reaction in the solid environment, which might be critical for the stabilization of radical species.¹⁵⁶ Due to the low or zero diffusion of the reactive species on the surface, the life time of the radical species could be dramatically increased, resulting in a more efficient immobilization reaction. Although reproducing the immobilization reaction under homogeneous conditions does not seem feasible, we conducted more experiments to obtain more direct evidence.

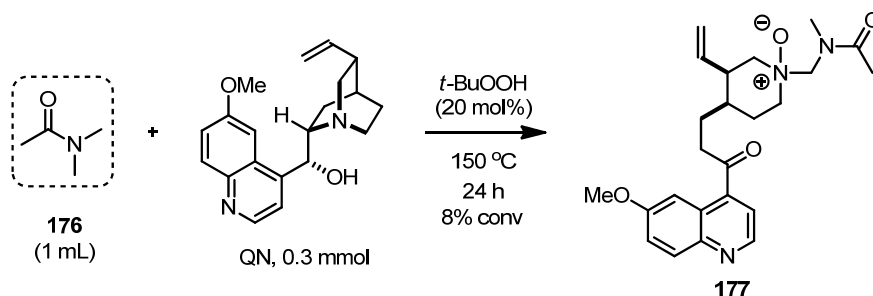
Since we presumed that the photochemical reaction conditions generate free-radicals on the surface of the solid support, we decided to mimic these reaction conditions by generating free-radicals through different approaches. As shown in Scheme 4-77, *tert*-butyl hydrogen peroxide could generate free-radical (**A**) on the cyclic amide at high temperature, which could perhaps be derived from the hydroxide radical. This radical

species can undergo a radical addition reaction to the olefin to generate a radical addition product **B**, stabilized by the α -heteroatom (oxygen) and quenched by a propagation mechanism (Scheme 4-86).



Scheme 4-86. Proposed mechanism for Scheme 4-77.

We presumed that this reaction pathway could be applied to our system to confirm the immobilization mechanism. Since the free-radical generation step using hydrogen peroxide derivatives could be more efficient than the photochemical reaction conditions, higher conversion to the desired product was expected. As shown in Scheme 4-87, we tested our hypothesis using *N,N*-dimethylacetamide (**176**) and quinine under the free-radical generation conditions (*t*-BuOOH, 150 °C). Surprisingly, we could obtain the product, quinotoxin derivative,^{157, 158, 159} with reasonable conversion to analyze by NMR and HR-MS. The quinoline ring system was intact and the new singlet signals (2.21 and 2.99 ppm) could be assigned to CH_3CO and $N-CH_3$ respectively. The reaction mixture gave only one set of the signals. Also the incorporation of the ketone was suggested by HRMS, (suggested mechanism in Scheme 4-89).

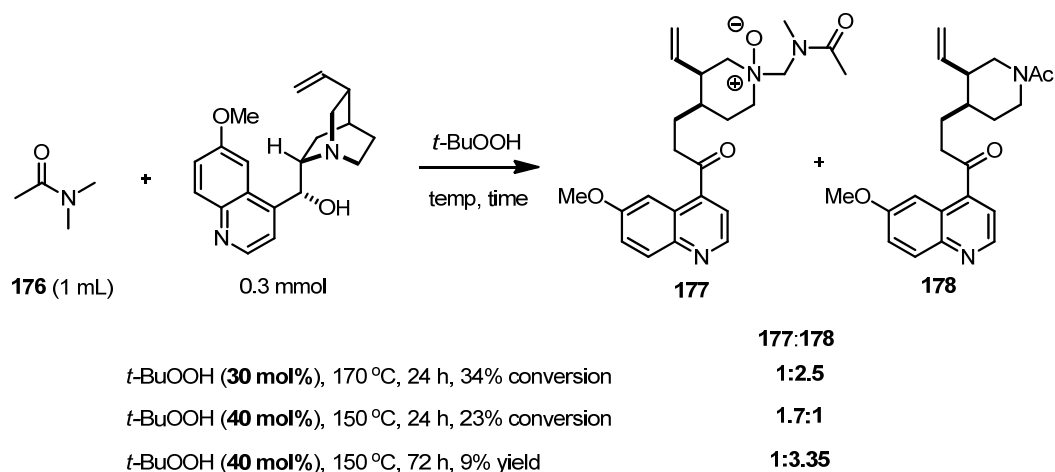


Scheme 4-87. Reaction of acetamide (**176**) and QN under free-radical generation conditions.

Optimization of the free-radical generation reaction conditions was conducted as briefly summarized in Scheme 4-88. Compound **178** was observed as a byproduct and separated by HPLC and confirmed by LC-MS and HR-MS. At higher temperature (170 °C), higher conversion was detected but the formation of compound **178** was more dominant. Decreasing the temperature and increasing the amount of *tert*-BuOOH indeed improved conversion and selectivity to product **177** (**177:178** = 1.7:1). However, increasing the reaction time

4. RESULTS AND DISCUSSION

under the same reaction conditions led to the formation of quinine (**178**), which implies that byproduct **178** could be generated more easily under these conditions than **177**. However, it cannot be ruled out that compound **178** is derived from compound **177** under free-radical generation conditions.



Scheme 4-88. Optimization of free-radical generation reaction conditions.

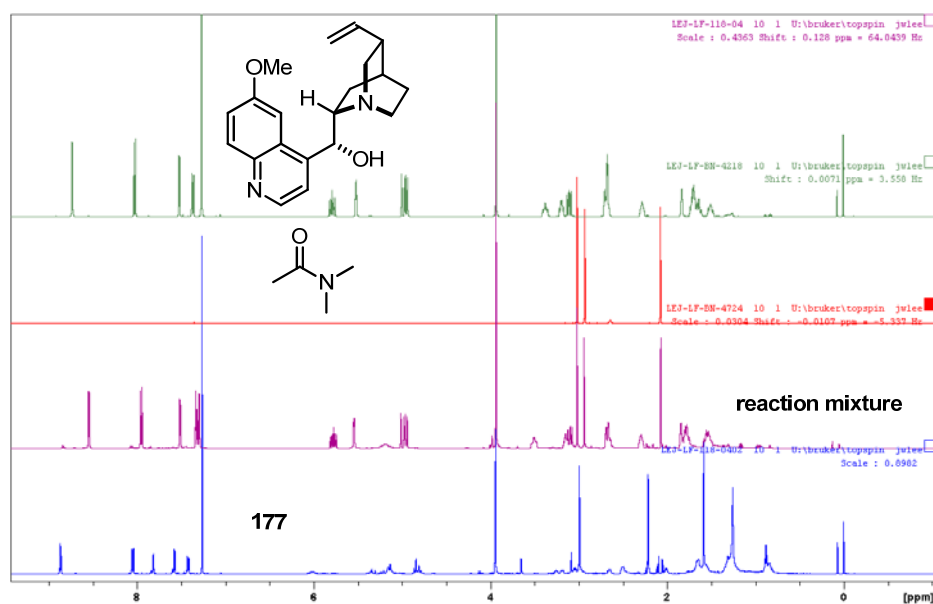
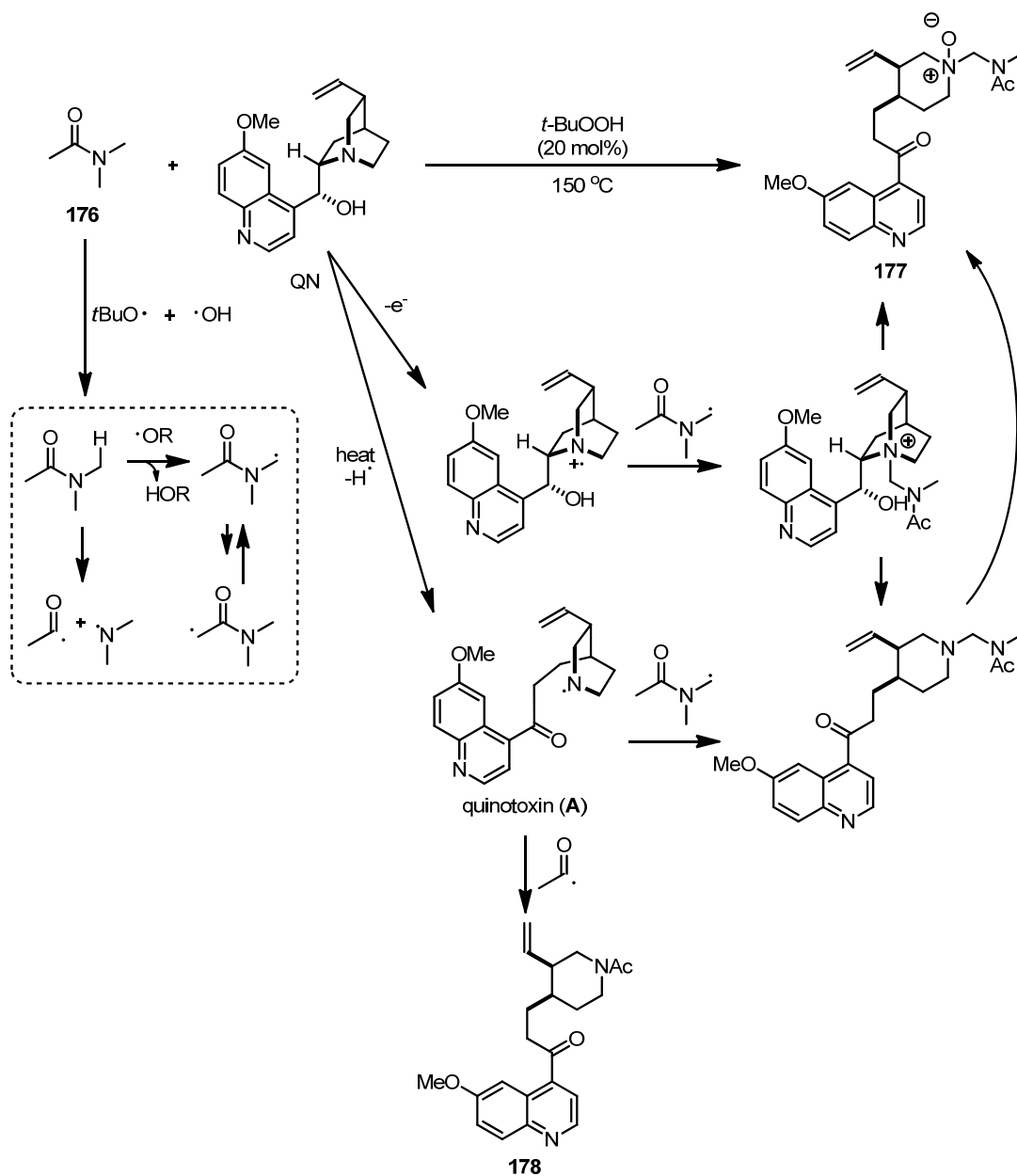


Figure 4-22. Comparison of ^1H NMR spectra of quinine, *N,N*-dimethylacetamide and reaction mixture and purified compound **177**.

The salt of cinchona alkaloids derivative **A** (quinotoxine) was isolated by Pasteur in 1853 and was used as a key intermediate for the synthesis of quinine derivatives.¹⁵⁹ The oxidation of tertiary amines is well-known reaction sequence in the presence of peroxide, which could explain the formation of *N*-oxide **177**.¹⁴³ Although this reaction is not relevant to our immobilization reaction conditions, the assignment of these by-products under free-radical reaction conditions would be beneficial for further studies regarding the immobilization mechanism.



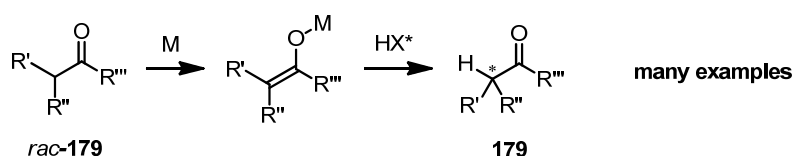
Scheme 4-89. Proposed reaction mechanism for the formation of coupled product **177**.

5. SUMMARY

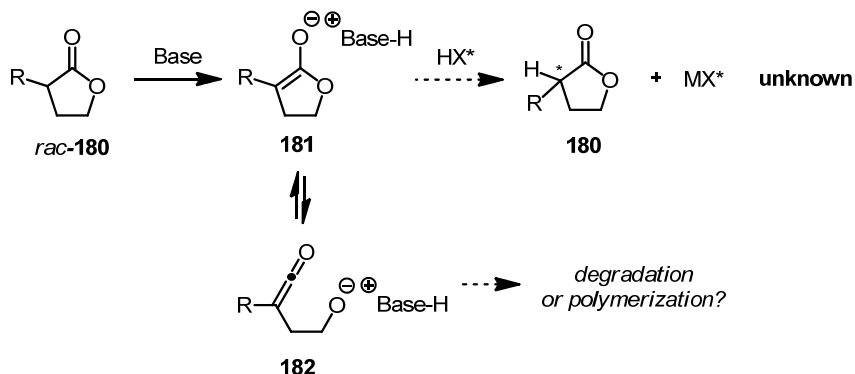
5.1. Deracemization of α -Substituted Hydrocoumarins *via* Asymmetric Protonation of Ketene Dithioacetals

Given the vast interest in asymmetric protonation reactions, as a strategy to access enantioenriched α -carbonyl compounds **179**, our research project focused on the preparation of chiral esters, particularly lactones **180**. Although asymmetric protonation using chiral auxiliaries and chiral proton donors can provide general access to chiral carbonyl compound such as esters, ketones and amides, the application of asymmetric protonation to cyclic lactones has been neglected (Scheme 5-1).

Asymmetric protonation of acyclic compounds:

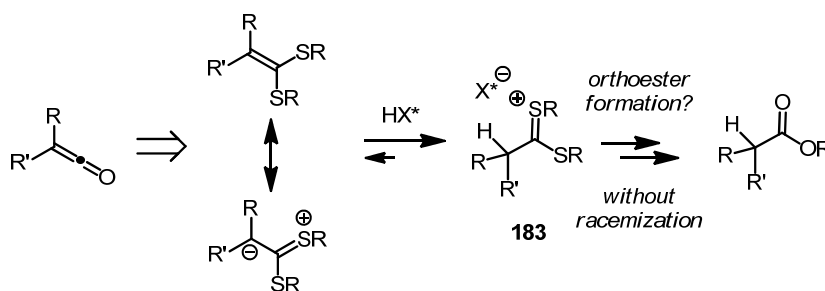


Asymmetric protonation of cyclic esters, lactones



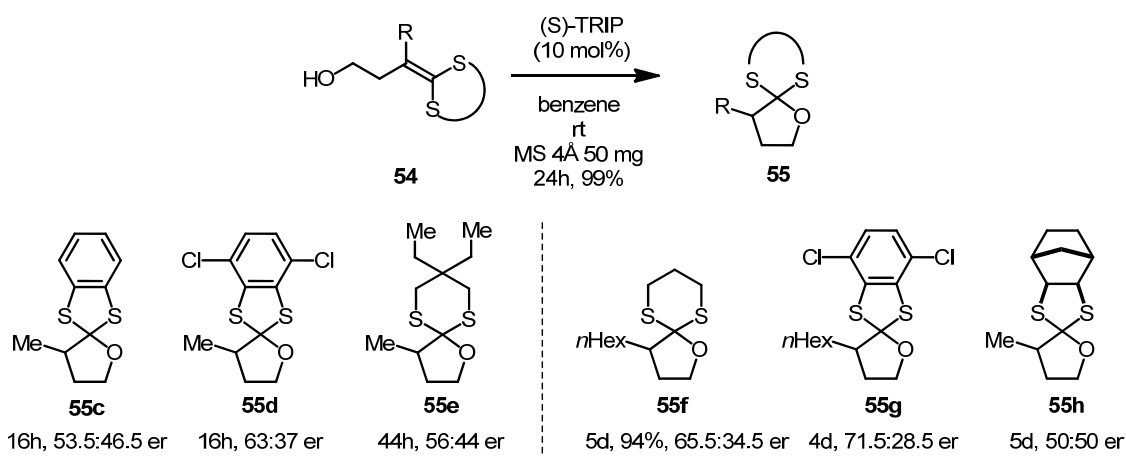
Scheme 5-1. Asymmetric protonation of carbonyl compounds.

α -Substituted lactones can be accessed *via* a simple alkylation strategy. Nevertheless, enolate **181** could be in an equilibrium with ketene intermediate **182** leading to low yields of the desired product (Scheme 5-1). To circumvent this problem, we have investigated asymmetric protonation of novel ketene dithioacetals. Ketene dithioacetals are protected ketenes, which have a negative charge density on the α -carbon, which usually undergoes protonation in the presence of Brønsted acids. Our goal was to obtain enantioenriched α -protonated carbonyl compounds through intermediate **183** and further functionalization without destroying the established stereogenic center (Scheme 5-2).



Scheme 5-2. Asymmetric protonation of dithioacetene acetal and transformation to the corresponding carbonyl compounds.

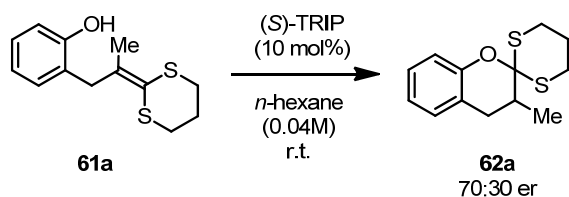
By exploring various dithiols as protecting groups, a facile cyclization reaction of ketene dithioacetals **54** under optimized reaction conditions was observed using TRIP as a Brønsted acid catalyst. A manipulation of the dithiol backbone gave no significant improvement of enantioselectivity as shown in Scheme 5-3. However, a slight increment of enantioselectivity was observed by changing the substituent at the α -position from methyl to *n*-hexyl. This result prompted us to investigate different substrate classes since the obtained enantioselectivity was greatly affected by α -substitution, and not by the dithiol moiety.



Scheme 5-3. Asymmetric protonation reaction of various ketene dithioacetals.

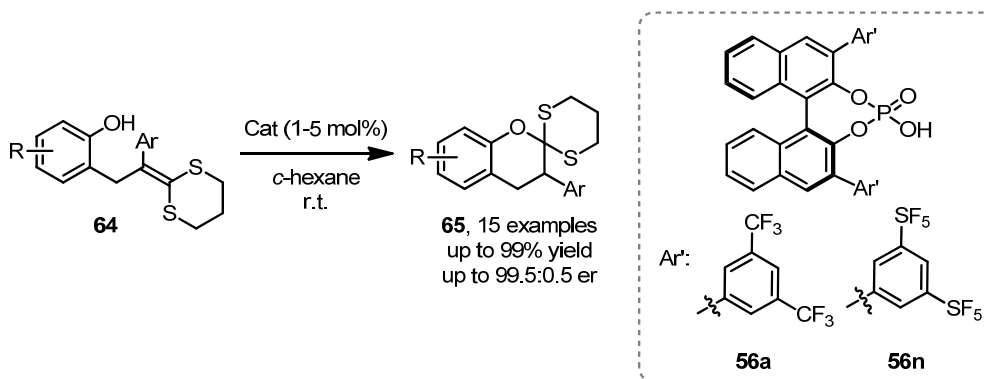
Prior to this work, no general method existed for the asymmetric synthesis of α -substituted hydrocoumarin in enantiopure form. We became interested in the synthesis of this class of molecules since they are known to be biologically active. However, asymmetric protonation of the ketene dithioacetal derived from α -methylhydrocoumarin **61a** gave only disappointing results in the presence of a catalytic amount of TRIP phosphoric acid after extensive screening of the reaction conditions (up to 70:30 er, Scheme 5-4).

5. SUMMARY



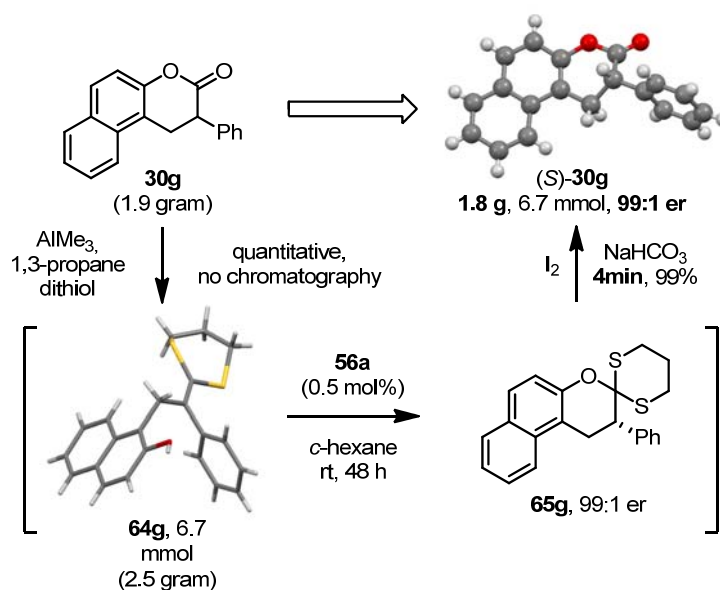
Scheme 5-4. Asymmetric protonation of α -methyl ketene dithioacetal derived from hydrocoumarin (**61a**).

Since it was observed that the α -substitution of ketene dithioacetals is critical for the enantioselectivity, we turned our attention to the α -aryl hydrocoumarin **30** as a substrate. Numerous naturally occurring hydrocoumarins, chromans and isoflavonoids possess an α -aryl substituent. Moreover, prior to this work, asymmetric synthesis of α -aryl hydrocoumarin was completely unknown. After extensive screening of various Brønsted acid catalysts and reaction conditions, high enantioselectivities of dithioacetals **65** were obtained (up to 99.6:0.4 er) with good chemical yields by using catalyst **56a** and novel SF₅ substituted catalyst **56n** (Scheme 5-5).



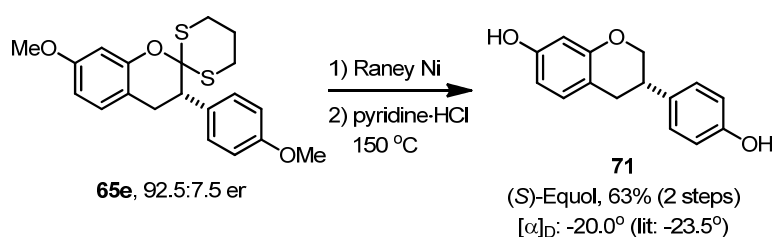
Scheme 5-5. Asymmetric protonation of ketene dithioacetals derived from α -arylhydrocoumarins **64**.

Further applications of our methodology were demonstrated by the large scale synthesis of enantiopure hydrocoumarin **30g**. This compound structurally resembles Splitomicin, which is an effective inhibitor for histone deacetylase.⁹¹ The synthesis of hydrocoumarin **30g** was commenced by preparing ketene dithioacetal **64g**, which was isolated by simple precipitation in cold ether (Scheme 5-6). The subsequent cyclization of ketene dithioacetal was conducted in the presence of 0.5 mol% of catalyst **56a** to afford enantiopure product **65g** with 99:1 er. These two intermediates were not isolated until the oxidative hydrolysis was completed. Under the optimized reaction conditions (I₂, NaHCO₃, 4 min), enantiopure hydrocoumarin (*S*)-**30g** was obtained with high yield after precipitation due to its low solubility. Therefore deracemization of hydrocoumarin **30g** was achieved in a large scale under the practical reaction conditions without any chromatographic purification.



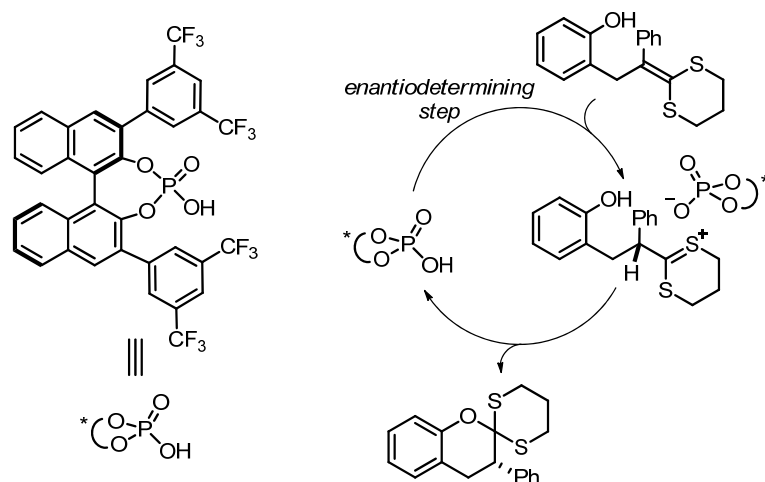
Scheme 5-6. Large scale deracemization of hydrocoumarin **30g**.

As showcased here, the dithioacetals could easily be removed by hydrogenolysis using Raney-Ni under hydrogen atmosphere. After deprotection of the dithioacetal using this method, we could access the chroman derivative without racemization of the stereogenic center. This prompted us to apply our methodology to the synthesis of natural products. For example, Equol is a natural product, which could be found in the human intestine. The deprotection reaction conditions were easily optimized and applied to dithioacetal **65e** to afford chroman **70**. After demethylation at high temperature using pyridine-HCl salt, we could obtain enantioenriched (S)-Equol with good yield over two steps (63% yield, Scheme 5-7).



Scheme 5-7. Reductive deprotection of dithioacetal and demethylation to afford (S)-Equol.

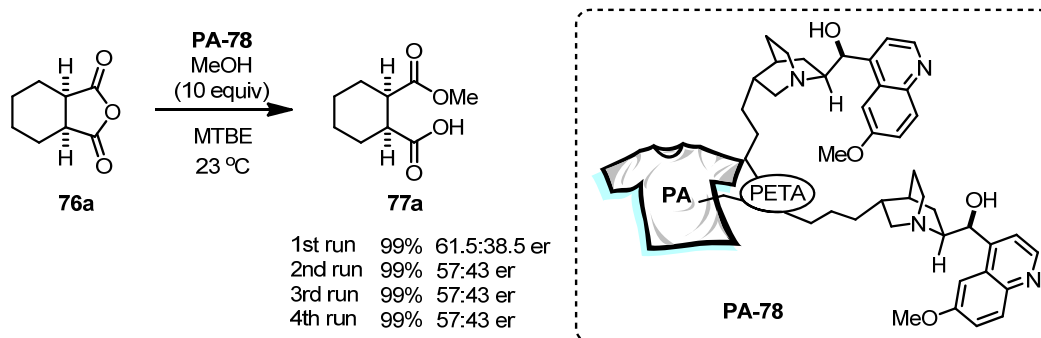
A plausible reaction mechanism of the asymmetric protonation of ketene dithioacetal is summarized in Scheme 5-8. It is well known that ketene dithioacetals **64** undergo spontaneous protonation under acidic conditions. Although the phenolic proton could be a proton source (pK_a of phenol in DMSO = 18), the enantiodetermining step must be the protonation step from the catalyst to the ketene dithioacetal, due to its higher acidity (pK_a of catalyst **56a** in DMSO = 2.63).¹⁶⁰ Although the protonated intermediate could be cyclized without catalyst to afford product **65**, the incorporation of the phosphonate could facilitate the reaction by stabilizing and activating the intermediate *via* hydrogen bonding and charge-charge interaction.



Scheme 5-8. A plausible reaction mechanism for the asymmetric protonation of ketene dithioacetal.

5.2. Textile Organocatalysis

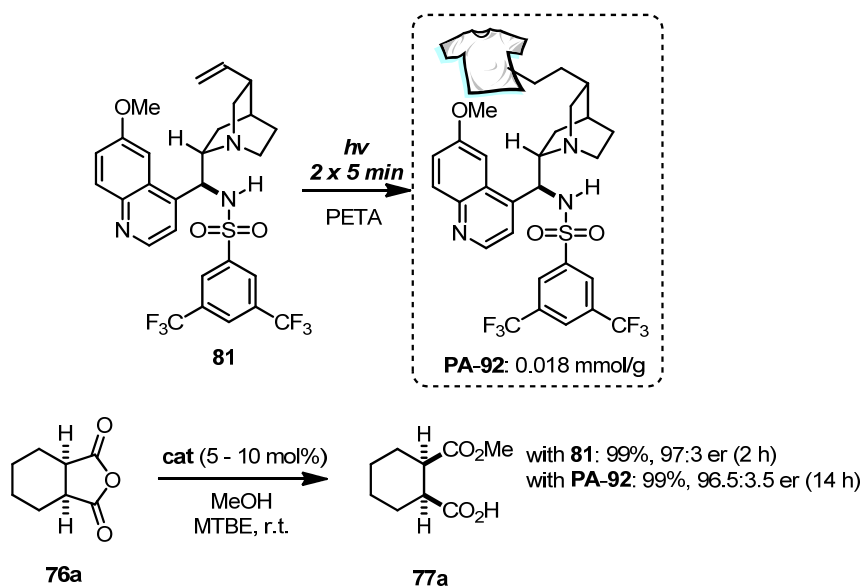
To provide a general methodology for preparing heterogeneous catalysts from homogenous catalysts without sophisticated functionalization and manipulation, we conducted a series of experiments regarding the preparation of textile-supported organocatalysts and their applications. Our results show a great potential of the methodology as a general platform for heterogeneous organocatalysis. A simple organocatalyst, quinine, was immobilized without any functionalization on the catalyst or the solid support. The irradiation reaction conditions enabled the facile preparation of chiral catalyst-immobilized textile **PA-78**. The obtained catalyst was used for the desymmetrization of *meso*-anhydride **76** to afford hemiester **77a** with good conversion and low enantioselectivity. However, further recycling experiments revealed that the catalyst could be used without significant erosion of enantioselectivity (Scheme 5-9).



Scheme 5-9. Application of quinine-immobilized textile organocatalyst **PA-78**.

Further investigation of bifunctional organocatalysts was focused on the sulfonamide-based catalyst **81**. The obtained textile catalyst, after extensive optimization studies, showed high enantioselectivity for the model reaction. Although the desymmetrization reaction could suffer from severe competition of the background

reaction, the heterogeneous catalysis with catalyst **PA-92** gave comparable activity and enantioselectivity to the homogeneous catalysis (Scheme 5-10).



Scheme 5-10. Preparation and application of textile-immobilized sulfonamide catalyst **PA-92**.

Textile catalyst **PA-92** could be reused for the reaction without any sophisticated recovery procedure for more than 250 cycles (Figure 5-1). Using 6-7 mol% of catalyst loading, we could obtain more than 95:5 er of the desired product with quantitative yield. Although the enantioselectivity of the catalyst slightly decreased after 150 cycles (94:6 er), we could obtain the same enantioselectivity as before (95:5 er) by increasing the catalyst loading to 10 mol %. This result demonstrates the remarkable stability of the textile catalyst. To the best of our knowledge, there is no precedent heterogeneous asymmetric catalyst, which can be used for more than 200 cycles without losing catalytic activity or enantioselectivity.

5. SUMMARY

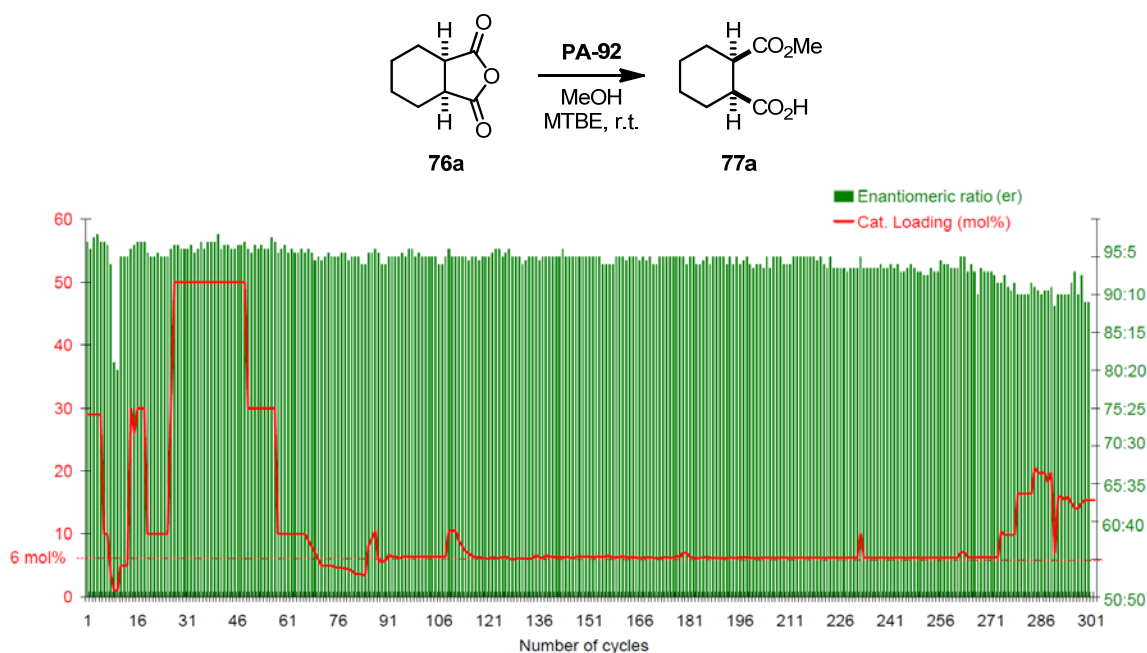
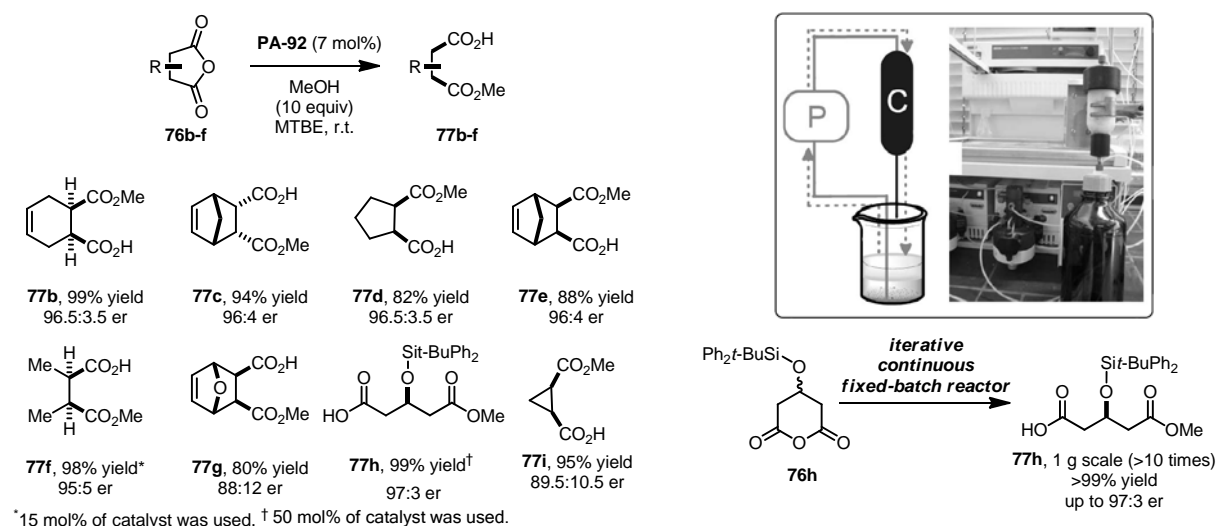


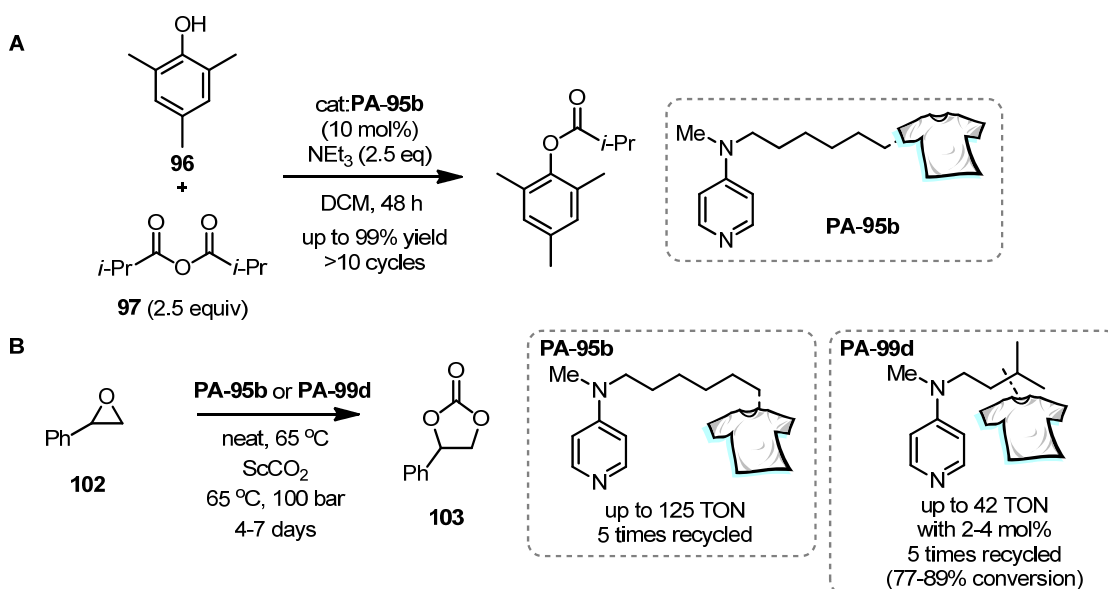
Figure 5-1. Recycling of textile catalyst PA-92 for the desymmetrization of *meso*-anhydride.

Notably, the textile catalyst could be prepared in large scale (20 sheets, >20g). The obtained catalysts were used to test the substrate scope (Scheme 5-11). Generally, the textile catalyst showed similar activity and enantioselectivity to the homogeneous catalyst, affording hemiesters **77** with high enantioselectivity. Further application of the textile catalyst was conducted by preparing a continuous fixed-batch reactor. After brief optimization of the reaction conditions, this system could provide optically enriched hemiester **77h** with quantitative yield in large scale (1-2 gram per each run). The obtained hemiester from 4-hydroxyglutaric anhydride could be used for the synthesis of Statin derivatives (Scheme 5-11).



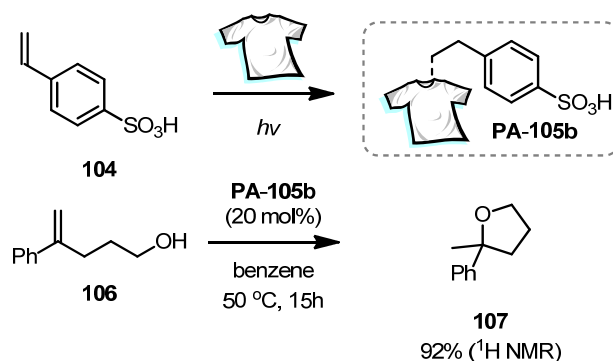
Scheme 5-11. Substrate scope of catalyst PA-92 and application of the textile catalyst to fixed-batch continuous reactor.

Next, the immobilization of various organocatalysts was attempted. First, Lewis basic DMAP derivatives were successfully immobilized and applied in the acylation of sterically bulky substrates (Scheme 5-12A). The catalyst could be recycled more than 10 times without erosion of its activity. Moreover, this catalyst was employed for the cyclic carbonate formation using an epoxide to afford a cyclic carbonate in supercritical CO₂ conditions (Scheme 5-12B). The catalyst showed reasonable stability under the harsh reaction conditions, which again showed the robustness of the heterogeneous catalyst.



Scheme 5-12. Application of textile catalysts prepared from DMAP-derivatives. Acylation reaction of phenol **96**. cyclic carbonate formation reaction using epoxide **102** catalyzed by catalysts **PA-95b** or **PA-99d**.

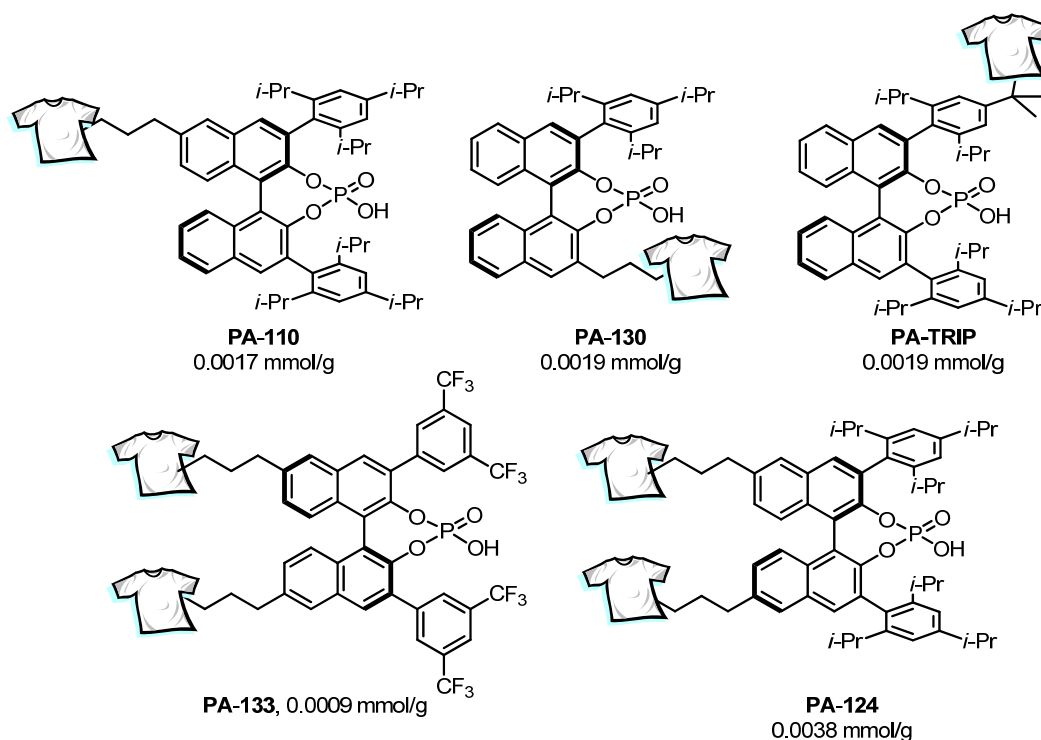
Further application of this immobilization methodology was conducted with Brønsted acid catalysts. From commercially available starting material (acid and polyamide), the highly acidic heterogeneous catalyst could be easily accessed. Then catalyst **PA-105b** was applied in a catalytic hydroetherification reaction of substrate **106** to afford a tetrahydrofuran derivative with good yield. This results again highlights the methodology since the procedure for the preparation of catalyst **PA-105b** is remarkably simple.



Scheme 5-13. Preparation and application of Brønsted acid immobilized textile catalyst **PA-105b**.

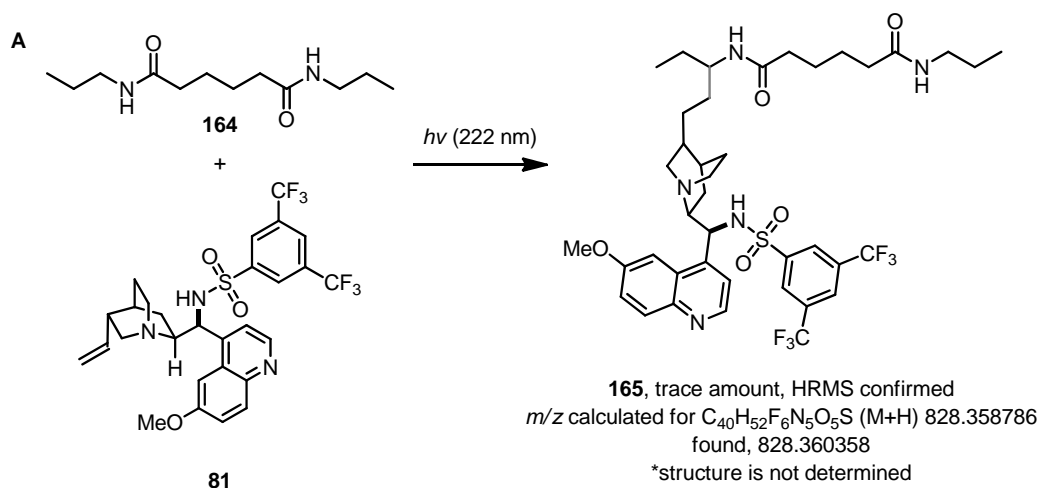
5. SUMMARY

We then turned our attention to the preparation of chiral phosphoric acid-immobilized textile catalysts. Several monomeric phosphoric acids containing an olefin functionality were prepared and immobilized on textile (Scheme 5-14). However, the catalytic activity and enantioselectivity of these catalysts was poor. Further optimization of the immobilization process for phosphoric acids is highly desirable. Nonetheless, immobilization could occur without the olefin functional group. For example TRIP was immobilized under irradiation conditions, presumably through formation of an isopropyl centered radical intermediate. This reaction profile could improve the synthetic procedure for the immobilization process, since the monomer requires no further functionalization.



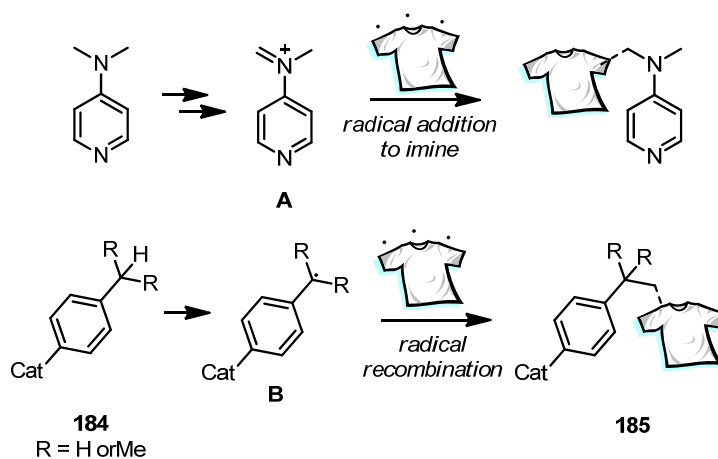
Scheme 5-14. Various immobilized phosphoric acids on polyamide.

To gain insight of the reaction mechanism, we conducted various experiments under photochemical reaction conditions and free-radical generation reaction conditions using “monomeric” polyamide in the presence of quinine and quinine sulfonamide catalyst **81**. As summarized in Scheme 5-15, the sulfonamide catalyst could be coupled with diamide **164** under irradiation conditions albeit in extremely low yield.



Scheme 5-15. Mechanistic studies on the immobilization process.

As mentioned previously, in the absence of the olefin functionality, we could obtain the immobilized organocatalyst in the case of electron-rich DMAP and toluene, cumene derived organocatalysts **184**. According to the obtained mechanistic evidence, we presumed that the excited surface of the textile could react with activated intermediates such as iminium cation (**A**) and cumene radical (**B**) (Scheme 5-16). This process could be very useful for the immobilization of various common organic catalysts, promoters and reagents due to the simplicity of the process. Further investigation on the immobilization of simple organic molecules such as metal-chelating reagents, phosphines and peptide for solid state synthesis would be desirable.

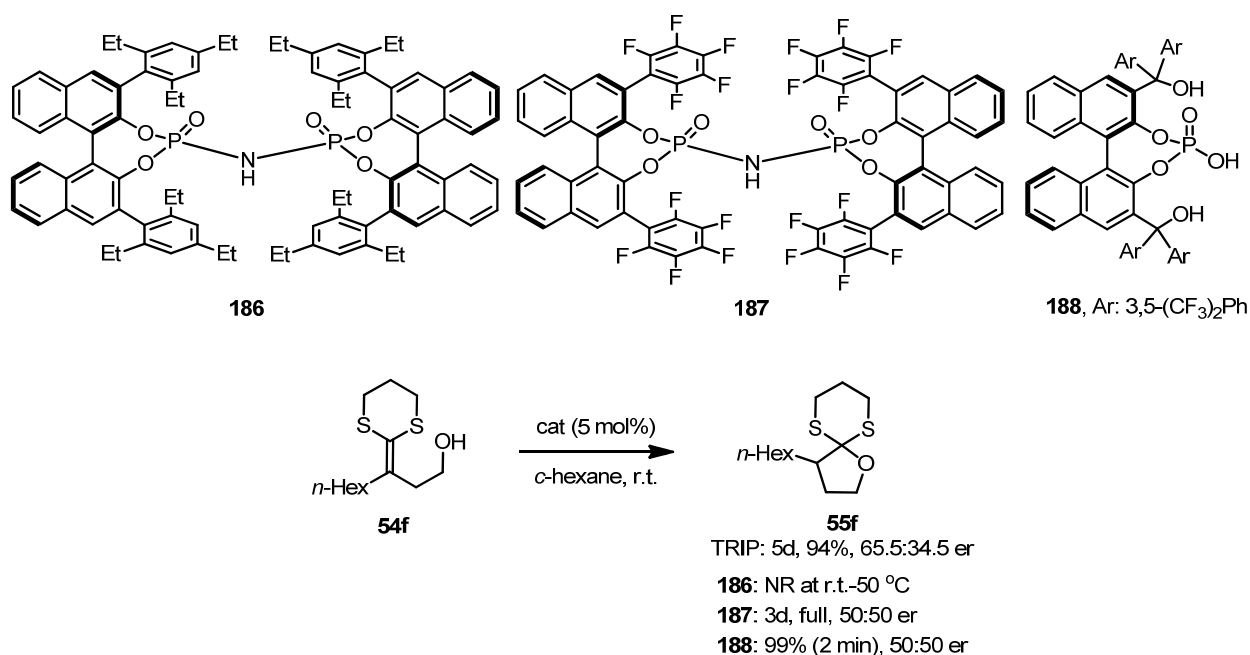


Scheme 5-16. Proposed immobilization mechanism of DMAP and cumene derived catalysts.

6. OUTLOOK

6.1. Asymmetric Protonation of Ketene Dithioacetals

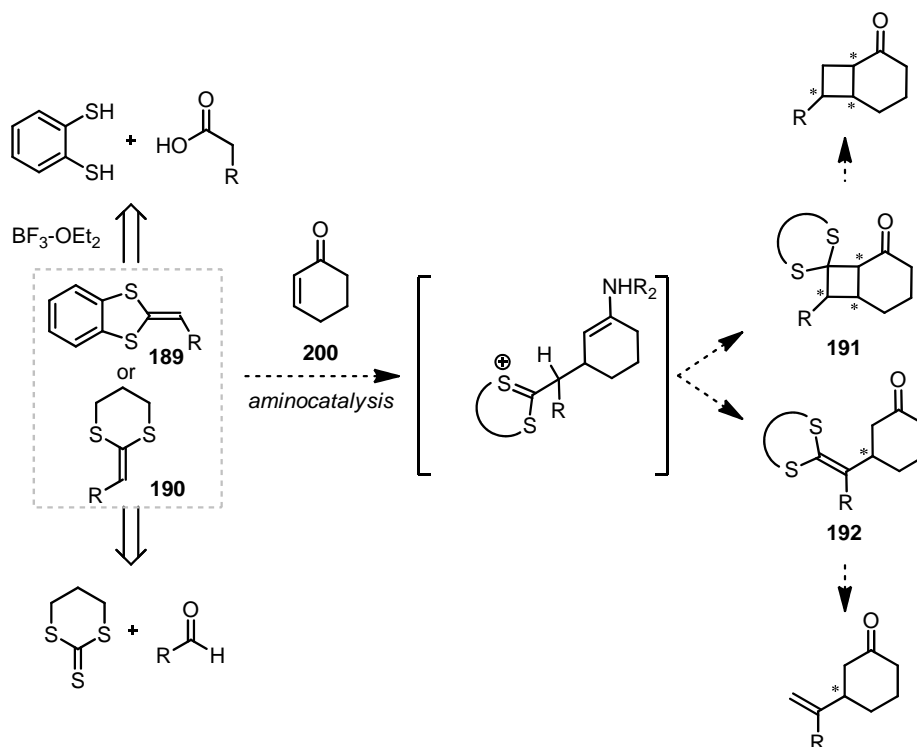
Although for α -arylhydrocoumarins we have achieved a highly enantioselective protonation reaction using a chiral Brønsted acid catalyst, α -alkylhydrocoumarins and simple lactones showed inferior enantioselectivities. This result could be improved through employment of new catalysts by rendering a more compact chiral environment. Imidodiphosphoric acid catalysts **186** and **187** were tested for this purpose, but due to the sterically hindered catalyst cavity, the reaction did not proceed even at higher reaction temperature (Scheme 6-1). On the other hand, stronger Brønsted acid catalyst **188** could facilitate the reaction, which takes more than 5 days under the standard reaction conditions. Catalyst **188** showed good activity for this reaction although the obtained product was racemic. The new catalyst developed by *Dr. Lars Ratjen* showed remarkable reactivity. Full conversion of the starting material to desired product **55f** was observed albeit with no enantioselection. Nonetheless these types of new catalysts are quite promising for the undeveloped asymmetric catalysis by fine-tuning of the chiral backbone to induce high enantioselectivity.



Scheme 6-1. Further screening of newly developed catalysts on the asymmetric protonation of ketene dithioacetal **54f**.

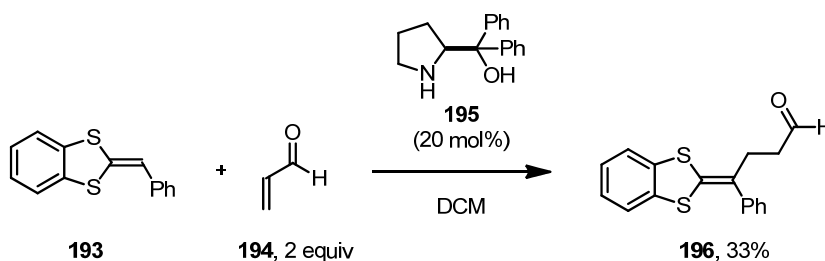
Another application of ketene dithioacetals can be achieved by using simple starting materials such as dithiol and carboxylic acids under Lewis acidic reaction conditions. The obtained ketene dithioacetals **189** and **190**

could undergo nucleophilic addition to a typical electrophile, an iminium ion, to give rise to complex molecules such as bicyclic compound **191** and Heck-type product **192**.



Scheme 6-2. Nucleophilic reaction of ketene dithioacetals **189** and **190**.

A preliminary result shows reasonable conversion of enal to 1,4-addition product **196** with 33% yield in the presence of secondary amine catalyst **195**. Further investigation of this reaction with cyclic compounds would be interesting (Scheme 6-3).

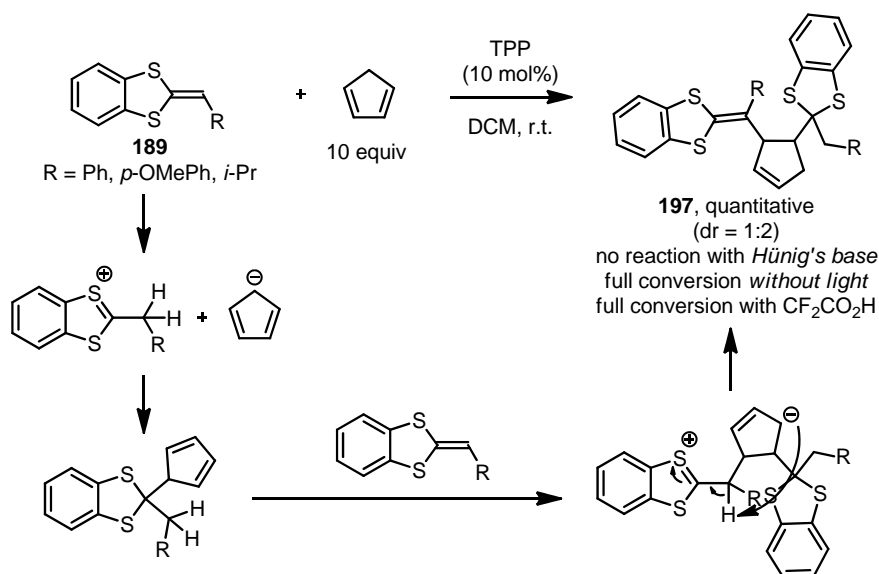


Scheme 6-3. 1,4-Addition of ketene dithioacetal **193** to acrolein.

The unique reactivity of ketene dithioacetals was also observed by treating substrate **189** with cyclopentadiene under photochemical reaction conditions. The reaction provided cyclic compound **197** which incorporates two molecules of ketene dithioacetal. The exact reaction mechanism is completely unclear at this stage but we suggest a reaction mechanism, which shows basic and nucleophilic properties of ketene dithioacetal. A brief optimization of the reaction conditions revealed that in the presence of base, the reaction was completely quenched. A catalytic amount of acid could promote the reaction efficiently, which implies that a trace amount

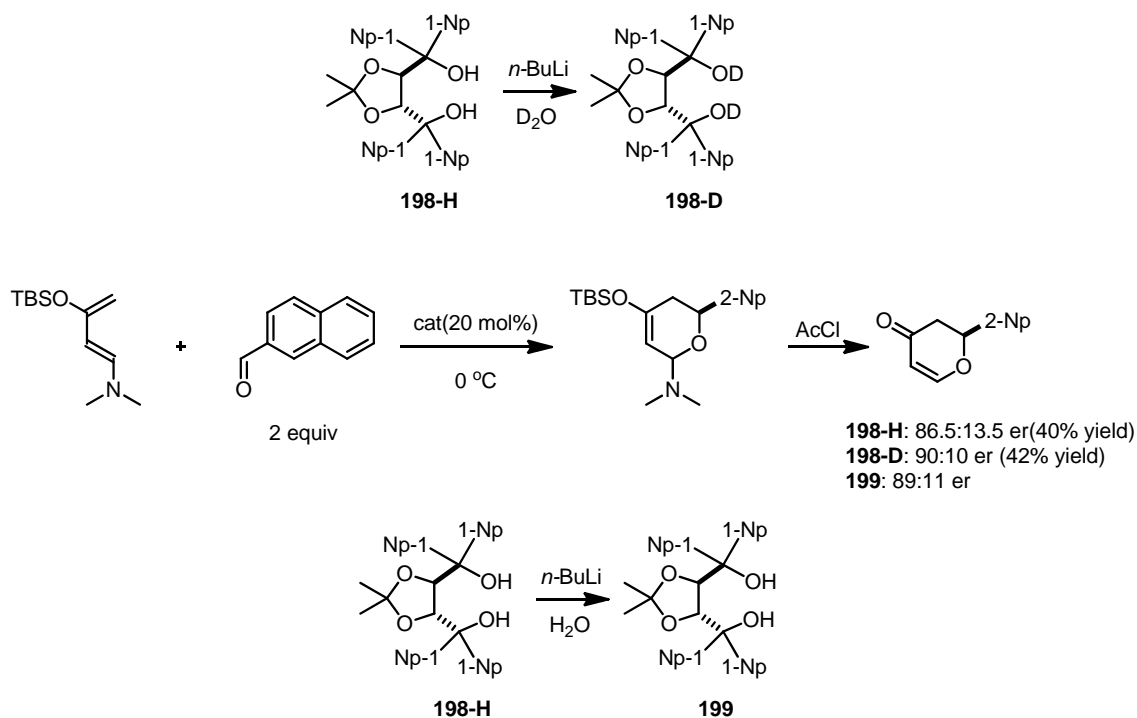
6. OUTLOOK

of Brønsted acid could be a reason for the reaction outcome in the presence of photosensitizer TPP (Triphenylpyrylium tetrafluoroborate salt).



Scheme 6-4. Unusual reactivity pattern of ketene dithioacetals **189** with cyclopentadiene.

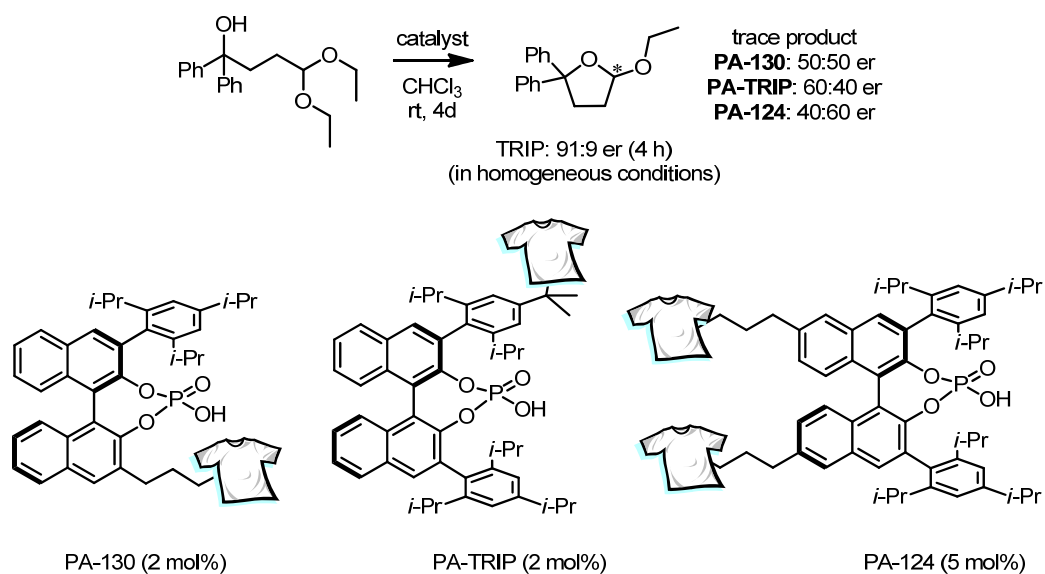
As mentioned in Chapter 4.2.6, we have observed a slight increase of enantioselectivity by using a deuterated substrate and catalyst (collaboration with *Dr. Ilija Čorić*). To confirm this hypothesis we conducted control experiments with common hydrogen-bonding donor catalyst TADDOL **198-H**. For the hetero Diels-Alder reaction reported by Rawal *et al.*⁵⁹ the catalyst **198-D** after deuteration showed higher enantioselectivity (90:10 er) compared to the protonated catalyst **198-H** (86.4:13.5 er). However, this effect could be derived from the alteration of the catalyst purity as shown by using re-protonated catalyst **199** for the catalysis to afford the product with slightly higher enantioselectivity (89:11 er).



Scheme 6-5. Effects of deuterated catalyst in asymmetric catalysis.

6.2. Textile Organocatalysis

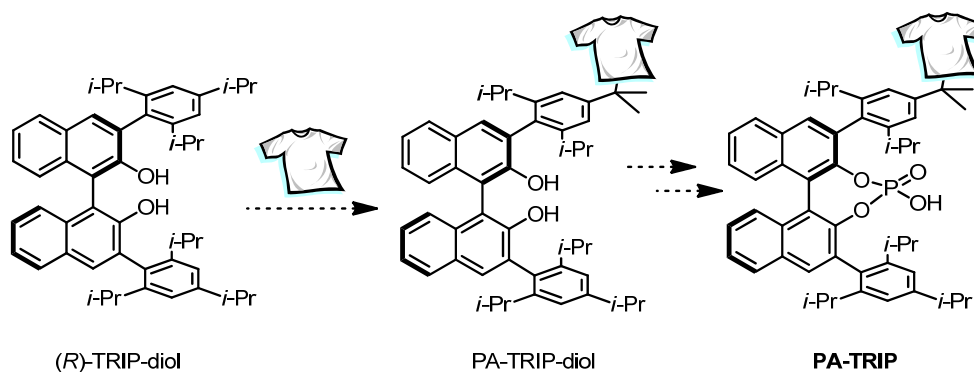
Although we have successfully prepared and applied textile catalysts for various catalytic transformations including asymmetric catalysis, we could not obtain any promising results with phosphoric acid derivatives. The obtained heterogeneous catalysts are generally less active than the corresponding homogeneous catalysts and show inferior enantioselectivity for transacetalization as shown in Scheme 6-6 (up to 60:40 er).¹⁶¹ This result could be improved by preparing the catalyst through a different pathway.



Scheme 6-6. Enantioselective transacetalization using textile-immobilized phosphoric acids.

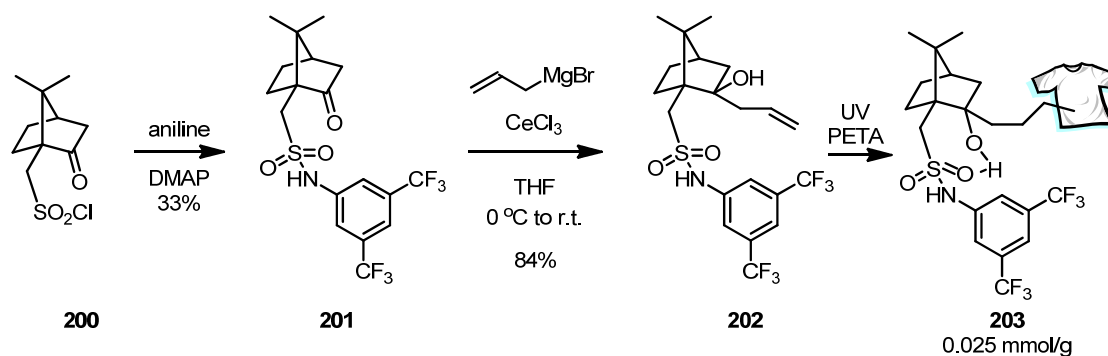
6. OUTLOOK

For example, a BINOL derivative could be immobilized under photochemical conditions. Because amide bonds can react under phosphoric acid formation reaction conditions (Vilsmeier–Haack reaction), a chemically more robust textile such as PET should be employed for the preparation of phosphoric acid-immobilized textile catalysts.



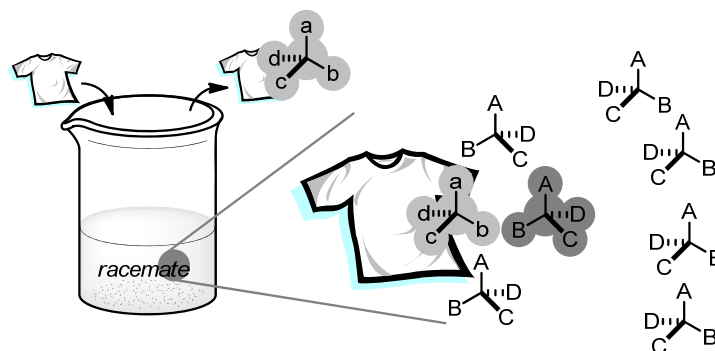
Scheme 6-7. Immobilization of BINOL-derived diol and further functionalization to provide phosphoric acids immobilized textiles.

The simple preparation (total 3 steps) of textile immobilized chiral organocatalyst is demonstrated as depicted in Scheme 6-8. A facile synthesis and immobilization of the olefin-functionalized sulfonamide **202**, which is potentially useful hydrogen-bonding donor catalyst, could find an application in asymmetric catalysis.



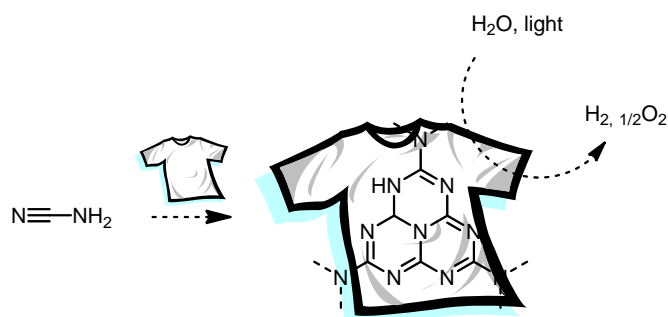
Scheme 6-8. Synthesis of new hydrogen bonding donor **202** with allyl functional group and its immobilization.

The obtained chiral functional textiles could be applied into various recognition processes, such as chiral host-guest interactions. Due to the high permeability for organic solvents and the high surface area of textile materials, enantioselective recognition of a racemic mixture by a chiral textile material would be desirable (Scheme 6-9). A similar approach was reported using chiral molecule-modified nanoparticles.¹⁶² A convenient preparation of chiral textiles can provide a more practical approach for this methodology. Further applications in microfluidic-like systems would be interesting using the textiles' capillary effect.¹⁶³



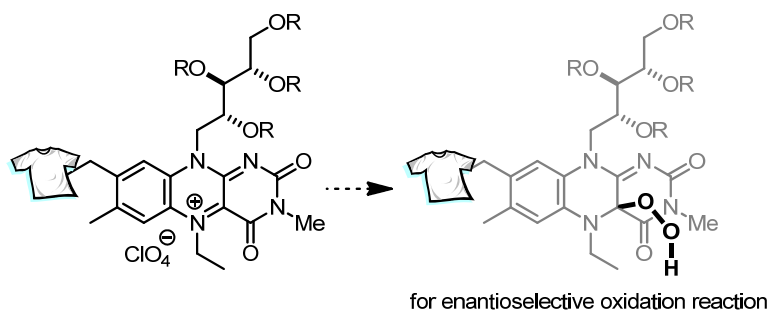
Scheme 6-9. Selective enantiomer fishing by chiral molecule modified textile materials.

Another application could be realized by employing organic photo-active polymers, such as carbon nitride, which is known for water splitting catalyst.¹⁶⁴ Carbon nitride is a graphene-like flat polymer with nitrogen doping. The synthesis is quite straightforward from aminonitrile. We presume that if the polymerization could occur on the surface of the textile materials, we could generate a photo-active textile for water splitting reaction under photochemical reaction conditions. This reaction could lead us to provide a simple device without any sophisticated cell assembly. We are currently working on the synthesis of carbon nitride polymer embedded textile materials and their analysis.



Scheme 6-10. Water splitting reaction under photochemical reaction conditions using CN-immobilized textile.

Riboflavin derivatives have been reported as chiral catalysts for the oxidation of sulfide.¹⁶⁵ We have observed that toluene could undergo photochemical activation for the immobilization reaction on textile materials. Using the inherent functionality of riboflavin's xylene group, it would be interesting to employ O-protected riboflavin as an oxidation catalyst in heterogeneous reaction conditions using hydrogen peroxide (Scheme 6-11). Since the textile materials could be sensitive to hydrogen peroxide, and undergo radical decomposition of the solid backbone, we are currently investigating textile materials, which can withstand harsh reaction conditions. Various textiles could be washed with bleach (NaOCl), however, it should be noted that immobilized organic molecules could be cleaved under radical generation conditions, which can be supported by our own experimental results.



Scheme 6-11. Enantioselective oxidation using riboflavin derivative-immobilized textiles.

Although the immobilization reaction conditions could be detrimental for certain molecules, which are light-sensitive, our methodology could be applied to various organic catalysts, ligands and reagents. Particularly, metal scavengers are attractive due to their vast employment in industry to remove transition metal impurities. These materials are extremely expensive from commercial sources. For example, Merrifield's resin immobilized TMEDA can coordinate to various transition metals (cobalt, copper, nickel, palladium and zinc). Our methodology could provide a TMEDA-immobilized textile using simply photochemical reaction conditions *via* iminium ion formation of TMEDA and radical reaction (Figure 6-1). Our methodology would allow the straightforward preparation of any kind of immobilized organic molecules under simple reaction conditions.

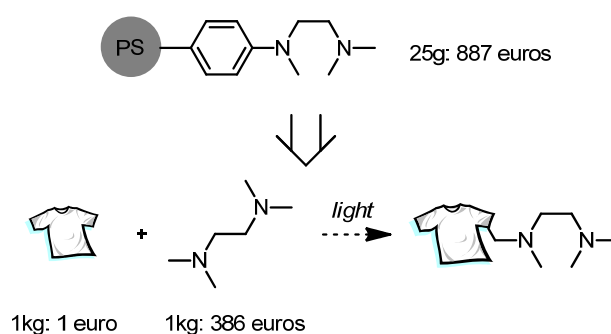


Figure 6-1. Comparison of conventional metal scavenger and textile-scavenger. (Prices are from the website of Sigma-Aldrich)

7. EXPERIMENTAL PART

7.1. General Experimental Conditions

Solvents and reagents

All solvents were purified by distillation before use following standard procedures. Absolute solvents were obtained by distillation over appropriate drying agent and then kept under an atmosphere of argon: diethyl ether, tetrahydrofuran, dichloromethane, triethylamine (calcium hydride), acetonitrile. Other commercial reagents were obtained from various sources and used without further purification.

Inert gas atmosphere

Air and moisture-sensitive reactions were conducted under an atmosphere of argon (*Air Liquide*, >99.5% purity). Unless otherwise stated, all cross-coupling and allylic alkylation reactions within this thesis were carried out under argon atmosphere.

Chromatographic methods

Whenever possible, reactions were monitored by thin layer chromatography (TLC) using silica gel pre-coated plastic sheets (0.2 mm, Machery-Nagel). Visualization was accomplished by irradiation with UV light at 254 nm and/or potassium permanganate (1.5 g KMnO_4 , 10 g K_2CO_3 , 1.25 mL 10% NaOH, 200 mL H_2O) or *p*-anisaldehyde (0.7 mL *p*-anisaldehyde, 250 mL EtOH, 9.5 mL conc. H_2SO_4 , 2.7 mL glacial AcOH) stains. Flash column chromatography was performed using Merck silica gel (60, particle size 0.040-0.063 mm) using a specified solvent mixture and elevated pressure.

High pressure liquid chromatography (HPLC) was performed on a Shimadzu LC-2010C system equipped with a spectrophotometer or a diode array. Commercial HPLC-grade solvents were used, and measurements were conducted at 25 °C. The chiral stationary phase of the columns is specified in each experiment.

7. EXPERIMENTAL PART

Nuclear magnetic resonance spectroscopy (NMR)

Proton and carbon NMR spectra were recorded on Bruker AV-500 or Bruker AV-400 or Bruker AV-300 spectrometer in deuterated solvents. Proton chemical shifts are reported in ppm (δ) relative to tetramethylsilane (TMS) with the solvent resonance employed as the internal standard (C_6D_6 , δ 7.16 ppm; $CDCl_3$, δ 7.26; THF- d_8 , δ 1.85 (OCH_2CH_2) ppm; CD_3OD , δ 3.31 ppm; $(CD_3)_2CO$, δ 2.05 ppm). Data are reported as follows: chemical shift, multiplicity (s = singlet, d = doublet, q = quartet, sept = septet, m = multiplet, br = broad), coupling constants (Hz) and integration. ^{13}C Chemical shifts are reported in ppm from tetramethylsilane (TMS) with the solvent resonance as the internal standard (C_6D_6 , δ 128.06 ppm; $CDCl_3$, δ 77.0; THF- d_8 , δ 25.6 (OCH_2CH_2) ppm; $(CD_3)_2CO$, δ 29.84 ppm).

Mass spectrometry (MS)

Mass spectra were measured on a Finnigan MAT 8200 (70 eV) or an Agilent 5973 (70 eV) spectrometer by electron ionization, chemical ionization, or fast atom/ion bombardment techniques. High resolution mass spectra were determined on a Bruker APEX III FTMS (7 T magnet). All masses are given in atomic units/elementary charge (m/z) and reported in percentage relative to the basic peak.

Specific rotation ($[\alpha]$)

Optical rotations were determined with Autopol IV polarimeter (Rudolph Research Analytical) using a 0.5 mL cell with a path length of 1 dm at 589 nm (sodium D-line) and 25 °C. Data are reported as follows: $[\alpha]_{\lambda}^{temp}$, concentration (c in g/100 mL), and solvent.

Determination of the optical purity

Enantiomeric ratios (er) were determined by chiral HPLC analysis by comparing samples with the appropriate racemic mixtures.

Melting point (mp)

All melting points were measured on a *Büchi* 540 Melting Point apparatus in open glass capillaries. The values are given in °C and are uncorrected.

Preparation of textile catalysts

For the preparation of textile catalysts, photo immobilization reactions was conducted by using an UV-Excimer-System by Heraeus Noblelight with a quasi monochromatic KrCl*-Excimer-Lamp with a wavelength of 222 nm (sample to light source: 8 cm) under argon atmosphere. Polyamid (6,6, weave by Gustav Schuessler Textilwarenfabrik GmbH & Co. KG) with an area weight of 170 g/m² was extracted with EtOH/H₂O for 8 h and with petroleumether for 8 h before use.

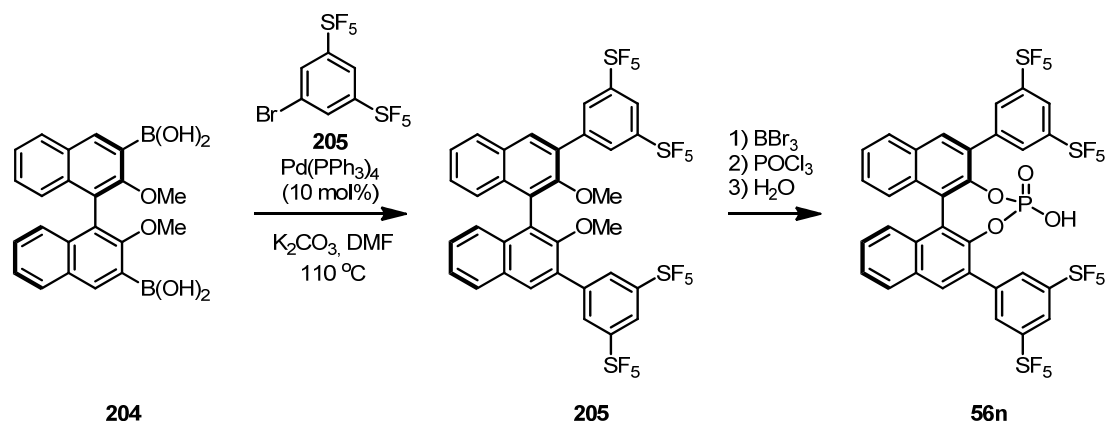
Elemental analysis

Microwave digestion for elemental analysis of sulphur was conducted with MarsXpress, CEM. Elemental analysis was measured with Varian 720-ES ICP/OES.

Electron Microscopy

SEM image of the textile was recorded with SEM S-3400 N II of Hitachi High-Technologies Europe GmbH.

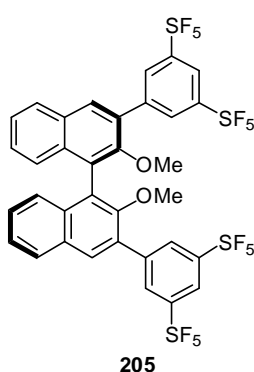
7.2. Synthesis of BINOL-Based Brønsted Acid Catalysts

7.2.1. Preparation SF₅-Substituted Phosphoric Acid 56n

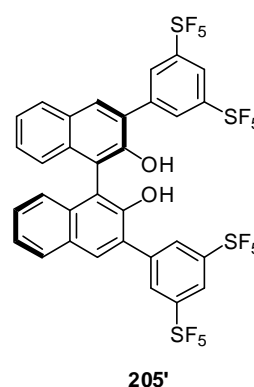
Suzuki coupling: Under argon atmosphere, to a two-neck round bottom flask, boronic acid **205** (1 equiv) and 3,5-bis(pentafluorothio)bromo benzene (4 equiv), tetrakis(triphenylphosphine) (0.2 equiv) and K₃PO₄ (9 equiv) was added and dried by applying reduced pressure and refilled with argon twice. Then DMF (0.02 M based on the boronic acid) was added and the reaction mixture was purged with argon for 30 min by bubbling argon and then heated to 110 °C and stirred for 3 days. After completion of starting material **204**, water (10 mL) and dichloromethane (15 mL) was added and extracted with dichloromethane three times and dried over MgSO₄. The crude reaction mixture was further purified by silica column chromatography (Ethylacetate:Hexane=1:4) to afford **205** (30% yield, not optimized).

Deprotection: To a solution of compound **205** in dichloromethane (0.02 M based on the **205**) BBr₃ (solution in DCM, 2M, 4 equiv) was added slowly at 0 °C and the reaction mixture warmed to room temperature. After 5 hrs, the reaction mixture was quenched with water (10 mL) and extracted with dichloromethane and the crude reaction mixture was further purified by silica chromatography (dichloromethane:hexane=1:10) to afford pure diol **205'** (75% yield).

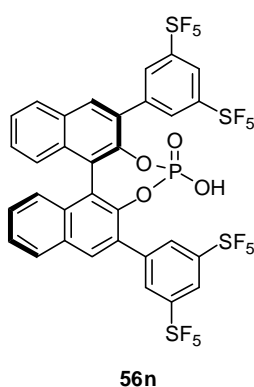
Phosphoric acid preparation: The diol **205'** was dissolved in anhydrous pyridine (0.01 M) and POCl₃ (2 equiv) was slowly added at 0 °C and the reaction mixture was stirred at room temperature overnight, then water (2 mL) was added to the reaction mixture and stirred for 1 hr. To the reaction mixture 6N HCl was added and extracted with dichloromethane and the combined organic layer was evaporated under the reduced pressure. The obtained crude mixture was purified by short silica chromatography and then the pure compound dissolved in toluene and washed with 6N HCl (10 mL x 3) The combined organic layer was concentrated under the reduced pressure to afford catalyst **56n** (89% yield).

(R)-2,2'-Dimethoxy,-3,3'-bis[3,5-bis(pentafluorothio)phenyl]-1,1'-binaphthalene (**205**)

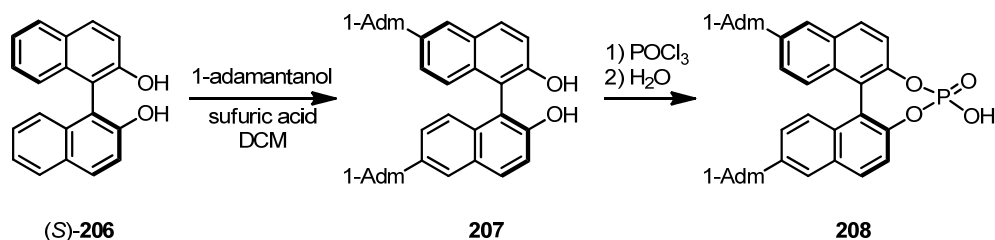
¹H NMR (500 MHz, CDCl₃), δ = 3.21 (s, 6H), 7.24 (d, J = 8.47 Hz, 2H), 7.38 (t, J = 7.66 Hz, 2H), 7.51 (t, J = 7.49 Hz, 2H), 8.00 (d, J = 8.21 Hz, 2H), 8.04 (s, 2H), 8.17 (t, J = 1.65 Hz, 2H), 8.36 (d, J = 1.71 Hz, 4H) ppm, **¹³C NMR** (125 MHz, CDCl₃), δ = 60.99, 122.79 (br), 125.73, 125.93, 126.02, 127.80, 128.55, 129.82 (br), 130.65, 131.21, 131.26, 134.35, 140.61, 153.21, 153.63 (t, J = 18.0 Hz) ppm. **¹⁹F NMR** (376 MHz, CDCl₃), δ = 62.94 (t, J = 16.5 Hz, 8F), 63.34 (t, J = 16.5 Hz, 8F), 81.92 (q, J = 150 Hz, 4F), **HRMS (ESI+)**, m/z calculated for C₃₄H₂₂O₂F₂₀S₄Na (M+Na⁺) 993.007562, found 993.007089.

(R)-2,2'-Diol,-3,3'-bis[3,5-bis(pentafluorothio)phenyl]-1,1'-binaphthalene (**205'**)

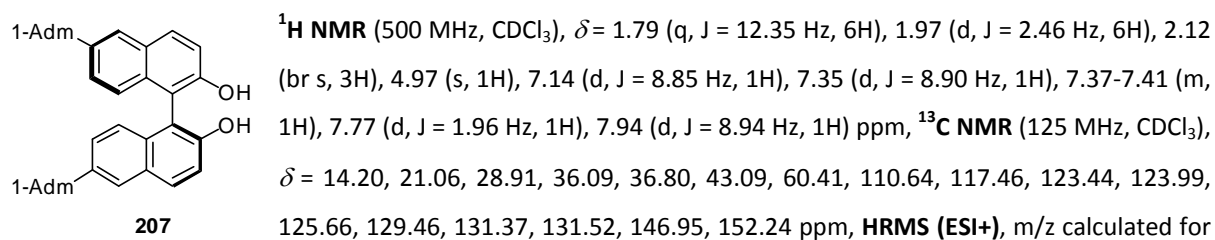
¹H NMR (500 MHz, CDCl₃), δ = 5.38 (s, 2H), 7.22 (d, J = 8.29 Hz, 2H), 7.44 (ddd, J = 8.15, 6.96, 1.21 Hz, 2H), 7.50 (ddd, J = 8.08, 6.84, 1.04 Hz, 2H), 8.02 (d, J = 7.97 Hz, 2H), 8.10 (s, 2H), 8.17 (t, J = 1.87 Hz, 2H), 8.33 (d, J = 1.83 Hz, 4H) ppm, **¹³C NMR** (125 MHz, acetone-*d*₆), δ = 114.88, 123.05, 124.96, 125.24, 128.55, 128.93, 129.65, 130.08, 131.65, 132.60, 135.72, 142.66, 152.21, 153.83 (quintet, J = 18.38 Hz) ppm, **¹⁹F NMR** (376 MHz, CDCl₃), δ = 62.94 (s, 8F), 63.34 (s, 8F), 81.99 (q, J = 152 Hz, 4F), **HRMS (ESI+)**, m/z calculated for C₃₂H₁₈O₂F₂₀S₄Na (M+Na⁺) 964.976258, found 964.976609.

(R)-3,3'-bis[3,5-bis(pentafluorothio)phenyl]-[1,1'-binaphthalene]-2,2'-diol phosphate (**56n**)

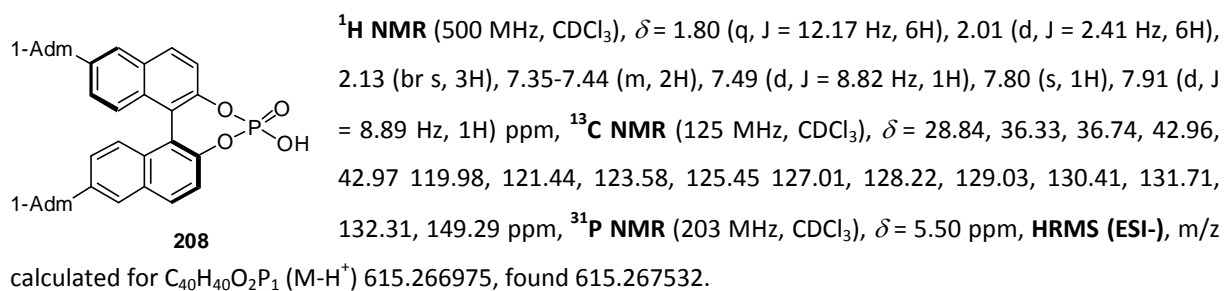
¹H NMR (500 MHz, CD₃OD), δ = 7.31 (d, J = 8.60 Hz, 2H), 7.38 (t, J = 7.64 Hz, 2H), 7.56 (t, J = 7.41 Hz, 2H), 8.15 (d, J = 8.27 Hz, 2H), 8.25-8.29 (m, 4H), 8.61 (s, 4H) ppm, **¹³C NMR** (125 MHz, CDCl₃), δ = 122.35, 123.54, 126.91, 126.98, 127.88, 128.76, 130.35, 131.51, 132.14, 132.49, 138.18, 143.59, 143.66, 153.31 (t, J = 18.90 Hz) ppm. **¹⁹F NMR** (376 MHz, CD₃OD), δ = 60.22 (s, 8F), 60.62 (s, 8F), 78.80 (q, J = 150.60 Hz, 4F), **³¹P NMR** (203 MHz, CDCl₃), δ = 5.23 ppm, **HRMS (ESI+)**, m/z calculated for C₃₂H₁₇O₄F₂₀PS₄Na (M+Na⁺) 1023.932025, found 1026.932956. $\alpha_D^{25} = -272.84^\circ$ (c = 0.34, MeOH).

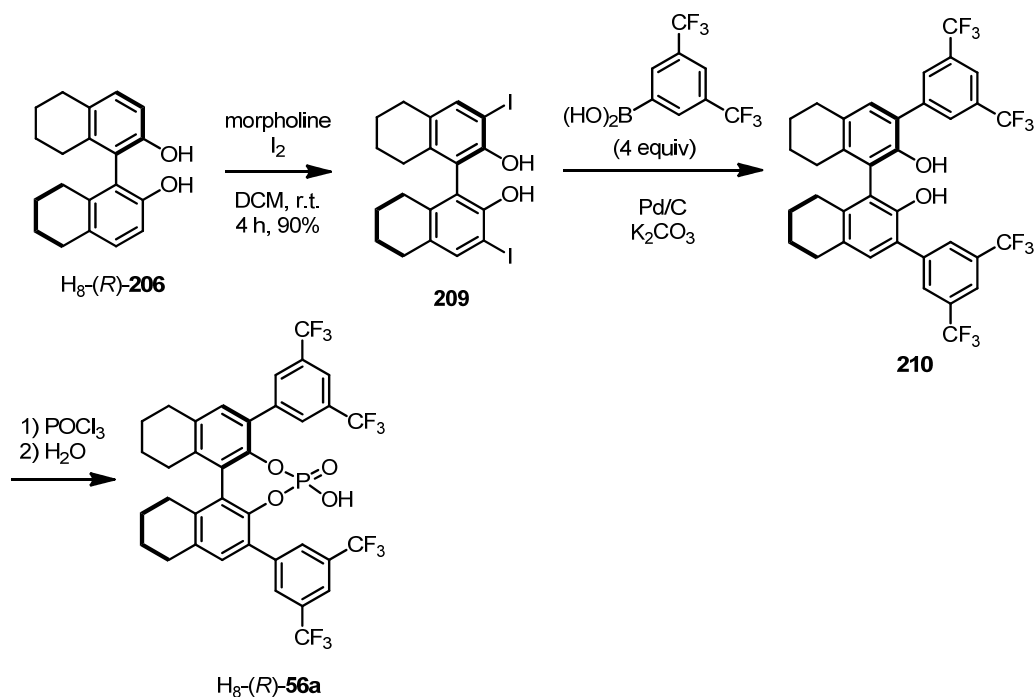
7.2.2. Preparation 6,6'-Adamantyl Substituted Phosphoric Acid^{166,167}

(S)-6,6'-di(adamantan-1-yl)-[1,1'-binaphthalene]-2,2'-diol (**207**)

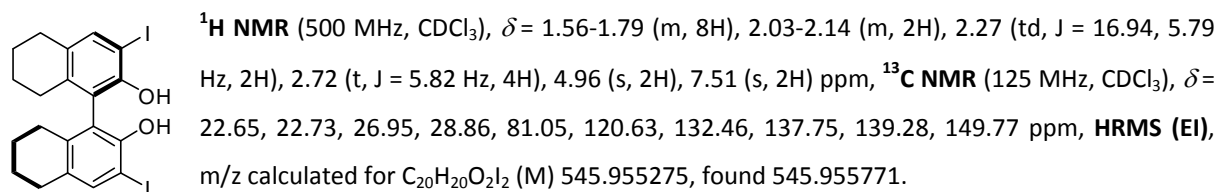


(S)-6,6'-di(adamantan-1-yl)-Binolphosphate (**208**)



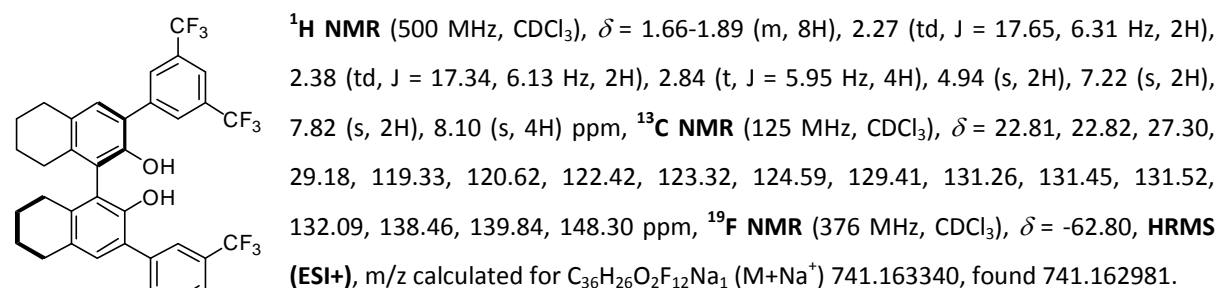
7.2.3. Preparation H₈-BINOL Derived Phosphoric Acid¹⁶⁸

(R)-3,3'-diiodo-5,5',6,6',7,7',8,8'-octahydro-[1,1'-binaphthalene]-2,2'-diol (**209**)



209

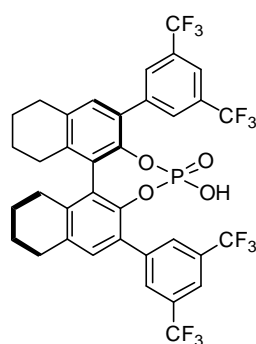
(R)-3,3'-diiodo-5,5',6,6',7,7',8,8'-octahydro-[1,1'-binaphthalene]-2,2'-diol (**210**)



210

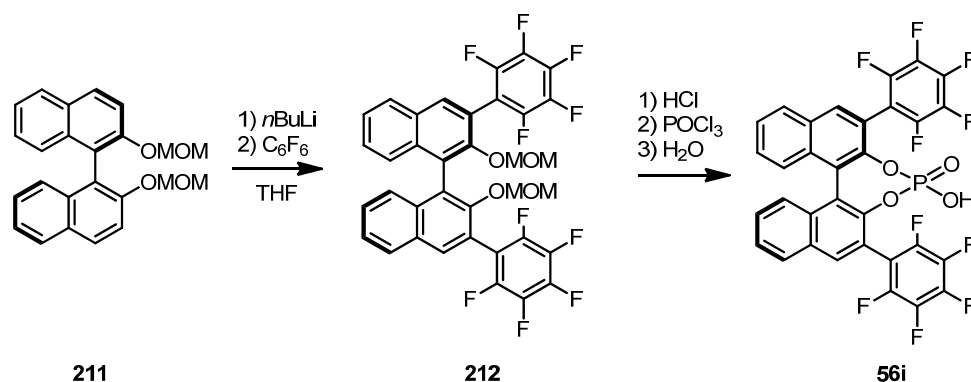
7. EXPERIMENTAL PART

(*R*)-3,3'-diiodo-5,5',6,6',7,7',8,8'-octahydro-[1,1'-binaphthalene]-2,2'-diol phosphate (H_8 -(*R*)-**56a**)

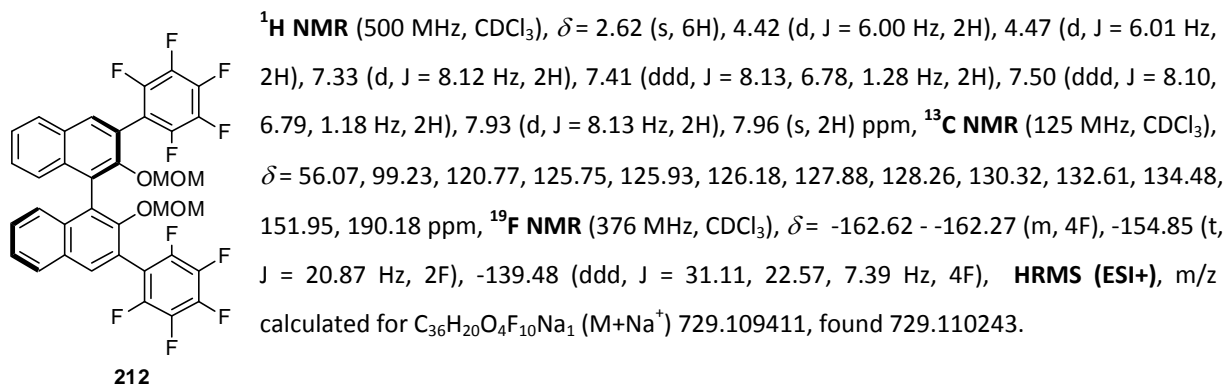


H_8 -(*R*)-**56a**

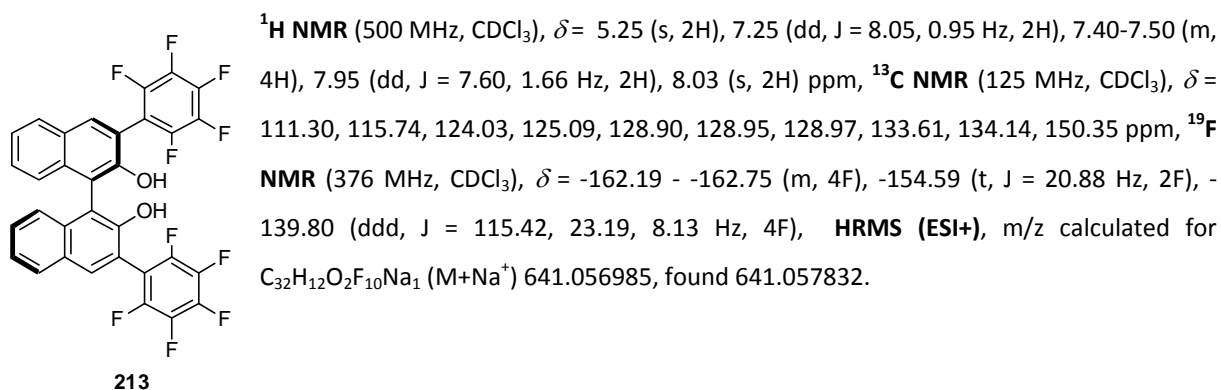
¹H NMR (500 MHz, CDCl₃), δ = 1.61-1.75 (m, 2H), 1.87 (td, *J* = 15.01, 7.02 Hz, 6H), 2.41 (td, *J* = 16.88, 5.48 Hz, 2H), 2.67-2.77 (m, 2H), 2.91 (s, 4H), 7.12 (s, 2H), 7.57 (s, 2H), 7.86 (s, 4H) ppm, ¹⁹F NMR (376 MHz, CDCl₃), δ = -62.92, ³¹P NMR (203 MHz, CDCl₃), δ = 2.72 ppm, HRMS (ESI+), *m/z* calculated for C₃₆H₂₄O₄F₁₂P₁ (M-H⁺) 779.122620, found 779.123230.

7.2.4. Preparation 3,3'-Pentafluorophenyl Substituted BINOL-Phosphoric Acid¹⁶⁹

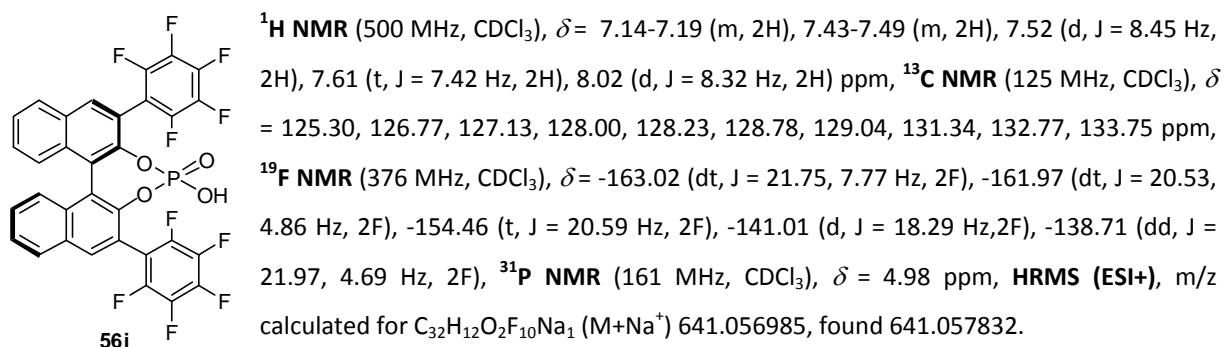
(*R*)-2,2'-bis(methoxymethoxy)-3,3'-bis(perfluorophenyl)-1,1'-binaphthalene (**212**)

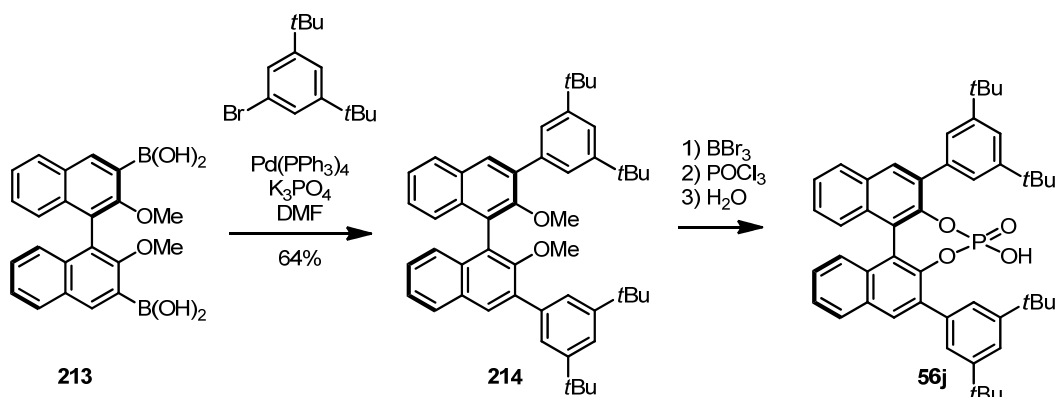


(*R*)-3,3'-bis(perfluorophenyl)-[1,1'-binaphthalene]-2,2'-diol (**213**)

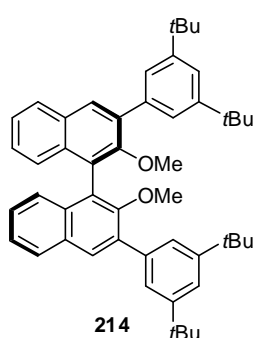


(*R*)-3,3'-bis(perfluorophenyl)-[1,1'-binaphthalene]-2,2'-diol phosphate (**56i**)



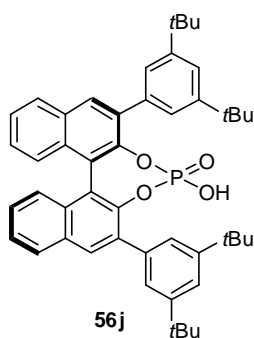
7.2.5. Preparation 3,3'-(3,5-(*t*Bu)₂C₆H₃) BINOL-Phosphoric Acid¹⁷⁰

(*R*)- 3,3'-bis(3,5-di-*tert*-butylphenyl)-2,2'-dimethoxy-1,1'-binaphthalene (**214**)



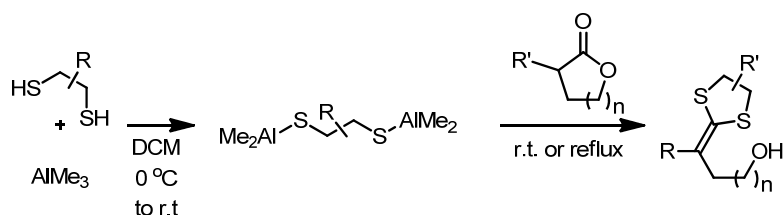
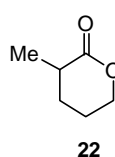
¹H NMR (500 MHz, CDCl₃), δ = 1.38 (s, 36H), 3.22 (s, 6H), 7.26 (s, 2H), 7.29-7.42 (m, 4H), 7.43 (t, *J* = 1.80 Hz, 2H), 7.60 (d, *J* = 1.83 Hz, 4H), 7.92 (d, *J* = 8.21 Hz, 2H), 7.98 (s, 2H)ppm, ¹³C NMR (125 MHz, CDCl₃), δ = 31.57, 34.95, 60.39, 120.98, 123.63, 124.79, 125.79, 125.91, 125.99, 127.98, 130.32, 130.75, 133.45, 135.96, 138.04, 150.52, 154.34. HRMS (ESI+), *m/z* calculated for C₅₀H₅₈O₂Na₁ (M+Na⁺) 713.432897, found 713.432859.

(*R*)-3,3'- bis(3,5-di-*tert*-butylphenyl)-[1,1'-binaphthalene]-2,2'-diol phosphate (**56j**)

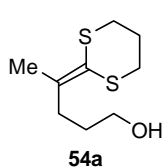


¹H NMR (500 MHz, CDCl₃), δ = 1.13 (s, 36H), 7.29 (td, *J* = 3.01, 2.38 Hz, 1H), 7.40-7.32 (m, 3H), 7.44 (dd, *J* = 12.68, 1.84 Hz, 1H), 7.50-7.46 (m, 1H), 7.94 (d, *J* = 6.86 Hz, 2H), ¹³C NMR (125 MHz, CDCl₃), δ = 31.57, 34.95, 60.39, 120.98, 123.63, 124.79, 125.79, 125.91, 125.99, 127.98, 130.32, 130.75, 133.45, 135.96, 138.04, 150.52, 154.34, ³¹P NMR (202 MHz, CDCl₃), δ = 2.90 ppm. HRMS (ESI+), *m/z* calculated for C₄₈H₅₃O₄PN₁ (M+Na) 747.357365, found 747.357937.

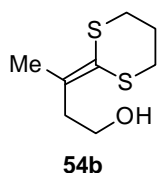
7.3. General Procedure for the Preparation of Dithioketene acetals from Lactones

3-methyltetrahydro-2H-pyran-2-one (**22**)

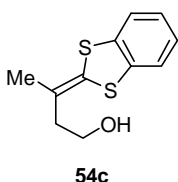
Lactone **22** was prepared by treating γ -valerolactone with freshly prepared LDA and MeI to give the desired product with 36% yield. ¹H NMR (500 MHz, CDCl₃), δ = 1.27 (d, J = 6.89 Hz, 3H), 1.50-1.62 (m, 1H), 1.91 (dd sext, J = 14.29, 6.91, 5.47 Hz, 2H), 2.10 (dt, J = 13.42, 6.75 Hz, 1H), 2.50-2.65 (m, 1H), 4.23-4.40 (m, 2H) ppm, ¹³C NMR (125 MHz, CDCl₃), δ = 16.69, 22.03, 27.10, 34.64, 68.55, 175.30 ppm, HRMS (EI), m/z calculated for C₆H₁₀O₂ (M) 114.068076, found 114.068061.

4-(1,3-dithian-2-ylidene)pentan-1-ol (**54a**)

¹H NMR (500 MHz, CDCl₃), δ = 1.73-1.63 (m, 2H), 1.76 (t, J = 6.04 Hz, 1H), 1.91 (s, 3H), 2.07-2.17 (m, 2H), 2.44 (t, J = 7.32 Hz, 2H), 2.83-2.93 (m, 4H), 3.62 (q, J = 6.10 Hz, 2H) ppm, ¹³C NMR (125 MHz, CDCl₃), δ = 20.09, 24.87, 30.15, 30.31, 30.35, 31.69, 61.82, 119.67, 139.65 ppm, HRMS (EI), m/z calculated for C₉H₁₆O₁S₂ (M) 204.064259, found 204.064114.

3-(1,3-dithian-2-ylidene)butan-1-ol (**54b**)

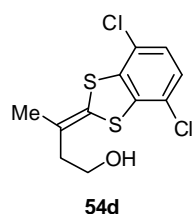
¹H NMR (500 MHz, toluene-*d*₈), δ = 0.72 (t, J = 5.22 Hz, 1H), 1.51-1.64 (m, 2H), 1.88 (s, 3H), 2.36-2.48 (m, 4H), 2.52 (t, J = 6.80 Hz, 2H), 3.43 (dd, J = 11.90, 6.57 Hz, 2H) ppm, ¹³C NMR (125 MHz, CDCl₃), δ = 21.05, 25.30, 30.23, 30.40, 40.01, 61.40, 129.54, 136.05 ppm, HRMS (EI), m/z calculated for C₈H₁₄O₁S₂ (M) 190.048610, found 190.048427.

3-(benzo[d][1,3]dithiol-2-ylidene)butan-1-ol (**54c**)

¹H NMR (500 MHz, CD₂Cl₂), δ = 1.47 (t, J = 5.76 Hz, 1H), 1.71 (s, 3H), 2.30 (t, J = 6.57 Hz, 2H), 3.64 (dd, J = 12.39, 6.47 Hz, 2H), 6.94-6.99 (m, 2H), 7.07-7.12 (m, 2H) ppm, ¹³C NMR (125 MHz, CDCl₃), δ = 21.49, 41.36, 60.50, 119.21, 121.73, 121.77, 125.59, 125.78, 125.83, 136.90, 136.94 ppm, HRMS (EI), m/z calculated for C₁₁H₁₂O₁S₂ (M) 224.032959, found 224.032761.

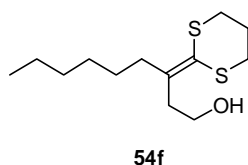
7. EXPERIMENTAL PART

3-(4,7-dichlorobenzo[d][1,3]dithiol-2-ylidene)butan-1-ol (**54d**)



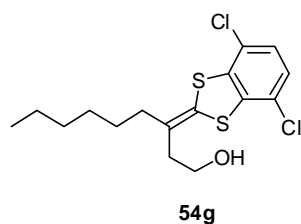
$^1\text{H NMR}$ (500 MHz, $\text{DMSO-}d_6$), δ = 1.78 (s, 3H), 2.26 (t, J = 6.64 Hz, 2H), 3.52 (t, J = 6.19 Hz, 2H), 7.29-7.41 (m, 2H) ppm, $^{13}\text{C NMR}$ (125 MHz, $\text{DMSO-}d_6$), δ = 21.00, 40.83, 59.95, 121.51, 122.58, 126.49, 126.54, 128.25, 129.16 ppm, **HRMS (EI)**, m/z calculated for $\text{C}_{11}\text{H}_{10}\text{O}_1\text{Cl}_2\text{S}_2$ (M) 291.955018, found 291.955141.

3-(1,3-dithian-2-ylidene)nonan-1-ol (**54f**)



$^1\text{H NMR}$ (500 MHz, toluene- d_8), δ = 0.88 (t, J = 4.45 Hz, 1H), 0.95 (t, J = 6.93 Hz, 3H), 1.22-1.38 (m, 6H), 1.49-1.49 (m, 2H), 1.57-1.67 (m, 2H), 2.33-2.55 (m, 6H), 2.64 (t, J = 7.03 Hz, 2H), 3.57 (dd, J = 12.62, 6.90 Hz, 2H) ppm, $^{13}\text{C NMR}$ (125 MHz, toluene- d_8), δ = 14.35, 23.13, 24.99, 28.67, 29.81, 29.99, 30.09, 32.20, 34.92, 37.84, 61.28, 123.88, 140.36 ppm, **HRMS (EI)**, m/z calculated for $\text{C}_{13}\text{H}_{24}\text{O}_1\text{S}_2$ (M) 260.126857, found 260.126712.

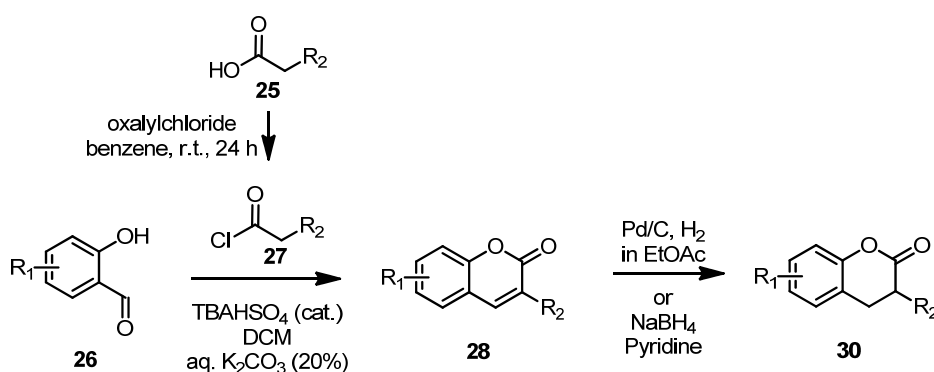
3-(4,7-dichlorobenzo[d][1,3]dithiol-2-ylidene)nonan-1-ol (**54g**)



$^1\text{H NMR}$ (500 MHz, C_6D_6), δ = 0.88 (t, J = 7.11 Hz, 3H), 1.10-1.37 (m, 8H), 1.96-2.01 (m, 2H), 2.17 (t, J = 6.86 Hz, 2H), 3.40 (t, J = 6.79 Hz, 2H), 6.36 (d, J = 0.84 Hz, 2H) ppm, $^{13}\text{C NMR}$ (125 MHz, $\text{DMSO-}d_6$), δ = 14.27, 23.04, 27.23, 29.52, 32.08, 36.12, 38.94, 60.34, 120.04, 123.23, 125.00, 126.51, 126.91, 127.33, 137.81, 137.94 ppm, **HRMS (ESI+)**, m/z calculated for $\text{C}_{16}\text{H}_{20}\text{O}_1\text{Cl}_2\text{S}_2$ (M) 385.022486, found 385.022150.

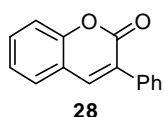
7.4. General Procedure for the Preparation of Coumarins and Hydrocoumarins and their dithioiketene acetals

7.4.1. Preparation of α -Aryl Coumarins and Hydrocoumarins



To a stirred solution of tetrabutyl ammonium hydrogensulfate (100 mg) and *o*-hydroxy aldehyde **26** (10 mmol) in dichloromethane (15 mL) and 20% aq. K_2CO_3 (30 mL) was added drop-wise a dichloromethane solution (15 mL) of α -arylacetylchloride **27** (12 mmol) at room temperature. The reaction mixture stirred for 24 - 48 h. The organic layer was extracted with dichloromethane (30 mL X 3) and dried with magnesium sulfate. The solvent was removed under reduced pressure and the residue was precipitated or crystallized in ethanol to give a pure solid coumarin **28** (ca 50% yield). A mixture of coumarin **28** (3 mmol) and palladium charcoal (10 wt%, 5 mol%) was stirred at room temperature in ethylacetate (10 mL) under pressure of hydrogen (1 – 5 bar). The conversion was followed by ^1H NMR. After reasonable conversion of coumarin **28** to hydrocoumarin **30**, the reaction mixture filtered over Celite and silica gel and concentrated under reduced pressure. The residue was precipitated or recrystallized in ethanol to afford pure hydrocoumarin **1** (45 - 98% yield). In the case of halogen substituted coumarin **28**, to a solution of coumarin **28** (3 mmol) in anhydrous pyridine (5 mL) was added sodium borohydride (1.3-1.5 equiv) at room temperature. After 30 min (after the reaction mixture turned to homogenous solution), the reaction quenched with 1N HCl (10 mL) and organic layer was extracted with diethylether and washed with 1N HCl (5 mL X 2). The combined organic phase was concentrated and filtered through short pad of a silica gel and washed with diethylether to afford hydrocoumarin **30** (46 - 87%) as a pure form or a mixture with coumarin **30** and used for the ketene thioacetal preparation after silica chromatography (nHexane:diethylether=4:1).

3-Phenylcoumarin (**28a**)

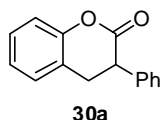


A colorless solid was obtained after precipitation in ethanol (45 %), Mp 152.6 °C, ^1H NMR (500 MHz, CDCl_3), δ = 7.27-7.34 (m, 1H), 7.35-7.49 (m, 4H), 7.50-7.57 (m, 2H), 7.67-7.75 (m, 2H), 7.82 (s, 1H) ppm, ^{13}C NMR (125 MHz, CDCl_3), δ = 116.46, 119.67, 124.49, 127.90, 128.36,

7. EXPERIMENTAL PART

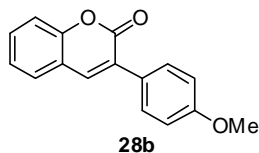
128.47, 128.53, 128.86, 131.40, 134.69, 139.87, 153.51, 160.59 ppm. **HRMS (ESI+)**, m/z calculated for $C_{15}H_{10}O_2Na$ ($M+Na^+$) 245.057297, found 245.057114.

3-Phenylhydrocoumarin (**30a**)



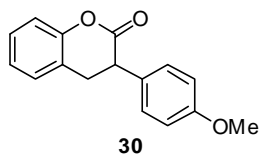
The reduction was conducted with Pd/C and H_2 (1 bar), colorless crystals were obtained after crystallization in ethanol (47 %), Mp 128.2 °C, 1H NMR (500 MHz, $CDCl_3$), δ = 3.23 (dd, J = 15.87, 6.19 Hz, 1H), 3.36 (dd, J = 15.84, 11.28 Hz, 1H), 3.98 (dd, J = 11.26, 6.19 Hz, 1H), 7.07-7.16 (m, 2H), 7.18-7.24 (m, 1H), 7.24-7.41 (m, 6H) ppm, ^{13}C NMR (125 MHz, $CDCl_3$), δ = 31.70, 45.60, 116.77, 122.63, 124.49, 127.85, 128.02, 128.09, 128.47, 128.85, 136.48, 151.70, 169.33 ppm. **HRMS (ESI+)**, m/z calculated for $C_{15}H_{12}O_2Na$ ($M+Na^+$) 247.072948, found 247.072841.

3-(4-Methoxyphenyl)coumarin (**28b**)



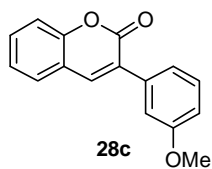
Colorless crystals were obtained after crystallization in diethylether (56 %), Mp 137.4 °C, 1H NMR (400 MHz, $CDCl_3$), δ = 3.85 (s, 3H), 6.93-7.01 (m, 2H), 7.27-7.30 (m, 1H), 7.35 (d, J = 8.03 Hz, 1H), 7.48-7.55 (m, 2H), 7.65-7.70 (m, 2H), 7.76 (s, 1H) ppm, ^{13}C NMR (100 MHz, $CDCl_3$), δ = 55.37, 113.91, 116.38, 119.83, 124.43, 127.06, 127.70, 127.87, 129.83, 131.01, 138.50, 153.29, 160.14, 160.81 ppm. **HRMS (ESI+)**, m/z calculated for $C_{16}H_{12}O_3Na$ ($M+Na^+$) 275.067865, found 275.067720.

3-(4-Methoxyphenyl)hydrocoumarin (**30b**)

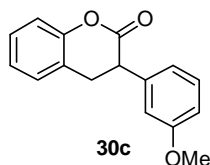


The reduction was conducted with Pd/C and H_2 (1 bar), colorless crystals were obtained after crystallization in diethylether (43 %), Mp 122.6 °C, 1H NMR (500 MHz, $CDCl_3$), δ = 3.21 (dd, J = 15.88, 6.18 Hz, 1H), 3.33 (dd, J = 15.83, 11.20 Hz, 1H), 3.80 (s, 3H), 3.93 (dd, J = 11.17, 6.20 Hz, 1H), 6.87-6.92 (m, 2H), 7.07-7.14 (m, 2H), 7.16-7.23 (m, 3H), 7.26-7.30 (m, 1H) ppm, ^{13}C NMR (125 MHz, $CDCl_3$), δ = 31.71, 44.79, 55.28, 114.27, 116.74, 122.73, 124.45, 128.01, 128.42, 128.43, 129.13, 151.70, 159.12, 169.67 ppm. **HRMS (ESI+)**, m/z calculated for $C_{16}H_{14}O_3Na$ ($M+Na^+$) 277.083512, found 277.083283.

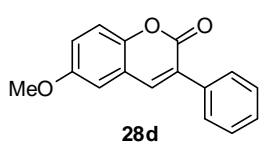
3-(3-Methoxyphenyl)coumarin (**28c**)



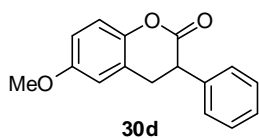
Colorless crystals were obtained after crystallization in ethanol (70 %), Mp 137.1 °C, 1H NMR (500 MHz, $CDCl_3$), δ = 3.86 (s, 3H), 6.96 (ddd, J = 8.31, 2.34, 1.18 Hz, 1H), 7.24-7.40 (m, 5H), 7.50-7.58 (m, 2H), 7.82 (m, 1H) ppm, ^{13}C NMR (125 MHz, $CDCl_3$), δ = 55.37, 114.20, 114.53, 116.46, 119.61, 120.91, 124.49, 127.93, 128.19, 129.49, 131.46, 136.02, 139.99, 153.52 ppm. **HRMS (ESI+)**, m/z calculated for $C_{16}H_{12}O_3Na$ ($M+Na^+$) 275.067865, found 275.067842.

3-(3-Methoxyphenyl)hydrocoumarin (**30c**)

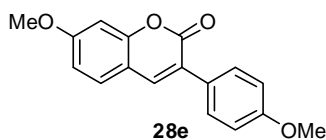
The reduction was conducted with Pd/C and H₂ (1 bar), colorless crystals were obtained after crystallization in diethylether (97 %), Mp 109.0 °C, ¹H NMR (500 MHz, CDCl₃), δ = 3.23 (dd, J = 15.89, 6.20 Hz, 1H), 3.35 (dd, J = 15.91, 11.10 Hz, 1H), 3.78 (s, 3H), 3.96 (dd, J = 11.01, 6.20 Hz, 1H), 6.78-6.82 (m, 1H), 6.85 (dd, J = 7.98, 2.05 Hz, 2H), 7.07-7.14 (m, 2H), 7.21 (d, J = 7.33 Hz, 1H), 7.26-7.31 (m, 2H) ppm, ¹³C NMR (125 MHz, CDCl₃), δ = 31.58, 45.57, 55.21, 113.12, 114.05, 116.75, 120.36, 122.57, 124.51, 128.03, 128.46, 129.86, 137.90, 151.68 ppm. HRMS (EI), m/z calculated for C₁₆H₁₄O₃ (M) 254.094294, found 254.094454.

6-Methoxy-3-phenylcoumarin (**28d**)

Pale yellow crystals were obtained after crystallization in ethanol (74 %), Mp 152.2 °C, ¹H NMR (400 MHz, CDCl₃), δ = 3.85 (s, 3H), 6.97 (d, J = 2.84 Hz, 1H), 7.10 (dd, J = 9.04, 2.90 Hz, 1H), 7.23-7.33 (m, 1H), 7.34-7.53 (m, 3H), 7.65-7.73 (m, 2H), 7.76 (s, 1H), ¹³C NMR (75 MHz, CDCl₃), δ = 55.84, 109.92, 117.47, 119.15, 120.01, 128.46, 128.56, 128.67, 128.85, 134.78, 139.70, 148.00, 156.14, 160.72 ppm. HRMS (ESI+), m/z calculated for C₁₆H₁₂O₃Na (M+Na⁺) 277.083517, found 277.083624.

6-Methoxy-3-phenylhydrocoumarin (**30d**)

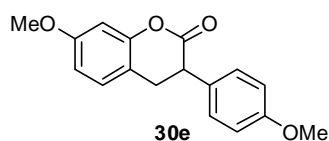
The reduction was conducted with Pd/C and H₂ (1 bar), colorless crystals were obtained after crystallization in ethanol (46 %), Mp 126.3 °C, ¹H NMR (400 MHz, CDCl₃), δ = 3.19 (dd, J = 15.89, 6.23 Hz, 1H), 3.32 (dd, J = 15.88, 10.80 Hz, 1H), 3.80 (s, 3H), 3.96 (dd, J = 10.79, 6.22 Hz, 1H), 6.72 (d, J = 2.93 Hz, 1H), 6.80 (dd, J = 8.88, 2.95 Hz, 1H), 7.02 (d, J = 8.87 Hz, 1H), 7.39-7.23 (m, 5H) ppm, ¹³C NMR (100 MHz, CDCl₃), δ = 31.63, 45.18, 55.34, 112.79, 113.08, 117.16, 123.16, 127.47, 127.72, 128.50, 136.22, 145.31, 155.87, 169.08 ppm. HRMS (ESI+), m/z calculated for C₁₆H₁₄O₃Na (M+Na⁺) 277.083517, found 277.0083624.

7-Methoxy-3-(4-methoxyphenyl)coumarin (**28e**)

Colorless crystals were obtained after crystallization in ethanol (61 %), Mp 188.1 °C, ¹H NMR (500 MHz, CDCl₃), δ = 3.85 (s, 3H), 3.88 (s, 3H), 6.83-6.89 (m, 2H), 6.94-6.98 (m, 2H), 7.40-7.44 (d, J = 8.20 Hz, 1H), 7.62-7.67 (m, 2H), 7.71 (s, 1H) ppm, ¹³C NMR (75 MHz, CDCl₃), δ = 55.36, 55.78, 100.38, 112.71, 113.49, 113.86, 124.44, 127.40, 128.62, 129.65, 138.75, 155.06, 159.82, 161.11, 162.32 ppm, HRMS (ESI+), m/z calculated for C₁₇H₁₄O₄Na (M+Na⁺) 305.078427, found 305.078366.

7. EXPERIMENTAL PART

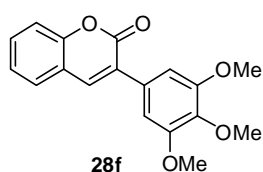
7-Methoxy-3-(4-methoxyphenyl)hydrocoumarin (**30e**)



Colorless crystals were obtained after crystallization in ethanol as a mixture with **1e'**, Mp 186.1 °C, $^1\text{H NMR}$ (400 MHz, CDCl_3), δ = 3.15 (dd, J = 15.72, 6.36 Hz, 1H), 3.25 (dd, J = 15.60, 10.64 Hz, 1H), 3.79 (s, 3H), 3.80 (s, 3H), 3.91 (dd, J = 9.30, 5.05 Hz, 1H), 6.62-6.70 (m, 2H), 6.84-6.91 (m, 2H), 7.09 (d, J = 8.22 Hz, 1H),

7.15-7.19 (m, 2H) ppm, **HRMS (ESI+)**, m/z calculated for $\text{C}_{17}\text{H}_{16}\text{O}_4\text{Na}$ ($\text{M}+\text{Na}^+$) 307.094076, found 307.094374.

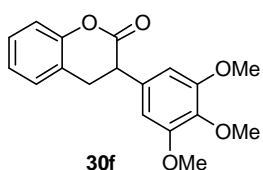
3-(3,4,5-trimethoxyphenyl)coumarin (**28f**)



Colorless crystals were obtained after crystallization in ethanol (55 %), Mp 147.2 °C, $^1\text{H NMR}$ (400 MHz, CDCl_3), δ = 3.90 (s, 3H), 3.93 (s, 6H), 6.95 (s, 2H), 7.31 (dt, J = 7.53, 1.07 Hz, 1H), 7.38 (d, J = 8.12 Hz, 1H), 7.59-7.50 (m, 2H), 7.80 (s, 1H) ppm, $^{13}\text{C NMR}$ (75 MHz, CDCl_3), δ = 56.33, 60.94, 106.08, 116.48, 119.62, 124.55, 127.86, 128.19,

130.20, 131.43, 138.91, 139.52, 153.18, 153.44, 160.56 ppm. **HRMS (ESI+)**, m/z calculated for $\text{C}_{18}\text{H}_{16}\text{O}_5\text{Na}$ ($\text{M}+\text{Na}^+$) 335.088991, found 335.088770.

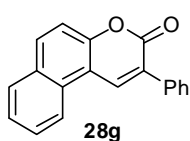
3-(3,4,5-trimethoxyphenyl)hydrocoumarin (**30f**)



The reduction was conducted with Pd/C (10 mol%) and H_2 (15 bar), Colorless crystals were obtained after crystallization in diethylether (55 %), Mp 172.8 °C, $^1\text{H NMR}$ (400 MHz, CDCl_3), δ = 3.25 (dd, J = 15.93, 6.39 Hz, 1H), 3.34 (dd, J = 15.89, 10.41 Hz, 1H), 3.80 (s, 6H), 3.83 (s, 3H), 3.93 (dd, J = 10.38, 6.39 Hz, 1H), 6.46 (s, 2H), 7.16-7.06 (m,

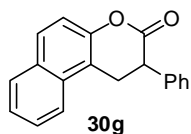
2H), 7.25-7.20 (m, 1H), 7.29 (m, 1H) ppm, $^{13}\text{C NMR}$ (75 MHz, CDCl_3), δ = 31.70, 45.75, 56.08, 60.79, 105.23, 116.73, 122.54, 124.59, 128.01, 128.52, 132.00, 137.60, 151.66, 153.41, 169.22 ppm. **HRMS (ESI+)**, m/z calculated for $\text{C}_{18}\text{H}_{18}\text{O}_5\text{Na}$ ($\text{M}+\text{Na}^+$) 337.104643, found 337.104376.

3-Phenyl-5,6-benzocoumarin (**28g**)

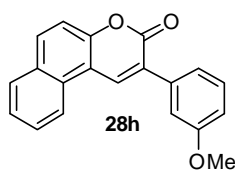


Crystals were obtained after crystallization in ethanol (34 %), Mp 143.4 °C, $^1\text{H NMR}$ (500 MHz, CDCl_3), δ = 7.41-7.48 (m, 1H), 7.48-7.54 (m, 3H), 7.59 (ddd, J = 8.01, 6.99, 1.00 Hz, 1H), 7.70 (ddd, J = 8.34, 6.96, 1.26 Hz, 1H), 7.79-7.83 (m, 2H), 7.94 (d, J = 8.08 Hz, 1H), 7.97-8.02 (m, 1H), 8.32 (d, J = 8.37 Hz, 1H), 8.61 (s, 1H) ppm, $^{13}\text{C NMR}$ (125 MHz, CDCl_3), δ = 113.78,

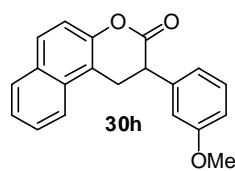
116.75, 121.45, 126.05, 127.33, 128.22, 128.59, 128.61, 128.90, 129.14, 130.37, 132.76, 135.12, 135.78, 153.22, 160.70 ppm. **HRMS (ESI+)**, m/z calculated for $\text{C}_{19}\text{H}_{12}\text{O}_2\text{Na}$ ($\text{M}+\text{Na}^+$) 295.072950, found 295.072828.

3,4-Dihydro-3-phenyl-5,6-benzocoumarin (**30g**)

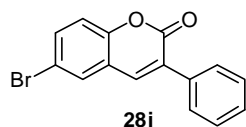
The reduction was conducted with Pd/C (10 mol%) and H₂ (1 bar), colorless crystals were obtained after crystallization in diethylether (59 %), Mp 166.9 °C, ¹H NMR (500 MHz, CDCl₃), δ = 3.57 (dd, *J* = 16.28, 11.27 Hz, 1H), 3.72 (dd, *J* = 16.30, 6.62 Hz, 1H), 4.10 (dd, *J* = 11.24, 6.61 Hz, 1H), 7.28 (d, *J* = 8.89 Hz, 1H), 7.30-7.41 (m, 6H), 7.48 (ddd, *J* = 8.02, 6.93, 0.96 Hz, 1H), 7.56 (ddd, *J* = 8.31, 6.89, 1.22 Hz, 1H), 7.80 (d, *J* = 8.90 Hz, 1H), 7.87 (m, 1H) ppm, ¹³C NMR (125 MHz, CDCl₃), δ = 28.15, 45.12, 115.62, 117.20, 122.75, 125.20, 127.24, 127.95, 128.18, 128.81, 128.95, 129.13, 130.82, 131.01, 136.70, 149.36 ppm. HRMS (EI), *m/z* calculated for C₁₉H₁₄O₂ (M⁺) 274.099377, found 274.099095.

3-(3-Methoxyphenyl)-benzocoumarin (**28h**)

A brown solid was obtained after crystallization in diethylether (40 %), Mp 130.8 °C, ¹H NMR (500 MHz, CDCl₃), δ = 3.89 (s, 3H), 6.99 (ddd, *J* = 7.99, 2.47, 1.31 Hz, 1H), 7.33-7.45 (m, 3H), 7.51 (d, *J* = 8.99 Hz, 1H), 7.56-7.61 (m, 1H), 7.70 (ddd, *J* = 8.31, 6.99, 1.19 Hz, 1H), 7.93 (d, *J* = 8.05 Hz, 1H), 7.99 (d, *J* = 8.99 Hz, 1H), 8.31 (d, *J* = 8.41 Hz, 1H), 8.63-8.60 (s, 1H) ppm, ¹³C NMR (125 MHz, CDCl₃), δ = 55.41, 113.71, 114.34, 114.45, 116.72, 120.98, 121.45, 126.05, 127.08, 127.22, 128.23, 129.12, 129.59, 130.35, 132.81, 135.88, 136.44, 153.21, 159.62, 160.56 ppm. HRMS (EI), *m/z* calculated for C₂₀H₁₄O₃ (M⁺) 302.094296, found 302.093991.

3,4-Dihydro-3-(3-methoxyphenyl)-benzocoumarin (**30h**)

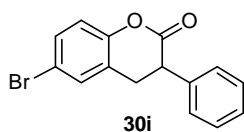
The reduction was conducted with Pd/C (10 mol%) and H₂ (1 bar), a white solid was obtained after precipitation in ethanol (34 %), Mp 140.6 °C, ¹H NMR (500 MHz, CDCl₃), δ = 3.57 (dd, *J* = 16.29, 11.13 Hz, 1H), 3.72 (dd, *J* = 16.31, 6.60 Hz, 1H), 3.78 (s, 3H), 4.08 (dd, *J* = 11.10, 6.59 Hz, 1H), 6.84-6.89 (m, 2H), 6.89-6.93 (m, 1H), 7.26-7.33 (m, 2H), 7.48 (ddd, *J* = 7.92, 6.93, 0.80 Hz, 1H), 7.56 (ddd, *J* = 8.35, 6.90, 1.10 Hz, 1H), 7.80 (d, *J* = 8.89 Hz, 1H), 7.85-7.89 (m, 2H) ppm, ¹³C NMR (125 MHz, CDCl₃), δ = 28.03, 45.11, 55.22, 113.25, 114.11, 115.59, 117.18, 120.40, 122.74, 125.20, 127.25, 128.80, 129.13, 129.96, 130.82, 131.01, 138.12, 149.34, 159.90, 169.05 ppm. HRMS (ESI+), *m/z* calculated for C₂₀H₁₆O₃Na (M+Na⁺) 327.099164, found 327.099156.

6-Bromo-3-phenylcoumarin (**28i**)

Colorless crystals were obtained after crystallization in diethylether (36 %), Mp 199.2 °C. ¹H NMR (500 MHz, CDCl₃), δ = 7.26 (d, *J* = 8.76 Hz, 1H), 7.40-7.50 (m, 3H), 7.62 (dd, *J* = 8.77, 2.30 Hz, 1H), 7.67-7.71 (m, 3H), 7.72-7.74 (s, 1H) ppm, ¹³C NMR (75 MHz, CDCl₃), δ = 117.02, 118.19, 121.22, 128.55, 128.56, 129.23, 129.53, 130.12, 134.09, 134.21, 138.28, 152.34, 159.89 ppm, HRMS (EI), *m/z* calculated for C₁₅H₉O₂Br (M) 299.978608, found 299.978928.

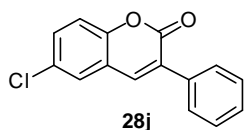
7. EXPERIMENTAL PART

6-Bromo-3-phenylhydrocoumarin (**30i**)



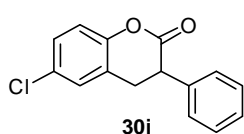
A white solid was obtained after silica chromatography (diethylether:nHexane = 1:3), (59 %), $^1\text{H NMR}$ (400 MHz, CDCl_3), δ = 3.22 (dd, J = 16.09, 6.25 Hz, 1H), 3.33 (dd, J = 16.04, 10.73 Hz, 1H), 3.97 (dd, J = 10.72, 6.27 Hz, 1H), 6.98 (d, J = 8.61 Hz, 1H), 7.22-7.26 (m, 2H), 7.29-7.42 (m, 5H) ppm, $^{13}\text{C NMR}$ (100 MHz, CDCl_3), δ = 31.42, 45.14, 114.38, 118.47, 124.61, 127.96, 128.01, 128.95, 130.83, 131.45, 135.91, 150.76, 168.48 ppm. **HRMS (ESI+)**, m/z calculated for $\text{C}_{15}\text{H}_{11}\text{O}_2\text{BrNa}$ ($\text{M}+\text{Na}^+$) 324.983473, found 324.983893.

6-Chloro-3-phenylcoumarin (**28j**)



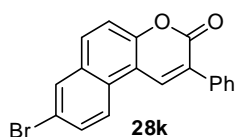
Colorless crystals were obtained after crystallization in ethanol (39 %), Mp 202.7 °C, $^1\text{H NMR}$ (500 MHz, CDCl_3), δ = 7.32 (d, J = 8.79 Hz, 1H), 7.40-7.50 (m, 4H), 7.53 (d, J = 2.42 Hz, 1H), 7.68-7.71 (m, 2H), 7.73 (s, 1H) ppm, $^{13}\text{C NMR}$ (125 MHz, CDCl_3), δ = 117.91, 120.70, 127.07, 128.54, 128.57, 129.23, 129.55, 129.73, 131.29, 134.22, 138.42, 151.86, 159.99 ppm. **HRMS (EI)**, m/z calculated for $\text{C}_{15}\text{H}_9\text{O}_2\text{Cl}$ (M) 256.029112, found 256.028951.

6-Chloro-3-phenylhydrocoumarin (**1j**)

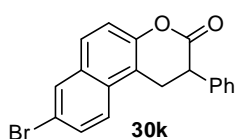


A white solid was obtained after silica chromatography (diethylether:nHexane = 1:10) as a mixture with **1j'** (6%), Mp 147.4 °C. $^1\text{H NMR}$ (400 MHz, CDCl_3), δ = 3.21 (dd, J = 16.06, 6.27 Hz, 1H), 3.33 (dd, J = 16.04, 10.74 Hz, 1H), 3.97 (dd, J = 10.72, 6.28 Hz, 1H), 7.03 (d, J = 8.64 Hz, 1H), 7.18-7.25 (m, 4H), 7.29-7.39 (m, 3H) ppm, $^{13}\text{C NMR}$ (75 MHz, CDCl_3), δ = 31.48, 45.12, 118.09, 124.17, 127.91, 127.96, 128.01, 128.49, 128.94, 129.53, 135.94, 150.22, 168.57 ppm, **HRMS (EI)**, m/z calculated for $\text{C}_{15}\text{H}_{11}\text{O}_2\text{Cl}$ (M) 258.044757, found 258.044558.

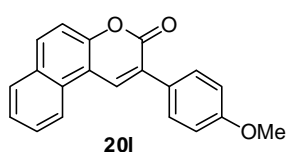
8-Bromo-2-phenyl-3H-naphtho[2,1-b]pyran-3-one (**28k**)



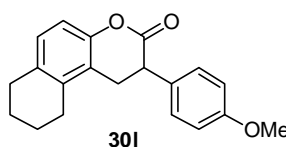
Colorless crystals were obtained after crystallization in ethanol (61 %), Mp 252.0 °C, $^1\text{H NMR}$ (500 MHz, CDCl_3), δ = 7.42-7.57 (m, 4H), 7.76 (dd, J = 8.94, 2.03 Hz, 1H), 7.80 (m, 2H), 7.90 (d, J = 9.01 Hz, 1H), 8.09 (d, J = 1.99 Hz, 1H), 8.18 (d, J = 9.01 Hz, 1H), 8.52 (s, 1H) ppm, $^{13}\text{C NMR}$ (125 MHz, CDCl_3), δ = 113.93, 118.00, 120.01, 123.26, 124.88, 127.74, 128.02, 128.62, 128.65, 129.11, 131.14, 131.44, 131.58, 134.86, 135.19, 143.75, 153.16, 160.36 ppm. **HRMS (ESI+)**, m/z calculated for $\text{C}_{19}\text{H}_{11}\text{O}_2\text{BrNa}$ ($\text{M}+\text{Na}^+$) 372.983474, found 372.983451.

8-Bromo-1,2-dihydro-2-phenyl-3H-naphtho[2,1-b]pyran-3-one (**30k**)

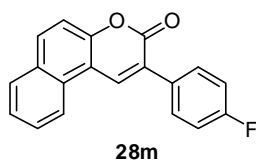
The reduction was conducted with NaBH₄ (1.3 equiv) in pyridine. A white solid was obtained after silica chromatography (diethylether: *n*Hexane = 1:10), Mp 183.7 °C. ¹H NMR (500 MHz, CDCl₃), δ = 3.57 (dd, *J* = 16.32, 11.20 Hz, 1H), 3.69 (dd, *J* = 16.33, 6.63 Hz, 1H), 4.11 (dd, *J* = 11.15, 6.61 Hz, 1H), 7.27-7.42 (m, 6H), 7.63 (dd, *J* = 8.99, 2.00 Hz, 1H), 7.73 (dd, *J* = 18.88, 8.97 Hz, 2H), 8.03 (d, *J* = 1.94 Hz, 1H) ppm, ¹³C NMR (100 MHz, CDCl₃), δ = 28.14, 44.96, 115.96, 118.42, 124.53, 128.06, 128.12, 128.25, 129.01, 129.62, 130.57, 130.77, 131.97, 136.43, 149.60, 168.76 ppm, HRMS (ESI+), *m/z* calculated for C₁₉H₁₃O₂BrNa (M+Na⁺) 374.999128, found 374.999349.

2-(4-methoxyphenyl)-3H-benzo[*f*]chromen-3-one (**28l**)

Colorless crystals were obtained after crystallization in ethanol (68 %), Mp 176.6 °C, ¹H NMR (500 MHz, CDCl₃), δ = 3.88 (s, 3H), 6.96-7.08 (m, 2H), 7.49 (d, *J* = 8.98 Hz, 1H), 7.57 (t, *J* = 7.26 Hz, 1H), 7.66-7.72 (m, 1H), 7.75-7.80 (m, 2H), 7.92 (d, *J* = 8.09 Hz, 1H), 7.96 (d, *J* = 9.00 Hz, 1H), 8.31 (d, *J* = 8.42 Hz, 1H), 8.53 (s, 1H) ppm, ¹³C NMR (125 MHz, CDCl₃), δ = 55.41, 113.90, 114.00, 116.71, 121.46, 125.96, 126.85, 127.46, 128.08, 129.09, 129.90, 130.36, 132.30, 134.36, 152.84, 160.18, 160.88 ppm. HRMS (ESI+), *m/z* calculated for C₂₀H₁₄O₃Na (M+Na⁺) 325.083516, found 325.083577.

2-(4-methoxyphenyl)-7,8,9,10-tetrahydro-1H-benzo[*f*]chromen-3(2H)-one (**30l**)

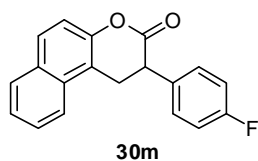
The reduction was conducted with Pd/C (10 mol%) and H₂ (11 bar), a white solid was obtained after chromatography (34 %), Colorless crystals were obtained after crystallization in ethanol (51 %), Mp 120.8 °C. ¹H NMR (400 MHz, CDCl₃), δ = 1.66-1.92 (m, 4H), 2.51-2.69 (m, 2H), 2.75 (t, *J* = 5.95 Hz, 2H), 3.08 (dd, *J* = 16.22, 11.19 Hz, 1H), 3.16 (dd, *J* = 16.22, 6.60 Hz, 1H), 3.80 (s, 3H), 3.86 (dd, *J* = 11.15, 6.61 Hz, 1H), 6.85 (d, *J* = 8.34 Hz, 1H), 6.87-6.91 (m, 2H), 6.99 (d, *J* = 8.35 Hz, 1H), 7.16-7.20 (m, 2H) ppm, ¹³C NMR (100 MHz, CDCl₃), δ = 22.65, 22.91, 26.58, 28.56, 29.50, 44.48, 55.29, 114.00, 114.29, 120.78, 128.82, 128.98, 129.18, 133.57, 134.76, 149.71, 159.12 ppm. HRMS (ESI+), *m/z* calculated for C₂₀H₂₀O₃Na (M+Na⁺) 331.130467, found 331.130665.

3-(4-Fluorophenyl)-benzocoumarin (**28m**)

Yellow crystals were obtained after crystallization in ethanol (52 %), Mp 249.7 °C, ¹H NMR (500 MHz, CDCl₃), δ = 7.16-7.22 (m, 2H), 7.52 (d, *J* = 9.00 Hz, 1H), 7.60 (ddd, *J* = 8.01, 6.99, 1.00 Hz, 1H), 7.71 (ddd, *J* = 8.34, 6.96, 1.25 Hz, 1H), 7.77-7.83 (m, 2H), 7.94 (d, *J* = 8.08 Hz, 1H), 8.01 (d, *J* = 8.99 Hz, 1H), 8.31 (d, *J* = 8.38 Hz, 1H), 8.57 (s, 1H) ppm, ¹³C NMR (125 MHz, CDCl₃), δ = 113.69, 115.51, 115.69, 116.72, 121.41, 126.12, 126.28, 128.28, 129.08, 129.17, 130.39, 130.45, 130.52, 131.12, 132.88, 135.57, 153.21, 160.65, 162.21, 164.13 ppm, ¹⁹F NMR (376 Hz, CDCl₃), δ = -112.27 ppm, HRMS (EI+), *m/z* calculated for C₁₉H₁₁O₂F (M+) 290.074309, found 290.074080.

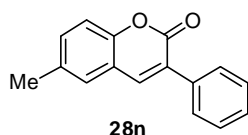
7. EXPERIMENTAL PART

3-(4-Fluorophenyl)-benzocoumarin (**30m**)



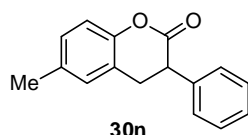
The reduction was conducted with NaBH_4 (1.4 equiv) in pyridine. A white solid was obtained after silica chromatography (DCM: *n*-hexane = 1:10), Mp 171.1 °C, $^1\text{H NMR}$ (500 MHz, CDCl_3), δ = 3.53 (dd, J = 16.24, 11.48 Hz, 1H), 3.72 (dd, J = 16.27, 6.59 Hz, 1H), 4.09 (dd, J = 11.47, 6.58 Hz, 1H), 7.04-7.12 (m, 2H), 7.26-7.35 (m, 3H), 7.43-7.52 (m, 1H), 7.58 (ddd, J = 8.32, 6.88, 1.28 Hz, 1H), 7.81 (d, J = 8.91 Hz, 1H), 7.88 (m, 2H) ppm, $^{13}\text{C NMR}$ (100 MHz, CDCl_3), δ = 28.23, 44.46, 115.45, 115.80, 116.01, 117.18, 122.70, 125.29, 127.33, 128.86, 129.27, 129.82, 129.90, 130.88, 130.99, 132.44, 132.48, 149.36, 161.15, 163.60, 169.00 ppm. $^{19}\text{F NMR}$ (376 Hz, CDCl_3), δ = -114.19 ppm, **HRMS (EI+)**, m/z calculated for $\text{C}_{19}\text{H}_{13}\text{O}_2\text{FNa}$ ($\text{M}+\text{Na}^+$) 315.079179, found 315.079560.

6-Methyl-3-phenylcoumarin (**28n**)



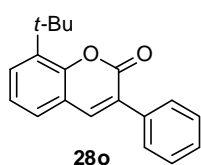
A white solid was obtained after precipitation in ethanol (74 %), Mp 155.9 °C, $^1\text{H NMR}$ (300 MHz, CDCl_3), δ = 2.41 (s, 3H), 7.22-7.28 (m, 1H), 7.29-7.49 (m, 5H), 7.66-7.72 (m, 2H), 7.75 (s, 1H) ppm, $^{13}\text{C NMR}$ (75 MHz, CDCl_3), δ = 20.79, 116.14, 119.40, 127.69, 128.16, 128.44, 128.52, 128.75, 132.44, 134.16, 134.85, 139.88, 151.65, 160.79 ppm. **HRMS (ESI+)**, m/z calculated for $\text{C}_{16}\text{H}_{12}\text{O}_2$ ($\text{M}+\text{Na}^+$) 259.072950, found 259.072713.

6-Methyl-3-phenylhydrocoumarin (**30n**)

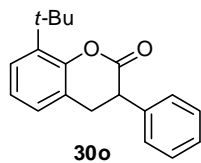


The reduction was conducted with Pd/C (10 mol%) and H_2 (1 bar). A white solid was obtained after precipitation in ethanol (53 %), Mp 127.4 °C, $^1\text{H NMR}$ (400 MHz, CDCl_3), δ = 2.32 (s, 3H), 3.18 (dd, J = 15.88, 6.24 Hz, 1H), 3.31 (dd, J = 15.85, 11.00 Hz, 1H), 3.95 (dd, J = 10.98, 6.25 Hz, 1H), 6.95-7.02 (m, 2H), 7.05-7.09 (m, 1H), 7.24-7.28 (m, 2H), 7.28-7.40 (m, 3H) ppm, $^{13}\text{C NMR}$ (100 MHz, CDCl_3), δ = 20.39, 31.38, 45.35, 116.11, 121.88, 127.44, 127.74, 128.08, 128.48, 128.57, 133.76, 136.32, 149.29, 169.16 ppm. **HRMS (ESI+)**, m/z calculated for $\text{C}_{16}\text{H}_{14}\text{O}_2$ ($\text{M}+\text{Na}^+$) 261.088602, found 261.088228.

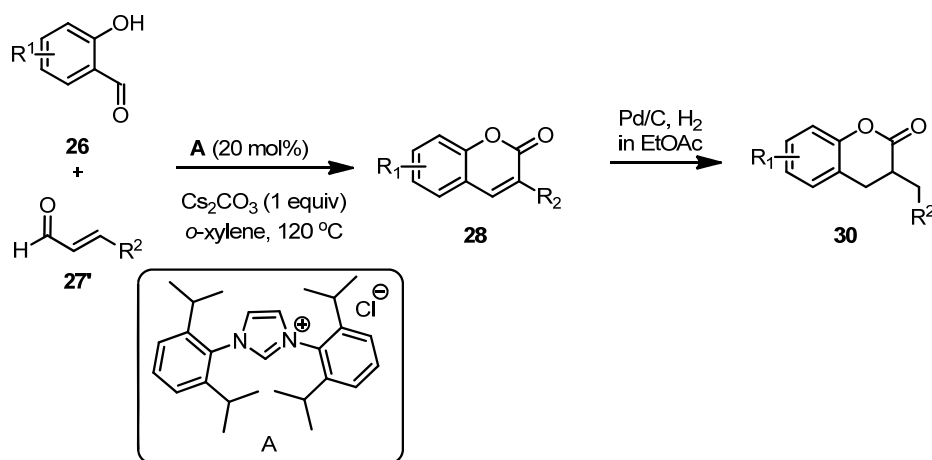
8-*tert*-Butyl-3-phenylcoumarin (**28o**)



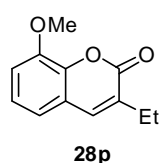
A white solid was obtained after precipitation in diethylether (51 %), Mp 121.1 °C. $^1\text{H NMR}$ (500 MHz, CDCl_3), δ = 1.55 (s, 9H), 7.18-7.26 (m, 1H), 7.36-7.41 (m, 2H), 7.42-7.46 (m, 2H), 7.51 (dd, J = 7.79, 1.50 Hz, 1H), 7.70-7.75 (m, 2H), 7.80 (s, 1H) ppm, $^{13}\text{C NMR}$ (125 MHz, CDCl_3), δ = 29.85, 34.94, 120.08, 124.00, 126.35, 127.29, 128.41, 128.47, 128.67, 128.89, 134.76, 137.64, 140.69, 152.22, 160.00 ppm. **HRMS (ESI+)**, m/z calculated for $\text{C}_{19}\text{H}_{18}\text{O}_2\text{Na}$ ($\text{M}+\text{Na}^+$) 301.119903, found 301.119918.

8-tert-Butyl-3-phenylhydrocoumarin (30o)

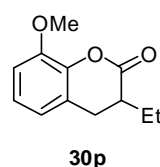
The reduction was conducted with Pd/C (10 mol%) and H₂ (1 bar), a white solid was obtained after precipitation in ethanol (97 %), Mp 129.9 °C, ¹H NMR (500 MHz, CDCl₃), δ = 1.45 (s, 9H), 3.20 (dd, *J* = 15.62, 5.90 Hz, 1H), 3.33 (dd, *J* = 15.60, 10.99 Hz, 1H), 3.94 (dd, *J* = 10.98, 5.90 Hz, 1H), 7.00-7.07 (m, 2H), 7.21-7.41 (m, 6H) ppm, ¹³C NMR (125 MHz, CDCl₃), δ = 29.94, 32.30, 34.80, 45.41, 123.49, 123.98, 125.92, 126.04, 127.70, 128.02, 128.78, 136.65, 137.99, 150.36, 169.02 ppm. HRMS (ESI+), *m/z* calculated for C₁₆H₂₀O₂ (M⁺) 280.146327, found 280.146495.

7.4.2. General Procedure for the Preparation of α -Alyl Coumarins and Hydrocoumarins¹⁷¹

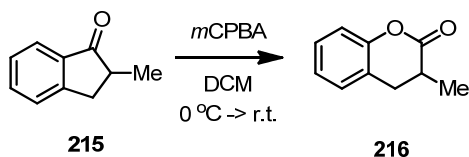
Procedure: In a 100 mL flask, salicylic aldehyde derivative **26** (2 mmol) and imidazolium salt **A** (0.4 mmol) and Cs_2CO_3 (2 mmol) were added, dried under vacuo and refilled with argon. Then *o*-xylene (50 mL) and enal **27'** (3 mmol) were added subsequently and the reaction mixture was heated to 120 °C and stirred for overnight. After 16 h, if no more enal was observed by TLC, additional enal substrate was added (3 mmol) to complete the reaction. In general, after 24 hr, the reaction was finished and the purified by silica chromatography to afford α -alkyl coumarin. The reduction was conducted using Pd/C (10 mol%) in ethylacetate as a solvent under 1 bar of hydrogen pressure for 24 hr.

3-Ethyl-8-methoxy-2H-chromen-2-one (**28p**)

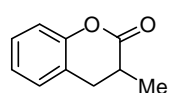
$^1\text{H NMR}$ (500 MHz, CDCl_3), δ = 1.26 (t, J = 7.44 Hz, 3H), 2.61 (dq, J = 7.42, 1.24 Hz, 2H), 3.96 (s, 3H), 6.99-7.04 (m, 2H), 7.18 (t, J = 7.96 Hz, 1H), 7.46 (t, J = 1.24 Hz, 1H) ppm, $^{13}\text{C NMR}$ (125 MHz, CDCl_3), δ = 12.23, 23.85, 56.19, 112.39, 118.65, 120.26, 124.06, 131.60, 137.55, 142.69, 147.03, 161.22 ppm. **HRMS (ESI+)**, m/z calculated for $\text{C}_{12}\text{H}_{12}\text{O}_3 \text{ Na}_1 (\text{M}^+)$ 227.067868, found 227.067715.

3-Ethyl-8-methoxychroman-2-one (**30p**)

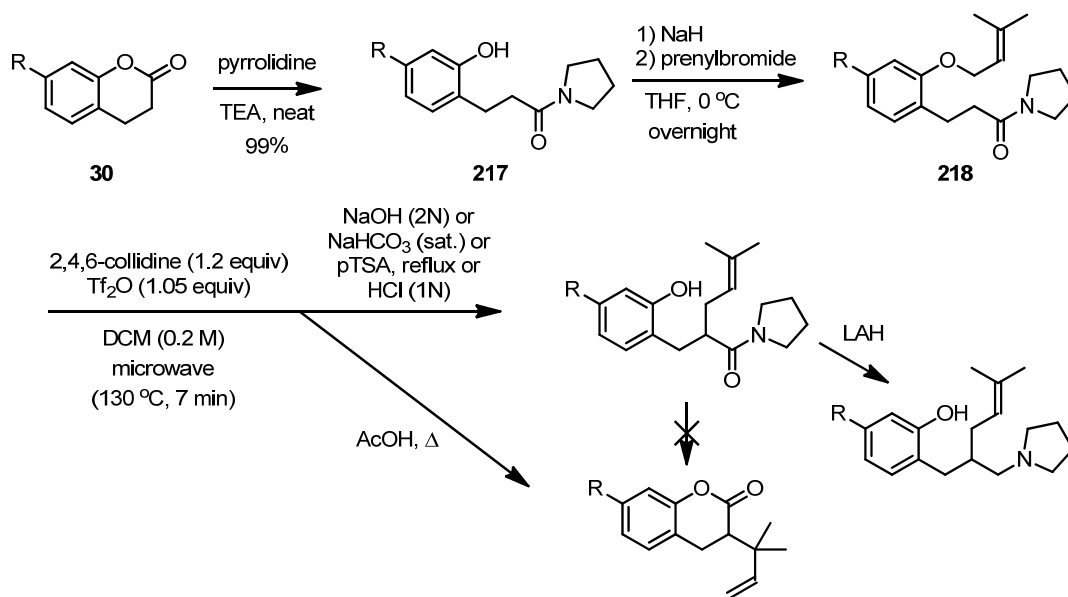
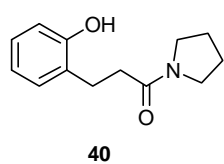
$^1\text{H NMR}$ (500 MHz, CDCl_3), δ = 1.05 (t, J = 7.45 Hz, 3H), 1.53-1.68 (m, 1H), 1.91-2.02 (m, 1H), 2.57-2.66 (m, 1H), 2.81 (dd, J = 15.73, 10.94 Hz, 1H), 3.02 (dd, J = 15.75, 5.93 Hz, 1H), 3.88 (s, 3H), 6.76 (d, J = 7.58 Hz, 1H), 6.85 (d, J = 8.14 Hz, 1H), 7.03 (t, J = 7.92 Hz, 1H) ppm, $^{13}\text{C NMR}$ (125 MHz, CDCl_3), δ = 11.33, 22.78, 28.96, 40.37, 56.01, 110.91, 119.62, 123.76, 124.13, 140.78, 147.39, 170.16 ppm.

7.4.3. Typical Procedure for the Preparation of α -Methyl Hydrocoumarin

Procedure: In a 50 mL flask, 2-methyl-1-indanone (**215**, 6 mmol) was dissolved in DCM (30 mL) at 0 °C then *m*CPBA (3 equiv) was added at the same temperature and the reaction mixture was stirred overnight. After checking conversion by GC/MS (16h, 72% conversion), 2 equiv of *m*CPBA was added additionally to complete reaction. After full conversion of indanone, the reaction mixture was quenched with NaHCO₃ and extracted with DCM. The combined organic layer was filtered through silicapad to afford off white solid **216** with 57% yield after evaporation of the solvent.

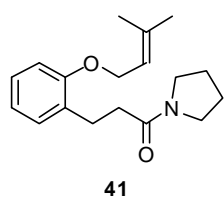
3-Methylchroman-2-one (216**)**

216 ¹H NMR (500 MHz, CDCl₃), δ = 1.38 (d, *J* = 6.49 Hz, 3H), 2.80 (tdd, *J* = 18.77, 12.16, 9.41 Hz, 2H), 2.98 (dd, *J* = 14.53, 5.08 Hz, 1H), 7.08 (ddd, *J* = 20.65, 13.55, 4.56 Hz, 2H), 7.18 (d, *J* = 7.42 Hz, 1H), 7.25 (dd, *J* = 12.06, 4.76 Hz, 1H) ppm, ¹³C NMR (125 MHz, CDCl₃), δ = 15.44, 31.70, 34.27, 116.66, 122.89, 124.27, 127.97, 128.25, 151.83, 171.64 ppm. HRMS (EI), *m/z* calculated for C₁₀H₁₀O₂ (M⁺) 162.068082, found 162.068151.

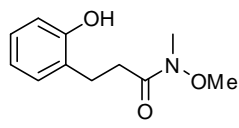
7.4.4. Typical Procedure for the Preparation of α -Prenyl Hydrocoumarin3-(2-Hydroxyphenyl)-1-(pyrrolidin-1-yl)propan-1-one (**40**)

¹H NMR (500 MHz, CDCl₃), δ = 1.68-1.81 (m, 2H), 1.81-1.92 (m, 2H), 2.49-2.66 (m, 2H), 2.84-2.90 (m, 2H), 3.26 (t, J = 6.79 Hz, 2H), 3.38 (t, J = 6.84 Hz, 2H), 6.75 (t, J = 7.29 Hz, 1H), 6.86 (d, J = 7.98 Hz, 1H), 6.98 (d, J = 7.27 Hz, 1H), 7.04 (t, J = 7.36 Hz, 1H), 9.78 (br s, 1H) ppm, ¹³C NMR (125 MHz, CDCl₃), δ = 24.28, 24.37, 25.94, 36.62, 46.19, 46.54, 118.22,

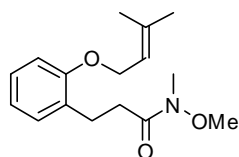
120.00, 127.99, 128.50, 130.60, 155.65, 172.33 ppm. HRMS (ESI⁺), m/z calculated for C₁₃H₁₇N₁O₂Na₁ (M+Na) 242.115151, found 242.114853.

3-((3-Methylbut-2-en-1-yl)oxy)phenyl)-1-(pyrrolidin-1-yl)propan-1-one (**41**)

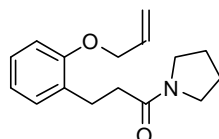
¹H NMR (500 MHz, CDCl₃), δ = 1.73 (s, 3H), 1.78 (s, 3H), 1.79-1.93 (m, 4H), 2.55 (dd, J = 9.22, 6.99 Hz, 2H), 2.96 (dd, J = 9.26, 6.94 Hz, 2H), 3.35 (t, J = 6.63 Hz, 2H), 3.46 (t, J = 6.74 Hz, 2H), 4.52 (d, J = 6.60 Hz, 2H), 5.43-5.51 (m, 1H), 6.82-6.90 (m, 2H), 7.18 (ddd, J = 9.55, 7.36, 1.62 Hz, 2H) ppm.

3-(2-Hydroxyphenyl)-N-methoxy-N-methylpropanamide (**217b**)**217b**

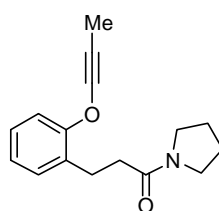
$^1\text{H NMR}$ (500 MHz, CDCl_3), δ = 2.83-2.89 (m, 2H), 2.92 (dd, J = 7.47, 3.91 Hz, 2H), 3.18 (s, 3H), 3.63 (s, 3H), 6.84 (dt, J = 7.43, 1.12 Hz, 1H), 6.92 (dd, J = 8.05, 0.95 Hz, 1H), 7.07 (dd, J = 7.51, 1.46 Hz, 1H), 7.12 (dt, J = 8.04, 1.65 Hz, 1H), 8.95 (br s, 1H) ppm, $^{13}\text{C NMR}$ (125 MHz, CDCl_3), δ = 23.78, 32.32, 33.82, 61.05, 118.00, 120.36, 127.98, 128.13, 130.64, 155.10, 175.18 ppm. **HRMS (ESI+)**, m/z calculated for $\text{C}_{11}\text{H}_{15}\text{N}_1\text{O}_3\text{Na}_1$ ($\text{M}+\text{Na}^+$) 232.094411, found 232.094495.

N-Methoxy-N-methyl-3-(2-((3-methylbut-2-en-1-yl)oxy)phenyl)propanamide (**218b**)**218b**

$^1\text{H NMR}$ (500 MHz, CDCl_3), δ = 1.73 (s, 3H), 1.78 (s, 3H), 2.70-2.74 (m, 2H), 2.91-2.98 (m, 2H), 3.18 (s, 3H), 3.61 (s, 3H), 4.53 (d, J = 6.51 Hz, 2H), 5.51-5.46 (m, 1H), 6.82-6.90 (m, 2H), 7.16-7.19 (m, 2H) ppm, $^{13}\text{C NMR}$ (125 MHz, CDCl_3), δ = 18.23, 25.75, 26.03, 32.05, 32.16, 61.12, 64.83, 111.41, 120.25, 120.36, 127.31, 129.92, 130.18, 137.11, 156.85, 174.44 ppm. **HRMS (ESI+)**, m/z calculated for $\text{C}_{16}\text{H}_{23}\text{N}_1\text{O}_3\text{Na}_1$ ($\text{M}+\text{Na}^+$) 300.157015, found 300.157259.

3-(2-(Allyloxy)phenyl)-1-(pyrrolidin-1-yl)propan-1-one (**218c**)**218c**

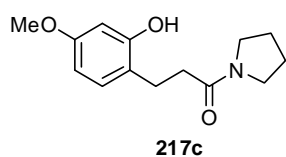
$^1\text{H NMR}$ (500 MHz, CDCl_3), δ = 1.78-1.96 (m, 4H), 2.51-2.61 (m, 2H), 2.97-3.03 (m, 2H), 3.32 (t, J = 6.68 Hz, 2H), 3.46 (t, J = 6.77 Hz, 2H), 4.55 (d, J = 5.05 Hz, 2H), 5.27 (d, J = 10.54 Hz, 1H), 5.41 (d, J = 17.28 Hz, 1H), 6.06 (ddd, J = 22.15, 10.37, 5.11 Hz, 1H), 6.83 (d, J = 8.16 Hz, 1H), 6.88 (t, J = 7.40 Hz, 1H), 7.15-7.21 (m, 2H) ppm, $^{13}\text{C NMR}$ (125 MHz, CDCl_3), δ = 24.43, 26.09, 26.49, 35.11, 45.57, 46.58, 68.68, 111.44, 117.16, 120.72, 127.34, 130.07, 130.37, 133.52, 156.46, 171.38 ppm. **HRMS (ESI+)**, m/z calculated for $\text{C}_{16}\text{H}_{21}\text{N}_1\text{O}_2\text{Na}_1$ ($\text{M}+\text{Na}^+$) 282.146451, found 282.146680.

3-(2-(Prop-1-yn-1-yloxy)phenyl)-1-(pyrrolidin-1-yl)propan-1-one (**218d**)**218d**

$^1\text{H NMR}$ (500 MHz, CDCl_3), δ = 1.81-7.90 (m, 7H, $-\text{CH}_3$ + 4H from pyrrolidine), 2.51-2.61 (m, 2H), 2.93-3.01 (m, 2H), 3.36 (t, J = 6.69 Hz, 2H), 3.46 (t, J = 6.79 Hz, 2H), 6.90 (t, J = 7.40 Hz, 1H), 6.94 (d, J = 8.07 Hz, 1H), 7.17-7.21 (m, 2H) ppm, $^{13}\text{C NMR}$ (125 MHz, CDCl_3), δ = 3.72, 24.45, 26.15, 26.54, 35.22, 45.56, 46.60, 56.43, 74.39, 83.29, 111.78, 121.13, 127.30, 130.24, 130.43, 155.82, 171.42 ppm. **HRMS (ESI+)**, m/z calculated for $\text{C}_{16}\text{H}_{21}\text{N}_1\text{O}_2\text{Na}_1$ ($\text{M}+\text{Na}^+$) 282.146451, found 282.146680.

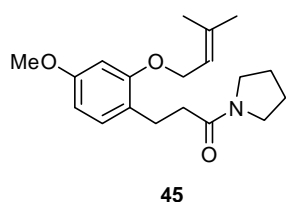
7. EXPERIMENTAL PART

3-(2-Hydroxy-4-methoxyphenyl)-1-(pyrrolidin-1-yl)propan-1-one (**217c**)



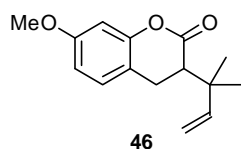
$^1\text{H NMR}$ (500 MHz, CDCl_3), δ = 1.79-1.87 (m, 2H), 1.93 (ddd, J = 13.88, 13.46, 7.08 Hz, 2H), 2.56-2.67 (m, 2H), 2.81-2.92 (m, 2H), 3.33 (t, J = 6.81 Hz, 2H), 3.46 (t, J = 6.88 Hz, 2H), 3.75 (s, 3H), 6.40 (dd, J = 8.31, 2.38 Hz, 1H), 6.51 (d, J = 2.29 Hz, 1H), 6.94 (d, J = 8.33 Hz, 1H), 9.92 (br s, 1H) ppm, $^{13}\text{C NMR}$ (125 MHz, CDCl_3), δ = 23.72, 24.28, 25.93, 36.78, 46.18, 46.54, 55.23, 103.00, 106.57, 120.64, 131.05, 156.62, 159.66, 172.51 ppm. **HRMS (ESI+)**, m/z calculated for $\text{C}_{14}\text{H}_{19}\text{N}_1\text{O}_3\text{Na}_1$ ($\text{M}+\text{Na}^+$) 272.125716, found 272.125800.

3-(4-Methoxy-2-((3-methylbut-2-en-1-yl)oxy)phenyl)-1-(pyrrolidin-1-yl)propan-1-one (**45**)



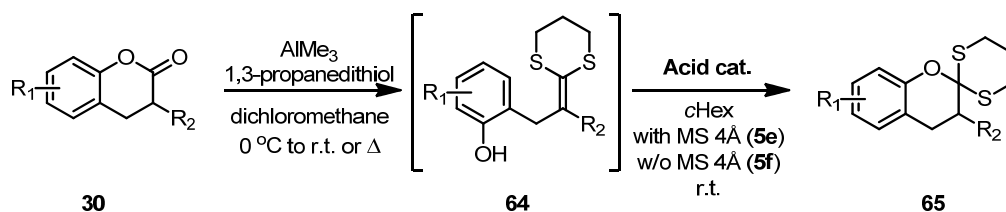
$^1\text{H NMR}$ (500 MHz, CDCl_3), δ = 1.73 (s, 3H), 1.78 (s, 3H), 1.80-1.93 (m, 4H), 2.45-2.64 (m, 2H), 2.89 (dd, J = 9.15, 6.92 Hz, 2H), 3.35 (t, J = 6.65 Hz, 2H), 3.46 (t, J = 6.76 Hz, 2H), 3.78 (s, 3H), 4.49 (d, J = 6.60 Hz, 2H), 5.47 (t, J = 6.59 Hz, 1H), 6.40 (dd, J = 8.20, 2.36 Hz, 1H), 6.44 (d, J = 2.29 Hz, 1H), 7.09 (d, J = 8.20 Hz, 1H) ppm, $^{13}\text{C NMR}$ (125 MHz, CDCl_3), δ = 18.24, 24.46, 25.79, 26.06, 26.13, 35.53, 45.53, 46.63, 55.36, 64.83, 99.50, 103.78, 120.00, 122.38, 130.42, 137.45, 157.62, 159.27, 171.68 ppm.

7-Methoxy-3-(2-methylbut-3-en-2-yl)chroman-2-one (**46**)



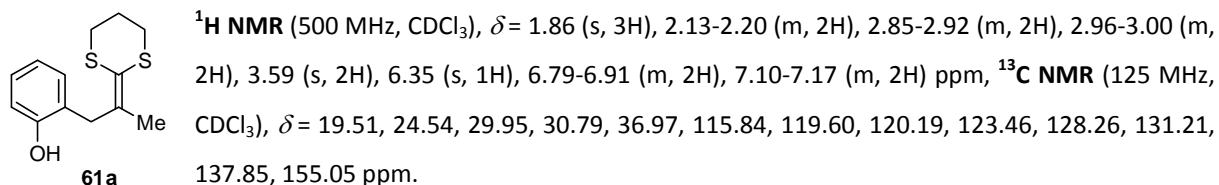
$^1\text{H NMR}$ (500 MHz, CDCl_3), δ = 1.16 (s, 3H), 1.23 (s, 3H), 2.57 (dd, J = 9.48, 6.35 Hz, 1H), 2.84 (dd, J = 15.92, 9.51 Hz, 1H), 2.95 (dd, J = 15.92, 6.33 Hz, 1H), 3.78 (s, 3H), 5.02 (dd, J = 14.07, 6.11 Hz, 2H), 5.87 (dd, J = 17.34, 10.85 Hz, 1H), 6.55 (d, J = 2.50 Hz, 1H), 6.62 (dd, J = 8.36, 2.54 Hz, 1H), 7.02 (d, J = 8.34 Hz, 1H) ppm, $^{13}\text{C NMR}$ (125 MHz, CDCl_3), δ = 23.47, 25.50, 26.31, 29.71, 48.30, 55.51, 101.89, 110.12, 112.64, 114.93, 128.24, 145.25, 152.33, 159.56, 168.64 ppm. **HRMS (ESI+)**, m/z calculated for $\text{C}_{15}\text{H}_{18}\text{O}_3\text{Na}_1$ ($\text{M}+\text{Na}$) 269.114815, found 269.114838.

7.4.5. General Procedure for the Preparation of Hydrocoumarin Ketene Dithioacetals and Their Asymmetric Protonation¹⁷²

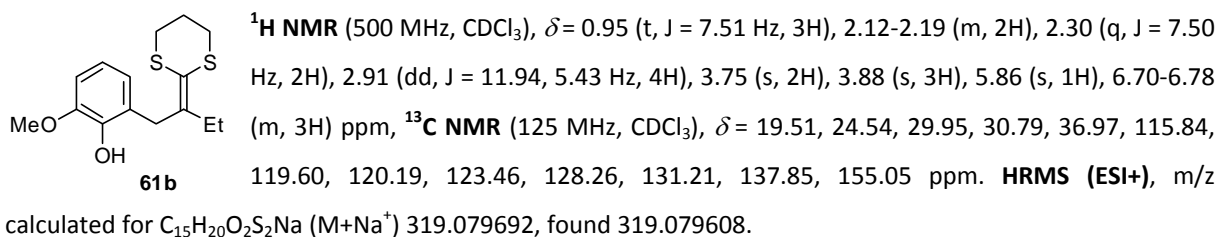


To a stirred solution of 1,3-propanedithiol (1.1 equiv) in dichloromethane (5 mL) under argon, trimethylaluminium solution in hexane (2 M, 2.2 equiv) was added dropwise at 0 °C and the reaction mixture warmed to room temperature (turbid solution). After 30 min, a solution of hydrocoumarin **30** (0.5 mmol) in dichloromethane (5 mL) was added dropwisely at room temperature or 0 °C. The reaction was followed by TLC (diethylether:*n*-Hexane=3:1) until the starting material consumed completely. Then, a few drops of triethylamine was added and the reaction mixture evaporated under vacuo at 25 °C and diluted with diethylether (20 mL) and 10 % aq. NaHCO₃ (10 mL) and stirred vigorously for 15 min and the organic layer separated and dried over Na₂SO₄ and concentrated under reduced pressure. The obtained residue further purified by silica chromatography (diethylether:*n*-hexane=4:1) to afford ketene dithioacetal and stored as a solution in diethylether (0.16 M) at -20 °C or **used for the asymmetric protonation reaction immediately to prevent a spontaneous cyclization.**

2-(2-(1,3-Dithian-2-ylidene)propyl)phenol (**61a**)

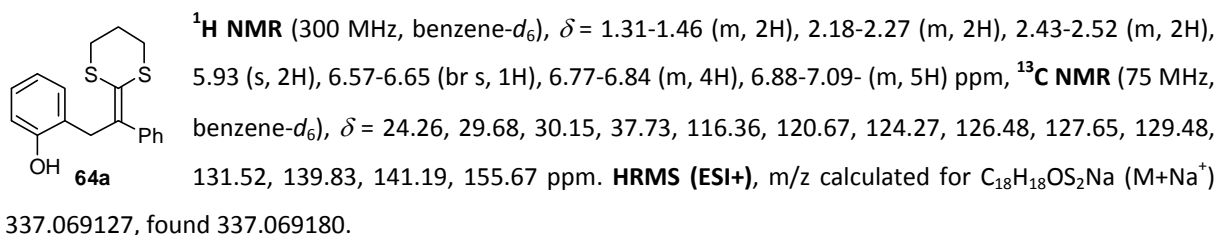


2-(2-(1,3-Dithian-2-ylidene)butyl)-6-methoxyphenol (**61b**)

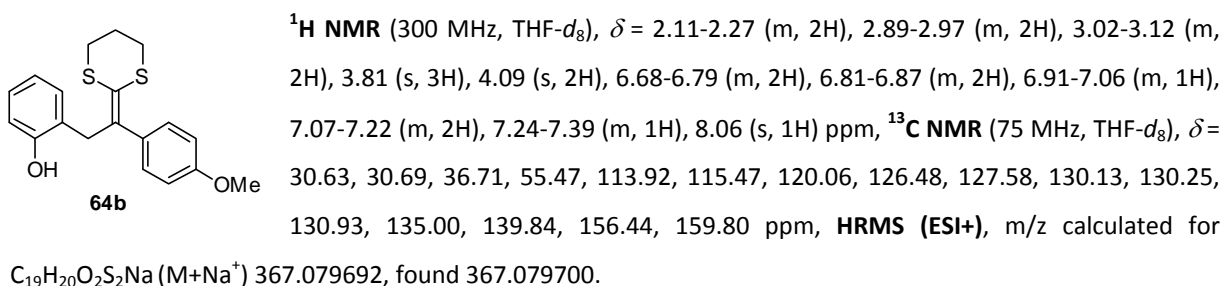


7. EXPERIMENTAL PART

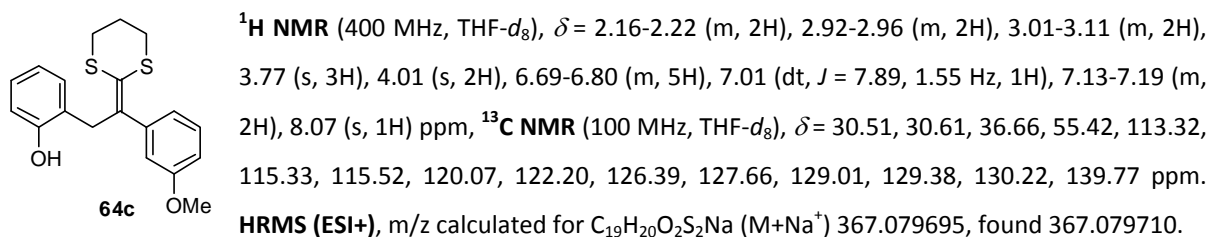
2-(2-(1,3-Dithian-2-ylidene)-2-phenylethyl)phenol (**64a**)



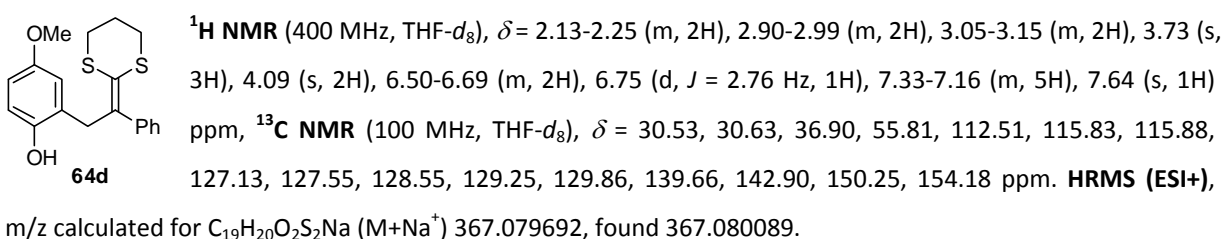
2-(2-(1,3-Dithian-2-ylidene)-2-(4-methoxyphenyl)ethyl)phenol (**64b**)



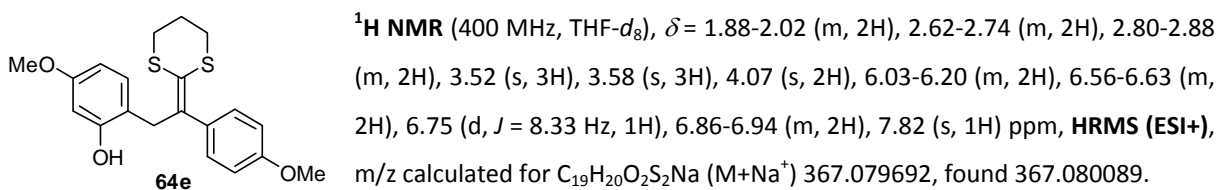
2-(2-(1,3-Dithian-2-ylidene)-2-(3-methoxyphenyl)ethyl)phenol (**64c**)

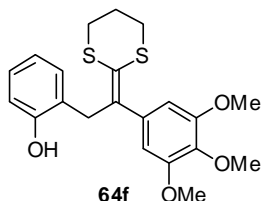


2-(2-(1,3-Dithian-2-ylidene)-2-phenylethyl)-4-methoxyphenol (**64d**)

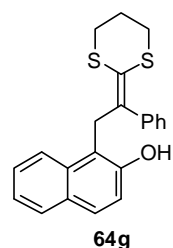


2-(2-(1,3-Dithian-2-ylidene)-2-(4-methoxyphenyl)ethyl)-5-methoxyphenol (**64e**)

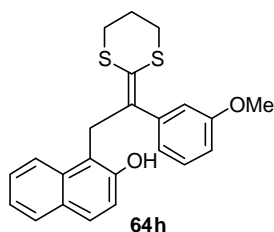


2-(2-(1,3-Dithian-2-ylidene)-2-(3,4,5-trimethoxyphenyl)ethyl)phenol (**64f**)

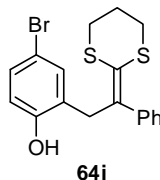
64f $^1\text{H NMR}$ (400 MHz, THF- d_8), δ = 2.13-2.27 (m, 2H), 2.88-2.99 (m, 2H), 3.06-3.13 (m, 2H), 3.76 (s, 3H), 3.77 (s, 6H), 4.09 (s, 2H), 6.45 (s, 2H), 6.78 (m, 2H), 7.03 (t, J = 7.63 Hz, 1H), 7.17 (d, J = 7.47 Hz, 1H), 8.12 (s, 1H) ppm, $^{13}\text{C NMR}$ (100 MHz, THF- d_8), δ = 30.51, 30.63, 36.45, 56.48, 56.65, 60.61, 107.69, 115.58, 120.08, 126.63, 127.70, 128.43, 130.41, 137.78, 138.94, 139.93, 153.99, 156.49 ppm. **HRMS (ESI+)**, m/z calculated for $\text{C}_{21}\text{H}_{24}\text{O}_4\text{S}_2\text{Na}$ ($\text{M}+\text{Na}^+$) 427.100821, found 427.100638.

1-(2-(1,3-Dithian-2-ylidene)-2-phenylethyl)naphthalen-2-ol (**64g**)

64g $^1\text{H NMR}$ (500 MHz, CDCl_3), δ = 2.15-2.21 (m, 2H), 2.77-2.89 (m, 2H), 3.13-3.22 (m, 2H), 4.29 (s, 2H), 6.20 (s, 1H), 6.74-6.77 (m, 2H), 7.02-7.12 (m, 4H), 7.13-7.21 (m, 2H), 7.43-7.51 (m, 1H), 7.60 (d, J = 8.82 Hz, 1H), 7.63-7.67 (m, 1H) ppm, $^{13}\text{C NMR}$ (125 MHz, CDCl_3-d_1), δ = 24.15, 29.71, 30.26, 31.39, 115.12, 117.89, 122.63, 123.17, 124.51, 125.84, 127.18, 127.89, 128.12, 128.35, 128.59, 128.93, 133.44, 139.79, 139.96, 152.71 ppm. **HRMS (ESI+)**, m/z calculated for $\text{C}_{22}\text{H}_{20}\text{O}_1\text{S}_2\text{Na}$ ($\text{M}+\text{Na}^+$) 387.084728, found 387.084904.

1-(2-(1,3-Dithian-2-ylidene)-2-(3-methoxyphenyl)ethyl)naphthalen-2-ol (**64h**)

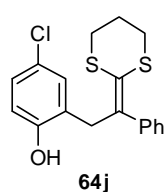
64h $^1\text{H NMR}$ (500 MHz, THF- d_8), δ = 2.21-2.30 (m, 2H), 2.88-2.96 (m, 2H), 3.29 (t, J = 6.36 Hz, 2H), 3.54 (s, 3H), 4.52 (s, 2H), 6.36-6.44 (m, 2H), 6.51-6.61 (m, 1H), 6.84-6.96 (m, 2H), 7.28 (dd, J = 14.76, 7.68 Hz, 1H), 7.42-7.58 (m, 2H), 7.72 (d, J = 8.09 Hz, 1H), 8.12 (d, J = 8.40 Hz, 1H), 8.19 (s, 1H) ppm, $^{13}\text{C NMR}$ (125 MHz, THF- d_8), δ = 30.59, 30.78, 31.36, 55.14, 113.69, 114.48, 118.08, 118.54, 122.39, 123.11, 124.93, 125.99, 126.79, 128.48, 128.64, 129.10, 129.93, 135.73, 141.72, 142.63 ppm. **HRMS (ESI+)**, m/z calculated for $\text{C}_{23}\text{H}_{22}\text{O}_2\text{S}_2\text{Na}$ ($\text{M}+\text{Na}^+$) 417.095346, found 417.095445.

2-(2-(1,3-Dithian-2-ylidene)-2-phenylethyl)-4-bromophenol (**64i**)

64i $^1\text{H NMR}$ (400 MHz, THF- d_8), δ = 1.24-1.42 (m, 2H), 2.11-2.24 (m, 2H), 2.33-2.51 (m, 2H), 3.75 (s, 2H), 5.78 (s, 1H), 6.38-6.51 (m, 1H), 6.87-7.04 (m, 8H) ppm, **HRMS (ESI+)**, m/z calculated for $\text{C}_{18}\text{H}_{17}\text{O}_1\text{BrS}_2\text{Na}$ ($\text{M}+\text{Na}^+$) 414.979655, found 414.979747.

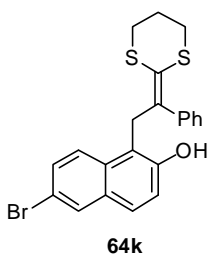
7. EXPERIMENTAL PART

2-(2-(1,3-Dithian-2-ylidene)-2-phenylethyl)-4-chlorophenol (**64j**)



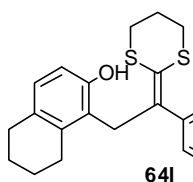
$^1\text{H NMR}$ (300 MHz, THF- d_8), δ = 2.13-2.29 (m, 2H), 2.92-3.01 (m, 2H), 3.06-3.15 (m, 2H), 4.08 (s, 2H), 6.70 (d, J = 8.49 Hz, 1H), 7.01 (dd, J = 8.50, 2.60 Hz, 1H), 7.13 (d, J = 2.59 Hz, 1H), 7.17-7.37 (m, 5H), 8.47 (br s, 1H) ppm, $^{13}\text{C NMR}$ (75 MHz, THF- d_8), δ = 30.45, 30.51, 36.49, 116.70, 124.71, 127.44, 127.68, 128.61, 128.65, 129.79, 138.44, 142.53, 155.23 ppm. **HRMS (ESI+)**, m/z calculated for $\text{C}_{18}\text{H}_{17}\text{O}_1\text{ClS}_2\text{Na}$ ($\text{M}+\text{Na}^+$) 371.030155, found 371.029880.

1-(2-(1,3-Dithian-2-ylidene)-2-phenylethyl)-6-bromonaphthalen-2-ol (**64k**)



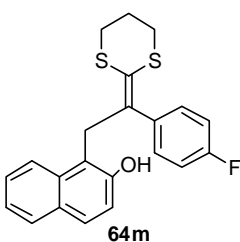
$^1\text{H NMR}$ (500 MHz, THF- d_8), δ = 2.20-2.31 (m, 2H), 2.87-2.98 (m, 2H), 3.25-3.33 (m, 2H), 4.50 (s, 2H), 6.81-6.84 (m, 2H), 6.93 (dd, J = 8.79, 3.29 Hz, 1H), 6.99-7.04 (m, 3H), 7.48 (d, J = 8.80 Hz, 1H), 7.59 (dd, J = 9.07, 2.10 Hz, 1H), 7.92 (d, J = 2.11 Hz, 1H), 8.07 (d, J = 9.07 Hz, 1H), 8.41 (s, 1H) ppm, $^{13}\text{C NMR}$ (125 MHz, THF- d_8), δ = 30.56, 30.83, 31.25, 116.75, 118.49, 119.72, 126.44, 127.06, 127.21, 127.82, 127.89, 129.82, 129.91, 131.09, 134.17, 141.32, 141.51, 154.24 ppm. **HRMS (ESI+)**, m/z calculated for $\text{C}_{22}\text{H}_{19}\text{O}_1\text{BrS}_2\text{Na}$ ($\text{M}+\text{Na}^+$) 464.995305, found 464.995389.

1-(2-(1,3-dithian-2-ylidene)-2-(4-methoxyphenyl)ethyl)-5,6,7,8-tetrahydronaphthalen-2-ol (**64l**)

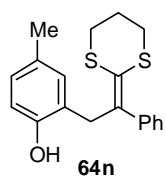


$^1\text{H NMR}$ (400 MHz, THF- d_8), δ = 1.67-1.82 (m, 5H), 2.14-2.23 (m, 2H), 2.62-2.72 (m, 3H), 2.83-2.91 (m, 2H), 3.09-3.17 (m, 2H), 3.76 (s, 3H), 4.10 (s, 2H), 6.41 (d, J = 8.14 Hz, 1H), 6.60-6.76 (m, 3H), 6.83-6.92 (m, 2H), 7.52 (s, 1H) ppm, $^{13}\text{C NMR}$ (100 MHz, THF- d_8), δ = 24.40, 24.76, 25.85, 27.69, 30.61, 30.64, 30.75, 32.13, 55.30, 113.21, 113.31, 124.38, 125.62, 128.29, 128.43, 130.89, 133.86, 138.00, 140.91, 154.36, 159.53 ppm. **HRMS (ESI+)**, m/z calculated for $\text{C}_{23}\text{H}_{26}\text{O}_2\text{S}_2\text{Na}$ ($\text{M}+\text{Na}^+$) 421.126644, found 421.126331.

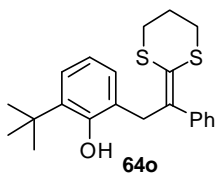
1-(2-(1,3-dithian-2-ylidene)-2-(4-fluorophenyl)ethyl)naphthalen-2-ol (**64m**)



$^1\text{H NMR}$ (400 MHz, THF- d_8), δ = 2.20-2.31 (m, 2H), 2.90-2.96 (m, 2H), 3.25-3.32 (m, 2H), 4.50 (s, 2H), 6.69-6.78 (m, 2H), 6.78-6.85 (m, 2H), 6.90 (d, J = 8.78 Hz, 1H), 7.26-7.34 (m, 1H), 7.49 (ddd, J = 8.38, 6.80, 1.25 Hz, 1H), 7.54 (d, J = 8.77 Hz, 1H), 7.73 (d, J = 8.15 Hz, 1H), 8.12 (d, J = 8.55 Hz, 1H), 8.20 (s, 1H) ppm, $^{13}\text{C NMR}$ (100 MHz, THF- d_8), δ = 29.70, 29.91, 30.47, 113.49, 113.70, 116.95, 117.61, 122.33, 123.89, 125.75, 126.05, 127.93, 128.34, 129.07, 130.75 ppm. **HRMS (ESI+)**, m/z calculated for $\text{C}_{22}\text{H}_{19}\text{O}_1\text{FS}_2\text{Na}$ ($\text{M}+\text{Na}^+$) 405.075356, found 405.074990.

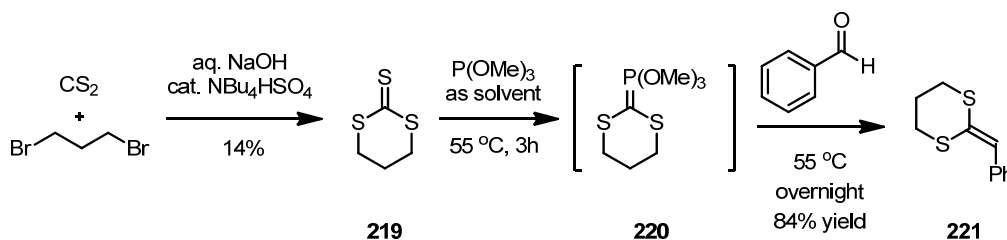
2-(2-(1,3-dithian-2-ylidene)-2-phenylethyl)-4-methylphenol (**64n**)

$^1\text{H NMR}$ (300 MHz, benzene- d_6), δ = 1.33-1.43 (m, 2H), 1.95 (s, 3H), 2.19-2.25 (m, 2H), 2.44-2.52 (m, 2H), 3.95 (s, 2H), 5.74 (s, 1H), 6.59-6.64 (m, 1H), 6.69-6.84 (m, 2H), 6.89-7.09 (m, 5H) ppm, $^{13}\text{C NMR}$ (75 MHz, benzene- d_6), δ = 20.74, 24.26, 29.68, 30.16, 37.85, 116.27, 123.95, 126.31, 127.65, 128.50, 129.05, 129.37, 129.50, 132.13, 140.04, 141.24 ppm.

2-(2-(1,3-dithian-2-ylidene)-2-phenylethyl)-6-tert-butylphenol (**64o**)

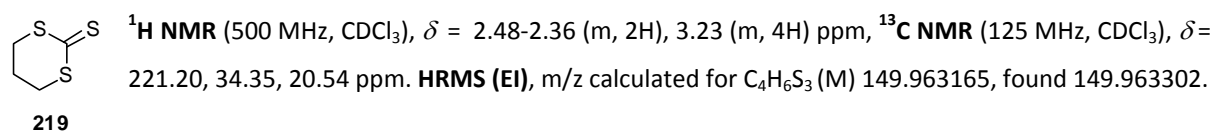
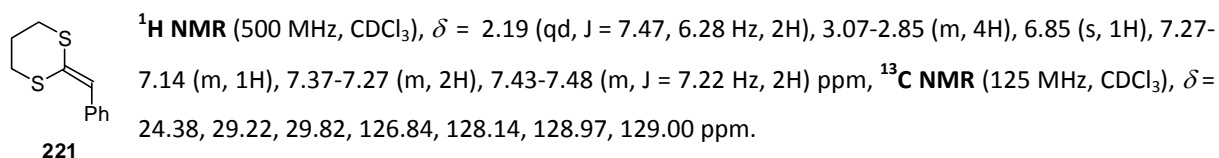
$^1\text{H NMR}$ (500 MHz, benzene- d_6), δ = 1.39 (s, 9H), 2.11-2.21 (m, 2H), 2.80-2.87 (m, 2H), 3.08-3.13 (m, 2H), 3.89 (s, 2H), 5.93 (s, 1H), 6.54 (dd, J = 7.46, 1.83 Hz, 1H), 6.56-6.60 (m, 1H), 6.87-6.94 (m, 2H), 7.08 (dd, J = 7.56, 1.73 Hz, 1H), 7.25-7.20 (m, 3H) ppm, $^{13}\text{C NMR}$ (125 MHz, benzene- d_6), δ = 24.07, 29.62, 29.72, 30.18, 34.76, 37.73, 119.26, 123.64, 125.32, 127.36, 128.05, 128.57, 129.10, 136.24, 139.53, 140.08 ppm. **HRMS (ESI-)**, m/z calculated for $\text{C}_{22}\text{H}_{25}\text{O}_1\text{S}_2$ (M-H^+) 369.135234, found 369.135142.

7.4.6. Typical Procedure for the Preparation of Ketene Dithioacetals from Benzaldehyde

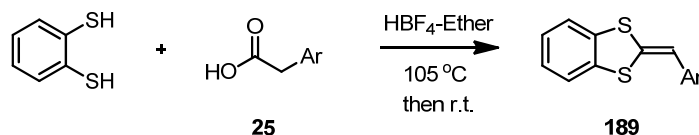


Trithiocarbonate formation: In a 250 mL flask, CS_2 (80 mL) and 33% aq. NaOH (NaOH 40 g in 80 mL of H_2O) were added and stirred vigorously for 30 min. Then NBu_4HSO_4 (0.1 equiv) was added and the reaction mixture turned to deep red color and oily. 1,3-Dibromopropane (1 equiv, 78.8 mmol) was added slowly to prevent polymerization and the reaction mixture was stirred overnight (the reaction mixture turned yellow at this step). The reaction mixture was then diluted with cold CS_2 , extracted with cold CS_2 and washed with water. The combined organic phase was evaporated and dissolved in methanol to precipitate trithiocarbonate **219** with 14% yield.¹⁷³

Dithioacetone formation: In a 25 mL flask, trithiocarbonate (1.33 mmol) was dissolved with trimethylphosphite (4 mL) and stirred for 3 hr at 55 °C. After consuming trithiocarbonate (checked by GC/MS), benzaldehyde (1.33 mmol) was added and stirred at 55 °C overnight. The reaction was followed by GC/MS to check conversion of the in-situ generated ylide intermediate. Then the reaction mixture was hydrolyzed with aq. NaOH and purified with silica chromatography (Hexane only, R_f of the product: 0.9) to afford ketene dithioacetal **221**.

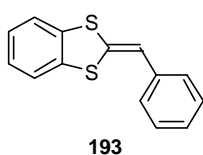
1,3-dithiane-2-thione (**219**)2-benzylidene-1,3-dithiane (**221**)

7.4.7. Typical Procedure for the Preparation of Ketene Dithioacetals from α -Arylaceticacids



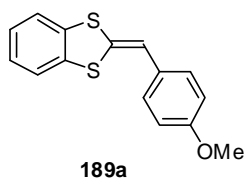
Procedure: In a 10 mL tube vial, 1,2-benzenedithiol (2.25 mmol) and phenylacetic acid (**25**, 2 mmol) was added and dissolved with HBF_4 -ether complex (2.5 mL). Then the vial was sealed and heated to 105 °C for 10 min. The reaction mixture was then cooled to room temperature and diluted with acetonitrile to precipitate the desired compound and purified by silica pad/ether to afford pure product **189** with 31 % yield as a white solid then by time the color changed to purple (but the ^1H NMR is identical as before).

2-Benzylidenebenzo[d][1,3]dithiole (**193**)



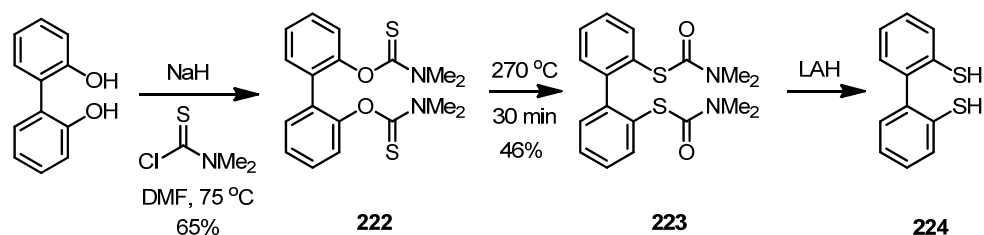
^1H NMR (500 MHz, CDCl_3), δ = 6.56 (s, 1H), 7.06-7.15 (m, 2H), 7.16-7.21 (m, 1H), 7.21-7.27 (m, 2H), 7.33-7.40 (m, 4H), ^{13}C NMR (125 MHz, CDCl_3), δ = 114.66, 120.92, 121.68, 125.57, 125.94, 126.00, 126.96, 128.52, 132.47, 134.70, 136.34, 136.55 ppm. **HRMS (EI)**, m/z calculated for $\text{C}_{14}\text{H}_{10}\text{S}_2$ (M) 242.022396, found 242.022236.

2-(4-Methoxybenzylidene)benzo[d][1,3]dithiole (**189a**)



^1H NMR (500 MHz, CDCl_3), δ = 3.97 (s, 3H), 6.50 (s, 1H), 6.86-6.99 (m, 2H), 7.03-7.12 (m, 2H), 7.21-2.29 (m, 4H), ^{13}C NMR (125 MHz, CDCl_3), δ = 55.32, 113.95, 114.64, 120.90, 121.65, 125.50, 125.87, 128.30, 129.55, 134.87, 136.34, 157.80 ppm. **HRMS (ESI+)**, m/z calculated for $\text{C}_{15}\text{H}_{14}\text{O}_1\text{S}_2$ ($\text{M}+\text{H}^+$) 273.040238, found 273.040719.

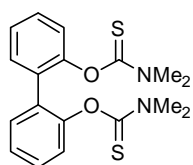
7.4.8. Preparation of Dithiols



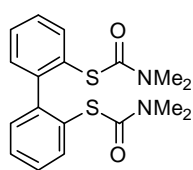
Thiocarbamate formation: NaH (4 equiv, 43 mmol) was added to a solution of biphenol (11 mmol) in DMF (45 mL) and stirred at 0 °C. After 30 min, thiocarbamoylchloride (5 equiv, 53 mmol) was added slowly and the reaction temperature was increased to 75 °C and stirred overnight. The reaction mixture was then poured into aq. NaOH solution to precipitate organic residue. The solid was filtered and washed with aq. NaOH and water then dissolved in DCM and washed with water to give desired product **222** with 65% yield after evaporation of solvent.

Newmann-Kwart rearrangement: The reaction conditions for Newmann-Kwart rearrangement was optimized by using melting-point apparatus. Substrate **222** was added in a 10 mL vial equipped with a stirring bar for high temperature reaction. After being evacuated and purged with argon several times, the reaction vessel was sealed under positive pressure to avoid any oxygen or water promoted reactions. After 30 min at 270 °C, the reaction mixture was cooled to room temperature and then purified by silica chromatography (diethylether:*n*-hexane=3:2, $R_f = 0.2$) to afford pure product **223** with 46-53% yield (the yield dependent on the reaction scale)

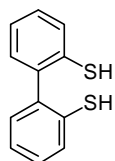
Reduction: Thiocarbamate (**223**, 2.12 mmol) was dissolved in THF (25 mL) and then LAH (21.17 mmol, 10 equiv) was added slowly at 0 °C. Then the reaction mixture was stirred for 16 hr at reflux temperature. After completion of the reaction (checked by TLC, diethylether, $R_f = 0.1$) the reaction was quenched with aq. NH_4Cl then HCl (1N) and extracted with diethylether to afford dithiol **224** (yellow solid) after evaporation of solvent. (92% of yield).

O,O'-[1,1'-Biphenyl]-2,2'-diyl bis(dimethylcarbamothioate) (**222**)**222**

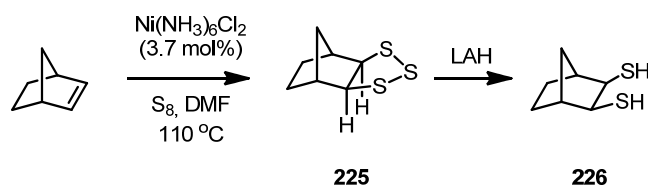
$^1\text{H NMR}$ (500 MHz, CDCl_3), $\delta = 3.03$ (s, 6H), 3.26 (s, 6H), 7.19 (dd, $J = 8.09, 0.92$ Hz, 2H), 7.26 (dt, $J = 7.51, 1.16$ Hz, 2H), 7.40 (ddd, $J = 18.15, 7.76, 1.64$ Hz, 4H), $^{13}\text{C NMR}$ (125 MHz, CDCl_3), $\delta = 38.45, 43.06, 123.96, 125.50, 128.41, 130.72, 131.30, 151.35, 187.19$ ppm. **HRMS (ESI+)**, m/z calculated for $\text{C}_{18}\text{H}_{20}\text{N}_2\text{O}_2\text{S}_2\text{Na}$ ($\text{M}+\text{Na}^+$) 383.085844, found 383.086073.

S,S'-[1,1'-Biphenyl]-2,2'-diyl bis(dimethylcarbamothioate) (**223**)**223**

$^1\text{H NMR}$ (500 MHz, CDCl_3), δ = 2.88 (s, 12H), 7.27-7.32 (m, 2H), 7.36-7.42 (m, 4H), 7.59-7.62 (m, 2H), $^{13}\text{C NMR}$ (125 MHz, CDCl_3), δ = 30.31, 36.91, 128.02, 128.45, 128.82, 130.71, 136.87, 145.60, 166.54 ppm. **HRMS (ESI+)**, m/z calculated for $\text{C}_{18}\text{H}_{20}\text{N}_2\text{O}_2\text{S}_2\text{Na}$ ($\text{M}+\text{Na}^+$) 383.085843, found 383.085950.

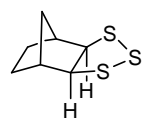
[1,1'-Biphenyl]-2,2'-dithiol (**224**)**224**

$^1\text{H NMR}$ (500 MHz, CDCl_3), δ = 3.29 (s, 2H), 7.18 (dd, J = 7.42, 1.52 Hz, 2H), 7.21-7.25 (m, 2H), 7.28 (dd, J = 7.44, 1.55 Hz, 2H), 7.41 (dd, J = 7.68, 1.04 Hz, 2H), $^{13}\text{C NMR}$ (125 MHz, CDCl_3), δ = 125.78, 128.69, 129.35, 130.23, 131.77, 138.95 ppm. **HRMS (EI)**, m/z calculated for $\text{C}_{12}\text{H}_{10}\text{S}_2$ (M) 218.022398, found 218.022177.



Cycloaddition: In a 250 mL flask, norbornene (21 mmol), nickel hexaamine dichloride (3.7 mol%, 0.2 mmol) and sulfur flower (2g, 8 mmol) was dissolved in DMF (60 mL) and then the reaction mixture was stirred at 110 °C overnight. The reaction was then cooled to room temperature and filtered on silica-pad with pentane. The organic residue was washed with water to provide desired product **225** (yellow oil) with 76% yield after evaporation of organic solvents.¹⁷⁴

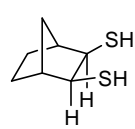
Reduction: The thiocarbamate (7.88 mmol) was dissolved in THF (30 mL) and then LAH (15.76 mmol, 2 equiv) was added slowly with water bath. Then the reaction mixture was stirred under reflux for 16 hr. After completion of the reaction (checked by TLC, Hexane, R_f = 0.3) the reaction was quenched with water and extracted with diethylether to afford dithiol **226** after evaporation of solvent (94% of yield).

Hexahydro-4,7-methanobenzo[d][1,2,3]trithiole (**225**)**225**

$^1\text{H NMR}$ (500 MHz, CDCl_3), δ = 1.07 (p, J = -1.#J Hz, 1H), 1.30-1.24 (m, 1H), 1.77-1.71 (m, 1H), 1.97-1.90 (m, 1H), 2.47 (td, J = 4.47, 1.55 Hz, 1H), 3.65 (d, J = 1.72 Hz, 1H), $^{13}\text{C NMR}$ (125 MHz, CDCl_3), δ = 27.59, 32.31, 40.75, 69.82 ppm. **HRMS (EI)**, m/z calculated for $\text{C}_7\text{H}_{10}\text{S}_3$ (M) 189.994465, found 189.994396.

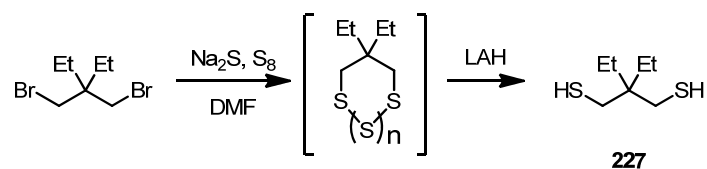
7. EXPERIMENTAL PART

Bicyclo[2.2.1]heptane-2,3-dithiol (**226**)



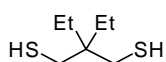
226

$^1\text{H NMR}$ (500 MHz, CDCl_3), δ = 1.12-1.25 (m, 1H), 1.29 (dd, J = 7.89, 2.14 Hz, 2H), 1.58-1.62 (m, 2H), 1.87 (dd, J = 4.62, 1.88 Hz, 2H), 1.95 (tdd, J = 7.65, 3.91, 2.10 Hz, 1H), 2.25 (td, J = 4.47, 1.55 Hz, 2H), 3.24 (td, J = 4.60, 1.87 Hz, 2H), $^{13}\text{C NMR}$ (125 MHz, CDCl_3), δ = 28.88, 32.70, 47.73, 48.19 ppm. **HRMS (EI)**, m/z calculated for $\text{C}_7\text{H}_{12}\text{S}_2$ (M) 160.038047, found 160.038116.



227

2,2-Diethylpropane-1,3-dithiol (**227**)



227

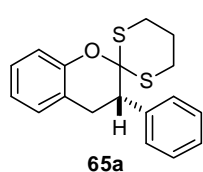
$^1\text{H NMR}$ (500 MHz, CDCl_3), δ = 0.91 (t, J = 7.47 Hz, 3H), 1.57 (q, J = 7.46 Hz, 2H), 2.89 (s, 1H), $^{13}\text{C NMR}$ (125 MHz, CDCl_3), δ = 9.18, 28.38, 48.39 ppm.

7.4.9. General Procedure for Asymmetric Protonation Reactions

Procedure for the **condition A** in Scheme 4-28: To a round bottom flask (100 mL), a solution of ketene dithioacetal **2** (0.1 mmol) in diethylether was added and dried under reduced pressure to remove remaining diethylether. The substrate **64** was dissolved with cyclohexane (50 mL). To the solution, molecular sieves (4Å, 30 mg) and catalyst **56a** (5 mol%) were added successively at room temperature and stirred for 24-48 hrs. After consumption of the starting material **64** (followed by TLC, diethylether/*n*Hexane=1:4), the solvent was removed under reduced pressure and the product **65** was purified by silica chromatography (neutralized silica with ammonia) using diethylether and *n*-hexane as an eluent. The enantiomeric excess was determined by HPLC analysis using chiral stationary phase. (The racemate was prepared using diphenylphosphate as a catalyst instead of catalyst **56a** in dichloromethane as a solvent).

Procedure for the **condition B** in Scheme 4-28: To a round bottom flask (25 mL), a solution of ketene dithioacetal **64** (0.1 mmol) in diethylether was added and dried under reduced pressure to remove diethylether. The remaining substrate **64** was dissolved with cyclohexane (12.5 mL). To the solution, catalyst **56n** (5 mol%) was added at room temperature and stirred for 3-13 days. After consumption of the starting material **64** (followed by TLC, diethylether/*n*Hexane=1:4), the solvent was removed under reduced pressure and the product **65** was purified by silica chromatography (neutralized silica with ammonia) using diethylether and *n*-hexane as an eluent. The enantiomeric excess was determined by HPLC analysis using chiral stationary phase.

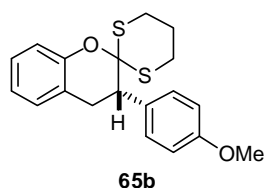
(*S*)-3-Phenylspiro[chroman-2,2'-[1,3]dithiane] (**65a**)



¹H NMR (500 MHz, benzene-*d*₆), δ = 1.41-1.37 (m, 1H), 1.56 (ttd, J = 13.85, 12.43, 3.25 Hz, 1H), 2.04-2.15 (m, 2H), 2.89 (dd, J = 16.89, 6.43 Hz, 1H), 3.03 (ddd, J = 13.98, 12.71, 2.76 Hz, 1H), 3.11 (dd, J = 16.89, 8.57 Hz, 1H), 3.20 (ddd, J = 14.00, 12.47, 2.78 Hz, 1H), 3.42 (dd, J = 8.52, 6.45 Hz, 1H), 6.82-6.89 (m, 2H), 6.98-7.12 (m, 5H), 7.36-7.41 (m, 2H) ppm, ¹³C NMR (125 MHz, CDCl₃), δ = 24.98, 26.80, 26.86, 29.43, 48.74, 90.00, 117.16, 122.08, 122.42, 127.48, 127.91, 128.32, 129.03, 129.33, 138.99, 151.70 ppm, HRMS (ESI+), m/z calculated for C₁₈H₁₈O₁S₂Na (M+Na⁺) 337.069128, found 337.069036. The enantiomeric ratio was determined by HPLC analysis using Daicel Chiralcel OD-3 column: *n*Hept:*i*PrOH = 99:1, flow rate 1.0 mL/min, λ = 254 nm: τ_{major} = 8.02 min, τ_{minor} = 11.96 min. α_D^{25} = +38.60° (c = 0.28, THF).

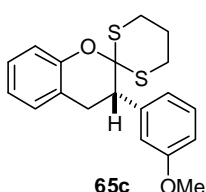
7. EXPERIMENTAL PART

(S)-3-(4-Methoxyphenyl)spiro[chroman-2,2'-[1,3]dithiane] (**65b**)



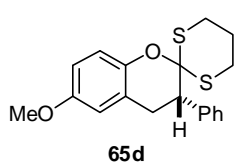
¹H NMR (500 MHz, CDCl₃), δ = 1.89-2.02 (m, 1H), 2.11-2.17 (m, 1H), 2.60-2.73 (m, 2H), 3.23 (d, J = 7.28 Hz, 2H), 3.31-3.39 (m, 1H), 3.42-3.50 (m, 2H), 3.79 (s, 3H), 6.82-6.88 (m, 2H), 6.97-7.02 (m, 2H), 7.09-7.23 (m, 2H), 7.23-7.30 (m, 1H) ppm, **¹³C NMR** (125 MHz, CDCl₃), δ = 24.95, 26.74, 26.80, 29.51, 47.87, 55.13, 90.32, 113.60, 117.07, 121.98, 122.46, 127.38, 129.27, 129.96, 130.93, 151.64, 159.13 ppm, **HRMS (ESI+)**, m/z calculated for C₁₉H₂₀O₂S₂Na (M+Na⁺) 367.079697, found 367.079811. The enantiomeric ratio was determined by HPLC analysis using Daicel Chiralcel OD-3 column: *n*Hept:*i*PrOH = 98:2, flow rate 1.0 mL/min, λ = 254 nm: τ_{major} = 12.22 min, τ_{minor} = 21.69 min. α_D^{25} = +39.77° (c = 1.72, Et₂O).

(S)-3-(3-methoxyphenyl)spiro[chroman-2,2'-[1,3]dithiane] (**65c**)



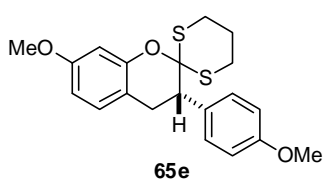
¹H NMR (400 MHz, CDCl₃), δ = 1.86-2.05 (m, 1H), 2.09-2.19 (m, 1H), 2.59-2.72 (m, 2H), 3.24 (d, J = 7.24 Hz, 2H), 3.29-3.41 (m, 1H), 3.41-3.52 (m, 2H), 3.75 (s, 3H), 6.84 (ddd, J = 8.26, 2.54, 0.88 Hz, 1H), 6.89-7.03 (m, 4H), 7.12 (ddd, J = 7.53, 1.62, 0.72 Hz, 1H), 7.17-7.24 (m, 2H) ppm, **¹³C NMR** (100 MHz, CDCl₃), δ = 24.94, 26.77, 26.84, 29.42, 48.73, 55.06, 89.88, 112.91, 114.99, 117.05, 121.36, 121.99, 122.34, 127.42, 129.15 ppm, **HRMS (ESI+)**, m/z calculated for C₁₉H₂₀O₂S₂Na (M+Na⁺) 367.079695, found 367.079306. The enantiomeric ratio was determined by HPLC analysis using Daicel Chiralcel OD-3 column: *n*Hept:*i*PrOH = 96:4, flow rate 1.0 mL/min, λ = 254 nm: τ_{major} = 6.84 min, τ_{minor} = 18.95 min. α_D^{25} = +50.91° (c = 0.06, THF).

(S)-6-Methoxy-3-phenylspiro[chroman-2,2'-[1,3]dithiane] (**65d**)



¹H NMR (500 MHz, CDCl₃), δ = 1.86-2.03 (m, 1H), 2.09-2.18 (m, 1H), 2.61-2.69 (m, 2H), 3.15-3.52 (m, 5H), 3.78 (s, 3H), 6.65-6.68 (m, 1H), 6.78 (dd, J = 8.85, 3.01 Hz, 1H), 6.95 (d, J = 8.85 Hz, 1H), 7.27-7.37 (m, 5H) ppm, **¹³C NMR** (125 MHz, CDCl₃), δ = 24.95, 26.76, 29.77, 48.55, 55.56, 89.88, 113.52, 117.79, 122.99, 127.83, 128.28, 128.94, 138.99, 145.64, 154.58, 151.64, 159.13 ppm. **HRMS (ESI+)**, m/z calculated for C₁₉H₂₀O₂S₂Na (M+Na⁺) 367.079692, found 367.080073. The enantiomeric ratio was determined by HPLC analysis using Daicel Chiralcel OD-3 column: *n*Hept:*i*PrOH = 98:2, flow rate 1.0 mL/min, λ = 206 nm: τ_{major} = 9.21 min, τ_{minor} = 12.61 min. α_D^{25} = +33.00° (c = 1.00, THF).

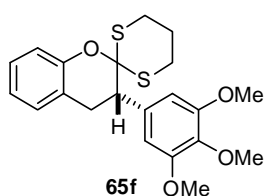
(S)-7-Methoxy-3-(4-methoxyphenyl)spiro[chroman-2,2'-[1,3]dithiane] (**65e**)



¹H NMR (400 MHz, CDCl₃), δ = 1.88-2.01 (m, 1H), 2.09-2.19 (m, 1H), 2.66 (td, J = 14.14, 3.55 Hz, 2H), 3.08-3.23 (m, 2H), 3.30-3.39 (m, 1H), 3.41-3.51 (m, 2H), 3.78 (s, 3H), 3.81 (s, 3H), 6.62-6.53 (m, 2H), 6.80-6.87 (m, 2H), 7.01 (d, J = 8.30 Hz, 1H), 7.22-7.27 (m, 2H) ppm, **¹³C NMR** (100 MHz, CDCl₃), δ = 24.96, 26.76, 26.81, 28.90, 48.02, 55.14, 55.38, 90.47, 102.17, 108.72, 113.60, 114.39, 129.73, 129.98, 131.08, 152.34, 159.14 ppm, **HRMS (ESI+)**, m/z calculated for C₂₀H₂₂O₃S₂Na (M+Na⁺) 397.090262, found 397.090293. The

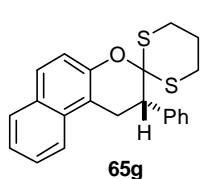
enantiomeric ratio was determined by HPLC analysis using Daicel Chiralcel OD-3 column: *n*Hept:*i*PrOH = 90:10, flow rate 1.0 mL/min, $\lambda = 254$ nm: $\tau_{\text{major}} = 6.23$ min, $\tau_{\text{minor}} = 17.77$ min. $\alpha_D^{25} = +43.53^\circ$ ($c = 0.17$, THF).

(*S*)-3-(3,4,5-Trimethoxyphenyl)spiro[chroman-2,2'-[1,3]dithiane] (**65f**)



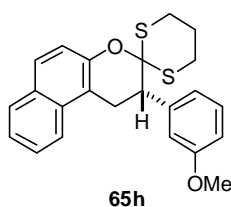
$^1\text{H NMR}$ (500 MHz, CDCl_3), $\delta = 1.89$ -2.09 (m, 1H), 2.12-2.22 (m, 1H), 2.63-2.75 (m, 2H), 3.20 (dd, $J = 16.94, 7.71$ Hz, 1H), 3.29 (dd, $J = 16.96, 6.40$ Hz, 1H), 3.32-3.41 (m, 1H), 3.41-3.44 (m, 1H), 3.45-3.53 (m, 1H), 3.77 (s, 6H), 3.83 (s, 3H), 6.55 (s, 2H), 6.96-7.03 (m, 2H), 7.14 (d, $J = 6.86$ Hz, 1H), 7.17-7.22 (m, 1H) ppm, $^{13}\text{C NMR}$ (125 MHz, CDCl_3), $\delta = 25.00, 26.89, 29.65, 48.76, 55.91, 60.82, 89.83, 105.97, 116.95, 122.04, 122.25, 127.50, 129.23, 134.35, 137.40, 151.63, 152.77$ ppm. **HRMS (ESI+)**, m/z calculated for $\text{C}_{21}\text{H}_{24}\text{O}_4\text{S}_2\text{Na}$ ($\text{M}+\text{Na}^+$) 427.100842, found 427.101472. The enantiomeric ratio was determined by HPLC analysis using Daicel Chiralcel OD-3 column: *n*Hept:*i*PrOH = 85:15, flow rate 1.0 mL/min, $\lambda = 254$ nm: $\tau_{\text{minor}} = 6.04$ min, $\tau_{\text{major}} = 6.95$ min. $\alpha_D^{25} = +55.00^\circ$ ($c = 0.20$, THF).

(*S*)-2-Phenyl-1,2-dihydrospiro[benzo[*f*]chromene-3,2'-[1,3]dithiane] (**65g**)



$^1\text{H NMR}$ (500 MHz, CDCl_3), $\delta = 1.90$ -2.05 (m, 1H), 2.11-2.19 (m, 1H), 2.62-2.71 (m, 2H), 3.38 (dt, $J = 13.90, 2.64$ Hz, 1H), 3.43-3.52 (m, 2H), 3.56 (dd, $J = 17.00, 6.74$ Hz, 1H), 3.68 (t, $J = 7.13$ Hz, 1H), 7.25 (s, 1H), 7.28-7.36 (m, 3H), 7.37-7.44 (m, 3H), 7.46-7.53 (m, 1H), 7.74 (d, $J = 8.88$ Hz, 1H), 7.82 (dd, $J = 8.21, 3.90$ Hz, 2H) ppm, $^{13}\text{C NMR}$ (125 MHz, CDCl_3), $\delta = 24.95, 26.86, 26.88, 26.94, 48.72, 89.94, 114.89, 118.54, 122.15, 124.05, 126.64, 127.97, 128.18, 128.39, 128.61, 129.07$ ppm. **HRMS (ESI+)**, m/z calculated for $\text{C}_{22}\text{H}_{20}\text{O}_1\text{S}_2\text{Na}$ ($\text{M}+\text{Na}^+$) 387.084780, found 387.085093. The enantiomeric ratio was determined by HPLC analysis using Daicel Chiralcel OD-3 column: *n*Hept:*i*PrOH = 98:2, flow rate 1.0 mL/min, $\lambda = 230$ nm: $\tau_{\text{major}} = 8.44$ min, $\tau_{\text{minor}} = 12.50$ min. $\alpha_D^{25} = +97.00^\circ$ ($c = 0.20$, THF). For (*R*)-configured product: $\alpha_D^{25} = -81.20^\circ$ ($c = 1.50$, THF).

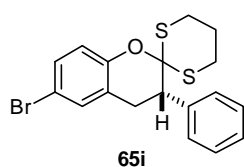
(*S*)-2-(3-Methoxyphenyl)-1,2-dihydrospiro[benzo[*f*]chromene-3,2'-[1,3]dithiane] (**65h**)



$^1\text{H NMR}$ (400 MHz, CDCl_3), $\delta = 1.89$ -2.07 (m, 1H), 2.08-2.19 (m, 1H), 2.66 (dddd, $J = 7.94, 6.23, 4.35, 3.29$ Hz, 2H), 3.36 (ddd, $J = 13.98, 12.78, 2.73$ Hz, 1H), 3.41-3.54 (m, 3H), 3.60-3.68 (m, 1H), 3.76 (s, 3H), 6.82-6.88 (m, 1H), 6.99-7.01 (m, 2H), 7.20-7.25 (m, 1H), 7.38 (ddd, $J = 7.94, 6.86, 1.09$ Hz, 1H), 7.49 (ddd, $J = 8.44, 6.86, 1.30$ Hz, 1H), 7.73 (d, $J = 8.84$ Hz, 1H), 7.79-7.83 (m, 2H) ppm, $^{13}\text{C NMR}$ (100 MHz, CDCl_3), $\delta = 24.94, 26.84, 26.89, 26.96, 48.80, 55.11, 89.88, 112.91, 114.86, 115.16, 118.47, 121.40, 122.11, 124.00, 126.59, 128.15, 128.56, 129.28, 129.72, 132.43, 140.55, 149.02, 159.35$ ppm. **HRMS (ESI+)**, m/z calculated for $\text{C}_{23}\text{H}_{23}\text{O}_2\text{S}_2\text{Na}$ ($\text{M}+\text{Na}^+$) 417.095346, found 417.095445. The enantiomeric ratio was determined by HPLC analysis using Daicel Chiralcel AS-H column: *n*Hept:*i*PrOH = 98:2, flow rate 1.0 mL/min, $\lambda = 236$ nm: $\tau_{\text{minor}} = 10.99$ min, $\tau_{\text{major}} = 12.44$ min. $\alpha_D^{25} = +99.60^\circ$ ($c = 0.50$, THF).

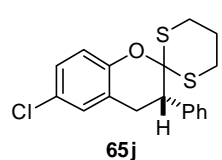
7. EXPERIMENTAL PART

(S)-6-Bromo-3-phenylspiro[chroman-2,2'-[1,3]dithiane] (**65i**)



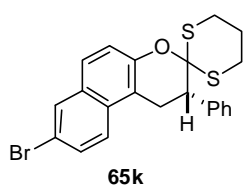
$^1\text{H NMR}$ (500 MHz, CDCl_3), δ = 1.86-2.05 (m, 1H), 2.07-2.20 (m, 1H), 2.65 (td, J = 14.27, 3.82 Hz, 2H), 3.26-3.15 (m, 2H), 3.25-3.45 (m, 2H), 3.49 (t, J = 7.32 Hz, 1H), 6.90 (d, J = 8.51 Hz, 1H), 7.25-7.31 (m, 8H) ppm, $^{13}\text{C NMR}$ (125 MHz, CDCl_3), δ = 24.75, 26.73, 26.76, 29.19, 48.21, 90.09, 114.33, 118.86, 124.61, 128.01, 128.34, 128.91, 128.96, 130.43, 131.89, 138.45, 150.83 ppm. **HRMS (ESI+)**, m/z calculated for $\text{C}_{18}\text{H}_{17}\text{O}_1\text{BrS}_2\text{Na}$ ($\text{M}+\text{Na}^+$) 414.979655, found 414.979747. The enantiomeric ratio was determined by HPLC analysis using Daicel Chiralcel OD-3 column: $n\text{Hept}:i\text{PrOH}$ = 98:2, flow rate 1.0 mL/min, λ = 206 nm: τ_{major} = 6.57 min, τ_{minor} = 8.78 min. α_D^{25} = $+51.30^\circ$ (c = 0.23, THF).

(S)-6-Chloro-3-phenylspiro[chroman-2,2'-[1,3]dithiane] (**65j**)

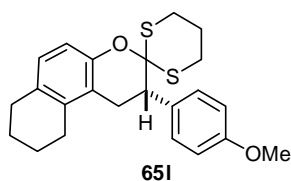


$^1\text{H NMR}$ (400 MHz, CDCl_3), δ = 1.84-2.04 (m, 1H), 2.07-2.20 (m, 1H), 2.60-2.70 (m, 2H), 3.15-3.29 (m, 2H), 3.30-3.45 (m, 2H), 3.49 (t, J = 7.14 Hz, 1H), 6.94 (d, J = 8.62 Hz, 1H), 7.08-7.20 (m, 2H), 7.31 (br s, 5H) ppm, $^{13}\text{C NMR}$ (100 MHz, CDCl_3), δ = 24.79, 26.75, 26.79, 29.32, 48.31, 90.20, 118.41, 124.08, 126.90, 127.55, 128.00, 128.34, 128.94, 128.97, 138.51, 150.34 ppm. **HRMS (ESI+)**, m/z calculated for $\text{C}_{18}\text{H}_{17}\text{OClS}_2\text{Na}$ ($\text{M}+\text{Na}^+$) 371.030160, found 371.030023. The enantiomeric ratio was determined by HPLC analysis using Daicel Chiralcel OD-3 column: $n\text{Hept}:i\text{PrOH}$ = 96:4, flow rate 1.0 mL/min, λ = 210 nm: τ_{major} = 5.37 min, τ_{minor} = 6.86 min. α_D^{25} = $+45.73^\circ$ (c = 1.50, THF).

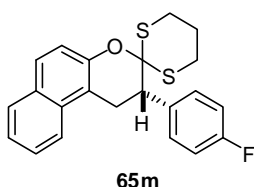
(S)-8-bromo-2-phenyl-1,2-dihydrospiro[benzo[*f*]chromene-3,2'-[1,3]dithiane] (**65k**)



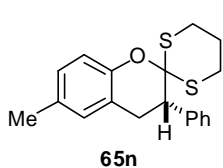
$^1\text{H NMR}$ (500 MHz, CDCl_3), δ = 1.88-2.07 (m, 1H), 2.09-2.22 (m, 1H), 2.67 (d, J = 14.15 Hz, 2H), 3.36 (t, J = 13.61 Hz, 1H), 3.41-3.56 (m, 3H), 3.66 (t, J = 7.24 Hz, 1H), 7.25 (m, 1H), 7.31-7.35 (m, 3H), 7.32-7.45 (m, 2H), 7.55 (d, J = 8.68 Hz, 1H), 7.64 (d, J = 8.94 Hz, 1H), 7.68 (d, J = 9.00 Hz, 1H), 7.97 (s, 1H) ppm, $^{13}\text{C NMR}$ (125 MHz, CDCl_3), δ = 24.83, 26.78, 26.83, 30.30, 48.60, 90.07, 115.18, 117.79, 119.64, 123.91, 127.23, 128.01, 128.37, 128.99, 129.77, 130.45, 130.89, 131.01, 138.79, 149.33 ppm. **HRMS (ESI+)**, m/z calculated for $\text{C}_{22}\text{H}_{19}\text{OS}_2\text{BrNa}$ ($\text{M}+\text{Na}^+$) 464.995308, found 464.995270. The enantiomeric ratio was determined by HPLC analysis using Daicel Chiralcel OD-3 column: $n\text{Hept}:i\text{PrOH}$ = 96:4, flow rate 1.0 mL/min, λ = 241 nm: τ_{major} = 8.17 min, τ_{minor} = 10.37 min. α_D^{25} = $+109.33^\circ$ (c = 0.15, THF).

(S)-2-(4-Methoxyphenyl)-1,2,7,8,9,10-hexahydrospiro[benzo[f]chromene-3,2'-[1,3]dithiane] (**65l**)

¹H NMR (400 MHz, CDCl₃), δ = 1.69-1.85 (m, 4H), 1.90-2.00 (m, 1H), 2.08-2.16 (m, 1H), 2.55 (t, J = 6.07 Hz, 2H), 2.59-2.69 (m, 2H), 2.75 (t, J = 5.91 Hz, 2H), 2.90-3.08 (m, 2H), 3.32 (ddd, J = 13.91, 12.92, 2.66 Hz, 1H), 3.39-3.45 (m, 1H), 3.46-3.50 (m, 1H), 6.82 (d, J = 8.31 Hz, 1H), 6.83-6.88 (m, 2H), 6.95 (d, J = 8.32 Hz, 1H), 7.26-7.31 (m, 2H) ppm, **¹³C NMR** (100 MHz, CDCl₃), δ = 22.75, 22.94, 25.01, 26.06, 26.78, 26.82, 27.62, 29.51, 48.12, 55.10, 89.62, 113.60, 114.36, 120.63, 127.98, 129.94, 130.74, 131.33, 135.59, 149.25, 159.09 ppm. **HRMS (ESI+)**, m/z calculated for C₂₃H₂₆O₂S₂Na (M+Na⁺) 421.126644, found 421.127231. The enantiomeric ratio was determined by HPLC analysis using Daicel Chiralcel OD-3 column: *n*Hept:*i*PrOH = 90:10, flow rate 1.0 mL/min, λ = 241 nm: τ_{major} = 5.40 min, τ_{minor} = 17.6 min. α_D^{25} = +26.18° (c = 2.20, THF).

(S)-2-(4-Fluorophenyl)-1,2-dihydrospiro[benzo[f]chromene-3,2'-[1,3]dithiane] (**65m**)

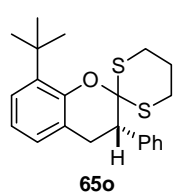
¹H NMR (400 MHz, CDCl₃), δ = 1.90-2.05 (m, 1H), 2.12-2.22 (m, 1H), 2.68 (td, J = 14.00, 3.47 Hz, 2H), 3.33-3.51 (m, 2H), 3.55 (dd, J = 17.02, 6.78 Hz, 1H), 3.67 (t, J = 7.07 Hz, 1H), 6.95-7.07 (m, 2H), 7.24 (d, J = 8.88 Hz, 1H), 7.34-7.44 (m, 2H), 7.50 (ddd, J = 8.36, 6.88, 1.23 Hz, 1H), 7.74 (d, J = 8.85 Hz, 1H), 7.79-7.85 (m, 2H) ppm, **¹³C NMR** (125 MHz, CDCl₃), δ = 24.86, 26.79, 26.82, 27.01, 47.88, 89.81, 114.57, 115.15, 115.32, 118.46, 122.05, 124.09, 126.66, 128.26, 128.60, 129.74, 130.54, 130.61, 132.37, 134.82, 134.84, 149.00, 161.44, 163.40 ppm, **¹⁹F NMR** (376 Hz, CDCl₃), δ = -114.38 ppm, **HRMS (ESI+)**, m/z calculated for C₂₂H₁₉OFS₂Na (M+Na⁺) 405.075357, found 405.075677. The enantiomeric ratio was determined by HPLC analysis using Daicel Chiralcel AD-3 column: *n*Hept:*i*PrOH = 98:2, flow rate 1.0 mL/min, λ = 236 nm: τ_{minor} = 11.66 min, τ_{major} = 14.39 min. α_D^{25} = +88.75° (c = 0.80, THF).

(S)-6-Methyl-3-phenylspiro[chroman-2,2'-[1,3]dithiane] (**65n**)

¹H NMR (400 MHz, CDCl₃), δ = 1.88-2.02 (m, 1H), 2.09-2.18 (m, 1H), 2.30 (s, 3H), 2.64 (ddd, J = 13.96, 7.13, 3.40 Hz, 2H), 3.12-3.26 (m, 2H), 3.25-3.46 (m, 2H), 3.50 (t, J = 7.10 Hz, 1H), 6.90-6.94 (m, 2H), 7.01 (dd, J = 8.25, 1.55 Hz, 1H), 7.26-7.38 (m, 5H) ppm, **¹³C NMR** (100 MHz, CDCl₃), δ = 20.71, 24.95, 26.76, 26.78, 29.38, 48.68, 89.86, 116.85, 121.95, 127.80, 128.13, 128.26, 128.95, 129.64, 131.40, 139.06, 149.47 ppm, **HRMS (ESI+)**, m/z calculated for C₁₉H₂₀O₁S₂Na (M+Na⁺) 351.084780, found 351.084376. The enantiomeric ratio was determined by HPLC analysis using Daicel Chiralcel OD-3 column: *n*Hept:*i*PrOH = 98:2, flow rate 1.0 mL/min, λ = 212 nm: τ_{major} = 5.34 min, τ_{minor} = 7.57 min. α_D^{25} = +33.88° (c = 0.75, THF).

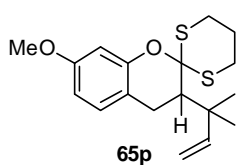
7. EXPERIMENTAL PART

(S)-8-tert-Butyl-3-phenylspiro[chroman-2,2'-[1,3]dithiane] (**65o**)



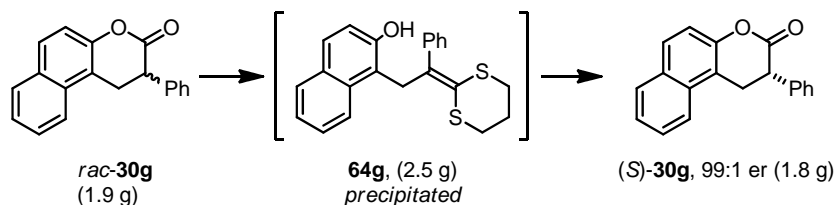
$^1\text{H NMR}$ (400 MHz, CDCl_3), δ = 1.51 (s, 9H), 1.89-2.04 (m, 1H), 2.13-2.23 (m, 1H), 2.61-2.75 (m, 2H), 3.26 (dd, J = 16.81, 7.34 Hz, 1H), 3.31-3.46 (m, 3H), 3.52 (t, J = 6.85 Hz, 1H), 6.87-6.95 (m, 1H), 6.96-7.00 (m, 1H), 7.14-7.19 (m, 4H), 7.21-7.27 (m, 3H), 7.18-7.36 (m, 3H) ppm, $^{13}\text{C NMR}$ (100 MHz, CDCl_3), δ = 24.50, 26.51, 26.73, 29.75, 30.27, 34.97, 48.42, 90.67, 120.93, 121.64, 125.08, 127.67, 127.77, 128.03, 129.17, 137.43, 139.25, 150.65 ppm, **HRMS (ESI+)**, m/z calculated for $\text{C}_{22}\text{H}_{26}\text{OS}_2\text{Na}$ ($\text{M}+\text{Na}^+$) 393.131727, found 393.131773. The enantiomeric ratio was determined by HPLC analysis using Daicel Chiralcel OD-3 column: $n\text{Hept}:i\text{PrOH}$ = 99:1, flow rate 1.0 mL/min, λ = 221 nm: τ_{major} = 3.76 min, τ_{minor} = 6.54 min. α_D^{25} = +8.60° (c = 1.00, THF).

7-Methoxy-3-(2-methylbut-3-en-2-yl)spiro[chroman-2,2'-[1,3]dithiane] (**65p**)



$^1\text{H NMR}$ (500 MHz, CDCl_3), δ = 1.23 (s, 3H), 1.40 (s, 3H), 1.53-1.60 (m, 1H), 1.78 (dddd, J = 16.13, 13.00, 8.12, 4.36 Hz, 1H), 2.08 (td, J = 13.74, 3.62 Hz, 1H), 2.29 (ddd, J = 11.79, 5.11, 3.26 Hz, 2H), 2.68 (dd, J = 16.37, 5.52 Hz, 1H), 2.90 (dd, J = 15.95, 11.80 Hz, 1H), 2.99-3.06 (m, 1H), 3.42 (s, 3H), 3.55 (dt, J = 13.38, 2.66 Hz, 1H), 5.03 (ddd, J = 10.63, 6.72, 5.59 Hz, 2H), 6.07 (dd, J = 17.65, 10.47 Hz, 1H), 6.53 (dd, J = 8.35, 2.54 Hz, 1H), 6.62 (d, J = 2.51 Hz, 1H), 6.83 (d, J = 8.36 Hz, 1H) ppm, **HRMS (ESI+)**, m/z calculated for $\text{C}_{18}\text{H}_{24}\text{O}_2\text{S}_2\text{Na}$ ($\text{M}+\text{Na}^+$) 359.110996, found 359.111233. The enantiomeric ratio was determined by HPLC analysis using Daicel Chiralcel AD-3 column: $n\text{Hept}:i\text{PrOH}$ = 99:1, flow rate 1.0 mL/min, λ = 221 nm: τ_{major} = 5.10 min, τ_{minor} = 5.55 min.

7.4.10. Gram-scale Deprotection and Application of Thioacetal-Protected Hydrocoumarin Products – Oxidative Hydrolysis

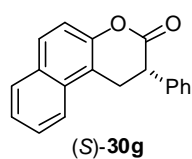


Procedure: *Ketene dithioacetal preparation:* To a stirred solution of 1,3-propanedithiol (1.1 equiv) in dichloromethane (30 mL) under argon, trimethylaluminium solution in hexane (2 M, 2.2 equiv) was added dropwise at 0 °C and the reaction mixture warmed to room temperature. After 30 min, a solution of hydrocoumarin **30** (6.9 mmol) in dichloromethane (30 mL) was added dropwisely at 0 °C. Then the reaction mixture was stirred under reflux for 16 hrs. When the starting material is completely consumed (check by TLC), the reaction mixture was cooled to room temperature and a few drops of triethylamine was added to avoid smell of the dithiol. The reaction mixture was evaporated under vacuo, diluted with diethylether (50 mL) and 10 % aq. NaHCO₃ (50 mL) and stirred vigorously for 15 min. Then the organic layer separated, dried over Na₂SO₄ and concentrated under reduced pressure at 25 °C. The obtained pale yellow jelly-like residue was dissolved in distilled diethylether (minimum amount, ca. 20 mL) in a round bottom flask (100 mL). The volume of the solvent was slowly reduced by blowing aron through a needle and pure thioketene acetal **64g** was precipitated out from the solution as a white solid (water has to be prevented). After filtration of the solid under aron atmosphere, **64g** was washed with ice-cold diethylether and dried under argon (98% yield) then used for asymmetric protonation without further purification.

Asymmetric protonation and deprotection of thioacetal: To a solution of **64g** (2.5 gram) in cyclohexane (90 mL), catalyst **56a** (26 mg, 0.5 mol%) was added and the solution was stirred for 48 hrs. After full conversion, ca. 60% of the solvent was evaporated under reduced pressure and the residue was dissolved in THF/H₂O (60/12 mL). Then NaHCO₃ (6.4 equiv) and iodine (3.4 equiv)¹⁰⁹ were added successively and the reaction mixture was stirred for 4 minutes, quenched with saturated aq. Na₂S₂O₃, extracted with MTBE and dried over Na₂SO₄. Then the volume of the solvent was slowly reduced under vacuo and ethanol was added to recrystallize the product (S)-**30g** at room temperature. Colorless crystals were formed, filtered and dried under the vacuo to afford (S)-**30g** with 99:1 er (99%).

7. EXPERIMENTAL PART

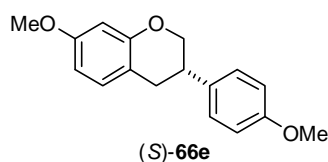
(S)-3,4-Dihydro-3-phenyl-5,6-benzocoumarin ((S)-**30g**)



The enantiomeric ratio was determined by reverse phase HPLC analysis using Daicel Chiralcel OJ-RH column: acetonitrile:water:MeOH (gradient), 0-3 min: acetonitrile:water = 30:70, 3-20 min: MeOH = 100%, flow rate 1.0 mL/min, $\lambda = 221$ nm: $\tau_{\text{major}} = 12.25$ min, $\tau_{\text{minor}} = 14.93$ min. $\alpha_D^{25} = +72.00^\circ$ ($c = 0.05$, THF).

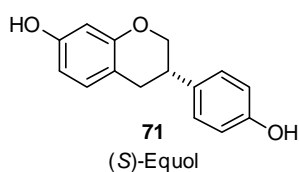
7.4.11. Application of Thioacetal-Protected Hydrocoumarin Products via Reductive Cleavage to the Synthesis of (S)-Equol

(S)-7-Methoxy-3-(4-methoxyphenyl)chroman ((S)-**66e**)



Cleavage of dithioacetal: To a round bottom flask equipped with stirring bar, dithioacetal protected hydrocoumarin **65e** was added and dried under vacuo and refilled with hydrogen gas. Under hydrogen atmosphere, acetone (0.03M) and Raney-Ni (Aldrich, H₂O slurry, 0.15mL for 0.1 mmol of **65e**) were added and stirred overnight. The reaction mixture was filtered through celite and purified by silica chromatography to give **66e** (67% yield). ¹H NMR (400 MHz, CDCl₃), $\delta = 2.88$ -3.01 (m, 2H), 3.12-3.23 (m, 1H), 3.77 (s, 3H), 3.81 (s, 3H), 3.98 (t, $J = 10.54$ Hz, 1H), 4.27-4.35 (m, 1H), 6.43 (d, $J = 2.54$ Hz, 1H), 6.48 (dd, $J = 8.35, 2.57$ Hz, 1H), 6.86-6.92 (m, 2H), 6.96-7.01 (m, 1H), 7.13-7.21 (m, 2H) ppm, ¹³C NMR (100 MHz, CDCl₃), $\delta = 31.52, 37.55, 54.94, 54.98, 70.78, 101.02, 106.93, 113.83, 125.14, 127.96, 129.82, 133.08, 154.66, 158.27, 158.81$ ppm, HRMS (ESI+), m/z calculated for C₁₇H₁₈O₃Na (M+Na⁺) 293.114811, found 293.114658.

(S)-Equol (**71**)



¹H NMR (500 MHz, DMSO-*d*₆), $\delta = 2.72$ -2.88 (m, 2H), 2.96-3.05 (m, 1H), 3.89 (t, $J = 10.46$ Hz, 1H), 4.14 (ddd, $J = 10.48, 3.48, 1.96$ Hz, 1H), 6.18 (d, $J = 2.31$ Hz, 1H), 6.28 (dd, $J = 8.19, 2.41$ Hz, 1H), 6.67-6.76 (m, 2H), 6.86 (d, $J = 8.15$ Hz, 1H), 7.10 (d, $J = 8.52$ Hz, 2H), 9.16 (s, 1H), 9.28 (s, 1H) ppm, ¹³C NMR (125 MHz, DMSO-*d*₆), $\delta = 31.26, 37.11, 70.21, 102.42, 107.92, 112.52, 115.20, 128.29, 130.04, 131.61, 154.46, 156.11, 156.45$ ppm, HRMS (ESI-), m/z calculated for C₁₅H₁₃O₃Na (M⁻) 241.087023, found 241.087214. $\alpha_D^{25} = -20.00^\circ$ ($c = 0.10$, EtOH).

7.5. X-ray Structure Analysis Parameters

7.5.1. X-ray Structure Analysis Parameters for 64g

X-ray Structure of ketene dithioacetal **64g**

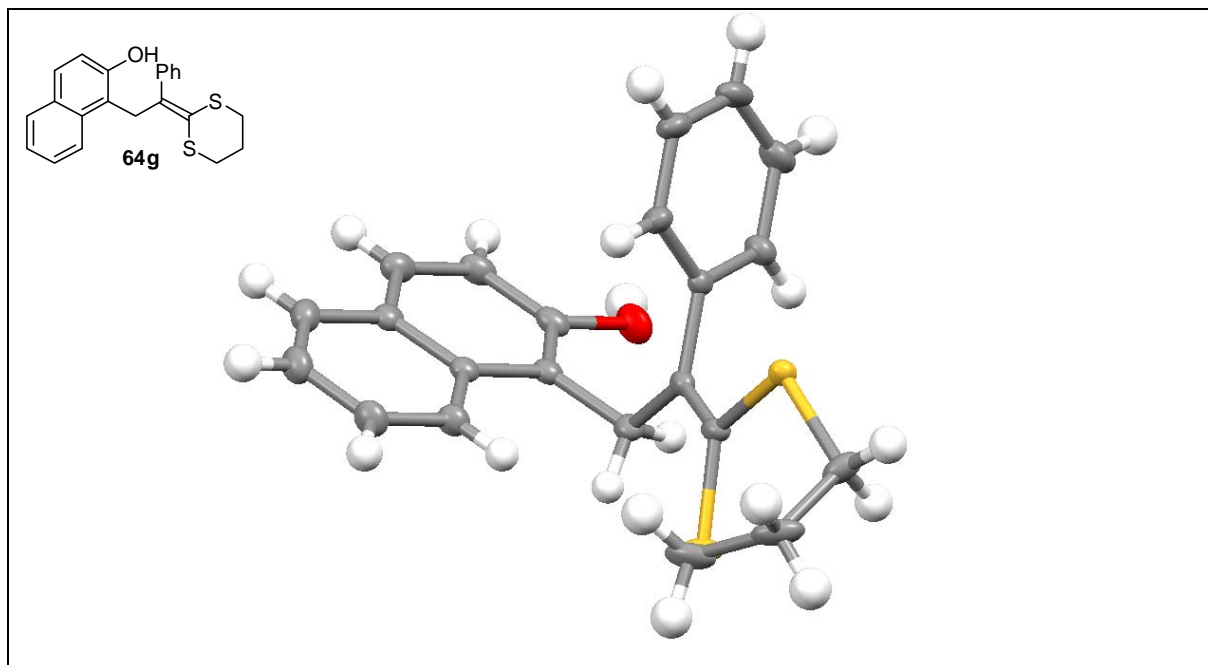


Table 7-1. Crystal data and structure refinement.

Identification code	7472	
Empirical formula	C ₂₂ H ₂₀ O ₂ S ₂	
Color	colourless	
Formula weight	364.50 g · mol ⁻¹	
Temperature	100 K	
Wavelength	0.71073 Å	
Crystal system	MONOCLINIC	
Space group	P2₁/n, (no. 14)	
Unit cell dimensions	a = 9.7476(4) Å	α = 90°.
	b = 15.9436(10) Å	β = 108.461(5)°.
	c = 12.1996(11) Å	γ = 90°.
Volume	1798.4(2) Å ³	
Z	4	
Density (calculated)	1.346 Mg · m ⁻³	
Absorption coefficient	0.303 mm ⁻¹	
F(000)	768 e	
Crystal size	0.24 x 0.15 x 0.10 mm ³	
θ range for data collection	2.67 to 33.11°.	

7. EXPERIMENTAL PART

Index ranges	-14 ≤ h ≤ 14, -24 ≤ k ≤ 24, -18 ≤ l ≤ 18	
Reflections collected	62063	
Independent reflections	6826 [R _{int} = 0.0442]	
Reflections with I > 2σ(I)	5464	
Completeness to θ = 33.11°	99.9 %	
Absorption correction	Gaussian	
Max. and min. transmission	0.97 and 0.95	
Refinement method	Full-matrix least-squares on F ²	
Data / restraints / parameters	6826 / 0 / 227	
Goodness-of-fit on F ²	1.081	
Final R indices [I > 2σ(I)]	R ₁ = 0.0394	wR ² = 0.0847
R indices (all data)	R ₁ = 0.0570	wR ² = 0.0921
Largest diff. peak and hole	0.427 and -0.313 e · Å ⁻³	

Table 7-2. Atomic coordinates and equivalent isotropic displacement parameters (Å²).
U_{eq} is defined as one third of the trace of the orthogonalized U_{ij} tensor.

	x	y	z	U _{eq}
S(1)	0.7810(1)	0.8849(1)	0.7413(1)	0.025(1)
S(2)	0.9650(1)	0.9459(1)	0.5994(1)	0.018(1)
O(1)	1.2234(1)	0.6262(1)	0.8726(1)	0.028(1)
C(1)	0.9229(1)	0.8648(1)	0.6840(1)	0.017(1)
C(2)	0.6576(1)	0.9409(1)	0.6195(1)	0.033(1)
C(3)	0.7120(2)	1.0272(1)	0.5982(1)	0.034(1)
C(4)	0.8764(2)	1.0351(1)	0.6398(1)	0.027(1)
C(5)	1.0026(1)	0.7943(1)	0.7065(1)	0.016(1)
C(6)	1.1259(1)	0.7834(1)	0.6601(1)	0.016(1)
C(7)	1.2680(1)	0.7863(1)	0.7343(1)	0.023(1)
C(8)	1.3832(1)	0.7763(1)	0.6911(1)	0.030(1)
C(9)	1.3577(2)	0.7626(1)	0.5741(1)	0.029(1)
C(10)	1.2172(2)	0.7587(1)	0.5000(1)	0.027(1)
C(11)	1.1014(1)	0.7693(1)	0.5427(1)	0.022(1)
C(12)	0.9785(1)	0.7242(1)	0.7825(1)	0.020(1)
C(13)	0.9908(1)	0.6375(1)	0.7363(1)	0.018(1)
C(14)	1.1141(1)	0.5902(1)	0.7846(1)	0.021(1)
C(15)	1.1289(1)	0.5086(1)	0.7451(1)	0.024(1)
C(16)	1.0196(1)	0.4748(1)	0.6562(1)	0.024(1)
C(17)	0.8902(1)	0.5203(1)	0.6030(1)	0.019(1)

C(18)	0.7763(1)	0.4850(1)	0.5114(1)	0.024(1)
C(19)	0.6519(2)	0.5293(1)	0.4623(1)	0.027(1)
C(20)	0.6356(1)	0.6101(1)	0.5032(1)	0.025(1)
C(21)	0.7448(1)	0.6469(1)	0.5901(1)	0.022(1)
C(22)	0.8766(1)	0.6025(1)	0.6436(1)	0.017(1)

Table 7-3. Bond lengths [Å] and angles [°].

C(1)-C(5)	1.3446(16)	C(1)-S(1)	1.7652(11)
C(1)-S(2)	1.7824(12)	C(2)-C(3)	1.526(2)
C(2)-S(1)	1.8216(14)	C(3)-C(4)	1.525(2)
C(4)-S(2)	1.8106(12)	C(5)-C(6)	1.4924(15)
C(5)-C(12)	1.5158(16)	C(6)-C(11)	1.3937(16)
C(6)-C(7)	1.3949(16)	C(7)-C(8)	1.3926(18)
C(8)-C(9)	1.387(2)	C(9)-C(10)	1.383(2)
C(10)-C(11)	1.3952(17)	C(12)-C(13)	1.5126(17)
C(13)-C(14)	1.3824(16)	C(13)-C(22)	1.4257(16)
C(14)-O(1)	1.3758(15)	C(14)-C(15)	1.4108(19)
C(15)-C(16)	1.3680(19)	C(16)-C(17)	1.4207(17)
C(17)-C(18)	1.4184(17)	C(17)-C(22)	1.4218(16)
C(18)-C(19)	1.3668(19)	C(19)-C(20)	1.409(2)
C(20)-C(21)	1.3739(17)	C(21)-C(22)	1.4306(16)
C(5)-C(1)-S(1)	123.08(9)	C(5)-C(1)-S(2)	120.06(8)
S(1)-C(1)-S(2)	116.77(6)	C(3)-C(2)-S(1)	113.94(10)
C(4)-C(3)-C(2)	113.80(11)	C(3)-C(4)-S(2)	112.70(10)
C(1)-C(5)-C(6)	120.19(10)	C(1)-C(5)-C(12)	123.29(10)
C(6)-C(5)-C(12)	116.47(10)	C(11)-C(6)-C(7)	119.01(11)
C(11)-C(6)-C(5)	120.81(10)	C(7)-C(6)-C(5)	120.18(10)
C(8)-C(7)-C(6)	120.25(12)	C(9)-C(8)-C(7)	120.33(12)
C(10)-C(9)-C(8)	119.84(12)	C(9)-C(10)-C(11)	120.09(12)

7. EXPERIMENTAL PART

C(6)-C(11)-C(10)	120.48(12)	C(13)-C(12)-C(5)	113.59(9)
C(14)-C(13)-C(22)	118.66(11)	C(14)-C(13)-C(12)	120.05(11)
C(22)-C(13)-C(12)	121.29(10)	O(1)-C(14)-C(13)	117.33(11)
O(1)-C(14)-C(15)	120.90(11)	C(13)-C(14)-C(15)	121.77(11)
C(16)-C(15)-C(14)	119.73(11)	C(15)-C(16)-C(17)	121.12(12)
C(18)-C(17)-C(16)	121.17(11)	C(18)-C(17)-C(22)	120.23(11)
C(16)-C(17)-C(22)	118.60(11)	C(19)-C(18)-C(17)	120.34(12)
C(18)-C(19)-C(20)	120.08(12)	C(21)-C(20)-C(19)	121.15(12)
C(20)-C(21)-C(22)	120.31(12)	C(17)-C(22)-C(13)	120.11(10)
C(17)-C(22)-C(21)	117.86(11)	C(13)-C(22)-C(21)	122.03(11)
C(1)-S(1)-C(2)	99.44(6)	C(1)-S(2)-C(4)	101.27(6)

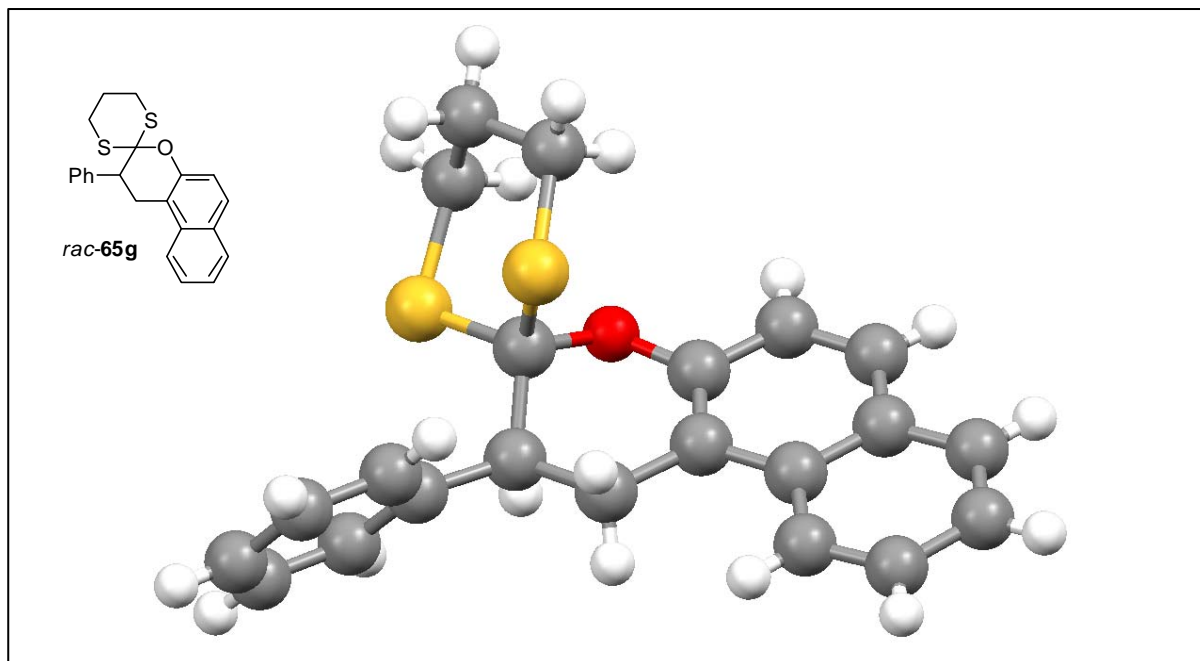
Table 7-4. Anisotropic displacement parameters (\AA^2).

The anisotropic displacement factor exponent takes the form:

$$-2\pi^2 [h^2 a^{*2} U_{11} + \dots + 2 h k a^* b^* U_{12}]$$

	U11	U22	U33	U23	U13	U12
S(1)	0.020(1)	0.038(1)	0.019(1)	0.005(1)	0.011(1)	0.009(1)
S(2)	0.015(1)	0.017(1)	0.021(1)	0.000(1)	0.007(1)	0.002(1)
O(1)	0.020(1)	0.034(1)	0.024(1)	0.008(1)	-0.001(1)	-0.001(1)
C(1)	0.014(1)	0.023(1)	0.015(1)	0.000(1)	0.005(1)	0.001(1)
C(2)	0.018(1)	0.058(1)	0.025(1)	0.010(1)	0.010(1)	0.015(1)
C(3)	0.034(1)	0.047(1)	0.027(1)	0.011(1)	0.017(1)	0.025(1)
C(4)	0.036(1)	0.023(1)	0.023(1)	-0.001(1)	0.010(1)	0.012(1)
C(5)	0.015(1)	0.019(1)	0.014(1)	-0.002(1)	0.004(1)	-0.002(1)
C(6)	0.017(1)	0.013(1)	0.021(1)	0.000(1)	0.008(1)	0.000(1)
C(7)	0.017(1)	0.027(1)	0.025(1)	0.001(1)	0.007(1)	-0.001(1)
C(8)	0.018(1)	0.033(1)	0.040(1)	0.002(1)	0.010(1)	0.000(1)
C(9)	0.028(1)	0.024(1)	0.044(1)	0.001(1)	0.023(1)	0.004(1)
C(10)	0.033(1)	0.025(1)	0.030(1)	-0.005(1)	0.019(1)	0.002(1)
C(11)	0.022(1)	0.023(1)	0.023(1)	-0.005(1)	0.009(1)	0.001(1)

C(12)	0.022(1)	0.023(1)	0.016(1)	0.001(1)	0.008(1)	-0.001(1)
C(13)	0.016(1)	0.021(1)	0.016(1)	0.004(1)	0.007(1)	0.000(1)
C(14)	0.016(1)	0.026(1)	0.019(1)	0.008(1)	0.006(1)	0.000(1)
C(15)	0.019(1)	0.026(1)	0.028(1)	0.010(1)	0.009(1)	0.005(1)
C(16)	0.026(1)	0.020(1)	0.029(1)	0.006(1)	0.013(1)	0.004(1)
C(17)	0.021(1)	0.019(1)	0.019(1)	0.004(1)	0.010(1)	0.000(1)
C(18)	0.030(1)	0.022(1)	0.023(1)	0.000(1)	0.010(1)	-0.004(1)
C(19)	0.026(1)	0.031(1)	0.023(1)	0.000(1)	0.003(1)	-0.006(1)
C(20)	0.020(1)	0.027(1)	0.025(1)	0.005(1)	0.002(1)	0.002(1)
C(21)	0.019(1)	0.023(1)	0.022(1)	0.004(1)	0.004(1)	0.002(1)
C(22)	0.017(1)	0.019(1)	0.016(1)	0.004(1)	0.007(1)	0.000(1)

7.5.2. X-ray Structure Analysis Parameters for *rac*-65g**Table 7-5.** Crystal data and structure refinement.

Identification code	7392
Empirical formula	C ₂₂ H ₂₀ O S ₂
Color	colourless
Formula weight	364.50 g • mol ⁻¹
Temperature	150 K
Wavelength	1.54178 Å
Crystal system	TRICLINIC
Space group	P ⁻ 1, (no. 2)
Unit cell dimensions	a = 8.437(6) Å α = 86.568(14)°. b = 9.321(7) Å β = 71.428(15)°. c = 12.345(9) Å γ = 78.708(15)°.
Volume	902.4(11) Å ³
Z	2
Density (calculated)	1.341 Mg • m ⁻³
Absorption coefficient	2.711 mm ⁻¹
F(000)	384 e
Crystal size	0.26 x 0.12 x 0.12 mm ³
θ range for data collection	3.78 to 67.14°.
Index ranges	-9 ≤ h ≤ 9, -11 ≤ k ≤ 11, -14 ≤ l ≤ 14

Reflections collected 38515
 Independent reflections 3092 [Rint = 0.0532]
 Reflections with $I > 2\sigma(I)$ 2920
 Completeness to $\theta = 67.14^\circ$ 96.2 %
 Absorption correction Gaussian
 Max. and min. transmission 0.77 and 0.57
 Refinement method Full-matrix least-squares on F2
 Data / restraints / parameters 3092 / 0 / 226
 Goodness-of-fit on F2 1.041
 Final R indices [$I > 2\sigma(I)$] R1 = 0.0338 wR2 = 0.0943
 R indices (all data) R1 = 0.0352 wR2 = 0.0953
 Largest diff. peak and hole 0.321 and -0.225 e \cdot Å⁻³

Table 7-6. Atomic coordinates and equivalent isotropic displacement parameters (Å²).

U_{eq} is defined as one third of the trace of the orthogonalized U_{ij} tensor.

	x	y	z	U_{eq}
C(1)	0.7633(2)	0.7588(2)	0.7086(1)	0.027(1)
C(2)	0.8013(2)	0.8417(2)	0.5173(1)	0.028(1)
C(3)	0.9232(2)	0.8757(2)	0.4150(2)	0.033(1)
C(4)	0.8931(2)	0.8702(2)	0.3140(2)	0.036(1)
C(5)	0.7429(2)	0.8285(2)	0.3090(2)	0.032(1)
C(6)	0.7151(3)	0.8114(2)	0.2035(2)	0.040(1)
C(7)	0.5696(3)	0.7715(2)	0.2003(2)	0.042(1)
C(8)	0.4438(3)	0.7477(2)	0.3021(2)	0.041(1)
C(9)	0.4667(2)	0.7614(2)	0.4059(2)	0.036(1)
C(10)	0.6175(2)	0.8007(2)	0.4127(1)	0.029(1)
C(11)	0.6489(2)	0.8092(2)	0.5190(1)	0.028(1)
C(12)	0.5205(2)	0.7783(2)	0.6304(1)	0.030(1)
C(13)	0.5703(2)	0.8112(2)	0.7342(1)	0.028(1)
C(14)	0.4588(2)	0.7586(2)	0.8463(1)	0.028(1)
C(15)	0.4250(2)	0.6164(2)	0.8624(2)	0.032(1)
C(16)	0.3170(2)	0.5758(2)	0.9652(2)	0.038(1)
C(17)	0.2415(2)	0.6750(2)	1.0536(2)	0.040(1)
C(18)	0.2760(3)	0.8158(2)	1.0394(2)	0.042(1)
C(19)	0.3837(2)	0.8564(2)	0.9366(2)	0.035(1)
C(20)	1.0546(2)	0.7412(2)	0.7719(2)	0.038(1)
C(21)	1.1109(2)	0.5807(2)	0.7372(2)	0.040(1)
C(22)	1.0555(2)	0.5449(2)	0.6385(2)	0.036(1)

7. EXPERIMENTAL PART

O(1)	0.8486(1)	0.8436(1)	0.6144(1)	0.030(1)
S(1)	0.8252(1)	0.8001(1)	0.8292(1)	0.034(1)
S(2)	0.8269(1)	0.5637(1)	0.6720(1)	0.030(1)

Table 7-7. Bond lengths [Å] and angles [°].

C(1)-O(1)	1.441(2)	C(1)-C(13)	1.539(3)	C(1)-S(1)	1.811(2)
C(1)-S(2)	1.834(2)	C(2)-C(11)	1.371(3)	C(2)-O(1)	1.380(2)
C(2)-C(3)	1.416(2)	C(3)-C(4)	1.355(3)	C(4)-C(5)	1.416(3)
C(5)-C(6)	1.418(3)	C(5)-C(10)	1.425(3)	C(6)-C(7)	1.363(3)
C(7)-C(8)	1.402(3)	C(8)-C(9)	1.373(3)	C(9)-C(10)	1.418(3)
C(10)-C(11)	1.429(3)	C(11)-C(12)	1.508(2)	C(12)-C(13)	1.534(3)
C(13)-C(14)	1.520(2)	C(14)-C(19)	1.387(3)	C(14)-C(15)	1.399(3)
C(15)-C(16)	1.387(3)	C(16)-C(17)	1.379(3)	C(17)-C(18)	1.388(3)
C(18)-C(19)	1.386(3)	C(20)-C(21)	1.522(3)	C(20)-S(1)	1.818(2)
C(21)-C(22)	1.512(3)	C(22)-S(2)	1.814(2)		
O(1)-C(1)-C(13)	107.88(13)	O(1)-C(1)-S(1)	106.15(11)	C(13)-C(1)-S(1)	109.57(12)
O(1)-C(1)-S(2)	109.80(11)	C(13)-C(1)-S(2)	111.47(11)	S(1)-C(1)-S(2)	111.76(9)
C(11)-C(2)-O(1)	123.03(15)	C(11)-C(2)-C(3)	122.33(17)	O(1)-C(2)-C(3)	114.64(16)
C(4)-C(3)-C(2)	119.47(17)	C(3)-C(4)-C(5)	121.03(16)	C(4)-C(5)-C(6)	121.81(17)
C(4)-C(5)-C(10)	119.13(17)	C(6)-C(5)-C(10)	119.06(18)	C(7)-C(6)-C(5)	121.01(18)
C(6)-C(7)-C(8)	120.20(18)	C(9)-C(8)-C(7)	120.57(19)	C(8)-C(9)-C(10)	120.87(18)
C(9)-C(10)-C(5)	118.26(17)	C(9)-C(10)-C(11)	122.30(16)	C(5)-C(10)-C(11)	119.42(17)
C(2)-C(11)-C(10)	118.44(15)	C(2)-C(11)-C(12)	120.53(16)	C(10)-C(11)-C(12)	121.00(16)
C(11)-C(12)-C(13)	112.20(15)	C(14)-C(13)-C(12)	113.20(14)	C(14)-C(13)-C(1)	115.69(14)
C(12)-C(13)-C(1)	108.93(14)	C(19)-C(14)-C(15)	118.00(16)	C(19)-C(14)-C(13)	118.77(15)
C(15)-C(14)-C(13)	123.22(15)	C(16)-C(15)-C(14)	120.79(16)	C(17)-C(16)-C(15)	120.45(17)
C(16)-C(17)-C(18)	119.37(17)	C(19)-C(18)-C(17)	120.17(18)	C(18)-C(19)-C(14)	121.21(17)
C(21)-C(20)-S(1)	114.14(13)	C(22)-C(21)-C(20)	113.09(16)	C(21)-C(22)-S(2)	113.99(14)
C(2)-O(1)-C(1)	115.17(13)	C(1)-S(1)-C(20)	99.99(9)	C(22)-S(2)-C(1)	99.29(8)

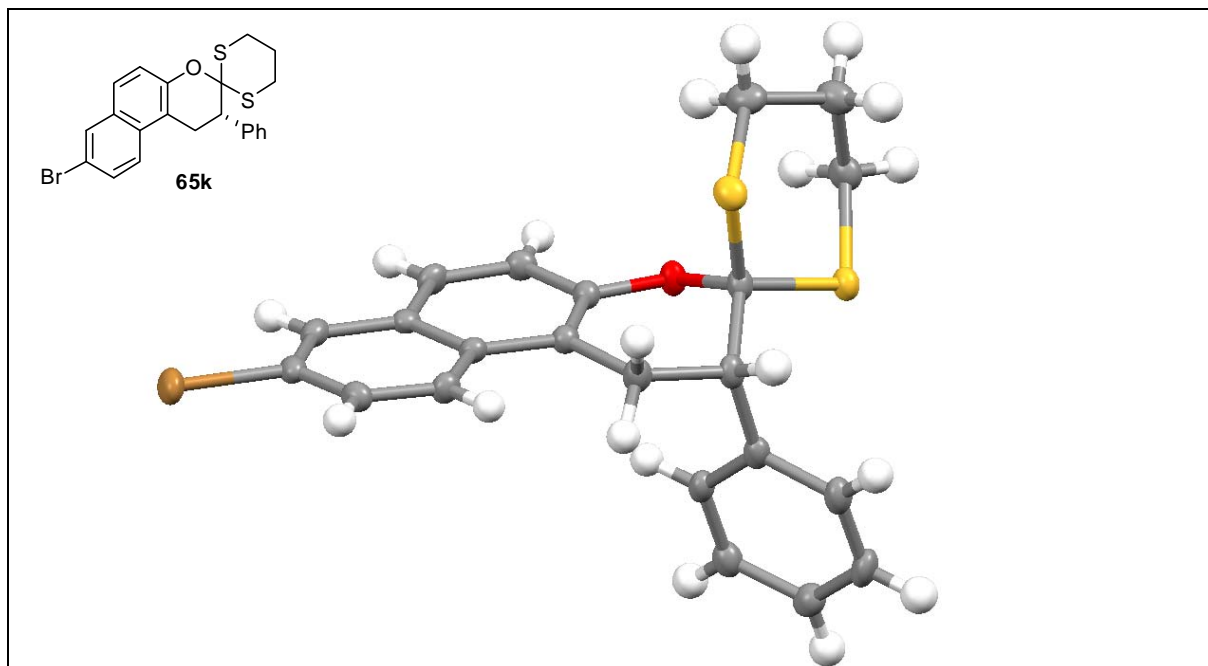
Table 7-8. Anisotropic displacement parameters (\AA^2).

The anisotropic displacement factor exponent takes the form:

$$-2\pi^2 [h^2 a^* 2U_{11} + \dots + 2 h k a^* b^* U_{12}].$$

C(1)	0.025(1)	0.025(1)	0.031(1)	0.001(1)	-0.007(1)
C(2)	0.027(1)	0.022(1)	0.033(1)	0.000(1)	-0.007(1)
C(3)	0.026(1)	0.030(1)	0.040(1)	-0.001(1)	-0.001(1)
C(4)	0.035(1)	0.031(1)	0.033(1)	0.002(1)	0.001(1)
C(5)	0.034(1)	0.024(1)	0.033(1)	0.001(1)	-0.006(1)
C(6)	0.047(1)	0.033(1)	0.032(1)	0.001(1)	-0.008(1)
C(7)	0.055(1)	0.034(1)	0.038(1)	-0.002(1)	-0.022(1)
C(8)	0.045(1)	0.036(1)	0.047(1)	0.001(1)	-0.023(1)
C(9)	0.036(1)	0.035(1)	0.038(1)	0.003(1)	-0.013(1)
C(10)	0.030(1)	0.022(1)	0.033(1)	0.001(1)	-0.009(1)
C(11)	0.025(1)	0.023(1)	0.032(1)	0.001(1)	-0.006(1)
C(12)	0.022(1)	0.035(1)	0.032(1)	0.003(1)	-0.007(1)
C(13)	0.024(1)	0.027(1)	0.033(1)	0.002(1)	-0.006(1)
C(14)	0.020(1)	0.031(1)	0.031(1)	0.003(1)	-0.008(1)
C(15)	0.026(1)	0.032(1)	0.034(1)	-0.001(1)	-0.007(1)
C(16)	0.034(1)	0.035(1)	0.044(1)	0.010(1)	-0.013(1)
C(17)	0.035(1)	0.048(1)	0.031(1)	0.008(1)	-0.003(1)
C(18)	0.041(1)	0.045(1)	0.032(1)	-0.003(1)	-0.002(1)
C(19)	0.033(1)	0.032(1)	0.036(1)	0.001(1)	-0.007(1)
C(20)	0.029(1)	0.039(1)	0.050(1)	-0.002(1)	-0.017(1)
C(21)	0.028(1)	0.038(1)	0.057(1)	0.000(1)	-0.017(1)
C(22)	0.026(1)	0.031(1)	0.049(1)	-0.004(1)	-0.009(1)
O(1)	0.025(1)	0.030(1)	0.034(1)	0.001(1)	-0.007(1)
S(1)	0.030(1)	0.037(1)	0.037(1)	-0.006(1)	-0.012(1)

7.5.3. X-ray Structure Analysis Parameters for 65k

**Table 7-9.** Crystal data and structure refinement.

Identification code	7448	
Empirical formula	$C_{22}H_{19}BrOS_2$	
Color	colorless	
Formula weight	$443.40 \text{ g} \cdot \text{mol}^{-1}$	
Temperature	130 K	
Wavelength	1.54184 \AA	
Crystal system	ORTHORHOMBIC	
Space group	$P2_1 2_1 2_1$, (no. 19)	
Unit cell dimensions	$a = 5.8076(4) \text{ \AA}$	$\alpha = 90^\circ$.
	$b = 9.5688(6) \text{ \AA}$	$\beta = 90^\circ$.
	$c = 34.268(2) \text{ \AA}$	$\gamma = 90^\circ$.
Volume	$1904.3(2) \text{ \AA}^3$	
Z	4	
Density (calculated)	$1.547 \text{ Mg} \cdot \text{m}^{-3}$	
Absorption coefficient	5.048 mm^{-1}	
F(000)	904 e	
Crystal size	$0.19 \times 0.15 \times 0.11 \text{ mm}^3$	
θ range for data collection	2.58 to 67.10° .	
Index ranges	$-6 \leq h \leq 6$, $-11 \leq k \leq 11$, $-37 \leq l \leq 40$	
Reflections collected	82904	

Independent reflections	3382 [$R_{\text{int}} = 0.0428$]	
Reflections with $I > 2\sigma(I)$	3376	
Completeness to $\theta = 67.10^\circ$	99.7 %	
Absorption correction	Gaussian	
Max. and min. transmission	0.62 and 0.36	
Refinement method	Full-matrix least-squares on F^2	
Data / restraints / parameters	3382 / 0 / 239	
Goodness-of-fit on F^2	1.115	
Final R indices [$I > 2\sigma(I)$]	$R_1 = 0.0188$	$wR^2 = 0.0477$
R indices (all data)	$R_1 = 0.0189$	$wR^2 = 0.0477$
Absolute structure parameter	-0.009(12)	
Largest diff. peak and hole	0.229 and -0.229 $e \cdot \text{\AA}^{-3}$	

Table 7-10. Atomic coordinates and equivalent isotropic displacement parameters (\AA^2).

U_{eq} is defined as one third of the trace of the orthogonalized U_{ij} tensor.

	x	y	z	U_{eq}
Br(1)	0.4750(1)	0.6677(1)	0.5854(1)	0.028(1)
S(1)	0.7172(1)	0.2377(1)	0.3025(1)	0.023(1)
S(2)	0.3571(1)	0.1814(1)	0.3645(1)	0.025(1)
O(1)	0.7863(2)	0.2822(1)	0.3764(1)	0.021(1)
C(1)	0.5988(3)	0.2907(2)	0.3492(1)	0.020(1)
C(2)	0.7523(3)	0.3429(2)	0.4124(1)	0.019(1)
C(3)	0.9101(3)	0.3011(2)	0.4414(1)	0.022(1)
C(4)	0.8951(3)	0.3563(2)	0.4782(1)	0.022(1)
C(5)	0.7174(3)	0.4526(2)	0.4877(1)	0.019(1)
C(6)	0.6935(3)	0.5065(2)	0.5261(1)	0.022(1)
C(7)	0.5140(4)	0.5931(2)	0.5342(1)	0.022(1)
C(8)	0.3514(4)	0.6326(2)	0.5061(1)	0.023(1)
C(9)	0.3755(3)	0.5840(2)	0.4685(1)	0.021(1)
C(10)	0.5589(3)	0.4935(2)	0.4582(1)	0.018(1)
C(11)	0.5827(3)	0.4404(2)	0.4193(1)	0.020(1)
C(12)	0.4278(3)	0.4900(2)	0.3869(1)	0.023(1)

7. EXPERIMENTAL PART

C(13)	0.5053(3)	0.4410(2)	0.3458(1)	0.021(1)
C(14)	0.7888(4)	0.0564(2)	0.3122(1)	0.027(1)
C(15)	0.5875(4)	-0.0335(2)	0.3255(1)	0.032(1)
C(16)	0.4946(4)	0.0114(2)	0.3649(1)	0.032(1)
C(17)	0.6739(4)	0.5382(2)	0.3256(1)	0.022(1)
C(18)	0.8740(4)	0.5858(2)	0.3439(1)	0.022(1)
C(19)	1.0287(4)	0.6712(2)	0.3243(1)	0.026(1)
C(20)	0.9857(4)	0.7109(2)	0.2859(1)	0.026(1)
C(21)	0.7875(4)	0.6656(2)	0.2676(1)	0.028(1)
C(22)	0.6322(4)	0.5812(2)	0.2872(1)	0.026(1)

Table 7-11. Bond lengths [Å] and angles [°].

Br(1)-C(7)	1.9073(18)	S(1)-C(1)	1.8132(19)
S(1)-C(14)	1.814(2)	S(2)-C(1)	1.827(2)
S(2)-C(16)	1.812(2)	O(1)-C(1)	1.436(2)
O(1)-C(2)	1.379(2)	C(1)-C(13)	1.541(3)
C(2)-C(3)	1.409(3)	C(2)-C(11)	1.378(3)
C(3)-C(4)	1.369(3)	C(4)-C(5)	1.421(3)
C(5)-C(6)	1.420(3)	C(5)-C(10)	1.423(3)
C(6)-C(7)	1.361(3)	C(7)-C(8)	1.401(3)
C(8)-C(9)	1.377(3)	C(9)-C(10)	1.417(3)
C(10)-C(11)	1.432(3)	C(11)-C(12)	1.506(3)
C(12)-C(13)	1.552(2)	C(13)-C(17)	1.516(3)
C(14)-C(15)	1.521(3)	C(15)-C(16)	1.515(3)
C(17)-C(18)	1.397(3)	C(17)-C(22)	1.400(3)
C(18)-C(19)	1.387(3)	C(19)-C(20)	1.393(3)
C(20)-C(21)	1.380(3)	C(21)-C(22)	1.385(3)
C(1)-S(1)-C(14)	101.22(9)	C(16)-S(2)-C(1)	100.20(10)
C(2)-O(1)-C(1)	116.67(14)	S(1)-C(1)-S(2)	112.60(10)
O(1)-C(1)-S(1)	105.59(12)	O(1)-C(1)-S(2)	111.35(12)
O(1)-C(1)-C(13)	111.71(15)	C(13)-C(1)-S(1)	109.08(13)

C(13)-C(1)-S(2)	106.58(13)	O(1)-C(2)-C(3)	114.76(16)
C(11)-C(2)-O(1)	122.71(16)	C(11)-C(2)-C(3)	122.49(17)
C(4)-C(3)-C(2)	119.87(17)	C(3)-C(4)-C(5)	120.46(17)
C(4)-C(5)-C(10)	119.05(17)	C(6)-C(5)-C(4)	121.24(17)
C(6)-C(5)-C(10)	119.70(18)	C(7)-C(6)-C(5)	119.07(18)
C(6)-C(7)-Br(1)	120.46(15)	C(6)-C(7)-C(8)	122.66(17)

Table 7-12. Anisotropic displacement parameters (\AA^2).

The anisotropic displacement factor exponent takes the form:

$$-2\pi^2 [h^2 a^{*2} U_{11} + \dots + 2 h k a^* b^* U_{12}].$$

	U_{11}	U_{22}	U_{33}	U_{23}	U_{13}	U_{12}
Br(1)	0.032(1)	0.034(1)	0.017(1)	-0.003(1)	0.004(1)	-0.002(1)
S(1)	0.023(1)	0.026(1)	0.019(1)	-0.004(1)	0.002(1)	0.003(1)
S(2)	0.018(1)	0.029(1)	0.029(1)	-0.003(1)	0.004(1)	0.001(1)
O(1)	0.018(1)	0.027(1)	0.019(1)	-0.004(1)	-0.002(1)	0.007(1)
C(1)	0.017(1)	0.026(1)	0.018(1)	-0.003(1)	-0.002(1)	0.002(1)
C(2)	0.018(1)	0.020(1)	0.018(1)	-0.001(1)	0.001(1)	0.001(1)
C(3)	0.018(1)	0.022(1)	0.025(1)	0.001(1)	0.001(1)	0.004(1)
C(4)	0.019(1)	0.025(1)	0.022(1)	0.005(1)	-0.004(1)	0.004(1)
C(5)	0.020(1)	0.017(1)	0.021(1)	0.002(1)	0.000(1)	-0.002(1)
C(6)	0.023(1)	0.023(1)	0.019(1)	0.004(1)	-0.002(1)	-0.003(1)
C(7)	0.028(1)	0.022(1)	0.018(1)	0.000(1)	0.003(1)	-0.005(1)
C(8)	0.022(1)	0.021(1)	0.024(1)	-0.003(1)	0.005(1)	0.002(1)
C(9)	0.020(1)	0.024(1)	0.020(1)	0.002(1)	-0.001(1)	0.005(1)
C(10)	0.018(1)	0.017(1)	0.019(1)	0.002(1)	0.001(1)	0.001(1)
C(11)	0.019(1)	0.020(1)	0.019(1)	0.000(1)	0.000(1)	0.001(1)
C(12)	0.021(1)	0.026(1)	0.021(1)	-0.001(1)	-0.002(1)	0.008(1)
C(13)	0.019(1)	0.027(1)	0.018(1)	-0.003(1)	-0.004(1)	0.005(1)
C(14)	0.026(1)	0.028(1)	0.029(1)	-0.005(1)	0.003(1)	0.006(1)
C(15)	0.031(1)	0.027(1)	0.039(1)	-0.003(1)	0.007(1)	0.001(1)
C(16)	0.028(1)	0.029(1)	0.040(1)	0.004(1)	0.010(1)	0.000(1)
C(17)	0.024(1)	0.022(1)	0.019(1)	-0.002(1)	-0.001(1)	0.008(1)
C(18)	0.026(1)	0.024(1)	0.017(1)	0.000(1)	-0.003(1)	0.005(1)
C(19)	0.024(1)	0.028(1)	0.025(1)	-0.005(1)	-0.002(1)	0.006(1)
C(20)	0.027(1)	0.027(1)	0.025(1)	0.001(1)	0.006(1)	0.005(1)
C(21)	0.034(1)	0.035(1)	0.016(1)	0.002(1)	-0.001(1)	0.008(1)
C(22)	0.026(1)	0.031(1)	0.020(1)	-0.003(1)	-0.004(1)	0.008(1)

7.5.4. X-ray Structure Analysis Parameters for (S)-30g

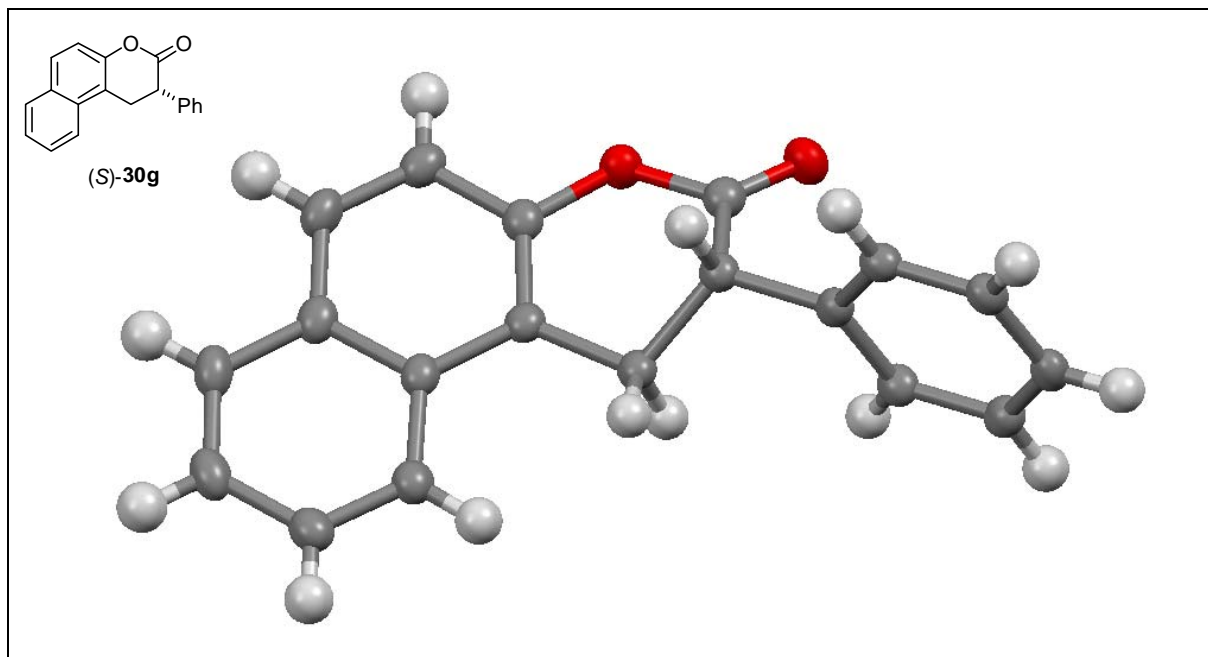


Table 7-13. Crystal data and structure refinement.

Identification code	7617	
Empirical formula	$C_{19}H_{14}O_2$	
Color	colourless	
Formula weight	$274.30 \text{ g} \cdot \text{mol}^{-1}$	
Temperature	100 K	
Wavelength	1.54184 \AA	
Crystal system	MONOCLINIC	
Space group	$P2_1$, (no. 4)	
Unit cell dimensions	$a = 8.0149(2) \text{ \AA}$	$\alpha = 90^\circ$.
	$b = 5.5448(2) \text{ \AA}$	$\beta = 91.373(2)^\circ$.
	$c = 14.9950(4) \text{ \AA}$	$\gamma = 90^\circ$.
Volume	$666.20(3) \text{ \AA}^3$	
Z	2	
Density (calculated)	$1.367 \text{ Mg} \cdot \text{m}^{-3}$	
Absorption coefficient	0.698 mm^{-1}	
F(000)	288 e	
Crystal size	$0.70 \times 0.14 \times 0.03 \text{ mm}^3$	

θ range for data collection	2.95 to 66.88°.	
Index ranges	-9 ≤ h ≤ 9, -6 ≤ k ≤ 6, -17 ≤ l ≤ 17	
Reflections collected	28189	
Independent reflections	2260 [$R_{\text{int}} = 0.0774$]	
Reflections with $I > 2\sigma(I)$	2066	
Completeness to $\theta = 66.88^\circ$	98.6 %	
Absorption correction	Gaussian	
Max. and min. transmission	0.98 and 0.75	
Refinement method	Full-matrix least-squares on F^2	
Data / restraints / parameters	2260 / 1 / 191	
Goodness-of-fit on F^2	1.029	
Final R indices [$I > 2\sigma(I)$]	$R_1 = 0.0387$	$wR^2 = 0.0917$
R indices (all data)	$R_1 = 0.0444$	$wR^2 = 0.0962$
Absolute structure parameter	0.6(3)	
Extinction coefficient	0.0149(18)	
Largest diff. peak and hole	0.157 and -0.164 e · Å ⁻³	

Table 7-14. Atomic coordinates and equivalent isotropic displacement parameters (Å²).

U_{eq} is defined as one third of the trace of the orthogonalized U_{ij} tensor.

	x	y	z	U_{eq}
C(1)	-0.0494(2)	-0.5835(4)	-0.7082(1)	0.026(1)
C(2)	-0.1811(2)	-0.4705(4)	-0.6510(1)	0.024(1)
C(3)	-0.3322(2)	-0.4001(4)	-0.7110(1)	0.025(1)
C(4)	-0.2743(2)	-0.2382(4)	-0.7843(1)	0.024(1)
C(5)	-0.1140(2)	-0.2653(4)	-0.8130(1)	0.025(1)
C(6)	-0.0438(2)	-0.1136(4)	-0.8769(1)	0.029(1)
C(7)	-0.1358(3)	0.0702(4)	-0.9125(1)	0.031(1)
C(8)	-0.3036(3)	0.1068(4)	-0.8876(1)	0.027(1)
C(9)	-0.4025(3)	0.2960(4)	-0.9242(1)	0.032(1)
C(10)	-0.5638(3)	0.3292(4)	-0.8988(1)	0.033(1)
C(11)	-0.6338(3)	0.1744(4)	-0.8360(1)	0.031(1)
C(12)	-0.5425(2)	-0.0104(4)	-0.7993(1)	0.028(1)
C(13)	-0.3736(2)	-0.0502(4)	-0.8227(1)	0.025(1)
C(14)	-0.2218(2)	-0.6279(4)	-0.5723(1)	0.024(1)
C(15)	-0.1699(2)	-0.5612(4)	-0.4865(1)	0.025(1)
C(16)	-0.2065(2)	-0.7056(4)	-0.4139(1)	0.026(1)
C(17)	-0.2934(2)	-0.9196(4)	-0.4263(1)	0.027(1)

7. EXPERIMENTAL PART

C(18)	-0.3471(2)	-0.9868(4)	-0.5116(1)	0.028(1)
C(19)	-0.3113(2)	-0.8419(4)	-0.5838(1)	0.026(1)
O(1)	-0.0117(2)	-0.4545(3)	-0.7838(1)	0.028(1)
O(2)	0.0271(2)	-0.7638(3)	-0.6937(1)	0.031(1)

Table 7-15. Bond lengths [Å] and angles [°].

C(1)-C(2)	1.512(3)	C(1)-O(1)	1.380(2)
C(1)-O(2)	1.190(3)	C(2)-C(3)	1.542(3)
C(2)-C(14)	1.510(3)	C(3)-C(4)	1.502(3)
C(4)-C(5)	1.373(3)	C(4)-C(13)	1.424(3)
C(5)-C(6)	1.402(3)	C(5)-O(1)	1.395(3)
C(6)-C(7)	1.359(3)	C(7)-C(8)	1.419(3)
C(8)-C(9)	1.417(3)	C(8)-C(13)	1.430(3)
C(9)-C(10)	1.369(3)	C(10)-C(11)	1.401(3)
C(11)-C(12)	1.367(3)	C(12)-C(13)	1.425(3)
C(14)-C(15)	1.393(3)	C(14)-C(19)	1.395(3)
C(15)-C(16)	1.388(3)	C(16)-C(17)	1.386(3)
C(17)-C(18)	1.390(3)	C(18)-C(19)	1.385(3)
O(1)-C(1)-C(2)	114.89(17)	O(2)-C(1)-C(2)	127.46(18)
O(2)-C(1)-O(1)	117.61(17)	C(1)-C(2)-C(3)	108.87(15)
C(14)-C(2)-C(1)	111.77(17)	C(14)-C(2)-C(3)	114.90(15)
C(4)-C(3)-C(2)	109.02(15)	C(5)-C(4)-C(3)	118.18(18)
C(5)-C(4)-C(13)	118.12(18)	C(13)-C(4)-C(3)	123.63(17)
C(4)-C(5)-C(6)	122.82(19)	C(4)-C(5)-O(1)	122.06(18)
O(1)-C(5)-C(6)	115.04(17)	C(7)-C(6)-C(5)	119.66(18)
C(6)-C(7)-C(8)	120.86(19)	C(7)-C(8)-C(13)	118.76(19)
C(9)-C(8)-C(7)	121.94(19)	C(9)-C(8)-C(13)	119.30(19)
C(10)-C(9)-C(8)	121.0(2)	C(9)-C(10)-C(11)	120.0(2)
C(12)-C(11)-C(10)	120.7(2)	C(11)-C(12)-C(13)	121.3(2)

C(4)-C(13)-C(8)	119.75(17)	C(4)-C(13)-C(12)	122.61(18)
C(12)-C(13)-C(8)	117.64(18)	C(15)-C(14)-C(2)	120.25(18)
C(15)-C(14)-C(19)	118.75(18)	C(19)-C(14)-C(2)	121.00(18)
C(16)-C(15)-C(14)	120.47(19)	C(17)-C(16)-C(15)	120.30(18)
C(16)-C(17)-C(18)	119.71(19)	C(19)-C(18)-C(17)	119.9(2)
C(18)-C(19)-C(14)	120.84(18)	C(1)-O(1)-C(5)	120.61(14)

Table 7-16. Anisotropic displacement parameters (\AA^2).

The anisotropic displacement factor exponent takes the form:

$$-2\pi^2 [h^2 a^{*2} U_{11} + \dots + 2 h k a^* b^* U_{12}].$$

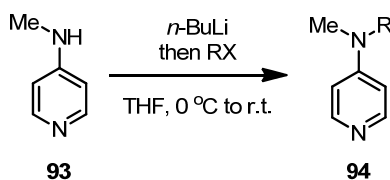
	U_{11}	U_{22}	U_{33}	U_{23}	U_{13}	U_{12}
C(1)	0.028(1)	0.026(1)	0.025(1)	-0.002(1)	-0.001(1)	-0.002(1)
C(2)	0.025(1)	0.021(1)	0.026(1)	-0.002(1)	-0.001(1)	-0.001(1)
C(3)	0.026(1)	0.023(1)	0.027(1)	0.000(1)	-0.002(1)	-0.002(1)
C(4)	0.026(1)	0.023(1)	0.023(1)	-0.003(1)	-0.001(1)	-0.004(1)
C(5)	0.030(1)	0.023(1)	0.024(1)	-0.003(1)	-0.002(1)	-0.002(1)
C(6)	0.033(1)	0.029(1)	0.025(1)	-0.005(1)	0.004(1)	-0.007(1)
C(7)	0.040(1)	0.030(1)	0.024(1)	0.001(1)	0.003(1)	-0.008(1)
C(8)	0.037(1)	0.023(1)	0.022(1)	-0.003(1)	-0.001(1)	-0.004(1)
C(9)	0.046(1)	0.026(1)	0.024(1)	0.002(1)	-0.004(1)	-0.002(1)
C(10)	0.043(1)	0.026(1)	0.029(1)	-0.001(1)	-0.010(1)	0.003(1)
C(11)	0.031(1)	0.029(1)	0.033(1)	-0.002(1)	-0.005(1)	0.000(1)
C(12)	0.031(1)	0.028(1)	0.026(1)	-0.001(1)	-0.003(1)	-0.002(1)
C(13)	0.030(1)	0.023(1)	0.021(1)	-0.001(1)	-0.002(1)	-0.003(1)
C(14)	0.023(1)	0.021(1)	0.029(1)	0.001(1)	0.002(1)	0.002(1)
C(15)	0.024(1)	0.023(1)	0.029(1)	-0.003(1)	-0.001(1)	0.000(1)
C(16)	0.025(1)	0.029(1)	0.023(1)	-0.001(1)	0.000(1)	0.003(1)
C(17)	0.025(1)	0.026(1)	0.029(1)	0.004(1)	0.004(1)	0.005(1)

7. EXPERIMENTAL PART

C(18)	0.027(1)	0.021(1)	0.034(1)	-0.001(1)	0.002(1)	0.001(1)
C(19)	0.028(1)	0.021(1)	0.027(1)	-0.004(1)	-0.002(1)	0.001(1)
O(1)	0.029(1)	0.029(1)	0.027(1)	0.000(1)	0.004(1)	0.002(1)
O(2)	0.032(1)	0.029(1)	0.033(1)	-0.001(1)	0.000(1)	0.007(1)

7.6. Preparation of Organocatalysts for Immobilization

7.6.1. Preparation of DMAP Derivatives¹⁷⁵



General procedure: To a solution of N-methylpyridine (**93**, 11 mmol) in THF (25 mL) at 0 °C, *n*-BuLi (2.5 M in *n*-hexane, 1.1 equiv., 4.89 mL) was added slowly and then stirred for 1.5 hours, then the corresponding RX (1.1 equiv.) was added at room temperature and the reaction was stirred for 24-48 hours. After consumption of the starting material (TLC: ethylacetate and a drop of methanol) water (10 mL) was added and the organic phase was extracted with MTBE or ethylacetate (20 mL X 3), dried over Na₂SO₄ and concentrated under reduced pressure. The obtained product could be purified by silica chromatography or used for the immobilization without purification (the purity of the products was confirmed by ¹H NMR).

N-(Hex-5-en-1-yl)-N-methylpyridin-4-amine (**94a**)

¹H NMR (300 MHz, CDCl₃), δ = 1.35-1.50 (m, 2H), 1.53-1.66 (m, 2H), 2.05-2.17 (m, 2H), 2.96 (s, 3H), 3.27-3.37 (m, 2H), 4.84-5.13 (m, 2H), 5.79 (tdd, *J* = 16.91, 10.15, 6.68 Hz, 1H), 6.46 (dd, *J* = 5.00, 1.60 Hz, 2H), 8.20 (dd, *J* = 4.99, 1.59 Hz, 2H) ppm, ¹³C NMR (75 MHz, CDCl₃), δ = 24.94, 25.05, 32.33, 36.29, 50.17, 105.24, 113.78, 137.12, 148.74, 152.10 ppm. HRMS (EI), *m/z* calculated for C₁₂H₁₈N₂ (M) 190.147000, found 190.147160.

N-Allyl-N-methylpyridin-4-amine (**94b**)

¹H NMR (500 MHz, CDCl₃), δ = 2.99 (s, 3H), 3.95 (td, *J* = 4.60, 1.62 Hz, 2H), 5.02-5.23 (m, 2H), 5.80 (tdd, *J* = 15.16, 9.86, 4.81 Hz, 1H), 6.49 (dd, *J* = 5.02, 1.53 Hz, 2H), 8.21 (dd, *J* = 5.01, 1.54 Hz, 2H) ppm, ¹³C NMR (125 MHz, CDCl₃), δ = 37.22, 53.70, 106.68, 116.61, 131.96, 149.92, 153.55 ppm. HRMS (EI), *m/z* calculated for C₉H₁₂N₂ (M) 148.100049, found 148.099981.

(*E/Z*)-N-(But-2-en-1-yl)-N-methylpyridin-4-amine (**94c**)

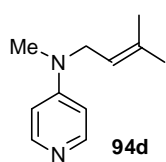
¹H NMR (500 MHz, CDCl₃), δ = 1.69 (ddd, *J* = 6.40, 2.86, 1.38 Hz, 3H, **E-1b**), 1.72-1.76 (m, 3H, **Z-1b**), 2.95 (s, 3H, **E-1b**), 2.96 (s, 3H, **Z-1b**), 3.89-3.84 (m, 2H, **E-1b**), 3.98 (d, *J* = 6.37 Hz, 2H, **Z-1b**), 5.47-5.33 (m, 1H, **E/Z-1b** overlapped), 5.52-5.62 (m, 1H, **E-1b**), 5.64-5.74 (m, 1H, **Z-1b**), 6.49 (dd, *J* = 5.03, 1.55 Hz, 2H, **E/Z-1b** overlapped), 8.17-8.22 (m, 2H, **E/Z-1b** overlapped)

94c (*E/Z* = 4:1)

7. EXPERIMENTAL PART

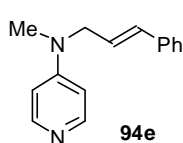
ppm, ^{13}C NMR (125 MHz, CDCl_3), δ = 13.10, 17.67, 36.95, 36.98, 48.05, 52.99, 106.68, 106.82, 124.69, 125.23, 127.66, 128.14, 149.66, 149.72, 153.62 ppm (For **Z-1b**, the quaternary aromatic carbon next to the nitrogen is not detected), HRMS (EI), m/z calculated for $\text{C}_9\text{H}_{14}\text{N}_2$ (M) 162.115700, found 162.115547.

N-Methyl-N-(3-methylbut-2-en-1-yl)pyridin-4-amine (**94d**)



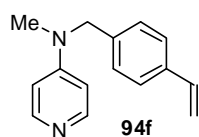
^1H NMR (500 MHz, CDCl_3), δ = 1.74 (d, J = 0.95 Hz, 6H), 2.93 (s, 3H), 3.91 (d, J = 6.40 Hz, 2H), 5.06-5.19 (m, 1H), 6.48 (dd, J = 5.02, 1.54 Hz, 2H), 8.20 (dd, J = 5.12, 1.35 Hz, 2H) ppm, ^{13}C NMR (125 MHz, CDCl_3), δ = 17.97, 25.70, 36.85, 49.11, 106.78, 119.38, 135.75, 149.82, 153.61 ppm, HRMS (EI), m/z calculated for $\text{C}_{11}\text{H}_{16}\text{N}_2$ (M) 176.131347, found 176.131186.

N-Cinnamyl-N-methylpyridin-4-amine (**94e**)

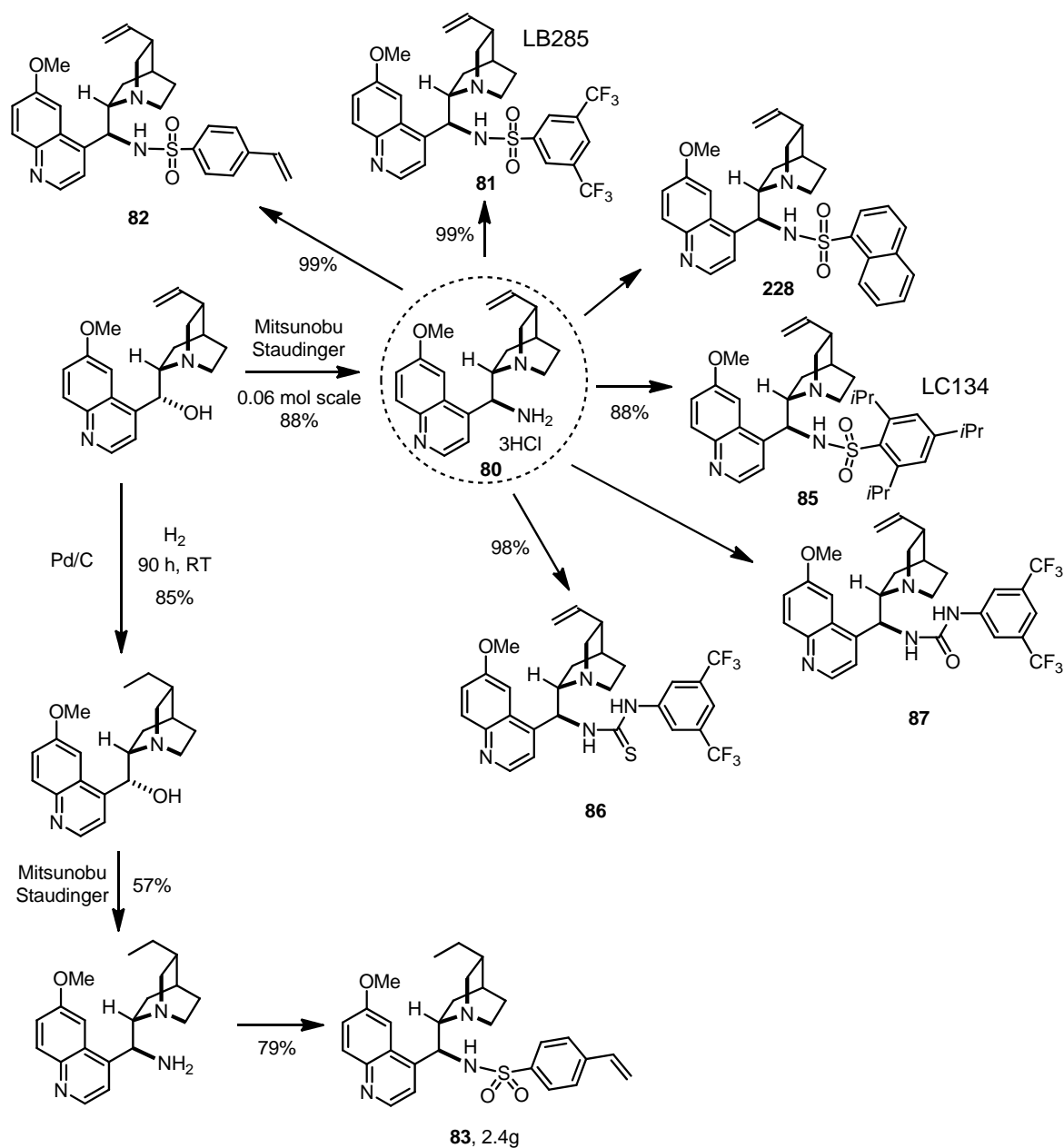


^1H NMR (500 MHz, CDCl_3), δ = 3.03 (s, 3H), 4.11 (dd, J = 5.34, 1.61 Hz, 2H), 6.17 (td, J = 15.91, 5.35 Hz, 1H), 6.46 (d, J = 15.96 Hz, 1H), 6.56 (dd, J = 4.99, 1.58 Hz, 2H), 7.21-7.26 (m, 1H), 7.28-7.36 (m, 4H), 8.23 (dd, J = 4.99, 1.57 Hz, 2H) ppm, ^{13}C NMR (125 MHz, CDCl_3), δ = 37.20, 53.32, 106.80, 123.64, 126.36, 127.78, 128.63, 131.80, 136.37, 149.99, 153.60 ppm. HRMS (ESI+), m/z calculated for $\text{C}_{15}\text{H}_{16}\text{N}_2\text{Na}$ ($\text{M}+\text{Na}^+$) 247.120563, found 247.120464.

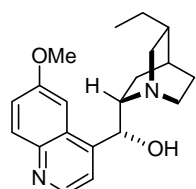
N-Methyl-N-(4-vinylbenzyl)pyridin-4-amine (**94f**)



^1H NMR (500 MHz, CDCl_3), δ = 3.07 (s, 3H), 4.56 (s, 2H), 5.24 (dd, J = 10.91, 0.56 Hz, 1H), 5.73 (dd, J = 17.59, 0.65 Hz, 1H), 6.54 (dd, J = 4.99, 1.59 Hz, 2H), 6.69 (dd, J = 17.59, 10.90 Hz, 1H), 7.12 (d, J = 8.19 Hz, 2H), 7.37 (d, J = 8.17 Hz, 2H), 8.22 (dd, J = 5.00, 1.55 Hz, 2H) ppm, ^{13}C NMR (125 MHz, CDCl_3), δ = 37.80, 54.81, 106.75, 113.96, 126.65, 127.18, 136.28, 136.73, 136.82, 149.92, 153.86 ppm. HRMS (ESI+), m/z calculated for $\text{C}_{15}\text{H}_{17}\text{N}_2$ ($\text{M}+\text{H}^+$) 225.138625, found 225.138417.

7.6.2. Preparation of Cinchona Alkaloid Derivatives¹²¹

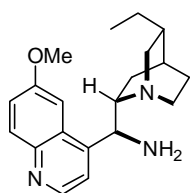
Hydroquinine (HQN)



¹H NMR (500 MHz, CDCl₃), δ = 0.79 (t, J = 7.36 Hz, 3H), 1.16-1.28 (m, 2H), 1.42 (ddd, J = 18.70, 10.17, 4.86 Hz, 3H), 1.72 (ddd, J = 17.39, 9.88, 4.54 Hz, 3H), 2.35 (ddd, J = 13.57, 4.08, 2.45 Hz, 1H), 2.55-2.66 (m, 1H), 3.05 (ddd, J = 23.51, 11.00, 7.20 Hz, 2H), 3.37-3.47 (m, 2H), 3.88 (s, 3H), 4.60 (s, 1H), 5.49 (d, J = 3.76 Hz, 1H), 7.23 (d, J = 2.63 Hz, 1H), 7.29 (dd, J = 9.20, 2.67 Hz, 1H), 7.47 (d, J = 4.51 Hz, 1H), 7.92 (d, J = 9.18 Hz, 1H), 8.54 (d, J = 4.50 Hz, 1H) ppm, ¹³C NMR (125 MHz, CDCl₃), δ = 12.11, 21.46, 25.48, 27.71, 28.37, 37.56, 43.35, 55.68, 58.70, 59.77, 72.04, 101.41, 118.48, 121.39, 126.67, 131.41, 144.11, 147.49, 148.18, 157.65 ppm.

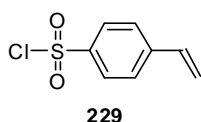
7. EXPERIMENTAL PART

9-*epi*-Amino-hydroquinine



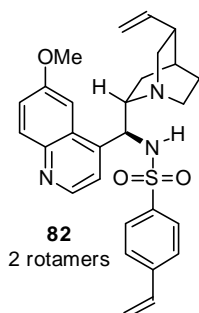
$^1\text{H NMR}$ (500 MHz, CDCl_3), δ = 0.75 (dd, J = 13.65, 7.50 Hz, 1H), 0.82 (t, J = 7.34 Hz, 3H), 1.18-1.63 (m, 7H), 2.24 (s, 2H), 2.53 (ddd, J = 13.63, 4.52, 2.37 Hz, 1H), 2.72-2.86 (m, 1H), 3.06 (d, J = 4.50 Hz, 1H), 3.23-3.16 (m, 1H), 3.26 (dd, J = 13.61, 9.88 Hz, 1H), 3.97 (s, 3H), 4.61 (s, 1H), 7.39 (dd, J = 9.19, 2.71 Hz, 1H), 7.48 (s, 1H), 7.67 (s, 1H), 8.04 (d, J = 9.20 Hz, 1H), 8.75 (d, J = 4.47 Hz, 1H) ppm, $^{13}\text{C NMR}$ (125 MHz, CDCl_3), δ = 12.08, 25.23, 25.81, 25.94, 27.62, 28.86, 37.46, 41.10, 55.55, 57.95, 61.75, 102.26, 119.88, 121.25, 128.80, 131.81, 144.75, 147.30, 147.88, 157.60 ppm. **HRMS (ESI+)**, m/z calculated for $\text{C}_{20}\text{H}_{27}\text{N}_3\text{ONa}$ ($\text{M}+\text{Na}^+$), 348.204631, found 348.2047234.

4-Vinylbenzene-1-sulfonyl chloride (**229**)



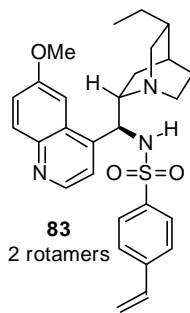
$^1\text{H NMR}$ (500 MHz, CDCl_3), δ = 5.55 (d, J = 10.90 Hz, 1H), 5.97 (d, J = 17.58 Hz, 1H), 6.79 (dd, J = 17.60, 10.88 Hz, 1H), 7.61 (d, J = 8.49 Hz, 2H), 8.00 (d, J = 8.60 Hz, 2H) ppm, $^{13}\text{C NMR}$ (125 MHz, CDCl_3), δ = 119.37, 127.14, 127.44, 134.81, 142.94, 144.42 ppm. **HRMS (EI)**, m/z calculated for $\text{C}_8\text{H}_7\text{O}_2\text{ClS}$ ($\text{M}+\text{Na}^+$), 201.985527, found 201.985321.

N-((S)-(6-Methoxyquinolin-4-yl)((1S,2S,4S,5R)-5-vinylquinuclidin-2-yl)methyl)-4-vinylbenzenesulfonamide (**82**)



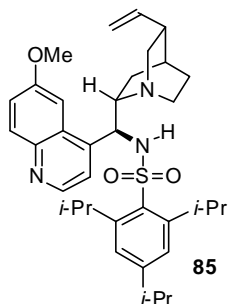
$^1\text{H NMR}$ (500 MHz, CDCl_3), δ = 0.85 (dd, J = 13.67, 7.08 Hz, 1H_{major}), 0.92 (dd, J = 13.44, 7.68 Hz, 1H_{minor}), 1.29 (ddd, J = 9.50, 7.68, 2.49 Hz, 1H), 1.47-1.78 (m, 3H), 2.29 (s, 1H), 2.71 (ddd, J = 16.28, 8.92, 2.31 Hz, 2H), 2.86 (dd, J = 8.37, 0.78 Hz, 1.5H), 3.24 (td, J = 13.80, 10.33 Hz, 1H), 3.34 (dd, J = 18.58, 9.41 Hz, 0.5H), 3.84 (s, 3H_{minor}), 3.98 (s, 3H_{major}), 4.36 (d, J = 10.85 Hz, 0.3H), 4.82-5.01 (m, 2.4H), 5.31 (d, J = 11.13 Hz, 1H_{minor}), 5.38 (d, J = 10.90 Hz, 1H_{major}), 5.53-5.71 (m, 1.3H), 5.77 (d, J = 17.57 Hz, 0.5H), 6.48 (dd, J = 17.53, 10.86 Hz, 1H_{minor}), 6.62 (dd, J = 17.56, 10.89 Hz, 1H_{major}), 6.92 (d, J = 8.32 Hz, 0.70H), 7.20 (ddd, J = 17.90, 14.28, 8.41 Hz, 2H), 7.29 (d, J = 4.58 Hz, 0.5H), 7.38 (ddd, J = 14.68, 7.75, 2.58 Hz, 2H), 7.51 (d, J = 2.69 Hz, 0.5H), 7.80 (d, J = 9.20 Hz, 1H_{minor}), 7.98 (d, J = 9.17 Hz, 1H_{major}), 8.50 (d, J = 4.58 Hz, 1H_{minor}), 8.62 (d, J = 4.31 Hz, 1H_{major}) ppm. **HRMS (ESI+)**, m/z calculated for $\text{C}_{28}\text{H}_{31}\text{N}_3\text{O}_3\text{SNa}$ ($\text{M}+\text{Na}^+$), 512.197835, found 512.197339.

N-((S)-((1S,2S,4S,5R)-5-Ethylquinuclidin-2-yl)(6-methoxyquinolin-4-yl)methyl)-4-vinylbenzenesulfonamide (**83**)



$^1\text{H NMR}$ (500 MHz, CDCl_3), δ = 0.76 (q, J = 7.47 Hz, 3H), 0.94-0.79 (m, 1H), 1.34-1.08 (m, 1H), 1.38-1.72 (m, 3H), 2.34-2.45 (m, 4H), 2.98-2.55 (m, 1H), 3.21 (ddd, J = 16.82, 13.81, 10.02 Hz, 3H), 3.30 (dd, J = 17.74, 9.71 Hz, 2H), 3.84 (s, 3H_{minor}), 3.98 (s, 3H_{major}), 4.33 (d, J = 10.83 Hz, 1H_{minor}), 4.92 (d, J = 10.54 Hz, 1H_{major}), 5.31 (d, J = 11.45 Hz, 1H_{minor}), 5.38 (d, J = 10.89 Hz, 1H_{major}), 5.65 (d, J = 17.56 Hz, 1H_{minor}), 5.78 (d, J = 17.56 Hz, 1H_{major}), 6.48 (dd, J = 17.54, 10.90 Hz, 1H_{minor}), 6.63 (dd, J = 17.57, 10.89 Hz, 1H_{major}), 6.93 (d, J = 8.33 Hz, 1H_{major}), 7.21 (ddd, J = 13.90, 10.87, 5.03 Hz, 3H), 7.43-7.28 (m, 3H), 7.54 (d, J = 2.68 Hz, 1H_{minor}), 7.81 (d, J = 9.20 Hz, 1H_{minor}), 7.99 (d, J = 9.17 Hz, 1H_{major}), 8.51 (d, J = 4.59 Hz, 1H_{major}), 8.62 (d, J = 4.32 Hz, 1H_{minor}) ppm, **HRMS (ESI+)**, m/z calculated for $\text{C}_{28}\text{H}_{33}\text{N}_3\text{O}_2\text{SNa}$ ($\text{M}+\text{Na}^+$), 514.213486, found 514.213814.

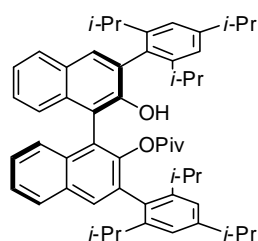
2,4,6-triisopropyl-N-((S)-(6-methoxyquinolin-4-yl)((1S,2S,4S,5R)-5-vinylquinuclidin-2-yl)methyl)benzenesulfonamide (**85**)



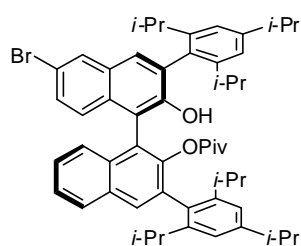
¹H NMR (500 MHz, CDCl₃), δ = 0.77 (d, J = 6.69 Hz, 6H), 0.97 (dd, J = 13.75, 7.21 Hz, 1H), 1.10 (d, J = 6.65 Hz, 1H), 1.19 (dd, J = 9.99, 3.84 Hz, 12H), 1.53-1.72 (m, 3H), 2.28 (s, 1H), 2.62-2.86 (m, 4H), 3.21 (ddd, J = 23.62, 14.97, 9.45 Hz, 2H), 3.83 (dd, J = 13.26, 6.53 Hz, 2H), 4.00 (s, 3H), 4.86-5.00 (m, 2H), 5.26-5.34 (m, 1H), 5.65 (ddd, J = 17.47, 10.34, 7.44 Hz, 2H), 6.88 (s, 2H), 7.09 (d, J = 4.59 Hz, 1H), 7.37 (dd, J = 9.20, 2.61 Hz, 1H), 7.51 (d, J = 2.56 Hz, 1H), 7.95 (d, J = 9.20 Hz, 1H), 8.32 (d, J = 4.58 Hz, 1H) ppm, ¹³C NMR (125 MHz, CDCl₃), δ = 23.58, 23.63, 23.99, 24.64, 24.90, 25.10, 27.37, 27.96, 29.57, 34.10, 39.54,

39.74, 40.31, 52.77, 55.66, 55.77, 61.92, 101.29, 114.64, 120.20, 121.35, 123.02, 128.51, 131.74, 133.74, 141.13, 142.98, 144.48, 146.97, 149.71, 152.57, 157.96 ppm. HRMS (ESI+), m/z calculated for C₃₅H₄₇N₃O₃SNa (M+Na⁺), 612.323034, found 612.322462.

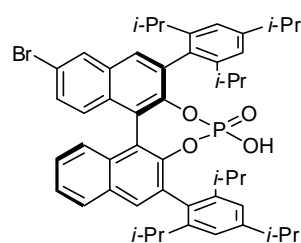
7.6.3. Preparation of Phosphate Derivatives for Immobilization on Textiles

(R)-2'-Hydroxy-3,3'-bis(2,4,6-triisopropylphenyl)-[1,1'-binaphthalen]-2-yl pivalate (**115**)**115**

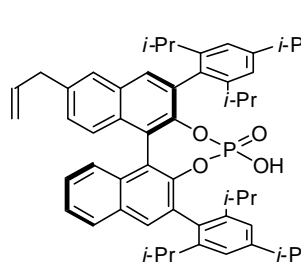
$^1\text{H NMR}$ (500 MHz, CDCl_3), δ = 1.08-1.22 (m, 32H), 1.23-1.28 (m, 13H), 2.67 (s, 2H), 2.82 (s, 2H), 2.93 (tdd, J = 20.43, 13.74, 6.90 Hz, 12H), 5.34 (s, 1H), 6.99-7.09 (m, 2H), 7.11 (s, 2H), 7.25-7.39 (m, 4H), 7.53-7.42 (m, 2H), 7.70 (s, 1H), 7.78 (d, J = 7.63 Hz, 1H), 7.91 (s, 1H), 7.93 (d, J = 8.17 Hz, 1H) ppm. **HRMS (ESI+)**, m/z calculated for $\text{C}_{55}\text{H}_{66}\text{O}_3\text{Na}$ ($\text{M}+\text{Na}^+$), 797.490416, found 797.490050.

(R)-6'-Bromo-2'-hydroxy-3,3'-bis(2,4,6-triisopropylphenyl)-[1,1'-binaphthalen]-2-yl pivalate (**116**)**116**

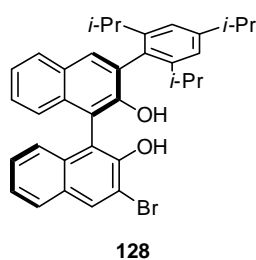
$^1\text{H NMR}$ (500 MHz, CDCl_3), δ = 0.97-1.23 (m, 18H), 1.23-1.28 (m, 10H), 1.31 (d, J = 6.93 Hz, 8H), 2.63 (s, 2H), 2.76 (s, 2H), 2.93 (tdd, J = 18.39, 13.80, 6.91 Hz, 2H), 7.10-7.01 (m, 1H), 7.23-7.09 (m, 3H), 7.44-7.32 (m, 3H), 7.54-7.48 (m, 1H), 7.62 (s, 1H), 7.91-7.95 (m, 3H) ppm. **HRMS (ESI+)**, m/z calculated for $\text{C}_{55}\text{H}_{65}\text{O}_3\text{BrNa}$ ($\text{M}+\text{Na}^+$), 875.400942, found 875.401186.

(R)-9-Bromo-4-hydroxy-2,6-bis(2,4,6-triisopropylphenyl)dinaphtho[2,1-d:1',2'-f][1,3,2]dioxaphosphepine 4-oxide (**121**)**121**

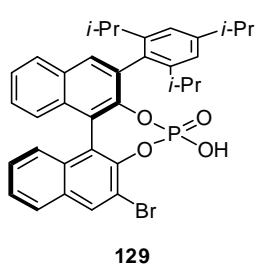
$^1\text{H NMR}$ (500 MHz, CDCl_3), δ = 0.82-0.95 (m, 6H), 1.07 (s, 12H), 1.12-1.20 (m, 6H), 1.23 (d, J = 6.69 Hz, 12H), 2.56-2.70 (m, 2H), 2.74 (s, 2H), 2.85 (td, J = 13.69, 6.72 Hz, 2H), 6.97 (s, 1H), 7.04 (d, J = 14.23 Hz, 2H), 7.07-7.22 (m, 1H), 7.28 (dd, J = 19.21, 9.79 Hz, 3H), 7.43 (t, J = 7.25 Hz, 1H), 7.66 (s, 1H), 7.76 (s, 1H), 7.85 (d, J = 8.16 Hz, 1H), 7.99 (s, 1H) ppm, $^{31}\text{P NMR}$ (202 MHz, CDCl_3), δ = 4.16 ppm. **HRMS (ESI-)**, m/z calculated for $\text{C}_{50}\text{H}_{55}\text{O}_4\text{BrP}$ ($\text{M}-\text{H}^+$), 829.302699, found 829.33210.

(R)-9-Allyl-4-hydroxy-2,6-bis(2,4,6-triisopropylphenyl)dinaphtho[2,1-d:1',2'-f][1,3,2]dioxaphosphepine 4-oxide (**110**)**110**

$^1\text{H NMR}$ (500 MHz, CDCl_3), δ = 0.78-0.96 (m, 6H), 1.08 (s, 12H), 1.17-1.28 (br s, 6H), 1.25 (br s, 12H), 2.79 (br s, 2H), 2.86 (br m, 4H), 3.53 (d, J = 6.53 Hz, 2H), 5.13 (dd, J = 22.16, 13.64 Hz, 2H), 6.05 (tdd, J = 16.74, 9.85, 6.75 Hz, 1H), 6.96 (s, 1H), 7.09 (d, J = 14.23 Hz, 2H), 7.08-7.25 (m, 1H), 7.28 (dd, J = 19.21, 9.79 Hz, 3H), 7.41 (t, J = 7.61 Hz, 1H), 7.61 (s, 1H), 7.68 (s, 1H), 7.74 (s, 1H), 7.84 (d, J = 7.95 Hz, 1H) ppm, $^{31}\text{P NMR}$ (202 MHz, CDCl_3), δ = 3.67 ppm. **HRMS (ESI-)**, m/z calculated for $\text{C}_{53}\text{H}_{60}\text{O}_4\text{P}$ ($\text{M}-\text{H}^+$), 791.423476, found 791.422469.

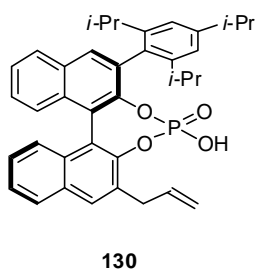
(R)-3-Bromo-3'-(2,4,6-triisopropylphenyl)-[1,1'-binaphthalene]-2,2'-diol (128)

¹H NMR (500 MHz, CDCl₃), δ = 1.12 (dd, *J* = 13.62, 6.89 Hz, 6H), 1.16 (t, *J* = 6.50 Hz, 6H), 1.31 (d, *J* = 6.88 Hz, 6H), 2.75 (td, *J* = 13.65, 6.83 Hz, 2H), 2.96 (td, *J* = 13.76, 6.87 Hz, 1H), 4.88 (s, 1H), 5.52 (s, 1H), 7.15 (d, *J* = 5.53 Hz, 2H), 7.20 (dd, *J* = 11.38, 8.53 Hz, 2H), 7.43-7.26 (m, 4H), 7.79 (d, *J* = 6.88 Hz, 2H), 7.88 (d, *J* = 8.07 Hz, 1H), 8.22 (s, 1H), **HRMS (ESI+)**, *m/z* calculated for C₃₅H₃₄O₂Br (M-H⁺), 565.174779, found 565.175031.

(R)-2-Bromo-4-hydroxy-6-(2,4,6-triisopropylphenyl)dinaphtho[2,1-d:1',2'-f][1,3,2]dioxaphosphepine 4-oxide (129)

¹H NMR (500 MHz, CDCl₃), δ = 0.94 (d, *J* = 6.78 Hz, 3H), 1.09 (dd, *J* = 11.68, 6.73 Hz, 6H), 1.15 (d, *J* = 6.72 Hz, 3H), 1.24 (dd, *J* = 6.32, 5.84 Hz, 6H), 2.53 (td, *J* = 13.62, 6.78 Hz, 1H), 2.70 (td, *J* = 13.39, 6.60 Hz, 1H), 2.89 (td, *J* = 13.77, 6.88 Hz, 1H), 7.05 (d, *J* = 16.78 Hz, 2H), 7.17 (d, *J* = 7.09 Hz, 1H), 7.31-7.25 (m, 4H), 7.47 (t, *J* = 7.20 Hz, 2H), 7.82 (d, *J* = 8.25 Hz, 1H), 7.85 (s, 1H), 7.87 (d, *J* = 8.25 Hz, 1H), 8.20 (s, 1H) ppm, **¹³C NMR** (125 MHz, CDCl₃), δ = 23.07, 23.59, 23.98, 24.08, 24.88, 26.51, 31.01, 31.12,

34.23, 120.44, 121.23, 123.57, 125.32, 125.82, 126.38, 126.74, 127.02, 127.18, 127.52, 128.17, 128.25, 129.06, 130.90, 131.68, 131.90, 132.20, 132.89, 133.48, 147.10, 147.88, 148.46 ppm. **³¹P NMR** (202 MHz, CDCl₃), δ = 3.91 ppm. **HRMS (ESI-)**, *m/z* calculated for C₃₅H₃₃O₄BrP (M-H⁺), 627.130552, found 627.130628.

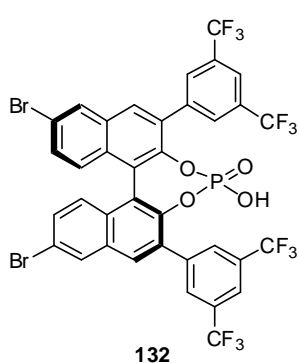
(R)-2-Allyl-4-hydroxy-6-(2,4,6-triisopropylphenyl)dinaphtho[2,1-d:1',2'-f][1,3,2]dioxaphosphepine 4-oxide (130)

¹H NMR (500 MHz, CDCl₃), δ = 0.95 (d, *J* = 6.58 Hz, 3H), 1.08 (d, *J* = 6.54 Hz, 3H), 1.13 (d, *J* = 4.13 Hz, 3H), 1.17 (d, *J* = 6.50 Hz, 3H), 1.21 (t, *J* = 6.82 Hz, 6H), 2.55 (td, *J* = 13.31, 6.57 Hz, 1H), 2.69 (td, *J* = 13.66, 6.97 Hz, 1H), 2.78-2.92 (m, 1H), 3.54 (dd, *J* = 14.93, 6.81 Hz, 1H), 3.70 (dd, *J* = 15.03, 5.11 Hz, 1H), 5.11 (t, *J* = 13.51 Hz, 2H), 6.11-5.97 (m, 1H), 7.04 (d, *J* = 20.40 Hz, 2H), 7.14-7.21 (m, 2H), 7.26-7.34 (m, 2H), 7.41-7.51 (m, 2H), 7.82 (s, 1H), 7.85-7.90 (m, 4H) ppm, **¹³C NMR** (125 MHz, CDCl₃), δ = 23.49, 23.91,

24.06, 24.95, 25.90, 26.53, 31.06, 34.18, 34.54, 120.36, 121.15, 125.31, 125.92, 127.37, 127.97, 128.24, 129.05, 130.17, 131.07, 131.81, 131.96, 132.26, 132.56, 135.24, 135.88, 137.86 ppm, **³¹P NMR** (202 MHz, CDCl₃), δ = 4.25 ppm. **HRMS (ESI-)**, *m/z* calculated for C₃₈H₃₈O₄P (M-H⁺), 589.251325, found 589.251829.

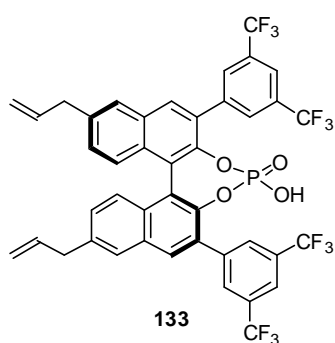
7. EXPERIMENTAL PART

(S)-2,6-Bis(3,5-bis(trifluoromethyl)phenyl)-9,14-dibromo-4-hydroxydinaphtho[2,1-d:1',2'-f][1,3,2]dioxaphosphine 4-oxide (**132**)



$^1\text{H NMR}$ (500 MHz, CDCl_3), δ = 7.16 (d, J = 9.10 Hz, 2H), 7.42 (d, J = 8.75 Hz, 2H), 7.62 (s, 2H), 7.85 (s, 2H), 8.07 (s, 4H), 8.15 (d, J = 1.53 Hz, 2H) ppm, $^{13}\text{C NMR}$ (125 MHz, CDCl_3), δ = 119.88, 120.43, 121.33, 122.05, 122.83, 124.22, 126.39, 126.62, 128.43, 130.00, 130.58, 130.65, 130.78, 130.88, 131.10, 131.36, 131.62, 132.13, 132.33, 138.69, 141.51, 144.90, 145.09 ppm, $^{31}\text{P NMR}$ (202 MHz, CDCl_3), δ = 2.76 ppm. **HRMS (ESI-)**, m/z calculated for $\text{C}_{36}\text{H}_{14}\text{O}_4\text{Br}_2\text{F}_{12}\text{P}$ (M-H^+), 926.881070, found 926.882062.

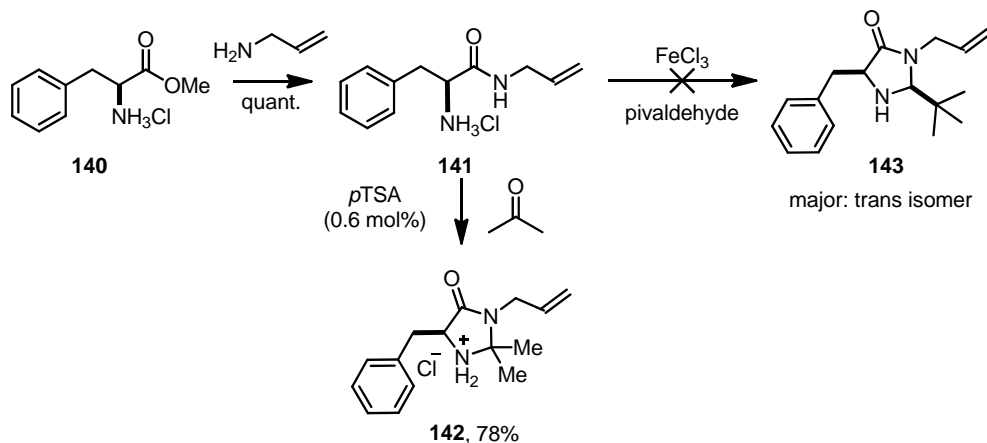
(S)-9,14-Diallyl-2,6-bis(3,5-bis(trifluoromethyl)phenyl)-4-hydroxydinaphtho[2,1-d:1',2'-f][1,3,2]dioxaphosphine 4-oxide (**133**)



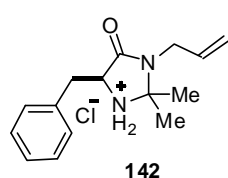
found 851.122256.

$^1\text{H NMR}$ (500 MHz, CDCl_3), δ = 3.58 (d, J = 6.59 Hz, 4H), 5.19-5.12 (m, 4H), 5.94-6.17 (m, 2H), 7.23-7.26 (m, 2H), 7.34 (d, J = 8.76 Hz, 2H), 7.65 (s, 2H), 7.79 (s, 2H), 7.95 (s, 2H), 8.06 (s, 4H) ppm, $^{13}\text{C NMR}$ (125 MHz, CDCl_3), δ = 40.00, 116.74, 119.95, 121.43, 122.13, 122.58, 124.30, 125.03, 126.47, 127.11, 127.30, 129.12, 129.94, 131.01, 131.17, 131.27, 131.45, 131.53, 131.62, 131.80, 136.58, 138.57, 138.92, 143.32 ppm, $^{31}\text{P NMR}$ (202 MHz, CDCl_3), δ = 4.11 ppm. **HRMS (ESI-)**, m/z calculated for $\text{C}_{42}\text{H}_{24}\text{O}_4\text{F}_{12}\text{P}$ (M-H^+), 851.122615,

7.6.4. Preparation of MacMillan-Type Catalyst

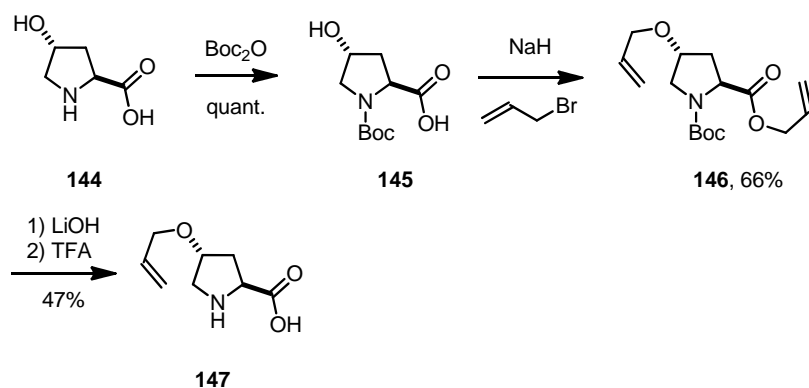


(S)-3-Allyl-5-benzyl-2,2-dimethyl-4-oxoimidazolidin-1-ium chloride (**142**)

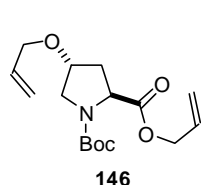


$^1\text{H NMR}$ (500 MHz, CD_3CN), δ = 1.63 (s, 3H), 1.76 (s, 3H), 3.37 (dd, J = 15.00, 4.89 Hz, 1H), 3.56 (dd, J = 14.95, 8.40 Hz, 1H), 3.86 (tdd, J = 16.49, 5.37, 1.51 Hz, 1H), 3.96 (tdd, J = 16.44, 5.68, 1.55 Hz, 1H), 4.42 (dd, J = 8.39, 5.07 Hz, 1H), 5.19 (ddd, J = 10.36, 2.70, 1.34 Hz, 1H), 5.33 (ddd, J = 17.19, 2.89, 1.51 Hz, 1H), 5.86-5.76 (m, 1H), 7.42-7.25 (m, 3H), 7.52 (t, J = -1.#J Hz, 2H), $^{13}\text{C NMR}$ (125 MHz, CD_3CN), δ = 23.29, 23.95, 33.09, 41.54, 57.39, 77.62, 126.82, 128.28, 129.32, 129.34, 132.61, 135.67, 166.15. **HRMS (ESI+)**, m/z calculated for $\text{C}_{15}\text{H}_{21}\text{N}_2\text{O}_1$ ($\text{M}+\text{H}^+$), 245.164837, found 245.164608.

7.6.5. Preparation of Proline-Derivative

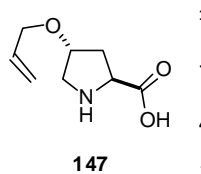


(2S,4R)-2-Allyl 1-tert-butyl 4-(allyloxy)pyrrolidine-1,2-dicarboxylate (**146**)



$^1\text{H NMR}$ (500 MHz, CDCl_3), δ = 1.41 (s, 9H), 2.09 (dd, J = 12.82, 6.37 Hz, 1H), 2.47-2.23 (m, 1H), 3.68-3.42 (m, 1H), 4.05-3.88 (m, 2H), 4.12 (q, J = 6.88 Hz, 1H), 4.37 (t, J = 7.55 Hz, 1H), 4.72-4.54 (m, 2H), 5.26 (ddd, J = 32.88, 23.43, 13.80 Hz, 4H), 5.90 (tdt, J = 15.60, 10.52, 5.10 Hz, 2H). **HRMS (ESI+)**, m/z calculated for $\text{C}_{16}\text{H}_{25}\text{NO}_5\text{Na}$ ($\text{M}+\text{Na}^+$), 334.162493, found 334.162539.

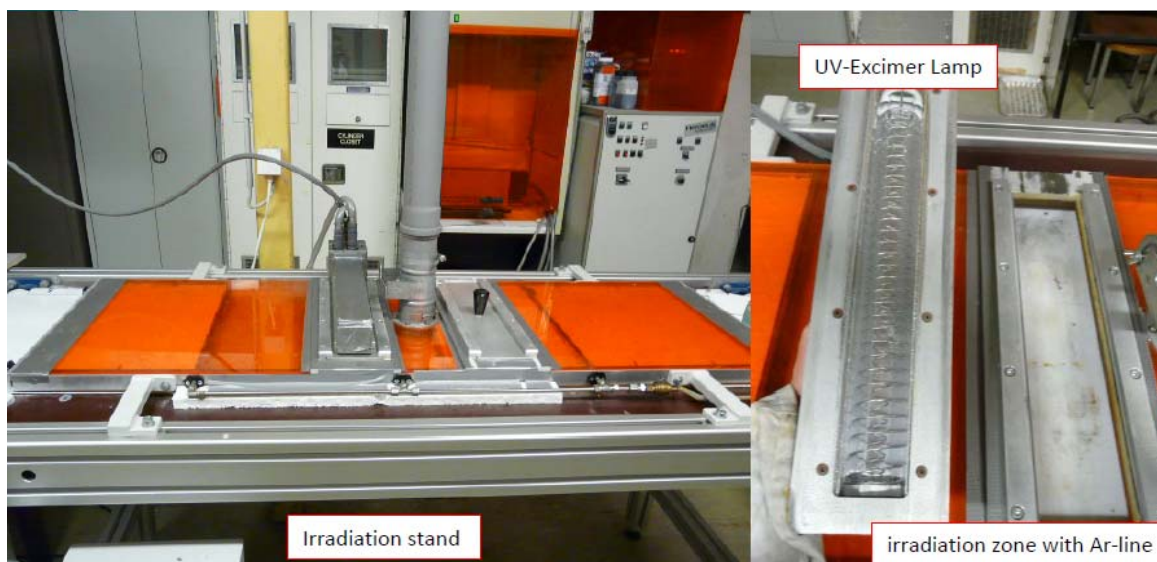
(2S,4R)-Allyl 4-(allyloxy)pyrrolidine-2-carboxylate (**147**)



$^1\text{H NMR}$ (400 MHz, CD_3CN), δ = 2.00 (tdd, J = 17.20, 10.64, 5.44 Hz, 1H), 2.36 (dd, J = 13.80, 7.52 Hz, 1H), 3.30 (d, J = 12.58 Hz, 1H), 3.43 (dd, J = 12.57, 4.38 Hz, 1H), 3.97-3.99 (m, 2H), 4.14 (dd, J = 10.51, 7.61 Hz, 1H), 4.21 (t, J = 4.41 Hz, 1H), 5.16 (ddd, J = 10.46, 3.04, 1.31 Hz, 1H), 5.29 (ddd, J = 17.27, 3.41, 1.66 Hz, 1H), 5.90 (tdd, J = 17.20, 10.64, 5.44 Hz, 1H), $^{13}\text{C NMR}$

(100 MHz, CD_3CN), δ = 34.82, 49.92, 59.70, 69.15, 77.15, 116.12, 134.55, 173.12 ppm. **HRMS (CI, isobutane)**, m/z calculated for $\text{C}_8\text{H}_{14}\text{NO}_3$ (M), 172.097372, found 172.097173.

7.7. General Procedure for the Preparation of Organocatalyst-Immobilized Textile Catalysts



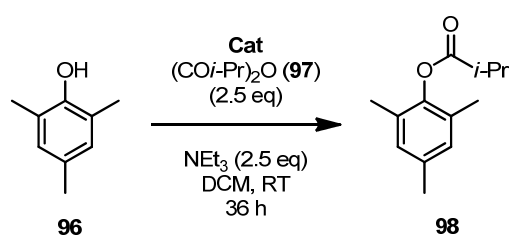
In the irradiation zone, the solution of organocatalyst and crosslinker PETA in acetonitrile (2 mL) was dropped on a textile piece (5 x 15 cm, 1.275 g) to soak uniformly. Then the sample was dried under air and irradiated both side for designated time. To increase catalyst loading on the surface, second irradiation was conducted if necessary under the same reaction conditions. After irradiation, the textile was removed from the irradiation zone and placed in a soxhlet extractor to remove remaining organic materials using MeOH, H₂O and ethylacetate. Catalyst loading was determined by following methods:

Surface sensitive acid base titration for nitrogen containing organic catalysts: The textile immersed in an aqueous HCl solution (pH 4) for 2 h. Then the catalyst was washed with water to remove excess HCl and dried. Titration was conducted with NaOH solution (0.02 M), 0.01 mL per 5 min. The change of the potential was measured (mV) by and plotted against the consumed HCl. Catalyst loading was determined by observing the inflection point.

ICP/OES for sulfur containing materials: After soxhlet extraction, the textile was subjected to a microwave digestion with HNO₃ (69 % ROTIPURAN[®] Supra) and sulphur contents was measured by ICP/OES and calibrated with Merck single element standard.

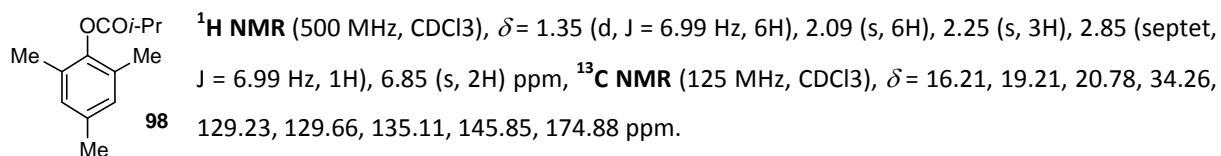
7.8. General Procedure for Applications of Textile Catalysts

7.8.1. General Procedure for Acylation of Phenol **96**

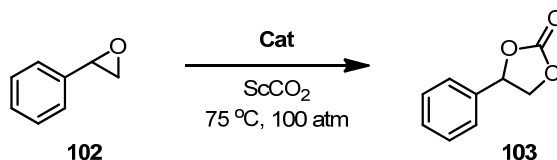


A 10 mL glass vial was equipped with textile catalyst **PA-99** and stirring bar. Then substrate **96** (0.1 mmol) was added and dissolved in DCM (2 mL). Triethylamine (0.25 mmol, 0.25 equiv) and anhydride **97** (0.25 mmol, 0.25 equiv) were then added subsequently and the reaction mixture was stirred at room temperature. The conversion was checked by GC/MS or ^1H NMR analysis of the crude reaction mixture. In some cases, the acylated product **98** was isolated and showed identical spectroscopic data.¹⁷⁶

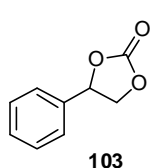
Mesityl isobutyrate (**98**)



7.8.2. General Procedure for Catalytic Cyclic Carbonate Formation Reaction

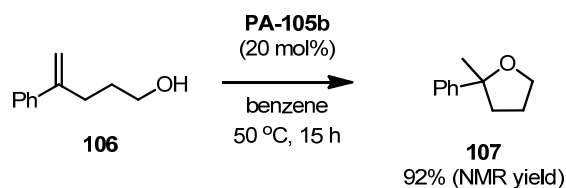


A 30 mL autoclave was equipped with textile catalyst **PA-95b** or (**PA-99d**) and stirring bar. Then epoxide **102** was added via syringe on the textile to soak the substrate. Then the autoclave was charged with CO₂ (65 bar) and then temperature was increased to 75 °C (the pressure was increased to ca. 100 bar). After 4-5 days, the autoclave was cooled to room temperature and CO₂ gas was released then the crude reaction mixture was checked by ¹H NMR. The carbonate **103** was isolated after silica chromatography (DCM:*n*-Hexane=2:1) and showed identical isolated yield compared to the conversion detected by ¹H NMR.

4-Phenyl-1,3-dioxolan-2-one (**103**)

¹H NMR (500 MHz, CDCl₃), δ = 4.33-4.37 (m, 1H), 4.80 (t, *J* = 8.41 Hz, 1H), 5.68 (t, *J* = 8.02 Hz, 1H), 7.29-7.51 (m, 5H) ppm, HRMS (EI), *m/z* calculated for C₉H₈O₃ (M) 164.047348, found 164.047256.

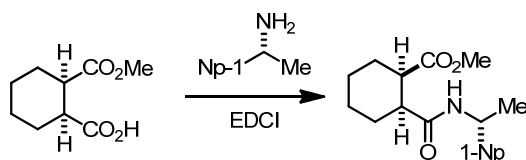
7.8.3. General Procedure for Hydroetherification of Alkene



A 10 mL glass vial was equipped with textile catalyst **PA-105b** and stirring bar. Then the substrate (0.1 mmol) was added, dissolved in benzene (2 mL) and the reaction mixture was stirred at 50 °C for 15 h. The conversion was checked by ¹H NMR analysis of the crude reaction mixture.

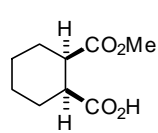
7.8.4. General Procedure for Desymmetrization of Anhydrides **76** and Recycling Experiments

A 15 mL glass vial was equipped with textile catalyst **PA-92** and stirring bar. *Meso*-anhydride **76a** (0.1 – 3.2 mmol) was added, dissolved in MTBE (14 mL), then methanol (2 - 30 equiv) was added and the reaction mixture was stirred at room temperature. The conversion was checked by TLC analysis (ethylacetate:*n*-hexane=1:4, and KMnO₄ stain). After full conversion of the starting material, the vial was washed with MTBE (10 mL x 2) and the combined organic solvent was concentrated under vacuo to afford the pure hemiester (in general, >97% isolated yield). Then the vial with the textile catalyst was used for next recycling step without any purification method. The detailed reaction conditions for recycling experiments are shown in Table S1. (The reaction conditions were optimized during the recycling experiments). Enantioselectivity of the obtained hemiester was recorded after a modification to the corresponding amide.

7.8.5. General Procedure for Desymmetrization of *meso*-Anhydrides

A 15 mL glass vial was equipped with textile catalyst **PA-92** and stirring bar. *Meso*-anhydride **76a** (0.27 mmol) was added, dissolved in MTBE (10 mL) then methanol (2.7 mmol, 10 equiv) was added and the reaction mixture was stirred at room temperature. The conversion was checked by TLC analysis (ethylacetate:*n*-hexane=1:4, and KMnO₄ stain). After full conversion of the starting material, the vial was washed with MTBE (10 mL x 2) and the combined organic solvent was concentrated under vacuo to afford the pure hemiester. The ¹H and ¹³C NMR spectra of crude reaction mixture were consistent with the reported values (1-4). Enantioselectivity of the obtained hemiester was recorded after a modification to the corresponding amide. **Meso*-cyclic anhydrides were prepared via condensation of the corresponding diacids if needed using acetyl chloride at 80 °C for 1.5-2 hrs then precipitated in diethylether/*n*-hexane or diethylether/pentane.

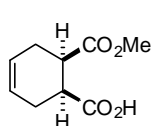
(1*S*,2*R*)-2-(Methoxycarbonyl)cyclohexanecarboxylic acid (**77a**)



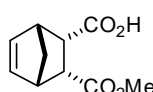
77a

¹H NMR (500 MHz, CDCl₃), δ = 1.36-1.60 (m, 4H), 1.73-1.83 (m, 2H), 1.96-2.09 (m, 2H), 2.79-2.89 (m, 2H), 3.22 (s, 3H), 11.18 (br s, 1H) ppm, ¹³C NMR (125 MHz, CDCl₃), δ = 23.60, 23.74, 25.92, 26.22, 42.29, 42.53, 51.70, 174.08, 180.37 ppm. The enantiomeric ratio was determined by HPLC analysis using Daicel Chiralcel OD-3 column: *n*-Hep:*i*-PrOH = 98:2, flow rate 1.0

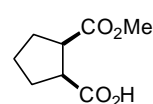
mL/min, λ = 254 nm: τ_{minor} = 16.34 min, τ_{major} = 18.84 min.

(1*R*,6*S*)-6-(Methoxycarbonyl)cyclohex-3-enecarboxylic acid (**77b**)**77b**

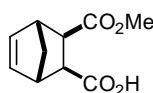
$^1\text{H NMR}$ (500 MHz, CDCl_3), δ = 2.27-2.46 (m, 2H), 2.59 (dt, J = 18.86, 18.56, 5.51 Hz, 2H), 3.15-2.97 (m, 2H), 3.70 (s, 3H), 5.69 (d, J = 4.56 Hz, 2H), 11.14 (br s, 1H) ppm, $^{13}\text{C NMR}$ (125 MHz, CDCl_3), δ = 25.73, 26.91, 39.47, 39.60, 51.92, 125.08, 125.15, 173.70, 179.42 ppm. The enantiomeric ratio was determined by HPLC analysis using Daicel Chiralcel OD-3 column: *n*-Hep:*i*-PrOH = 97:3, flow rate 1.0 mL/min, λ = 223 nm: τ_{minor} = 17.17 min, τ_{major} = 20.37 min.

(1*R*,2*S*,3*R*,4*S*)-3-(Methoxycarbonyl)bicyclo[2.2.1]hept-5-ene-2-carboxylic acid (**77c**)**77c**

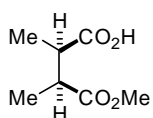
$^1\text{H NMR}$ (500 MHz, CDCl_3), δ = 1.34 (d, J = 8.60 Hz, 1H), 1.49 (d, J = 8.62 Hz, 1H), 3.18 (d, J = 18.18 Hz, 2H), 3.31 (ddd, J = 27.56, 10.25, 3.12 Hz, 2H), 3.59 (s, 3H), 6.21 (dd, J = 5.26, 2.92 Hz, 1H), 6.33 (dd, J = 5.39, 2.85 Hz, 1H), 10.14 (br s, 1H) ppm, $^{13}\text{C NMR}$ (125 MHz, CDCl_3), δ = 46.04, 46.59, 48.03, 48.25, 48.79, 51.51, 134.26, 135.63, 172.91, 178.63 ppm. The enantiomeric ratio was determined by HPLC analysis using Daicel Chiralcel AD-3 column: *n*-Hep:*i*-PrOH = 90:10, flow rate 0.7 mL/min, λ = 223 nm: τ_{major} = 4.95 min, τ_{minor} = 7.60 min.

(1*S*,2*R*)-2-(Methoxycarbonyl)cyclopentanecarboxylic acid (**77d**)**77d**

$^1\text{H NMR}$ (500 MHz, CDCl_3), δ = 1.57-1.74 (m, 1H), 1.82-1.93 (m, 1H), 1.93-2.12 (m, 4H), 3.04-3.12 (m, 2H), 3.66 (s, 3H), 10.84 (br s, 1H) ppm, $^{13}\text{C NMR}$ (125 MHz, CDCl_3), δ = 23.81, 28.66, 46.76, 46.84, 51.76, 174.38, 180.43 ppm. The enantiomeric ratio was determined by HPLC analysis using Daicel Chiralcel AS-H column: *n*-Hep:*i*-PrOH = 80:20, flow rate 1.0 mL/min, λ = 223 nm: τ_{major} = 11.21 min, τ_{minor} = 17.24 min.

(1*S*,2*S*,3*R*,4*R*)-3-(Methoxycarbonyl)bicyclo[2.2.1]hept-5-ene-2-carboxylic acid (**77e**)**77e**

$^1\text{H NMR}$ (500 MHz, CDCl_3), δ = 1.47-1.53 (m, 1H), 2.10 (d, J = 9.12 Hz, 1H), 2.65 (d, J = 1.68 Hz, 2H), 3.15-3.10 (m, 2H), 3.66 (s, 3H), 6.22 (t, J = 1.86 Hz, 2H), 10.29 (br s, 1H) ppm; $^{13}\text{C NMR}$ (125 MHz, CDCl_3), δ = 45.38, 45.79, 47.35, 47.45, 51.80, 137.89, 138.07, 173.89, 179.80 ppm. The enantiomeric ratio was determined by HPLC analysis using Daicel Chiralcel AD-3 column: *n*-Hep:*i*-PrOH = 95:5, flow rate 1.0 mL/min, λ = 224 nm: τ_{major} = 8.03 min, τ_{minor} = 9.27 min.

(2*S*,3*R*)-4-Methoxy-2,3-dimethyl-4-oxobutanoic acid (**77f**)**77f**

$^1\text{H NMR}$ (500 MHz, CDCl_3), δ = 1.20 (dd, J = 14.60, 6.62 Hz, 6H), 2.77 (pd, J = 21.30, 7.10 Hz, 2H), 3.70 (s, 3H) ppm, 11.23 (br s, 1H); $^{13}\text{C NMR}$ (125 MHz, CDCl_3), δ = 14.87, 14.95, 42.33, 42.75, 51.76, 175.26, 179.88 ppm. The enantiomeric ratio was determined by HPLC analysis using Daicel Chiralcel AD-3 column: *n*-Hep:*i*-PrOH = 95:5, flow rate 1.0 mL/min, λ = 204 nm: τ_{major} = 7.28 min, τ_{minor} = 8.04 min.

7. EXPERIMENTAL PART

7.8.6. Recycling Experiments for Desymmerization Reaction of 76a

Recycling number	Catalyst loading (mol%)	76a (mg)	MeOH (eq)	MeOH (uL)	Time	Conv (%) (isolated yield, %)	ee (%)
0	29	17	10	45	25h	99	94
1	29	17	10	45	23h	99	92
2	29	17	10	45	21h	99	95
3	29	17	10	45	22h	99	96
4	29	17	10	45	12h	99	94
5	10	49	10	129	29h	99 (97%)	94
6	10	49	10	129	14h	99 (99%)	93
7	4	141	10	369	25h	99	88
8	1	492	10	1291	23.5h	99	62
9	1	492	10	1291	9h	90	60
10	5	98	5	129	6h	80	90
11	5	98	3	77	30h	full	90
12	5	98	2	52	44h	full	90
13	30	16	10	43	10h	full	92
14	26	19	10	50	9h	full	93
15	30	16	10	43	12h	full	94
16	30	16	10	43	18h	full	94
17	30	16	10	43	24h	full (99%)	94
18	10	49	10	129	18h	full	91
19	10	49	10	129	14h	full (99%)	90
20	10	49	10	129	22h	full	90
21	10	49	10	129	24h	full	91
22	10	49	10	129	25h	full	90
23	10	49	10	129	24h	full	90
24	10	49	10	129	30h	full	90
25	30	16	10	43	30h	full	92
26	50	10	10	26	24h	full	93
27	50	10	10	26	24	full	93
28	50	10	10	26	14	full	92
29	50	10	20	52	4	full	92
30	50	10	30	77	2	full	92
31	50	10	30	77	5	full	93
32	50	10	30	77	24	full	91
33	50	10	30	77	24	full	92

34	50	10	30	77	24	full	94
35	50	10	30	77	24	full	92
36	50	10	30	77	18	full	94
37	50	10	30	77	24	full	94
38	50	10	30	77	24	full	94
39	50	10	30	77	7	full	96
40	50	10	30	77	24	full	92
41	50	10	30	77	24	full	93
42	50	10	30	77	24	full	93
43	50	10	30	77	24	full	92
44	50	10	30	77	24	full	92
45	50	10	30	77	24	full	93
46	50	10	30	77	24	full	93
47	50	10	30	77	24	full	94
48	30	16	10	43	25	full	92
49	30	16	10	43	24	full	91
50	30	16	10	43	18	full	93
51	30	16	10	43	34	full	92
52	30	16	10	43	24	full	93
53	30	16	10	43	24	full	92
54	30	16	10	43	23	full	92
55	30	16	10	43	24	full	95
56	30	16	10	43	24	full	94
57	10	49	10	129	48	full	91
58	10	49	10	129	17	full	92
59	10	49	10	129	24	full	93
60	10	49	10	129	24	full (99%)	91
61	10	49	10	129	24	full	92
62	10	49	10	129	24	full	91
63	10	49	10	129	24	full	91
64	10	49	10	129	19	full	92
65	10	49	10	129	21	full	91
66	9	55	9	129	21	full	92
67	8	62	8	129	24	full (99%)	91
68	7	70	7	129	24	full	89
69	6	82	6	129	21	full (99%)	90
70	5	98	5	129	27	full	89
71	5	98	5	129	18	full	90

7. EXPERIMENTAL PART

72	5	98	5	129	21	full	91
73	5	98	5	129	24	full	90
74	5	105	5	129	22	full	90
75	5	106	5	128	24	full	90
76	5	107	5	129	24	full	91
77	4	110	4	129	24	full	91
78	4	111	4	129	26	99	89
79	4	120	4	129	24	99	90
80	4	133	4	129	24	99	90
81	4	135	4	129	24	99	90
82	4	138	4	129	24	99	88
83	3	147	3	129	24	99	88
84	8	61	8	129	24	99	91
85	9	53	9	129	24	99	91
86	11	47	11	129	18	99	92
87	6	87	6	129	24	99	91
88	6	87	6	129	24	99	88
89	6	87	6	129	24	99	88
90	7	74	7	129	24	99	90
91	6	77	6	129	24	full (99%)	90
92	7	76	7	129	24	99	90
93	6	80	6	129	24	99	90
94	6	78	6	129	24	99	91
95	7	76	7	129	24	99	90
96	6	77	6	129	24	99	92
97	6	77	6	129	24	99	92
98	6	77	6	129	24	99	90
99	6	77	6	129	24	99	91
100	6	77	6	129	24	99	90
101	6	77	6	129	24	99	90
102	6	77	6	129	24	99	90
103	6	77	6	129	24	99	90
104	6	77	6	129	24	99	90
105	6	77	6	129	24	99	88
106	6	77	6	129	24	99	88
107	6	77	6	129	24	99	90
108	11	47	11	129	24	99	92
109	11	47	11	129	24	99	90
110	11	47	11	129	24	99	90

111	9	55	9	129	24	99	90
112	8	62	8	129	24	99	90
113	7	68	7	129	24	99	90
114	7	72	7	129	24	99	89
115	7	75	7	129	24	99	90
116	6	79	6	129	24	99	90
117	6	77	6	129	24	99	89
118	6	79	6	129	24	99	90
119	6	81	6	129	24	99	90
120	6	82	6	129	24	99	90
121	6	77	6	129	24	99	91
122	6	79	6	129	24	99	92
123	6	79	6	129	24	99	92
124	6	78	6	129	24	99	90
125	6	77	6	129	24	99	91
126	6	80	6	129	24	99	92
127	6	84	6	129	24	99	90
128	6	81	6	129	24	99	90
129	6	81	6	129	24	99	90
130	6	81	6	129	24	99	88
131	6	81	6	129	24	99	89
132	6	81	6	129	24	99 (99%)	90
133	6	81	6	129	24	99	90
134	7	75	7	129	24	99	90
135	6	78	6	129	24	99	89
136	6	79	6	129	24	99	90
137	7	75	7	129	24	99	90
138	6	78	6	129	24	99	90
139	7	76	7	129	24	99	90
140	6	79	6	129	24	99	90
141	6	76	6	129	24	99	90
142	6	79	6	129	24	99	92
143	6	77	6	129	24	99	90
144	6	78	6	129	24	99	90
145	6	81	6	129	24	99	90
146	6	77	6	129	24	99	90
147	6	76	6	129	24	99	90
148	6	77	6	129	24	99	90

7. EXPERIMENTAL PART

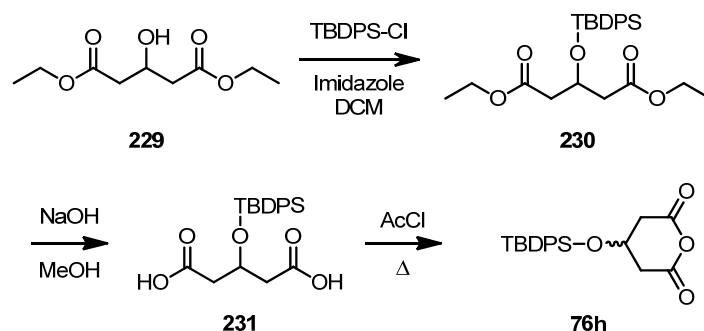
149	6	77	6	129	24	99	90
150	6	77	6	129	24	99	90
151	6	78	6	129	24	99	90
152	6	77	6	129	24	99	90
153	6	77	6	129	24	99	90
154	6	78	6	129	24	99	88
155	6	76	6	129	24	99	88
156	6	76	6	129	24	99	88
157	6	78	6	129	24	99	88
158	6	78	6	129	24	99	90
159	6	78	6	129	24	99	90
160	6	76	6	129	24	99	90
161	6	78	6	129	24	99	89
162	6	78	6	129	24	99	90
163	6	78	6	129	24	99	90
164	6	79	6	129	24	99	90
165	6	79	6	129	24	99	89
166	6	79	6	129	24	99 (99%)	90
167	6	78	6	129	24	99	89
168	6	78	6	129	24	99	90
169	6	79	6	129	24	99	88
170	6	80	6	129	24	99	88
171	6	80	6	129	24	99	90
172	6	78	6	129	24	99	90
173	6	78	6	129	24	99	90
174	6	79	6	129	24	99	90
175	6	79	6	129	24	99	90
176	7	75	7	129	24	99	90
177	6	78	6	129	24	99	90
178	7	70	7	129	24	99	90
179	7	71	7	129	24	99	88
180	6	77	6	129	24	99	90
181	6	79	6	129	24	99	90
182	6	81	6	129	24	99	88
183	6	79	6	129	24	99	88
184	6	79	6	129	24	99	89
185	6	77	6	129	24	99	90
186	6	79	6	129	24	99	88
187	6	79	6	129	24	99	90

188	6	80	6	129	24	99	90
189	6	79	6	129	24	99	90
190	6	80	6	129	24	99	90
191	6	79	6	129	24	99	88
192	6	79	6	129	24	99	90
193	6	79	6	129	24	99	88
194	6	80	6	129	24	99	90
195	6	78	6	129	24	99	88
196	6	78	6	129	24	99	89
197	6	78	6	129	24	99	90
198	6	79	6	129	24	99	88
199	6	80	6	129	24	99	87
200	6	79	6	129	24	99	88
201	6	79	6	129	24	99	88
202	6	79	6	129	24	99	87
203	6	79	6	129	24	99	90
204	6	79	6	129	24	99	87
205	6	79	6	129	24	99	90
206	6	79	6	129	24	99	90
207	6	79	6	129	24	99	90
208	6	79	6	129	24	99	88
209	6	79	6	129	24	99	88
210	6	79	6	129	24	99	88
211	6	79	6	129	24	99	90
212	6	79	6	129	24	99	90
213	6	79	6	129	24	99 (99%)	90
214	6	79	6	129	24	99	90
215	6	79	6	129	24	99	90
216	6	79	6	129	24	99	90
217	6	79	6	129	24	99	90
218	6	79	6	129	24	99	89
219	6	79	6	129	24	99	90
220	6	79	6	129	24	99	88
221	6	79	6	129	24	99	87
222	6	79	6	129	24	99	90
223	6	79	6	129	24	99	87
224	6	79	6	129	24	99	87
225	6	79	6	129	24	99	87

7. EXPERIMENTAL PART

226	6	79	6	129	24	99	87
227	6	79	6	129	24	99	87
228	6	79	6	129	48	99	87
229	6	79	6	129	48	99	87
230	6	79	6	129	48	99	87
231	10	49	10	129	24	99	90
232	6	79	6	129	48	99	87
233	6	79	6	129	48	99	87
234	6	79	6	129	48	99	87
235	6	79	6	129	48	99	87
236	6	79	6	129	48	99	87
237	6	79	6	129	48	99	88
238	6	79	6	129	48	99	87
239	6	79	6	129	48	99	87
240	6	79	6	129	48	99	88
241	6	79	6	129	48	99	87
242	6	79	6	129	24	99	88
243	6	79	6	129	48	99	86
244	6	79	6	129	24	99	86
245	6	79	6	129	48	99	87
246	6	79	6	129	48	99	88
247	6	79	6	129	48	99	87
248	6	79	6	129	48	99	86
249	6	79	6	129	48	99	86
250	6	79	6	129	48	99	85
251	6	79	6	129	48	99	85
252	6	79	6	129	48	99	87
253	6	79	6	129	48	99	86
254	6	79	6	129	48	99	89
255	6	79	6	129	48	99	88
256	6	79	6	129	48	99	87
257	6	79	6	129	48	99	87
258	6	79	6	129	48	99	87
259	6	79	6	129	48	99	90
260	6	79	6	129	48	99	90
261	6	79	6	129	48	99	86
262	6	79	6	129	48	99	88
263	6	79	6	129	48	99	86
264	6	79	6	129	48	99	80

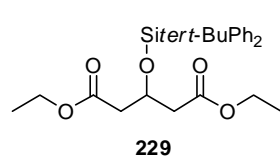
265	6	79	6	129	48	99	87
266	6	79	6	129	48	99	86
267	6	79	6	129	48	99	86
268	6	79	6	129	48	99	86
269	6	78	6	129	48	99	85
270	6	78	6	129	48	99	83
271	10	47	10	129	48	99	83
272	10	50	10	129	48	99	85
273	10	50	10	129	48	99	82
274	10	50	10	129	48	99	81
275	10	50	10	129	48	99	83
276	9	57	9	129	48	99	80

7.8.7. Synthesis of 4-*tert*-Butyldiphenylsilyloxy Glutaric Anhydride **76h**¹⁷⁷

Protection: To a solution of diester **229** (25g, 122 mmol) in DCM (100 mL), imidazole (13.843 g, 203 mmol, 1.6 equiv) and TBDPDS-Cl (35 mL, 134 mmol, 1.1 equiv) were added at 0 °C and the reaction mixture was stirred for 24 hrs. After full conversion of the starting material **229** (checked by TLC, ethylacetate:*n*-hexane=1:5, R_f =0.45) water (100 mL) was added, then the aqueous phase was extracted with DCM (50 mL x 3), dried over $MgSO_4$ and concentrated under vacuo to afford analytically pure (by 1H NMR) TBDPDS-protected diester **230** and used for next step without further purification.

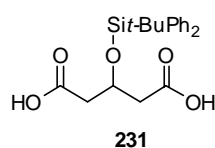
Hydrolysis: In a 500 mL round bottom flask with a magnetic stirring bar, the crude diester **230** was dissolved in methanol (160 mL) and cooled to 0 °C. NaOH (9.76g, 2 equiv) was added slowly, then the reaction mixture was warmed to room temperature and stirred for 24 hrs. After checking the completion of the reaction by TLC, methanol was evaporated under vacuo and the residue was dissolved in water (100 mL) washed in MTBE (50 mL) twice. Then the aqueous phase was acidified with HCl (6N solution, pH = ca. 2) and extracted with MTBE (100 mL x 3) to afford diacid **231** without purification.

Diethyl 3-((*tert*-butyldiphenylsilyl)oxy)pentanedioate (**229**)



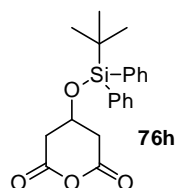
1H NMR (500 MHz, $CDCl_3$), δ = 1.02 (s, 9H), 1.18 (t, J = 7.14 Hz, 6H), 2.53 (dd, J = 15.16, 5.82 Hz, 4H), 2.60 (dd, J = 15.17, 6.39 Hz, 4H), 3.95-4.07 (m, 1H), 4.54 (p, J = 6.11 Hz, 1H), 7.34-7.49 (m, 6H), 7.67-7.72 (m, 4H) ppm, ^{13}C NMR (125 MHz, $CDCl_3$), δ = 14.08, 19.22, 26.79, 41.80, 60.38, 67.26, 127.59, 129.77, 133.49, 135.86, 170.82

ppm. HRMS (ESI+), m/z calculated for $C_{25}H_{34}O_5SiNa$ ($M+Na^+$) 465.206771, found 465.206733.

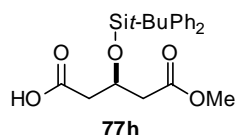
3-((*tert*-Butyldiphenylsilyl)oxy)pentanedioic acid (**231**)

$^1\text{H NMR}$ (500 MHz, CDCl_3), δ = 1.01 (s, 9H), 2.60 (dq, J = 15.53, 6.20 Hz, 4H), 4.48 (p, J = 6.23 Hz, 1H), 7.32-7.45 (m, 6H), 7.64-7.66 (m, 4H), 11.34 (br s, 1.8 H) ppm, $^{13}\text{C NMR}$ (125 MHz, CDCl_3), δ = 19.20, 26.80, 41.49, 66.62, 127.71, 129.93, 133.07, 135.82, 177.12 ppm.

HRMS (ESI-), m/z calculated for $\text{C}_{21}\text{H}_{24}\text{O}_5\text{SiNa}$ ($\text{M}-2\text{H}+\text{Na}^+$) 407.129622, found 407.129637.

4-((*tert*-Butyldiphenylsilyl)oxy)pentanedioic anhydride (**76h**)

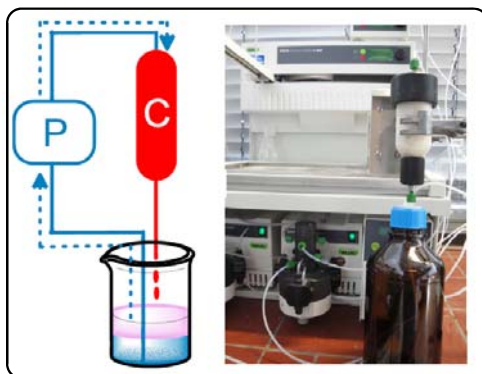
$^1\text{H NMR}$ (500 MHz, CDCl_3), δ = 1.04 (s, 9H), 2.58 (dd, J = 16.10, 2.45 Hz, 2H), 2.79-2.89 (m, 2H), 4.23-4.35 (m, 1H), 7.35-7.53 (m, 6H), 7.61-7.63 (m, 4H) ppm, $^{13}\text{C NMR}$ (125 MHz, CDCl_3), δ = 19.02, 26.69, 38.76, 62.76, 128.13, 130.44, 132.21, 135.60, 165.17 ppm. **HRMS (ESI+)**, m/z calculated for $\text{C}_{21}\text{H}_{24}\text{O}_4\text{SiNa}$ ($\text{M}+\text{Na}^+$) 391.133605, found 391.133483.

(R)-3-((*tert*-Butyldiphenylsilyl)oxy)-5-methoxy-5-oxopentanoic acid (**77h**)

$^1\text{H NMR}$ (500 MHz, CDCl_3), δ = 1.02 (s, 9H), 2.42-2.748 (m, 4H), 3.55 (s, 3H), 4.45-4.57 (m, 1H), 7.26-7.53 (m, 6H), 7.60-7.71 (m, 4H), 11.27 (br s, 1H) ppm, $^{13}\text{C NMR}$ (125 MHz, CDCl_3), δ = 19.22, 26.80, 41.48, 51.58, 66.90, 127.68, 129.88, 133.19, 133.31, 135.86,

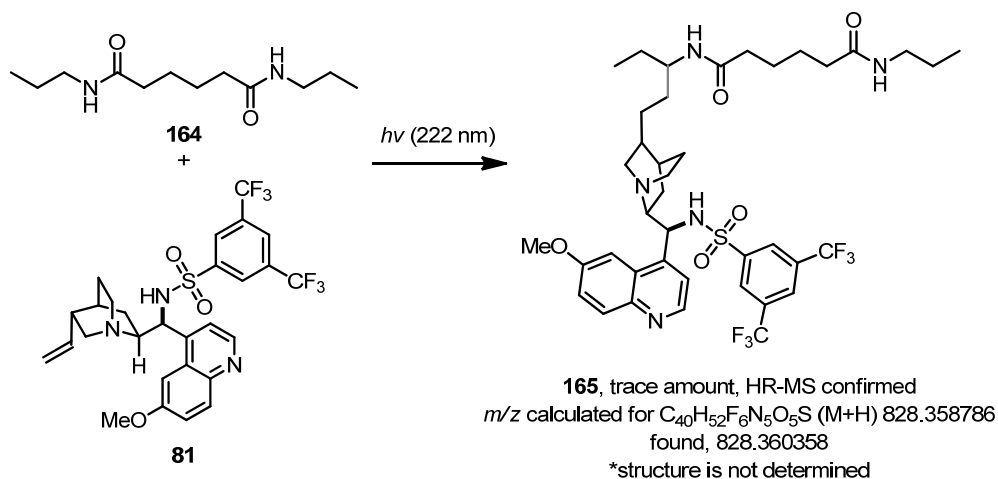
135.87, 171.15, 177.07 ppm. **HRMS (ESI+)**, m/z calculated for $\text{C}_{22}\text{H}_{28}\text{O}_5\text{SiNa}$ ($\text{M}+\text{Na}^+$) 423.159820, found 423.159889. The enantiomeric ratio was determined by HPLC analysis using Daicel Chiralcel OD-3 column: *n*-Hep:*i*-PrOH = 99:1, flow rate 1.0 mL/min, λ = 204 nm: τ_{minor} = 18.75 min, τ_{major} = 20.65 min.

7.8.8. Typical Procedure for Desymmetrization of *meso*-Anhydride **76h** using a Continuous Circulatory Reactor.

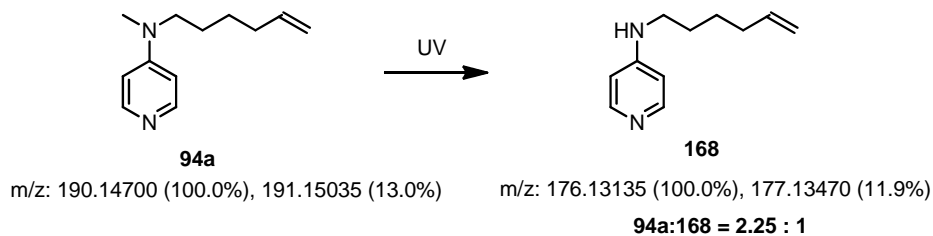


The reaction was conducted using BUCHI-Flash System. Textile catalyst **PA-92** (ca. 0.28 mmol of catalyst, 20 sheets) was packed in polypropylene cartridge (40 mm). The system was flushed with MTBE prior to the reaction. The connecting tubes (fluorinated ethylene propylene) were shortened as possible to prevent background reaction. After completion of starting material **76h**, the system was washed with additional MTBE in a separated bottle (500 mL). The combined organic solvents was dried under reduced pressure to afford pure product **77h** with quantitative yield.

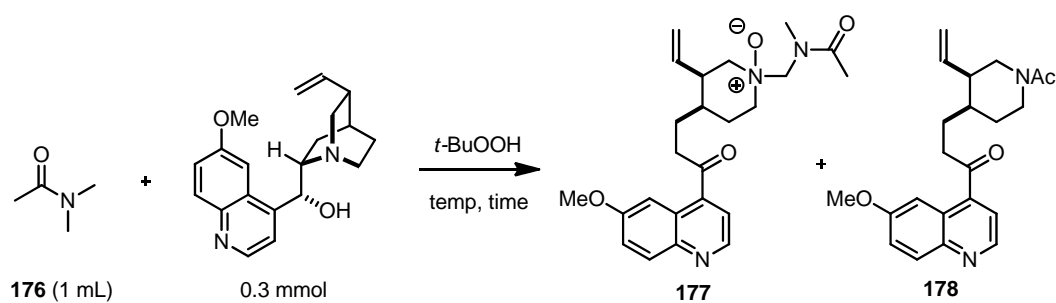
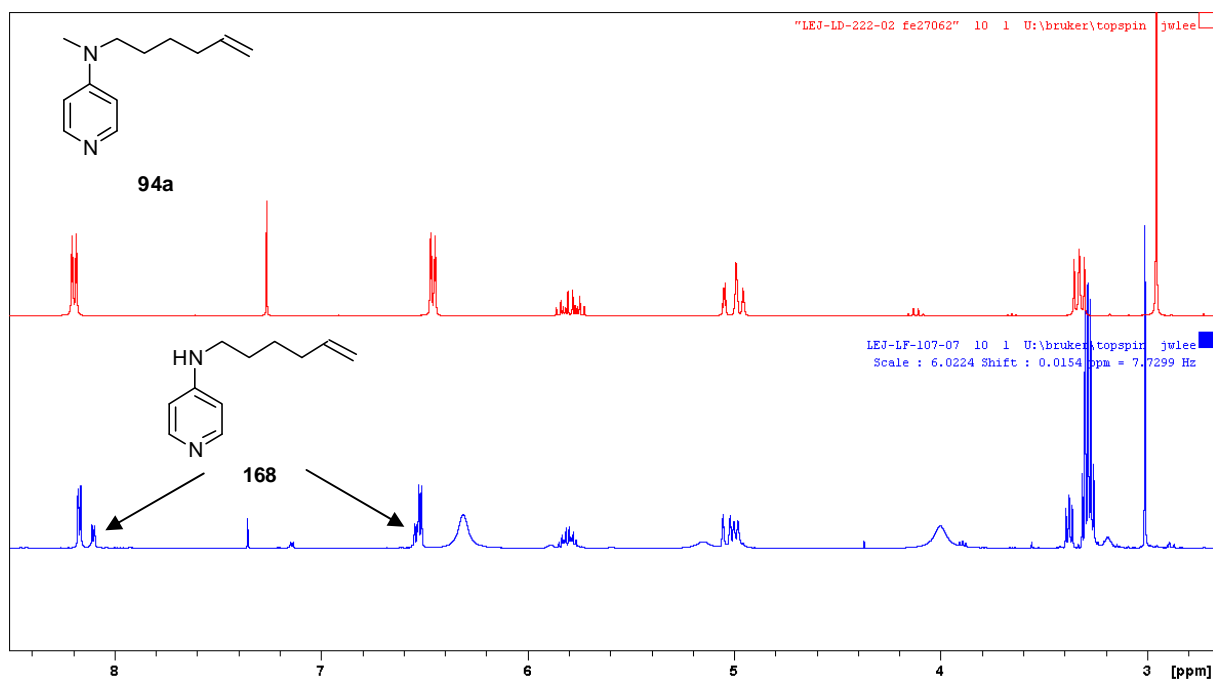
7.8.9. Typical Procedure for Radical-Mediated Reaction of "Monomeric" Amide and Cinchona Alkaloids.



Photochemical reaction conditions: In an irradiation chamber, organic substrates were dissolved in DCM and then irradiated with UV-light for designated time. After irradiation, the reaction mixture was evaporated and subjected to column chromatography for purification. The desired product (**165**) was isolated with less than 1% yield based on sulfonamide **81**.



7. EXPERIMENTAL PART



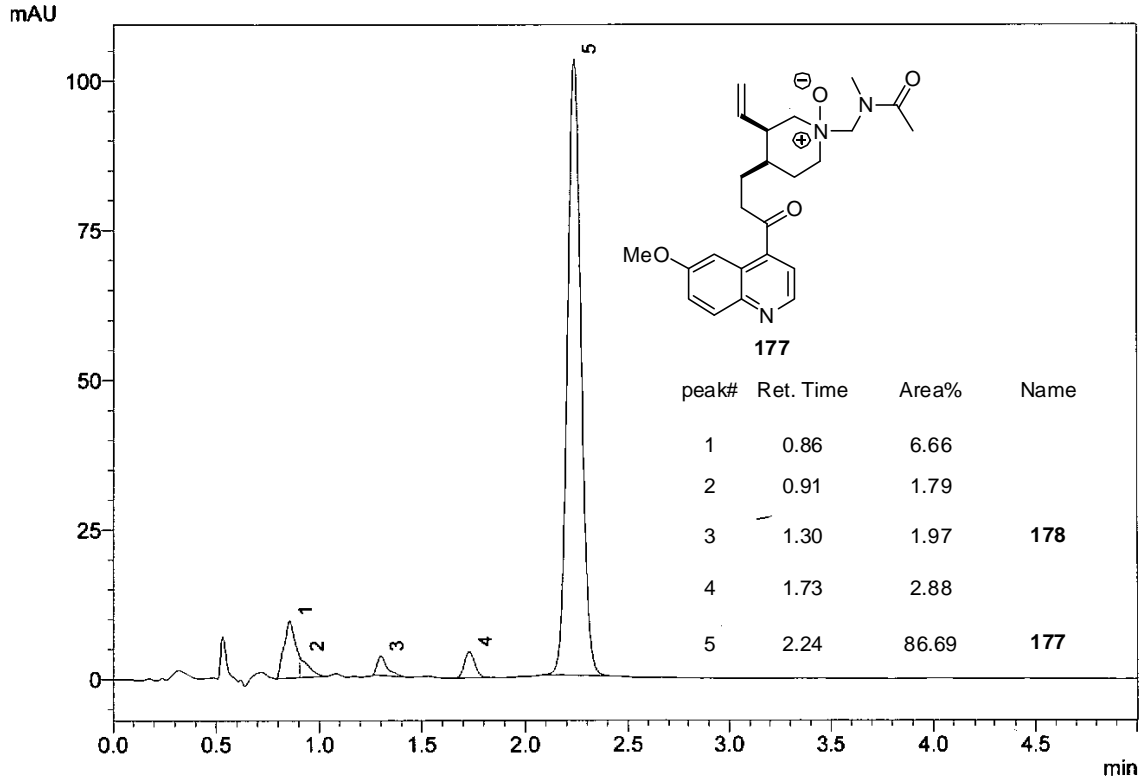
Free radical reaction conditions: In a vial, organic substrates were dissolved in *t*BuOOH solution in decane and heated for 24-48 h at 120 °C. The reaction mixture directly subjected to ¹H NMR analysis and then purified by silica column chromatography. Further purification of a mixture was conducted by HPLC using stationary phase, YMC ODS-A 5 mm, 20150 00058 and mobile phase, methanol/10 mmol TEAA (triethylammonium acetate) at pH 7. (NMR assignment of compound **177** and **178** was conducted by Petra Philips from NMR department)

Gerät : UFLC-20-2

Operator : Br
Sample Name : LEJ-LF-118-20
Vial # : 35
Injection Volume : 0.5 uL
Data File Name : LEJ-LF-118-20-04.lcd
Method File Name : Jiwong Lee_YMC.lcm

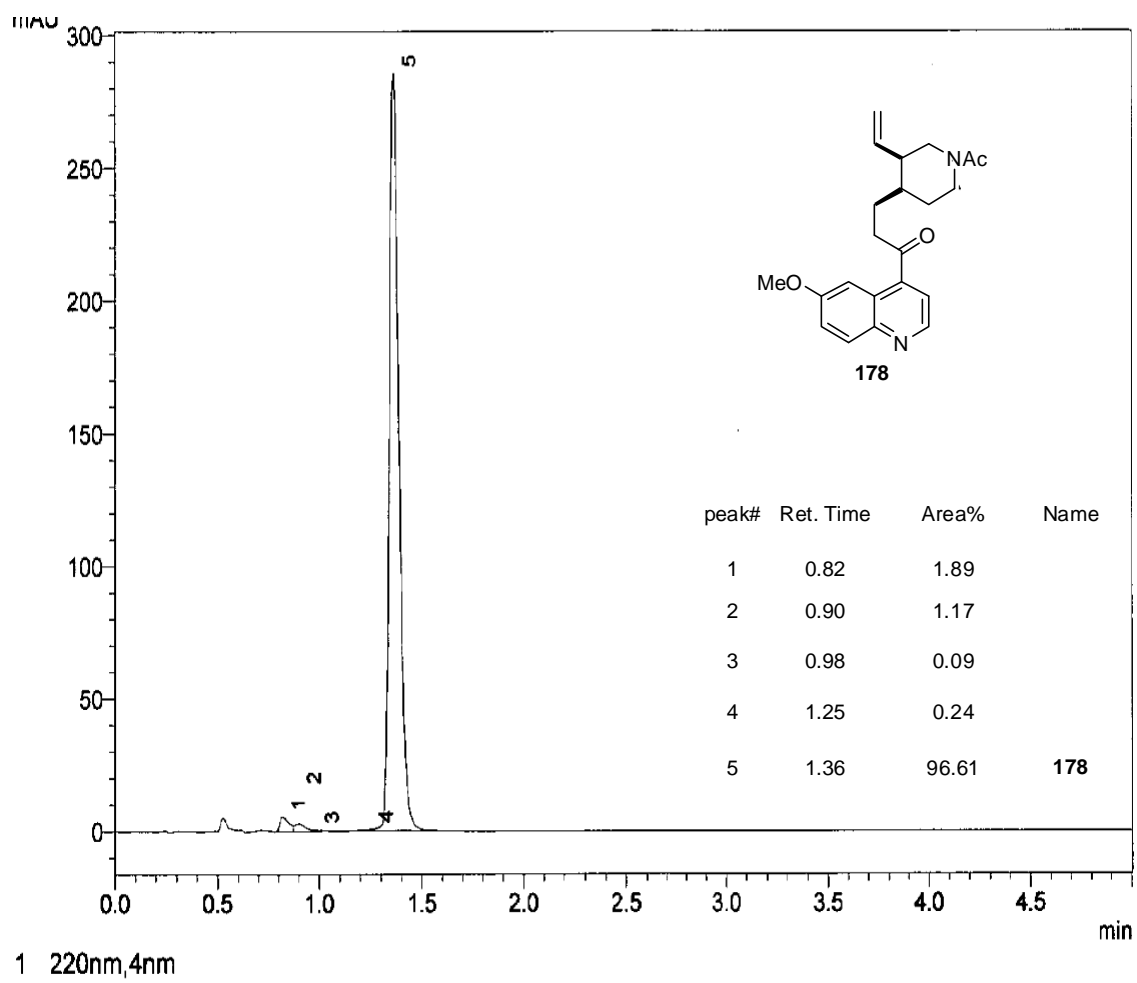
Data Acquired: 08.03.2013 12:13:57

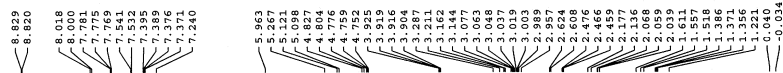
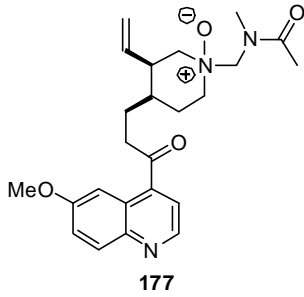
0.5 µ LEJ-LF-118-20 nach der Aufarbeitung
50 mm Eclipse Plus C18, 1.8 µm, 4.6 mm i.D., USUXG 03406
Methanol/10 mmol TEAA pH7 = 70:30
1.0 ml/min, 28.3 MPa, 308 K
220 nm



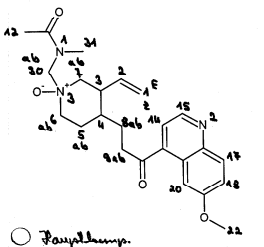
1 220nm,4nm

7. EXPERIMENTAL PART





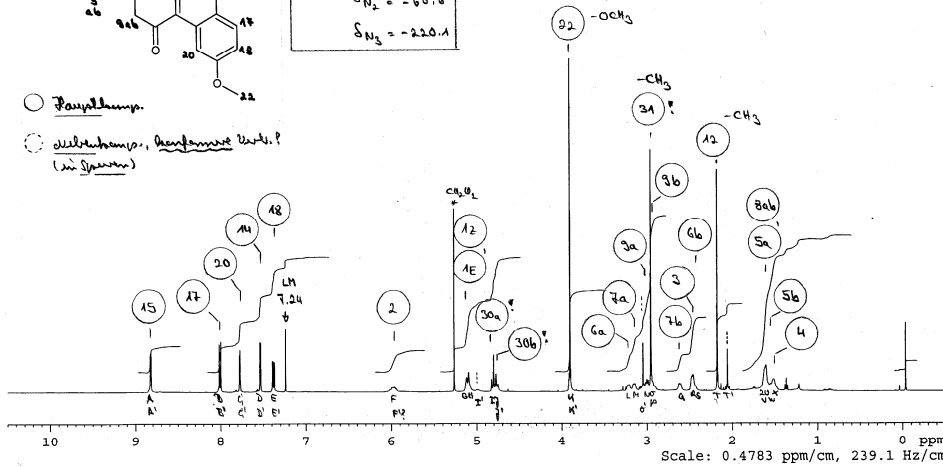
Struktur aus NMR:



$-\delta N$:

$\delta N_1 = -257.8$
 $\delta N_2 = -60.6$
 $\delta N_3 = -220.1$

- Hauptkomp.
- Nebenkomp., befeuchtet Wert? (in Spektrum)



4500012

NAME	1e1f11820
EXPNO	1
PROCNO	1
Time	20130318
Time	16.53
INSTRUM	spcpc
PROBHD	5 mm PABBO BB-
PULPROG	zgpg30
TD	32760
SOLVENT	CDCl3
NS	32
DS	4
SWH	8231.685 Hz
F2FRES	0.250967 Hz
AQ	1.992344 sec
RG	114
HNACQAF	42.000 usec
DS	10.00 usec
TE	298.0 K
D1	0.0100000 sec
TD0	1

AV500as:
 HSACSBFGP
 HNACQAF
 COSYDAP
 CONVDPM
 2-NOSYBPMH
 15V-HMRG

CHANNEL F1
 SFO1 497.870850 MHz
 NUCL1 13
 P1 10.00 usec
 SFO2 65336
 SP 499.8700275 MHz
 SWH 0
 LB 0.30 Hz
 GB 0
 PC 1.00

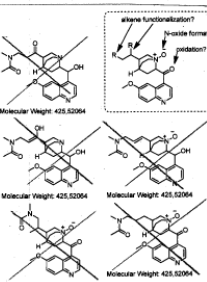
$\delta S, 26 \mu g, CDCl_3, \#2984$

SR = 27.50

(gem. Dr. Fuchs)
 LEJ-LF-118-20
 1H
 AV500as

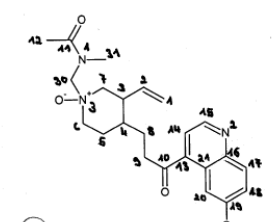
P. Plüsch

VORSCHLAG DES MITTRÄGERS



das nicht?

Struktur aus NMR:



$-\delta N$:

$\delta N_1 = -257.8$
 $\delta N_2 = -60.6$
 $\delta N_3 = -220.1$

- Hauptkomp.
- Nebenkomp., befeuchtet Wert? (in Spektrum)



CS01013

NAME	1e1f11820
EXPNO	1
PROCNO	1
Time	20130318
Time	11.30
INSTRUM	spcpc
PROBHD	5 mm PABBO BB-
PULPROG	zgpg30
TD	65336
SOLVENT	CDCl3
NS	14400
DS	64
SWH	39062.500 Hz
F2FRES	0.596046 Hz
AQ	0.4308108 sec
RG	2050
HNACQAF	12.800 usec
DS	10.00 usec
TE	298.0 K
D1	0.0100000 sec
D11	0.0300000 sec
TD0	1

AV500as:
 HSACSBFGP
 HNACQAF
 COSYDAP
 CONVDPM
 2-NOSYBPMH
 15V-HMRG

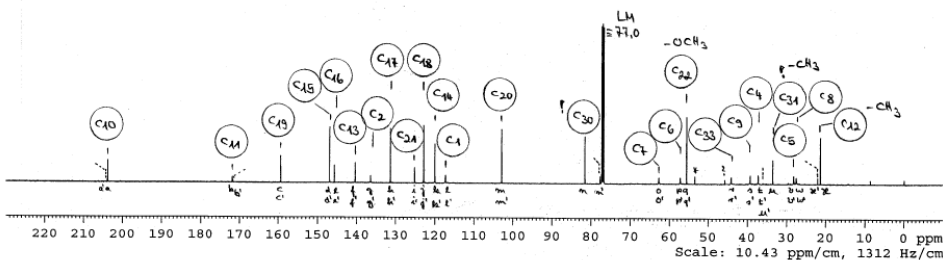
CHANNEL F1
 SFO1 125.7649800 MHz
 NUCL1 13C
 P1 10.00 usec
 SFO2 65336
 SP 125.6924191 MHz
 SWH 0
 LB 0.00 Hz
 GB 0
 PC 1.00

$\delta S, 26 \mu g, CDCl_3, \#2984$

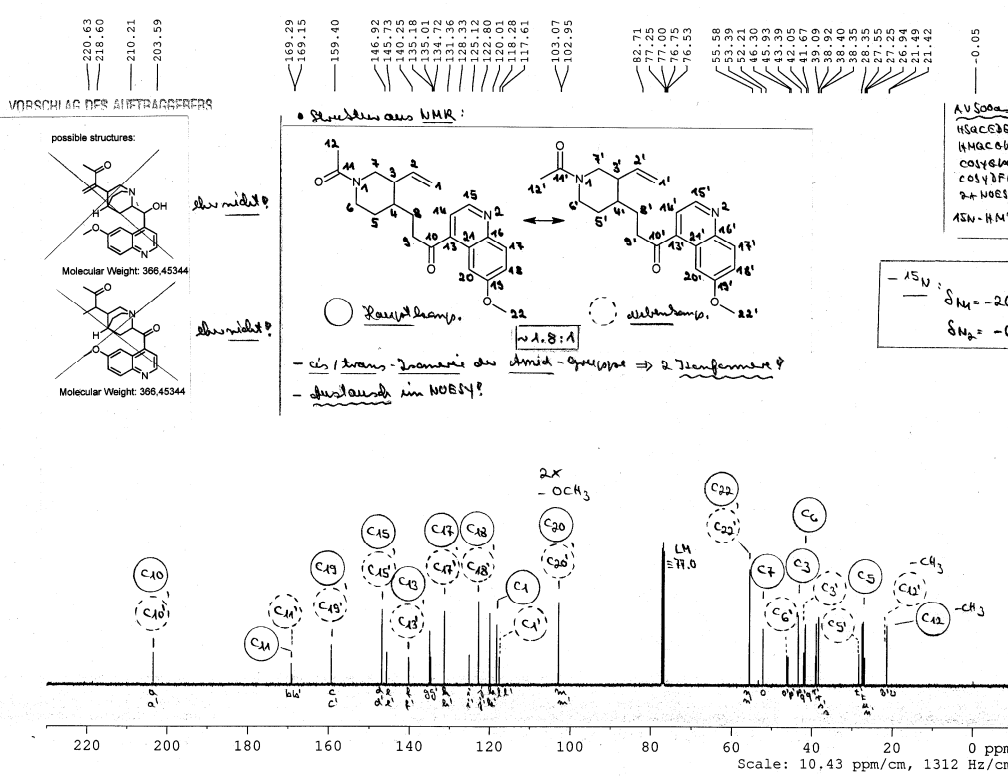
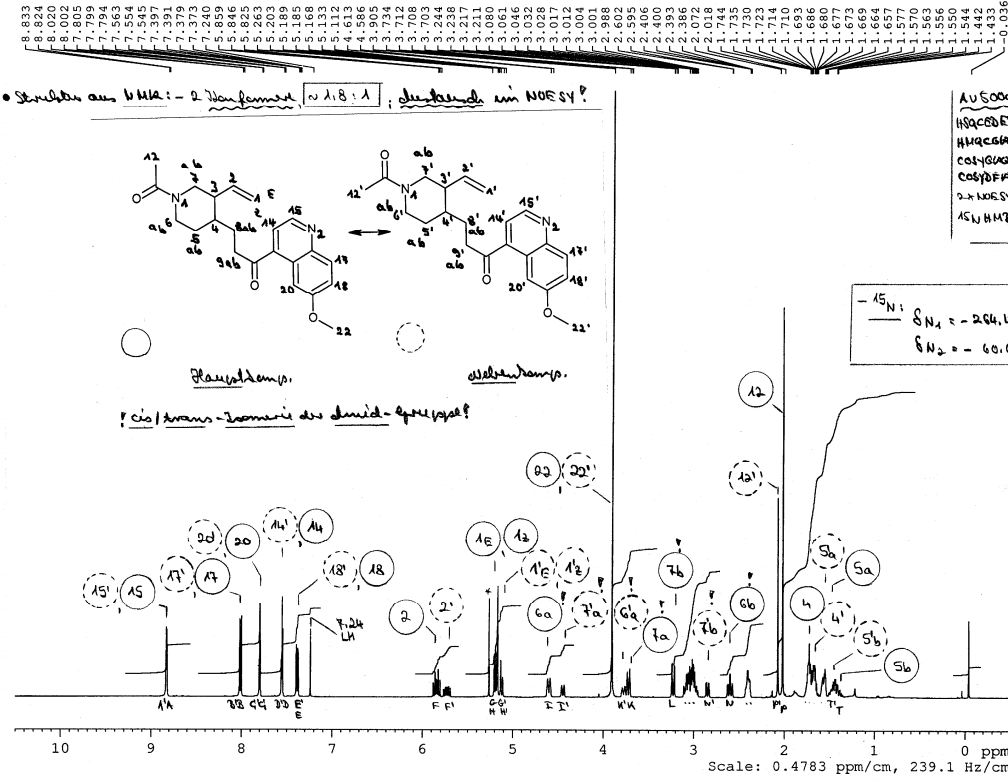
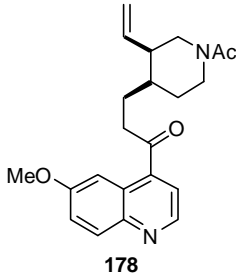
SR = 8.12

(gem. Dr. Fuchs)
 LEJ-LF-118-20
 13C(1H)
 AV500as

P. Plüsch



7. EXPERIMENTAL PART



7.8.10. X-ray Structure Analysis Parameters for CSA-Sulfonamide 203

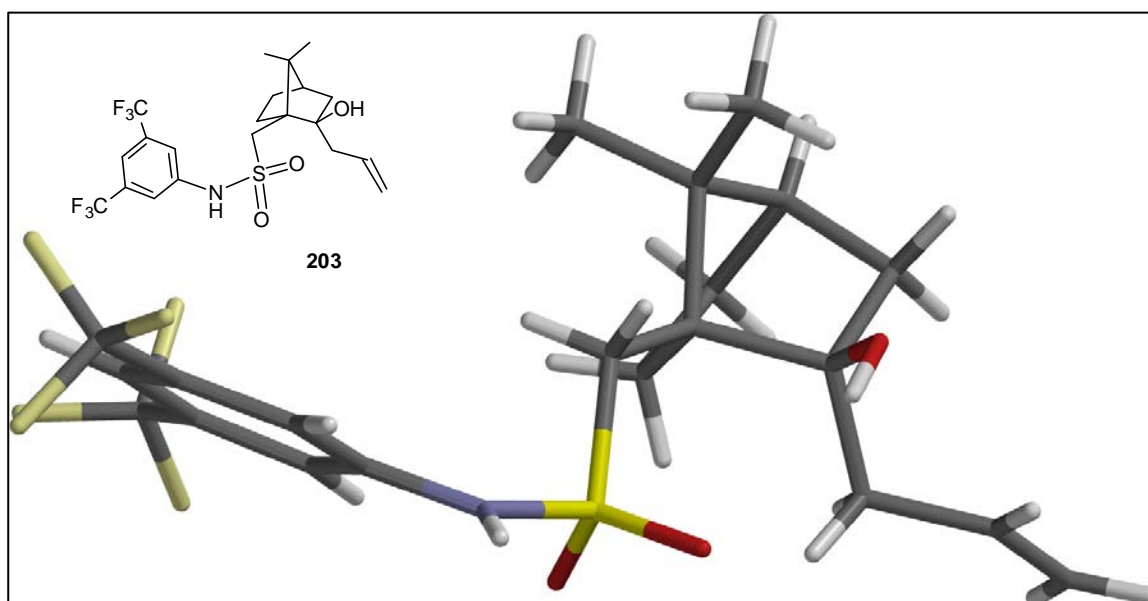


Table 7-17. Crystal data and structure refinement.

Identification code	7952	
Empirical formula	$C_{21}H_{25}F_6NO_3S$	
Color	colourless	
Formula weight	$485.48 \text{ g} \cdot \text{mol}^{-1}$	
Temperature	100 K	
Wavelength	1.54178 \AA	
Crystal system	RHOMBOHEDRAL	
Space group	R3, (no. 146)	
Unit cell dimensions	$a = 24.885(4) \text{ \AA}$	$\beta = 90^\circ$.
	$b = 24.885(4) \text{ \AA}$	$\beta = 90^\circ$.
	$c = 9.2565(15) \text{ \AA}$	$\beta = 120^\circ$.
Volume	$4964.2(14) \text{ \AA}^3$	
Z	9	
Density (calculated)	$1.462 \text{ Mg} \cdot \text{m}^{-3}$	
Absorption coefficient	1.985 mm^{-1}	
F(000)	2268 e	
Crystal size	$0.65 \times 0.12 \times 0.11 \text{ mm}^3$	
θ range for data collection	3.55 to 66.77° .	
Index ranges	$-28 \leq h \leq 29$, $-29 \leq k \leq 29$, $-10 \leq l \leq 10$	
Reflections collected	68773	
Independent reflections	3770 [$R_{\text{int}} = 0.0454$]	
Reflections with $I > 2\sigma(I)$	3731	

7. EXPERIMENTAL PART

Completeness to $\theta = 66.77^\circ$	99.9 %	
Absorption correction	Gaussian	
Max. and min. transmission	0.88 and 0.49	
Refinement method	Full-matrix least-squares on F^2	
Data / restraints / parameters	3770 / 1 / 292	
Goodness-of-fit on F^2	1.030	
Final R indices [$I > 2\sigma(I)$]	$R_1 = 0.0278$	$wR^2 = 0.0732$
R indices (all data)	$R_1 = 0.0281$	$wR^2 = 0.0734$
Absolute structure parameter	-0.006(12)	
Largest diff. peak and hole	0.301 and -0.278 e · Å ⁻³	

Table 7-18. Bond lengths [Å] and angles [°].

S(1)-O(1)	1.4391(13)	S(1)-O(2)	1.4425(14)
S(1)-N(1)	1.6346(15)	S(1)-C(1)	1.7755(18)
F(1)-C(20)	1.318(3)	F(2)-C(20)	1.331(3)
F(3)-C(20)	1.331(3)	F(4)-C(21)	1.331(3)
F(5)-C(21)	1.329(2)	F(6)-C(21)	1.329(3)
O(3)-C(7)	1.438(2)	N(1)-C(14)	1.414(2)
C(1)-C(2)	1.530(2)	C(2)-C(3)	1.543(2)
C(2)-C(7)	1.579(2)	C(2)-C(8)	1.582(3)
C(3)-C(4)	1.555(3)	C(4)-C(5)	1.538(3)
C(5)-C(6)	1.534(3)	C(5)-C(8)	1.551(3)
C(6)-C(7)	1.558(2)	C(7)-C(11)	1.544(3)
C(8)-C(9)	1.529(3)	C(8)-C(10)	1.540(3)
C(11)-C(12)	1.503(3)	C(12)-C(13)	1.314(3)
C(14)-C(19)	1.393(3)	C(14)-C(15)	1.399(3)
C(15)-C(16)	1.388(3)	C(16)-C(17)	1.392(3)
C(16)-C(20)	1.508(3)	C(17)-C(18)	1.392(3)
C(18)-C(19)	1.392(3)	C(18)-C(21)	1.497(3)
O(1)-S(1)-O(2)	118.65(8)	O(1)-S(1)-N(1)	104.89(8)
O(2)-S(1)-N(1)	108.89(8)	O(1)-S(1)-C(1)	109.63(8)
O(2)-S(1)-C(1)	109.15(8)	N(1)-S(1)-C(1)	104.67(8)
C(14)-N(1)-S(1)	124.46(12)	C(2)-C(1)-S(1)	117.40(12)
C(1)-C(2)-C(3)	115.84(15)	C(1)-C(2)-C(7)	116.72(14)
C(3)-C(2)-C(7)	107.81(14)	C(1)-C(2)-C(8)	110.46(14)
C(3)-C(2)-C(8)	100.95(14)	C(7)-C(2)-C(8)	103.19(14)
C(2)-C(3)-C(4)	102.67(15)	C(5)-C(4)-C(3)	103.51(15)
C(6)-C(5)-C(4)	108.47(17)	C(6)-C(5)-C(8)	102.22(15)
C(4)-C(5)-C(8)	102.77(16)	C(5)-C(6)-C(7)	104.19(14)
O(3)-C(7)-C(11)	108.75(15)	O(3)-C(7)-C(6)	108.02(15)

C(11)-C(7)-C(6)	110.74(14)	O(3)-C(7)-C(2)	111.47(14)
C(11)-C(7)-C(2)	115.88(15)	C(6)-C(7)-C(2)	101.59(14)
C(9)-C(8)-C(10)	106.56(17)	C(9)-C(8)-C(5)	114.73(17)
C(10)-C(8)-C(5)	113.21(16)	C(9)-C(8)-C(2)	115.96(15)
C(10)-C(8)-C(2)	114.17(17)	C(5)-C(8)-C(2)	92.07(14)
C(12)-C(11)-C(7)	112.88(17)	C(13)-C(12)-C(11)	124.8(2)
C(19)-C(14)-C(15)	119.78(16)	C(19)-C(14)-N(1)	122.39(16)
C(15)-C(14)-N(1)	117.83(16)	C(16)-C(15)-C(14)	119.60(18)
C(15)-C(16)-C(17)	121.30(18)	C(15)-C(16)-C(20)	119.79(18)
C(17)-C(16)-C(20)	118.89(17)	C(16)-C(17)-C(18)	118.37(17)
C(19)-C(18)-C(17)	121.27(18)	C(19)-C(18)-C(21)	118.67(18)
C(17)-C(18)-C(21)	120.03(17)	C(18)-C(19)-C(14)	119.58(17)
F(1)-C(20)-F(3)	106.20(19)	F(1)-C(20)-F(2)	108.3(2)
F(3)-C(20)-F(2)	104.65(18)	F(1)-C(20)-C(16)	113.37(16)
F(3)-C(20)-C(16)	111.51(17)	F(2)-C(20)-C(16)	112.24(18)
F(6)-C(21)-F(5)	106.8(2)	F(6)-C(21)-F(4)	106.79(18)
F(5)-C(21)-F(4)	106.18(18)	F(6)-C(21)-C(18)	112.65(17)
F(5)-C(21)-C(18)	112.32(17)	F(4)-C(21)-C(18)	111.70(19)

8. BIBLIOGRAPHY

- ¹ S. L. Miller, *Science* **1953**, *117*, 528.
- ² S. L. Miller, H. C. Urey, *Science* **1959**, *130*, 245.
- ³ A. Eschenmoser, *Tetrahedron* **2007**, *63*, 12821.
- ⁴ J. E. Hein, D. G. Blackmond, *Acc. Chem. Res.* **2012**, *45*, 2045.
- ⁵ K. Soai, T. Shibata, H. Morioka, K. Choji, *Nature* **1995**, *378*, 767.
- ⁶ M. Klussmann, H. Iwamura, S. P. Mathew, D. H. Wells, U. Pandya, A. Armstrong, D. G. Blackmond, *Nature* **2006**, *441*, 621.
- ⁷ Y. Ando, E. Fuse, W. D. Figg, *Clin. Cancer Res.* **2002**, *8*, 1964.
- ⁸ Z. Kovarik, Z. Radic, H. A. Berman, V. Simeon-Rudolf, E. Reiner, P. Taylor, *Biochem. J.* **2003**, *373*, 33.
- ⁹ Nobel prize 2001 nobel lecture, www.nobelprize.org
- ¹⁰ W. S. Knowles, M. J. Sabacky, *Chem. Commun.* **1968**, 1445.
- ¹¹ B. D. Vineyard, W. S. Knowles, M. J. Sabacky, G. L. Bachman, D. J. Weinkauff, *J. Am. Chem. Soc.* **1977**, *99*, 5946.
- ¹² G. Bredig, P. S. Fiske, *Biochem. Z.* **1912**, *46*, 7
- ¹³ H. Pracejus, *Justus Liebigs Ann. Chem.*, **1960**, *634*, 9.
- ¹⁴ Y. Orito, S. Imai, S. Niwa, Nguyengiahung, *J. Synth. Org. Chem. Jpn.* **1979**, *37*, 173.
- ¹⁵ K. T. Wan, M. E. Davis, *Nature* **1994**, *370*, 449.
- ¹⁶ K. Ding, Y. Uozumi, eds, *Handbook of Asymmetric Heterogeneous Catalysis*, Wiley-VCH, 2008.
- ¹⁷ Nobel prize 1984 nobel lecture, www.nobelprize.org
- ¹⁸ P. Barbaro, F. Liguori, *Chem. Rev.* **2009**, *109*, 515.
- ¹⁹ C. C. Tzschucke, C. Markert, W. Bannwarth, S. Roller, A. Hebel, R. Haag, *Angew. Chem. Int. Ed.* **2002**, *41*, 3964.
- ²⁰ H. C. Kolb, M. G. Finn, K. B. Sharpless, *Angew. Chem. Int. Ed.* **2001**, *40*, 2004.
- ²¹ Recent publication regarding the reaction mechanism, see: B. T. Worrell, J. A. Malik, V. V. Fokin, *Science* DOI: 10.1126/science.1229506.
- ²² W. H. Binder, R. Sachsenhofer, *Macromol. Rapid Comm.* **2007**, *28*, 15.
- ²³ Nobel prize 1920 nobel lecture, www.nobelprize.org
- ²⁴ Nobel prize 2007 nobel lecture, www.nobelprize.org
- ²⁵ W. H. Porter, *Pure. Appl. Chem.* **1991**, *63*, 1119.
- ²⁶ J. Gal, *Chirality* **2011**, *23*, 1.
- ²⁷ H. D. Flack, *Acta. Crystallogr. A* **2009**, *65*, 371.
- ²⁸ M. T. Reetz, *Angew. Chem. Int. Ed.* **2013**, *52*, 2658.
- ²⁹ A recent example, see: P. S. Coelho, E. M. Brustad, A. Kannan, F. H. Arnold, *Science* **2013**, *339*, 307.
- ³⁰ B. List, R. A. Lerner, C. F. Barbas, *J. Am. Chem. Soc.* **2000**, *122*, 2395.
- ³¹ Z. G. Hajos, D. R. Parrish, *J. Org. Chem.* **1974**, *39*, 1615.
- ³² A. B. Northrup, D. W. C. MacMillan, *J. Am. Chem. Soc.* **2002**, *124*, 2458.
- ³³ P. Garcia-Garcia, F. Lay, P. Garcia-Garcia, C. Rabalakos, B. List, *Angew. Chem. Int. Ed.* **2009**, *48*, 4363.
- ³⁴ A recent example, see: D. Almaşi, D. A. Alonso, E. Gómez-Bengo, C. Nájera, *J. Org. Chem.* **2009**, *74*, 6163.

- ³⁵ For reviews for asymmetric protonation, see: (a) J. T. Mohr, A. Y. Hong, B. M. Stoltz, *Nat. Chem.* **2009**, *1*, 359; (b) C. Fehr, *Angew. Chem. Int. Ed. Engl.* **1996**, *35*, 2567.
- ³⁶ L. Pu, H.-B. Yu, *Chem. Rev.* **2001**, *101*, 757.
- ³⁷ D. A. Evans, *Science* **1988**, *240*, 420.
- ³⁸ (a) H. Matsushita, M. Noguchi, M. Saburi, S. Yoshikawa, *Bull. Chem. Soc. Jpn.* **1975**, *48*, 3715; (b) H. Matsushita, M. Noguchi, S. Yoshikawa, *Chem. Lett.* **1975**, 1313; (c) H. Matsushita, Y. Tsujino, M. Noguchi, M. Saburi, S. Yoshikawa, *Bull. Chem. Soc. Jpn.* **1978**, *51*, 862.
- ³⁹ L. Duhamel, J. C. Plaquevent, *J. Am. Chem. Soc.* **1978**, *100*, 7415.
- ⁴⁰ L. Duhamel, J.-C. Plaquevent, *Tetrahedron Lett.* **1980**, *21*, 2521.
- ⁴¹ D. Potin, K. Williams, J. Rebek, *Angew. Chem. Int. Ed. Engl.* **1990**, *29*, 1420.
- ⁴² C. Fehr, *Angew. Chem. Int. Ed.* **2007**, *46*, 7119.
- ⁴³ C. Schaefer, G. C. Fu, *Angew. Chem. Int. Ed.* **2005**, *44*, 4606.
- ⁴⁴ J. T. Mohr, T. Nishimata, D. C. Behenna, B. M. Stoltz, *J. Am. Chem. Soc.* **2006**, *128*, 11348.
- ⁴⁵ I. Shimizu, T. Yamada, J. Tsuji, *Tetrahedron Lett.* **1980**, *21*, 3199.
- ⁴⁶ M. F. Carroll, *J. Chem. Soc.* **1940**, 704.
- ⁴⁷ C. H. Cheon, H. Yamamoto, *J. Am. Chem. Soc.* **2008**, *130*, 9246.
- ⁴⁸ D. Uruguchi, N. Kinoshita, T. Ooi, *J. Am. Chem. Soc.* **2010**, *132*, 12240.
- ⁴⁹ L. Duhamel, J.-C. Plaquevent, *Tetrahedron Lett.* **1977**, *18*, 2285.
- ⁵⁰ J. Steinreiber, K. Faber, H. Griengl, *Chem. Eur. J.* **2008**, *14*, 8060.
- ⁵¹ M. Barbero, S. Cadamuro, M. Ceruti, I. Degani, R. Fochi, V. Regondi, *Gazz Chim Ital* **1987**, *117*, 227.
- ⁵² T. E. Burghardt, *J. Sulfur Chem.* **2005**, *26*, 411.
- ⁵³ E. J. Corey, D. Seebach, *Angew. Chem. Int. Ed.* **1965**, *4*, 1075.
- ⁵⁴ M. Yus, C. Najera, F. Foubelo, *Tetrahedron* **2003**, *59*, 6147.
- ⁵⁵ E. J. Corey, D. J. Beames, *J. Am. Chem. Soc.* **1973**, *95*, 5829.
- ⁵⁶ E. J. Corey, A. P. Kozikowski, *Tetrahedron Lett.* **1975**, *16*, 925.
- ⁵⁷ T. Akiyama, *Chem. Rev.* **2007**, *107*, 5744.
- ⁵⁸ M. S. Sigman, E. N. Jacobsen, *J. Am. Chem. Soc.* **1998**, *120*, 4901.
- ⁵⁹ Y. Huang, A. K. Unni, A. N. Thadani, V. H. Rawal, *Nature* **2003**, *424*, 146.
- ⁶⁰ T. Akiyama, J. Itoh, K. Yokota, K. Fuchibe, *Angew. Chem. Int. Ed.* **2004**, *43*, 1566.
- ⁶¹ D. Uruguchi, M. Terada, *J. Am. Chem. Soc.* **2004**, *126*, 5356.
- ⁶² For reviews, see: (a) T. Akiyama, *Chem. Rev.* **2007**, *107*, 5744; (b) D. Kampen, C. M. Reisinger, B. List, *Top. Curr. Chem.* **2010**, *291*, 395; (c) M. Terada, *Synthesis* **2010**, 1929.
- ⁶³ D. Nakashima, H. Yamamoto, *J. Am. Chem. Soc.* **2006**, *128*, 9626.
- ⁶⁴ S. Vellalath, I. Čorić, B. List, *Angew. Chem. Int. Ed.* **2010**, *49*, 9749.
- ⁶⁵ I. Čorić, B. List, *Nature* **2012**, *483*, 315.
- ⁶⁶ I. Čorić, S. Müller, B. List, *J. Am. Chem. Soc.* **2010**, *132*, 17370.
- ⁶⁷ (a) N. Kann, *Molecules* **2010**, *15*, 6306; (b) A. F. Trindade, P. M. P. Gois, C. A. M. Afonso, *Chem. Rev.* **2009**, *109*, 418.

8. BIBLIOGRAPHY

- ⁶⁸ S. V. Ley, I. R. Baxendale, R. N. Bream, P. S. Jackson, A. G. Leach, D. A. Longbottom, M. Nesi, J. S. Scott, R. I. Storer, S. J. Taylor, *J. Chem. Soc. Perkin Trans. 1* **2000**, 3815.
- ⁶⁹ J. H. Hong, F. Zaera, *J. Am. Chem. Soc.* **2012**, *134*, 13056.
- ⁷⁰ For reviews on polymer-supported chiral organocatalysts, see: (a) F. Cozzi, *Adv. Synth. Catal.* **2006**, 348, 1367; (b) M. Benaglia, *New. J. Chem.* **2006**, *30*, 1525; (c) M. Gruttadauria, F. Giacalone, R. Noto, *Chem. Soc. Rev.* **2008**, *37*, 1666; (d) T. E. Kristensen, T. Hansen, *Eur. J. Org. Chem.* **2010**, 3179.
- ⁷¹ E. Buhleier, W. Wehner, F. Vögtle, *Synthesis* **1978**, 1978, 155.
- ⁷² (a) D. Astruc, F. Chardac, *Chem. Rev.* **2001**, *101*, 2991; (b) R. van Heerbeek, P. C. J. Kamer, P. W. N. M. van Leeuwen, J. N. H. Reek, *Chem. Rev.* **2002**, *102*, 3717.
- ⁷³ (a) X. Y. Chen, X. Yang, B. J. Holliday, *J. Am. Chem. Soc.* **2008**, *130*, 1546; (b) J. Schmidt, J. Weber, J. D. Epping, M. Antonietti, A. Thomas, *Adv. Mat.* **2009**, *21*, 702.
- ⁷⁴ (a) A. B. Powell, C. W. Bielawski, A. H. Cowley, *J. Am. Chem. Soc.* **2009**, *131*, 18232; (b) A. B. Powell, C. W. Bielawski, A. H. Cowley, *J. Am. Chem. Soc.* **2010**, *132*, 10184; (c) A. B. Powell, Y. Suzuki, M. Ueda, C. W. Bielawski, A. H. Cowley, *J. Am. Chem. Soc.* **2011**, *133*, 5218.
- ⁷⁵ C. Bleschke, J. Schmidt, D. S. Kundu, S. Blechert, A. Thomas, *Adv. Synth. Catal.* **2011**, *353*, 3101.
- ⁷⁶ D. S. Kundu, J. Schmidt, C. Bleschke, A. Thomas, S. Blechert, *Angew. Chem. Int. Ed.* **2012**, *51*, 5456.
- ⁷⁷ C. A. Wang, Z. K. Zhang, T. Yue, Y. L. Sun, L. Wang, W. D. Wang, Y. Zhang, C. Liu, W. Wang, *Chem. Eur. J.* **2012**, *18*, 6718.
- ⁷⁸ For reviews, see: (a) R. Dawson, A. I. Cooper, D. J. Adams, *Prog. Polym. Sci.* **2012**, *37*, 530; (b) N. B. McKeown, P. M. Budd, *Macromolecules* **2010**, *43*, 5163.
- ⁷⁹ Y. Arakawa, M. Wiesner, H. Wennemers, *Adv. Synth. Catal.* **2011**, *353*, 1201.
- ⁸⁰ T. J. Dickerson, N. N. Reed, K. D. Janda, *Chem. Rev.* **2002**, *102*, 3325; (b) D. E. Bergbreiter, *Chem. Rev.* **2002**, *102*, 3345.
- ⁸¹ Du Pont, United States Patent 2130523.
- ⁸² (a) L. B. Hu, M. Pasta, F. La Mantia, L. F. Cui, S. Jeong, H. D. Deshazer, J. W. Choi, S. M. Han, Y. Cui, *Nano Lett.* **2010**, *10*, 708; (b) M. Pasta, F. La Mantia, L. B. Hu, H. D. Deshazer, Y. Cui, *Nano Res.* **2010**, *3*, 452; (c) G. H. Yu, L. B. Hu, M. Vosgueritchian, H. L. Wang, X. Xie, J. R. McDonough, X. Cui, Y. Cui, Z. N. Bao, *Nano Lett.* **2011**, *11*, 2905; (d) M. D. Lima, S. L. Fang, X. Lepro, C. Lewis, R. Ovalle-Robles, J. Carretero-Gonzalez, E. Castillo-Martinez, M. E. Kozlov, J. Y. Oh, N. Rawat, C. S. Haines, M. H. Haque, V. Aare, S. Stoughton, A. A. Zakhidov, R. H. Baughman, *Science* **2011**, *331*, 51. (e) Y.-C. Li, J. Schulz, S. Mannen, C. Delhom, B. Condon, S. Chang, M. Zammarano, J. C. Grunlan, *ACS Nano* **2010**, *4*, 3325.
- ⁸³ (a) L. Xue, B. Jia, L. Tang, X. F. Ji, M. Y. Huang, Y. Y. Jiang, *Polym. Adv. Technol.* **2004**, *15*, 346. (b) S. Q. Wang, Z. W. Wang, L. C. Yang, J. L. Dong, C. Q. Chi, D. N. Sui, Y. Z. Wang, J. G. Ren, M. Y. Hung, Y. Y. Jiang, *J. Mol. Catal. A Chem.* **2007**, *264*, 60.
- ⁸⁴ A. Ricci, L. Bernardi, C. Gioia, S. Vierucci, M. Robitzer, F. Quignard, *Chem. Commun.* **2010**, 46, 6288.
- ⁸⁵ G. Bredig, F. Gerstner, H. Lang, *Biochem. Z.* **1935**, *282*, 88.
- ⁸⁶ (a) X. Zhang, Y.-J. Li, M.-Y. Huang, Y.-Y. Jiang, *Polym. Adv. Technol.* **2002**, *13*, 305; (b) L. Xue, D.-J. Zhou, L. Tang, X.-F. Ji, M.-Y. Huang, Y.-Y. Jiang, *React. Funct. Polym.* **2004**, *58*, 117.

- ⁸⁷ (a) D. Praschak, T. Bahnert, E. Schollmeyer, *Appl. Phys. A* **2000**, *71*, 577; (b) A. N. Netravali, T. Bahnert, *J. Adhes. Sci. Technol.* **2010**, *24*, 45.
- ⁸⁸ (a) K. Opwis, *Chem. Engineer. Trans.* **2010**, *20*, 19; (b) K. Opwis, D. Knittel, E. Schollmeyer, *Biotechnol. J.* **2007**, *2*, 347.
- ⁸⁹ D. A. Evans, M. D. Ennis, D. J. Mathre, *J. Am. Chem. Soc.* **1982**, *104*, 1737.
- ⁹⁰ B. M. Trost, *Angew. Chem. Int. Ed. Engl.* **1995**, *34*, 259.
- ⁹¹ A. Bedalov, T. Gattbonton, W. P. Irvine, D. E. Gottschling, J. A. Simon, *Proc. Natl. Acad. Sci. U.S.A.* **2001**, *98*, 15113; (b) M. Hirao, J. Posakony, M. Nelson, H. Hruby, M. F. Jung, J. A. Simon, A. Bedalov, *J. Biol. Chem.* **2003**, *278*, 52773; (c) S. Pagans, A. Pedal, B. J. North, K. Kaehlcke, B. L. Marshall, A. Dorr, C. Hetzer-Egger, P. Henklein, R. Frye, M. W. McBurney, H. Hruby, M. Jung, E. Verdin, M. Ott, *Plos. Biol.* **2005**, *3*, 210; (d) K. Drabikova, T. Perecko, R. Nosal, L. Rackova, G. Ambrozova, A. Lojek, J. Smidrkal, J. Harmatha, V. Jancinova, *Neuroendocrinol Lett.* **2010**, *31*, 73; (e) M. Weidenboerner, H. C. Jha, *Chem. Mikrobiol. Technol. Lebensm.* **1995**, *17*, 22.
- ⁹² (a) M. Versteeg, B. C. B. Bezuidenhoudt, D. Ferreira, K. J. Swart, *J. Chem. Soc. Chem. Comm.* **1995**, 1317; (b) L. Farkas, Gottsege, A. M. Nogradi, S. Antus, *J. Chem. Soc. Perkin Trans. 1* **1974**, 305.
- ⁹³ C. Decker, *Polym. Int.* **2002**, *51*, 1141.
- ⁹⁴ C. Liu, C. He, W. Shi, M. Chen, A. Lei, *Org. Lett.* **2007**, *9*, 5601.
- ⁹⁵ J. D. Rosen, T. D. Nelson, M. A. Huffman, J. M. McNamara, *Tetrahedron Lett.* **2003**, *44*, 365.
- ⁹⁶ A. E. Nibbs, K. A. Scheidt, *Eur. J. Org. Chem.* **2012**, 449.
- ⁹⁷ H. von Pechmann, W. Welsh, *Ber. Dtsch. Chem. Ges.* **1884**, *17*, 1646.
- ⁹⁸ G. Sabitha, A. V. S. Rao, *Synth. Commun.* **1987**, *17*, 341.
- ⁹⁹ Y. Kikugawa, S. Ikegami, S. I. Yamada, *Chem. Pharm. Bull.* **1969**, *17*, 98.
- ¹⁰⁰ R. Hernandezgalan, J. Salva, G. M. Massanet, I. G. Collado, *Tetrahedron* **1993**, *49*, 1701.
- ¹⁰¹ C. Madelaine, V. Valerio, N. Maulide, *Angew. Chem. Int. Ed.* **2010**, *49*, 1583.
- ¹⁰² B. Peng, D. H. O'Donovan, I. D. Jurberg, N. Maulide, *Chem. Eur. J.* **2012**, *18*, 16292.
- ¹⁰³ C. Madelaine, V. Valerio, N. Maulide, *Chem. Eur. J.* **2011**, *6*, 2224.
- ¹⁰⁴ R. M. Beesley, C. K. Ingold, J. F. Thorpe, *J. Chem. Soc. Transactions* **1915**, *107*, 1080.
- ¹⁰⁵ U. Gross, P. J. Gross, M. Shi, S. Brase, *Synlett* **2011**, 635.
- ¹⁰⁶ H. C. Xu, K. D. Moeller, *Angew. Chem. Int. Ed.* **2010**, *49*, 8004.
- ¹⁰⁷ F. M. Carlini, *Chim. Oggi* **2003**, *21*, 14.
- ¹⁰⁸ W. R. Dolbier, Jr., *Chim. Oggi* **2003**, *21*, 66.
- ¹⁰⁹ K. C. Nicolaou, M. E. Bunnage, D. G. McGarry, S. H. Shi, P. K. Somers, P. A. Wallace, X. J. Chu, K. A. Agrios, J. L. Gunzner, Z. Yang, *Chem. Eur. J.* **1999**, *5*, 599.
- ¹¹⁰ J. M. Heemstra, S. A. Kerrigan, D. R. Doerge, W. G. Helferich, W. A. Boulanger, *Org. Lett.* **2006**, *8*, 5441.
- ¹¹¹ U. Gerlach, S. Hunig, *Angew. Chem. Int. Ed. Engl.* **1987**, *26*, 1283.
- ¹¹² C. F. Bernasconi, D. E. Fairchild, C. J. Murray, *J. Am. Chem. Soc.* **1987**, *109*, 3409.
- ¹¹³ C. E. Song, *Cinchona Alkaloids in Synthesis & Catalysis*, WILEY-VCH, Weinheim, **2009**.
- ¹¹⁴ L. Canali, C. E. Song, D. C. Sherrington, *Tetrahedron: Asymm.* **1998**, *9*, 1029.
- ¹¹⁵ M. Studer, H.-U. Blaser, C. Exner, *Adv. Synth. Catal.* **2003**, *345*, 45.

8. BIBLIOGRAPHY

- ¹¹⁶ H.-U. Blaser, M. Studer, *Acc. Chem. Res.* **2007**, *40*, 1348.
- ¹¹⁷ C. E. Song, J. W. Yang, H.-J. Ha, *Tetrahedron: Asymm.* **1997**, *8*, 841.
- ¹¹⁸ D. Praschak, T. Bahnners, E. Schollmeyer, *Appl. Phys. A Mater.* **1998**, *66*, 69.
- ¹¹⁹ S. L. Gao, R. Hassler, E. Mader, T. Bahnners, K. Opwis, E. Schollmeyer, *Appl. Phys. B-Lasers O.* **2005**, *81*, 681.
- ¹²⁰ M. Y. Melnikov, N. V. Fok, *Russ. Chem. Rev.* **1980**, *49*, 131.
- ¹²¹ B. Vakulya, S. Varga, A. Csampai, T. Soos, *Org. Lett.* **2005**, *7*, 1967.
- ¹²² L.-W. Xu, J. Luo, Y. Lu, *Chem. Commun.* **2009**, 1807.
- ¹²³ S. J. Connon, *Chem. Commun.* **2008**, 2499.
- ¹²⁴ F. G. Bordwell, *Acc. Chem. Res.* **1988**, *21*, 456.
- ¹²⁵ T. Honjo, S. Sano, M. Shiro, Y. Nagao, *Angew. Chem. Int. Ed.* **2005**, *44*, 5838.
- ¹²⁶ J. P. Malerich, K. Hagihara, V. H. Rawal, *J. Am. Chem. Soc.* **2008**, *130*, 14416.
- ¹²⁷ Y. L. Liu, F. Zhou, J. J. Cao, C. B. Ji, M. A. Ding, J. A. Zhou, *Org. Biomol. Chem.* **2010**, *8*, 3847.
- ¹²⁸ J. W. Lee, T. H. Ryu, J. S. Oh, H. Y. Bae, H. Bin Jang, C. E. Song, *Chem. Commun.* **2009**, 7224.
- ¹²⁹ L. Wambach, M. Fischer, *US4874865 (1979)*.
- ¹³⁰ D. A. Annis, E. N. Jacobsen, *J. Am. Chem. Soc.* **1999**, *121*, 4147.
- ¹³¹ W. Steglich, G. Höfle, *Angew. Chem. Int. Ed. Engl.* **1969**, *8*, 981.
- ¹³² N. G. Anderson, *Org. Process. Res. Dev.* **2012**, *16*, 852.
- ¹³³ H. Hocke, Y. Uozumi, *Tetrahedron* **2003**, *59*, 619.
- ¹³⁴ B. J. Li, P. Chiu, *Eur. J. Org. Chem.* **2011**, 3932.
- ¹³⁵ P. Jain, J. C. Antilla, *J. Am. Chem. Soc.* **2010**, *132*, 11884.
- ¹³⁶ R. S. Givens, L. W. Kueper, *Chem. Rev.* **1993**, *93*, 55.
- ¹³⁷ A. Martínez, M. J. Webber, S. Müller, B. List, *Angew. Chem. Int. Ed.* **2013**, DOI: 10.1002/anie.201301618.
- ¹³⁸ B. List, P. Pojarliev, W. T. Biller, H. J. Martin, *J. Am. Chem. Soc.* **2002**, *124*, 827.
- ¹³⁹ S. A. Selkala, J. Tois, P. M. Pihko, A. M. P. Koskinen, *Adv. Synth. Catal.* **2002**, *344*, 941.
- ¹⁴⁰ C. Peters, M. Bacher, C. L. Buenemann, F. Kricek, J. M. Rondeau, K. Weigand, *ChemBiochem* **2007**, *8*, 1785.
- ¹⁴¹ O. Lifchits, C. M. Reisinger, B. List, *J. Am. Chem. Soc.* **2010**, *132*, 10227.
- ¹⁴² O. Lifchits, N. Demoulin, B. List, *Angew. Chem. Int. Ed.* **2011**, *50*, 9680.
- ¹⁴³ O. Lifchits, M. Mahlau, C. M. Reisinger, A. Lee, C. Farès, I. Polyak, G. Gopakumar, W. Thiel, B. List, *J. Am. Chem. Soc.* **2013**. DOI: 10.1021/ja402058v
- ¹⁴⁴ A. D. Kalugina, M. Y. Mel'nikov, *High. Energ. Chem.* **2007**, *41*, 385.
- ¹⁴⁵ T. Hashimoto, K. Maruoka, *Chem. Rev.* **2007**, *107*, 5656.
- ¹⁴⁶ A. G. Doyle, E. N. Jacobsen, *Chem. Rev.* **2007**, *107*, 5713.
- ¹⁴⁷ S. H. Youk, S. H. Oh, H. S. Rho, J. E. Lee, J. W. Lee, C. E. Song, *Chem. Commun.* **2009**, 2220.
- ¹⁴⁸ O. Gleeson, G. L. Davies, A. Peschiulli, R. Tekoriute, Y. K. Gun'ko, S. J. Connon, *Org. Biomol. Chem.* **2011**, *9*, 7929.
- ¹⁴⁹ BASF, *Ger. Offen.*, 3718563
- ¹⁵⁰ G. I. Nikishin, R. I. Mustafaer, *Bull. Acad. Sci. USSR. Div. Chem. Sci.* **1964**, *13*, 1745.
- ¹⁵¹ D. Elad, Sinnreic.J, *Chem. Commun.* **1965**, 471.

-
- ¹⁵² D. Elad, J. Sperling, *Chem. Commun.* **1968**, 655.
- ¹⁵³ S. F. Nelsen, J. T. Ippoliti, *J. Am. Chem. Soc.* **1986**, *108*, 4879.
- ¹⁵⁴ M. P. Sibi, N. A. Porter, *Acc. Chem. Res.* **1998**, *32*, 163.
- ¹⁵⁵ N. Ishida, Y. Shimamoto, M. Murakami, *Angew. Chem. Int. Ed.* **2012**, *51*, 11750.
- ¹⁵⁶ M. D. Cohen, *Tetrahedron* **1987**, *43*, 1211.
- ¹⁵⁷ J. I. Seeman, *Angew. Chem. Int. Ed.* **2007**, *46*, 1378.
- ¹⁵⁸ Y. Yanuka, A. Geryes, M. Heller, *Tetrahedron* **1987**, *43*, 911.
- ¹⁵⁹ A. C. Smith, R. M. Williams, *Angew. Chem. Int. Ed.* **2008**, *47*, 1736.
- ¹⁶⁰ P. Christ, A. G. Lindsay, S. S. Vormittag, J.-M. Neudörfl, A. Berkessel, A. C. O'Donoghue, *Chem. Eur. J.* **2011**, *17*, 8524.
- ¹⁶¹ (a) I. Čorić, S. Vellalath, B. List, *J. Am. Chem. Soc.* **2010**, *132*, 8536. Erratum: I. Čorić, S. Vellalath, B. List, *J. Am. Chem. Soc.* **2010**, *132*, 12155.
- ¹⁶² H. J. Choi, M. H. Hyun, *Chem. Commun.* **2009**, 6454.
- ¹⁶³ (a) A. W. Martinez, S. T. Phillips, G. M. Whitesides, *Proc. Natl. Acad. Sci. USA* **2008**, *105*, 19606; (b) A. W. Martinez, S. T. Phillips, M. J. Butte, G. M. Whitesides, *Angew. Chem. Int. Ed.* **2007**, *46*, 1318.
- ¹⁶⁴ X. C. Wang, K. Maeda, A. Thomas, K. Takanebe, G. Xin, J. M. Carlsson, K. Domen, M. Antonietti, *Nat. Mater.* **2009**, *8*, 76.
- ¹⁶⁵ (a) H. Iida, S. Iwahana, T. Mizoguchi, E. Yashima, *J. Am. Chem. Soc.* **2012**, *134*, 15103. Erratum: H. Iida, S. Iwahana, T. Mizoguchi, E. Yashima, *J. Am. Chem. Soc.* **2012**, *134*, 18150.
- ¹⁶⁶ J. Y. Yang, S. X. Wu, F. X. Chen, *Synlett* **2010**, 2725.
- ¹⁶⁷ J. Y. Yang, S. X. Wu, F. X. Chen, *Synlett* **2011**, 734.
- ¹⁶⁸ G. Pousse, A. Devineau, V. Dalla, L. Humphreys, M. C. Lasne, J. Rouden, J. Blanchet, *Tetrahedron* **2009**, *65*, 10617.
- ¹⁶⁹ N. Momiyama, H. Nishimoto, M. Terada, *Org. Lett.* **2011**, *13*, 2126.
- ¹⁷⁰ N. Momiyama, H. Nishimoto, M. Terada, *Org. Lett.* **2011**, *13*, 2126.
- ¹⁷¹ G. Sabitha, A. V. S. Rao, *Synth. Commun.* **1987**, *17*, 341.
- ¹⁷² K. D. Moeller, H. C. Xu, *Angew. Chem. Int. Ed.* **2010**, *49*, 8004.
- ¹⁷³ F. A. Carey, J. R. Neergaard, *J. Org. Chem.* **1971**, *36*, 2731.
- ¹⁷⁴ S. Poulain, S. Julien, E. Dunach, *Tetrahedron Lett.* **2005**, *46*, 7077.
- ¹⁷⁵ R. A. Shiels, C. W. Jones, *J. Mol. Catal. A Chem.* **2007**, *261*, 160.
- ¹⁷⁶ A. Sakakura, K. Kawajiri, T. Ohkubo, Y. Kosugi, K. Ishihara, *J. Am. Chem. Soc.* **2007**, *129*, 14775.
- ¹⁷⁷ C. H. Heathcock, C. R. Hadley, T. Rosen, P. D. Theisen, S. J. Hecker, *J. Med. Chem.* **1987**, *30*, 1858.

9.1 Erklärung

“Ich versichere, dass ich die von mir vorgelegte Dissertation selbständig angefertigt, die benutzten Quellen und Hilfsmittel vollständig angegeben und die Stellen der Arbeit – einschließlich Tabellen, Karten und Abbildungen –, die anderen Werken im Wortlaut oder dem Sinn nach entnommen sind, in jedem Einzelfall als Entlehnung kenntlich gemacht habe; dass diese Dissertation noch keiner anderen Fakultät oder Universität zur Prüfung vorgelegen hat; dass sie – abgesehen von unten angegebenen Teilpublikationen – noch nicht veröffentlicht worden ist sowie, dass ich eine solche Veröffentlichung vor Abschluss des Promotionsverfahrens nicht vornehmen werde. Die Bestimmungen der Promotionsordnung sind mir bekannt. Die von mir vorgelegte Dissertation ist von Herrn Professor Dr. Benjamin List betreut worden.“

Mülheim an der Ruhr, Juni 2013

Bisher sind folgende Teilpublikationen veröffentlicht worden:

“Deracemization of α -Aryl Hydrocoumarins via Catalytic Asymmetric Protonation of Ketene Dithioacetals”: J.-W. Lee, B. List, *J. Am. Chem. Soc.* **2012**, *134*, 18245.

“Process for the Immobilization of Catalysts on Textile Materials, the Obtained Textile Materials and the Use of Said Materials“ B. List, J.-W. Lee, T. Mayer-Gall, K. Opwis, Patent in application, EP 12170144.5-2104, 2012

9.2 Lebenslauf

Ji-Woong Lee

Geboren am 22. Dez 1982
in Seoul, Südkorea
Staatsangehörigkeit Koreanisch

Akademischer Werdegang

Promotion

09.2009 – 06.2013 Dissertation im Arbeitskreis von Prof. Dr. Benjamin List
Max-Planck-Institut für Kohlenforschung, Mülheim an der Ruhr
mit dem Titel „Unconventional Homogeneous and Heterogeneous
Asymmetric Organocatalysis“

Hochschulstudium

09.2007 – 08.2009 M.Sc. im Arbeitskreis von Prof. Dr. Choong Eui Song
Sungkyunkwan University, Korea
mit dem Titel „*Organic Reactions Promoted by Ionic Liquids and
Bifunctional Organocatalysts*“

03.2001 – 08.2007 Chemiestudium an der Sungkyunkwan University, Korea
GPA 3.95/4.50

Schulbildung

03.1998-02.2001 Wooshin High School, Seoul, Korea
03.1995-02.1998 Wooshin Middle School, Seoul, Korea
03.1989-02.1995 Onsu Elementary School, Seoul, Korea